Thermal Degradation Studies of Bionanocomposites

A Dissertation submitted to the
Indian Institute of Technology Guwahati
in the partial fulfillment of the requirements for the degree of

DOCTOR of PHILOSOPHY

By

Monika

Roll No: 136107017

Department of Chemical Engineering

Indian Institute of Technology Guwahati

Guwahati – 781039, Assam, India

February, 2019

Dedicated to

my Beloved Parents

who always Supported & Encouraged me to

Follow my Dreams

Department of Chemical Engineering

Indian Institute of Technology Guwahati

Guwahati-781039, India

STATEMENT

I hereby declare that the research matter embodied in the thesis entitled, "**Thermal Degradation Studies of Bionanocomposites**" is carried out by me at the Department of Chemical Engineering, Indian Institute of Technology Guwahati, Guwahati, Assam, India, under the supervision of **Prof. Vimal Katiyar** for the award of the degree of Doctor of Philosophy. To the best of my knowledge, the scientific work delineated in this thesis is achieved by me and has not been submitted to any other institute or university for the award of any degree or diploma.

In keeping up with the scientific tradition, all the work that has been adopted from elsewhere has been and duly acknowledged at the respective place in the thesis.

Guwahati

February 2019

(Ms. Monika)

Research Scholar

Roll No. 136107017

Department of Chemical Engineering

Indian Institute of Technology Guwahati

Guwahati-781039, Assam, India.

Dr. Vimal Katiyar

Professor
Department of Chemical Engineering
Indian Institute of Technology Guwahati
Guwahati-781039, Assam, India
Tel: +91-361-258-2278;
E-mail: vkatiyar@iitg.ac.in

CERTIFICATE

This is to certify that the thesis entitled "**Thermal Degradation Studies of Bionanocomposites**" is submitted by Ms. **Monika** for the award of PhD degree. The research work documented in this thesis has been carried out by her at CoE-SusPol, Department of Chemical Engineering, Indian Institute of Technology Guwahati under my supervision and has not been submitted to any other University or Institute for the award any degree or diploma.

Guwahati **Prof. Vimal Katiyar**

February, 2019 Thesis supervisor

Acknowledgements

At this moment of accomplishment, I owe my gratitude to numerous people who have contributed in many ways during this entire phase of my Ph. D journey and made it an unforgettable experience for me. Words seem inadequate to express my profound sense of gratitude for all those people who made my journey a wholesome.

First and foremost, I would like to express my appreciation to my advisor Professor Vimal Katiyar for his dedicated advice, scholarly input and consistent encouragement throughout the research work. His enthusiasm, positive disposition and integral view on research, has laid a deep impression on me. Sir has constantly forced me to remain focused on achieving my goals and I consider it as a great opportunity to do my doctoral programme under his guidance.

Besides my advisor, I would like to express my earnest thanks to my Doctoral Committee members Prof. Gopal Pugazhenthi (Department of Chemical Engineering), Dr. Pankaj Tiwari (Department of Chemical Engineering) and Dr. C. K. Jana (Department of Chemistry) for their insightful comments and positive appreciation.

Research is impossible without the required materials, instrument facilities and resources. I take this time to express my gratitude to the Center of Excellence for Sustainable Polymers (CoE-SusPol) and Central Instruments Facility (CIF), IIT Guwahati for providing me analytical facilities to work without hindrance. I am also thankful to the scientific staff of the chemical engineering department for helping me to carry out XRD analysis as part of my research work. Mr. Harsaraj Biswanath, Mr. Debojit and other non-technical staff of chemical department have been very helpful. My co-research fellows, Akhilesh Kumar Pal, Prodyut Dhar, Neelima Tripathi and Khalid Mahmood have all extended their support in a very special way, and I gained a lot from them, through their personal and scholarly interactions,

their suggestions at various points of my research programme. It's my pleasure to acknowledge my colleagues, especially, Melaku, Gourhari, Atanu, Naren and Sashanka for their help and good wishes. I am also indebted to my lab mates for providing fun-filled environment, especially Tabli, Pankaj, Munmi, Dolly, Deepshika, Naba, Neha and Kona.

I would like to pay high regards to my parents for their countless sacrifice, care and support, who made it possible for me to reach this stage in my life. Above all, I owe it all to Almighty God for granting me the wisdom, health and strength to undertake this research work and enabling me to its completion. I am thankful to Almighty God for his blessings beyond my belief.

Monika

Abstract

The aim of the current research is to develop poly (lactic acid) (PLA) based bionanocomposites which is motivated by the problems associated with the conventional polymers. The present research focuses on the development of environmental friendly packaging materials based on biopolymers such as polyesters, i.e. (PLA), polysaccharides (cellulose, chitosan and gum) and their structural complexes modified to a larger extent, to fulfil the requirements of the sustainable future. In order to meet the current demands of the industry and consumer needs, the addition of PLA with nano-functional biofiller is found to be a compelling alternative to the conventional plastic packaging. Nano-functional biofillers are considered to be most suitable alternatives to develop green biocomposites when incorporated into the PLA matrix which offer the advantages of biodegradability, renewability along with balanced properties. The melt processing of PLA with biofiller is a challenging task as the material undergoes thermal decomposition at elevated temperature and the shearing action results in the reduced melt strength. The modification of biofiller is one such strategy which may be adopted to overcome these limitations. Additionally, the chain extenders or radical initiators may lead to the enhancement in the melt strength during reactive extrusion with a wide range of processing window. Non isothermal TGA kinetics studies at dynamic heating regime along with the evolution of volatile components are observed using the unique thermogravimetry (TGA) and hyphenated TGA Fourier transform infrared spectroscopy (TG–FTIR) techniques. In the current research, a comprehensive kinetic model is employed, including (i) model free methods to investigate the parameters and (ii) generalized master plots to propose the thermal induced mechanism. The influence of biofiller on the degradation mechanism of nanobiocomposite is determined. The current research helps in understanding the fabrication process of PLA based nanobiocomposite films

along with its degradation mechanism. The effect of biofillers in tailoring the final properties of the fabricated films has also been presented.

Contents

List of Tables

List of Figures

List of Schemes

Nomenclature

Abbreviations

PLA	Poly (lactic acid)
PBS	Poly(butylenes succinate)
CNC	Cellulose Nanocrystals
GA	Gum Arabic
Chitosan	CH
TGA	Thermogravimetric analysis
DSC	Differential Scanning Calorimetry
FCH	Functionalized Chitosan
FG	Functionalized Gum arabic
DCP	Dicumyl Peroxide
GPC	Gel Permeation Chromatography
POM	Polarized Optical Microscopy
FWO	Flynn Wall Ozawa
CR	Coat-Redfern
FESEM	Field Emission Scanning Electron Microscopy
FTIR	Fourier Transmission Infra-Red Spectroscopy
DTG	Derative Thermograms
H2SO4	Sulphuric Acid

HNO3	Nitric Acid
H3PO4	Phosphoric Acid
HCl	Hydrochloric Acid
3D	Three Dimensions
2D	Two Dimensions
CO_2	Carbon dioxide
CO	Carbon mono-oxide
M_n	Number Average Molecular Weight
M_w	Weight Average Molecular Weight
OLLA	Oligo-L Lactic Acid
FETEM	Field Electron Transmission Electron Microscopy
XRD	X-Ray Diffraction
PDI	Polydispersity Index

Notations

α	Fractional Conversion
β	Rate of Heating
k	Rate Constant
θ	Diffraction Angle
T_{max}	Maximum Degradation Temperature
A	Pre-Exponential Factor
E_a	Activation Energy
n	Order of Reaction
R	Gas Constant
θ_c	Contact Angle
λ	Cu-Kα Radiation Wavelength
T_g	Glass Transition Temperature
T_{cc}	Cold Crystallization Temperature
T_c	Crystallization Temperature
T_m	Melting Temperature
G'	Storage Modulus
G"	Loss Modulus
X_c	Percentage Crystallinity
η^*	Complex Viscosity

ω	Angular Frequency
τ	Shear Stress
η	Viscosity
γ	Shear Rate
η'	Real Viscosity
η''	Imaginary Viscosity
θ_a	Apparent Nucleation Delay Time
ΔH_{cc}	Cold Crystallization Enthalpy
ΔH_c	Crystallization Enthalpy
ΔH_m	Melting Enthalpy
ΔG	Gibbs' Free Energy
ΔS	Entropy
ΔH_m^o	Standard Heat of Fusion

Chapter 1

Introduction and Literature Review

This chapter represents the basic fundamentals of bioplastics, their classification, with a brief review on the synthesis of poly (lactic acid) (PLA) and its properties. Addressing the limitations of PLA in various sectors, suitable alternative have been highlighted to improve its performances for end use applications possibly by forming blends and biocomposites. The advantages of natural biofillers such as cellulose nanocrystals, chitosan and gum arabic have been presented for their possible use as filler in the matrix of PLA. Further, a brief introduction on the melt processing technique and thermal degradation route for PLA has been dispensed along with the emphasis on reactive extrusion processing to improve the melt strength and compatibility of polymer matrix with filler. Further, discussion has been made on the kinetic of thermal degradation based on the experimental and computational approaches which are closely related to the current research work with the aim of fabrication biodegradable composite material without compromising quality of end product. Furthermore, the literature survey has been carried out with an emphasis on PLA and its PLA/PBS blend and biocomposite, kinetics of thermal degradation and the release of volatile species at elevated temperature. Subsequently, the objective of the current research work and its organization is presented.

1. INTRODUCTION

Plastics are considered to be as mechanically strong, inexpensive, moldable, durable, light weight and corrosion-resistant materials, which are utilized in diverse applications that add safety, comfort and convenience and have penetrated in almost all aspects of everyday lives **(Thompson et al., 2009; Brydson et al., 1999; Hopewell et al., 2009).** It is almost impossible to imagine the human life without plastics. Consumption of plastics is gradually increasing day by day and the annual plastic production is enhanced from two million tons in 1950 to 380 million tons in 2015 worldwide **(Jung et al., 2018)** which has subsequently led to the accumulation of 43% plastic debris in the landfills and more than 10 million tons in natural habitats (Jambeck et al., 2015). It is therefore essential to focus upon on the major challenges such as the environmental pollultants, volatile oil prices, waste management, etc. and utilized the resource judiciously. According to a forecast by **Yarsley et al.,** in 1945 the predictions had been made on "*how much brighter and cleaner a world would be than that which preceded this plastic age*"as during that time the potential of plastics for diverse applications had been estimated but the problems associated with plastics somehow remained unidentified

It has been found that approximately 40% of plastic being utilized in packaging sector including food and other packaging **(Coles et al., 2011)**. Conventional plastics are not easily decomposed and have a short service life, especially for packaging applications **(Hopewell et al., 2009)**. The useful life of a packaging material may be considered only up to a few minutes after purchasing the items; most of which usually generate to municipal solid-wastes. These annual waste generated by conventional plastics is about 67 million tons; of which the packaging waste accounts to approximately 18% of 10.4 million tons and this waste produced annually from

Europe and UK respectively **(Song et al., 2009)**. The concerns about the depletion of fossil based resources and sustainability issues have shifted the attention of the world towards replacing the conventional plastics with bio-plastics derived from renewable resources for their possible utilization in various sectors including packaging **(Emadian et al., 2017)**. As a result, significant progress has been made in developing bioplastics with properties comparable to that of conventional plastics **(Song et al., 2009)**. According to various agencies, less than 4% of total produced biomass has been utilized by the people, of which only a fraction of biomass is utilized for plastic production and chemical applications suggesting that the massive approaches have managed for further enhancement in the capacity **(Shen et al., 2009)**. The worldwide production capacities of these materials have been depicted by the dynamic rate of growth. The bio based and biodegradable materials lead to the reduction in human dependence on fossil oil resources by substituting them step by step. The other advantages include reduced carbon foot print, easy breakdown of their chains under environmental conditions, relatively less energy required for manufacturing along with lower environmental impact during their complete life cycle **(Chen et al., 2014)**. An urgent necessity of environmental friendly bio-plastic has been notified as an alternative to convention plastics in order to lower the environmental impact. The limitations of bio-plastic include their expensive nature and inferior properties compared to the existing commodity plastics. However it is possible to overcome these limitations by (i) fabricating novel biopolymers by developing new routes of polymerization and processing so as to minimize the consumption of energy, (ii) blending with other biopolymer and (iii) addition of bio-filler to tailor the properties of the end product for targeted applications. Introduction of other polymers or bio-filler is found to be a cost effective method to explore their potential and meet the expectations of the global market **(Imre et al., 2013)**.

1.1 BIOPLASTIC

1.1.1 *Definition and Classification*

The accepted definition of bioplastic is, "either bio-based polymer produced from the renewable resources or derived from the monomer which is extracted from the biomass." The bioplastic is either biobased or biodegradable or both **(Imre et al., 2013)**. Most importantly, it can be transformed into the article of desired shape along with obtaining better physiochemical properties using industrially viable processing techniques **(Pilla et al., 2011)**. The replacement of conventional plastics with the renewable ones is one of the prime attempts of the modern plastic markets. Figure 1.1 displays a broad classification of bioplastics **(Song et al., 2011; Yutaka et al., 2009)**.

- ***Biobased plastics originating from renewal resources***

This group of bioplastics consists of bio-based polyethylene (PE), bio-based propylene (PP), bio-based poly (ethylene terephthalate) (PET) which have been synthesized from the non-degradable biomass based monomers. These are non-biodegradable, but serve the same purpose as that of their fossil-based conventional counterparts. The use of bio-derived conventional counterparts might be adopted widely if they become more cost competitive in near future.

- ***Biobased and biodegradable plastic***

Several bioplastics are both "bio-based and biodegradable" which are classified according to their sources as follows:

(i) *Directly obtained from biomass*: These biopolymers are obtained directly from biological sources originated monomer with some chemical modifications of polysaccharides. The examples are thermoplastic starch and starch-based complex.

(ii) *Synthesized from biomass*: These biopolymers can be synthesized directly from the biomass monomers via biological and chemical transformations with a tendency to be processed at the industrial level. Poly (lactic acid) (PLA) and poly (glycolic acid) (PGA) can also be considered under this class. Among various bioplastics, PLA is the widely explored and adapted bioplastic in the modern market.

(iii) *Produced from micro-organism*: Such biopolymers are mainly synthesized in the presence of specific microbes using bioengineering techniques. The examples of these biopolymers include poly (hydroxyl alkanoates) (PHA) and their derivates such as poly (hydroxyl valerate) (PHV), poly (hydroxyl hexanoate) (PHH), poly (hydroxyl butyrate) (PHB), poly (glutamic acid) and bacterial cellulose.

- ***Biodegradable plastic originating from petroleum based feedstock***

Poly (butylene succinate) (PBS), polyvinyl alcohol (PVOH), poly (butylene succinate adipate) (PBSA) and poly (caprolactone) (PCL) are a class of biopolymers which are derived from petroleum based feedstock and exposed to enzymatic attacks due to the presence of many weak sites and in turn leading to the biodegradation of polymeric chains.

1.1.2 *Bioplastic Market*

According to Nova institute, bioplastics contribute nearly to 7.85 million tons production in the global market by 2019. The production capacity of the major bioplastic will be bio-based poly (ethylene terephthalate) (76.5%), biodegradable polyesters (6.6%), poly (lactic acid) (5.5%), bio-based polyethylene (2.5%), biodegradable starch blend (2.4%) and poly hydroxyl alkanoates (1.3% of the total production) and so on. Global bioplastic production capacities, as the report of 2019, are displayed in Figure 1.2 **(Imre et al., 2015)**.

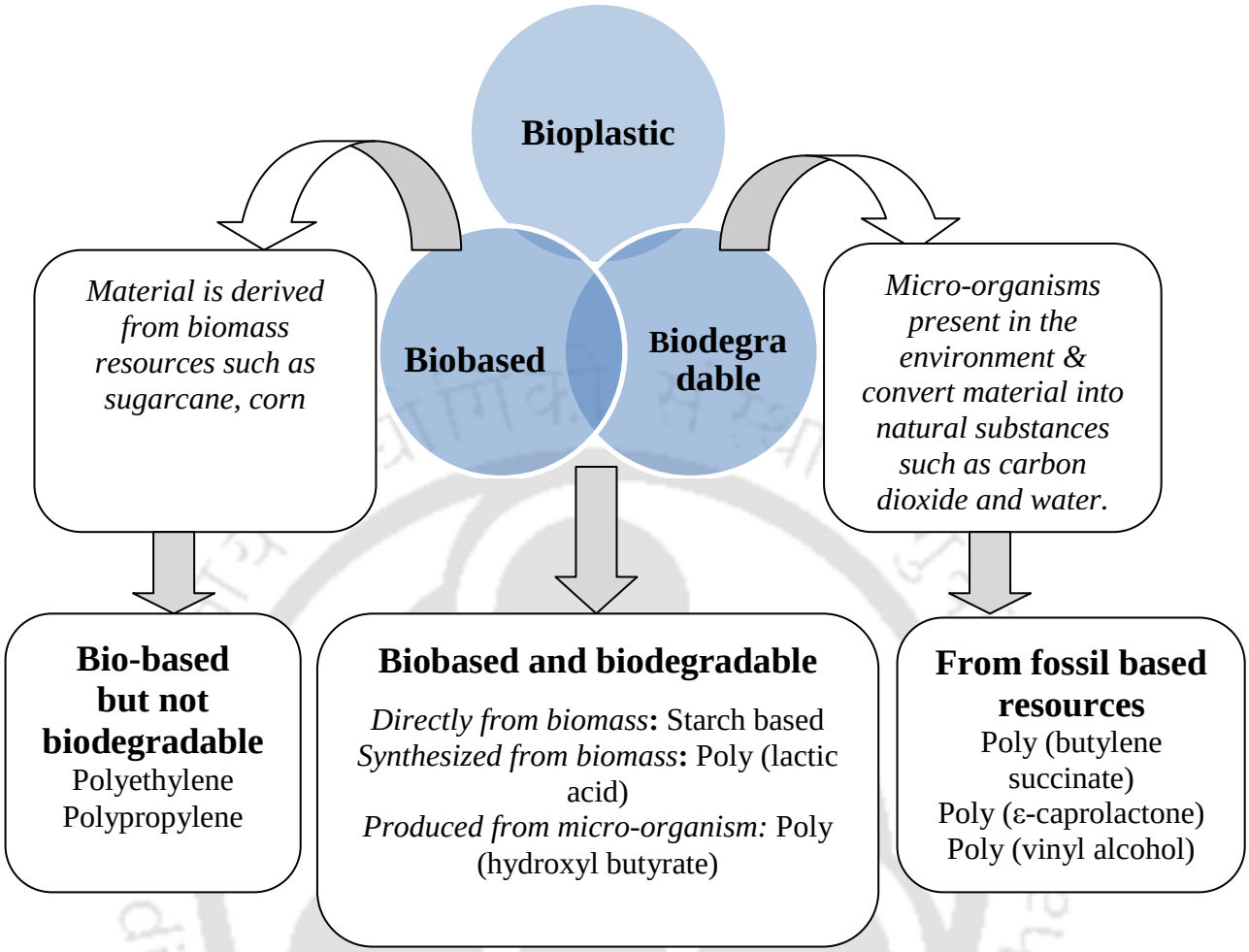

Figure 1.1: *Classification of bio-plastics.*

Recently, bioplastics have received much attention in replacing the conventional plastics in order to make the sustainable alternatives. Nowadays, government and scientists are preceding an eye on the mass production of sustainable bioplastics which mimic like conventional plastics.

1.1.3 *Applications*

Bioplastics are found to have enormous potential in various applications and they can further be broadly classified into two parts, as mentioned:

- ***Present end use of bioplastics***

Bioplastic have been utilized to make biodegradable and short-lived products such as extensive

packaging (shopping bags, tray and films for food items and compostable bag for waste material collection), disposable catering products **(Kumar et al., 2017)**, mulch films **(Tachibana et al., 2009)**, textile **(Aguiree et al., 2016)**, medical sectors including bone fixation, sutures **(Hamad et al., 2015)**, drug delivery and tissue engineering **(Brigham et al., 2012)**. Also, these are potentially used in pharmaceutical sectors to make pills and capsules along with durable products such as automotive interiors and mobile cases.

- ***Possible emerging end use of bioplastics***

The major emerging applications of bioplastic include 3D printing **(Chilson et al., 2015)**, metalized biaxially oriented PLA based food packaging films **(Aguiree et al., 2016; Auras et al., 2004)** and modified durable automotive products.

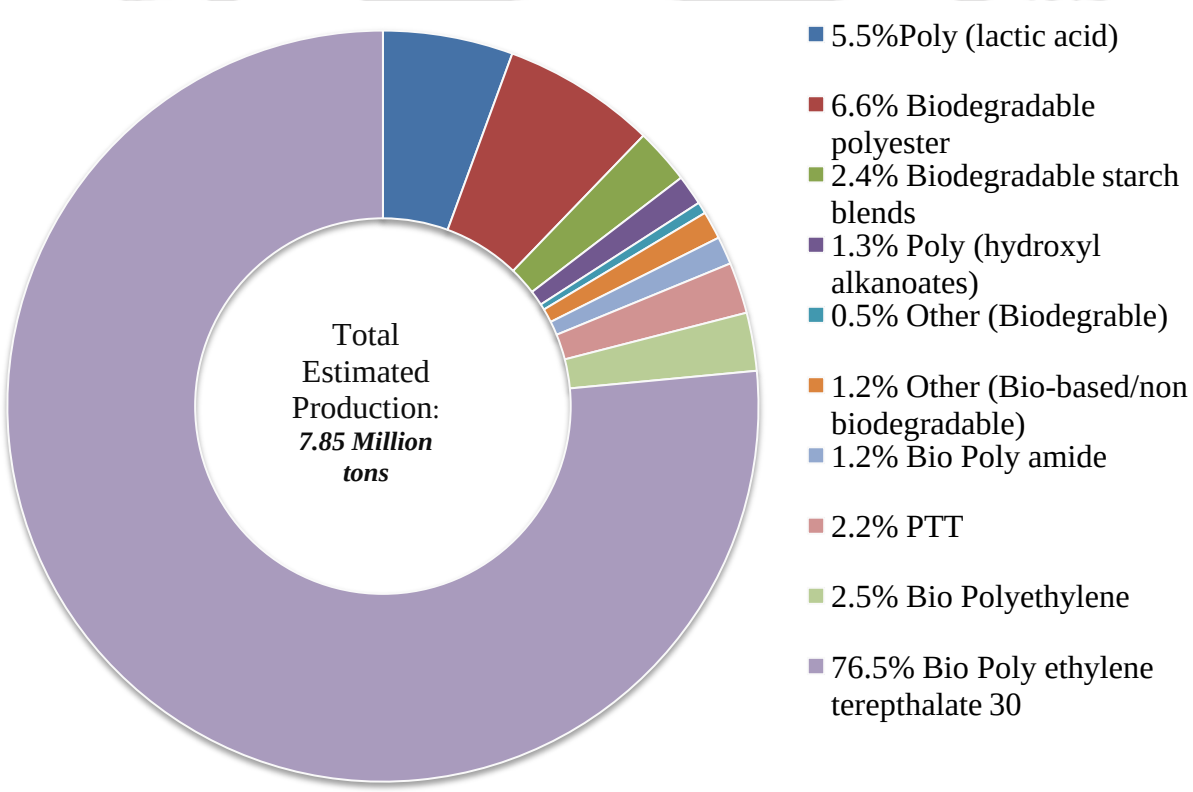

Figure 1.2: *Global bioplastic production capacities in 2019.*

1.1.4 *Current Challenges for Growing Market*

Major concerns of bioplastics are the performance limitations and the production cost of biomass based feed-stock. Generally, these factors are also responsible for restricting the growth rate of bioplastics in the global market. However, bio-based feed-stock is the prime issue and its increased production may influence the global food supply. For instance, enhancement in cost of corn as a result of bioethanol extraction affects the market significantly. As we know, one of the major impediments to the widespread acceptance of bioplastics is the difficulty to achieve competitive thermo-mechanical, and barrier characteristics while maintaining biodegradability in comparison to conventional plastics. On an industrial scale, the production cost of bioplastic is higher than that of conventional plastic. In fact, the manufacturing price of lactic acid is aimed to reduce to 0.8 US dollar per kg owing to the fact that the selling cost of PLA must be reduced approximately by half of its current cost, i.e. 2.2 US dollar per kg. Therefore, it is necessary to take vital steps to overcome these challenges and also help to grow the bioplastic market each year. Among various types of bioplastics, PLA is one of the most promising candidate and extensively used material with the brightest growth rate. It is also considered "green" eco friendly material. As we know, Nature Work LLC is the leading manufacturer of lactic acid and PLA at commercial scale **(Aguiree et al., 2016**). This work focuses on the development of PLA based biocomposites due to the promising future of PLA and its potential for replacing the conventional plastics.

1.1.5 *Poly (lactic acid) (PLA)*

Biodegradable PLA is one of the viable substitutes to the petrochemical based plastics. It is derived from lactic acid which is produced from renewable resources mainly the carbohydrate

riches, such as tapioca roots, sugarcane or corn starch **(Drumright et al., 2000; Auras et al., 2004)**. Life cycle of PLA has been discussed in scheme 1.1 **(Kijchavengul et al., 2008; Lim et al., 2008)**.

PLA can be produced by many routes such as polycondensation reaction, ring opening polymerization and solid state polymerization using the different kinds of metallic and biocatalysts **(Masutani et al., 2014; Yang et al., 2015)**. Direct polycondensation reaction requires removal of water continuously in the presence of vacuum to produce high molecular weight PLA. Although it requires high temperature and long reaction time and the molecular weight of PLA also depends on water removal efficiency. Nowadays, ring-opening polymerization is a preferred route in which high molecular weight PLA can be synthesized from lactide (cyclic dimer) has relatively more control of polymerization **(Rudnik et al., 2010)**. Due to the presence of chiral carbon atoms at two different positions in one monomer of lactide **(Auras et al., 2004)**, various form of stereoisomer's can be produced such as poly (L-lactic acid) (PLLA), poly (D-lactic acid) (PDLA) or racemic mixture of L and D **(Lopes et al., 2012)**. PLA has a dominant position because of its versatile applications in packaging (for fresh food, for baked items, thermoformed trays and cups, cast film, wrapping, foam, biaxial oriented film and short shelf life products that do not demand sophisticated barriers, laminated to paper boards), medical (sutures, orthopedics and scaffolds), pharmaceutical, edible coating, textile and chemical sectors **(Auras et al., 2010)**. It has relatively similar mechanical properties to conventional plastics such as poly (ethylene terephthalate) (PET) **(Vink et al., 2015)**. PLA can be easily processed using various techniques such as extrusion, thermoforming, injection, blow molding, spinning to get versatile products in the form of sheet, film, foam, molded articles or fibers to meet the customer demands **(Savioli et al., 2012)**. Also, PLA suffer from various drawbacks

such as its poor melt strength, low thermal stability, low elasticity, slow crystallization rate, poor barrier properties which has limited its commercial applications **(Nerkar et al., 2015)**. In this particular investigation, more emphasis has been laid on the stabilization and improvement of the melt strength to expand the processing window of PLA and its applicability. The present challenge for the scientists is to overcome the limitation of PLA through various approaches.

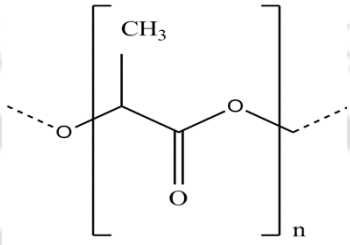

Figure 1.3: *Structure of PLA.*

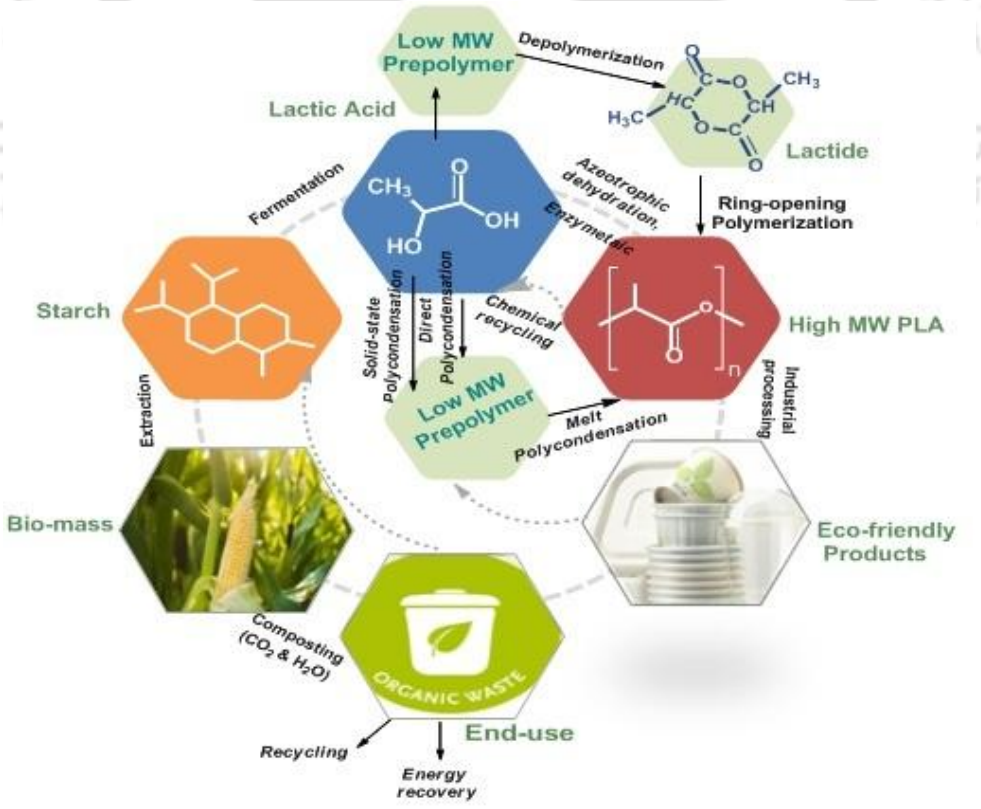

Scheme 1.1: *Life cycle of Poly (lactic acid).*

1.2 MODIFICATION METHODS

Several approaches such as blending with other biopolymers, loading of bio-fillers or plasticizers, modification of bio-fillers, fabrication of biocomposites with reactive and non-reactive compatibilization etc., have been developed in order to adjust the physiochemical properties of PLA for the modification of functionalities and cost reduction.

1.2.1 *Physical Blending of PLA*

Physical blending is one of the matured field which has been utilized for the melt mixing of polymeric materials without chemical reaction. The technique is useful to obtain versatile properties in relatively less time and low cost as compared to the generation of novel monomers and polymerization techniques. The primary role of blending of brittle biopolymers such as PLA with flexible biopolymers including poly (butylene succinate) (PBS), poly (butylenes succinate-co-adipate) (PBSA) and polycaprolactone (PCL) is to maintain the biodegradability, which improve the toughness **(Shibata et al., 2006; Jiang et al., 2006)**. In this research work, PLA/PBS blend is one of the best choices because the combination of two polymers gives the desired properties of each polymer. Physical properties of PLA and PBS are mentioned in Table 1.1 respectively. PBS will be discussed briefly in this section.

Poly (butylene succinate) (PBS): PBS is a bio-based aliphatic polyester, which permits the synthesis using melt polycondensation techniques, showing its appealing thermo-mechanical characteristics as well as tuned biodegradability including acceptable raw resources and production price. The synthesis of PBS usually is done by the reaction of 1, 4-butanediol with succinic acid under melt-polycondensation where the monomers can be derived from fossil feed-stock or renewable resources **(Cherykhunthod et al., 2015; Bahari et al. 1998)**. PBS shows high flexibility, impact strength and chemical resistance which is similar to polypropylene (PP).

Thus, PBS has attracted significant attention as a promising eco-friendly bio-plastic material. Nevertheless, applications of PBS are limited in the packaging applications due to its poor gas barrier (OTR), water vapors transmission rate (WVTR) and melt viscosity (η) properties. It is mainly used in biodegradable packaging at a commercial scale; the application of PBS has also gained attention in biomedical domain. The structure of PBS is displayed in Figure 1.4.

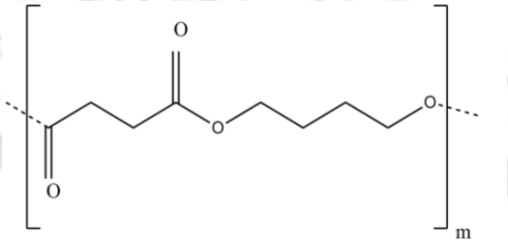

Figure 1.4: *Structure of PBS.*

Table 1.1: Material properties of PLA and PBS

Material properties	**Nature Work PLA 4032D**	**Bionelle PBS 1001 MD**
Physical properties		
Melt Flow Rate (g/10 min)	7	1-3
Density (g/cm^3)	1.24	1.26
Mechanical Properties		
Tensile Strength at yield (MPa)	60	31
Elongation at break (%)	6-10	660
Thermal properties		
Heat deflection temperature (°C)	40-45	97
Melting temperature (°C)	155-170	114
Glass transition temperature (°C)	55-56	-32

1.2.2 *Bionanocomposite*

Generally, the biocomposite refers to a composite fabricated by simple loading of bio-filler in the one or more biopolymers. The fabrication of PLA based biocomposite in the presence of various

bio-fillers such as cellulose **(Kamal et al., 2015)**, chitosan **(Li et al., 2004; Bonilla et al., 2013)**, chitin **(Nasrin et al., 2017)**, gum arabic **(Onyari et al., 2008)**, silk **(Patwa et al., 2018)**, etc. using a simple melt extrusion is an economical as well as ecologically viable technique. Common methods to fabricate the biocomposite with better performance include the surface treatment or modification of bio-filler, lamination of multilayer film and loading of bio-filler for enhancing the properties of PLA and their blend. In this framework, a nano size bio-filler has been chosen because of the small concentration of bio-filler in PLA giving rise to the prominent improvement in physiochemical properties of the polymeric matrix. As concerned, an inhomogeneous distribution of bio-filler into the PLA matrix may result in non-compatibility of bio-filler with matrix phase, which shows an adverse impact on properties. One of the possible solutions is the functionalization of polymeric chains on the filler surface to enhance the distribution of bio-filler in the matrix. Keeping this in mind, three different bio-fillers such as cellulose nanocrystals, chitosan and gum arabic have been used in this research work for the exploration of PLA properties.

Cellulose

Cellulose is a linear biopolymer, known as a complex carbohydrate or polysaccharide which is most abundantly available in nature. It can be extracted from plant based resources and which compromises of paired β-1,4 glycosidic-linked to d-glucose units **(Gurunathan et al., 2015; Ummartyotin et al., 2015)**. Due to the presence of highly active sites, its backbone can be grafted with polymers through different routes based on the targeted applications. The structure of cellulose has been adopted from **Gurunathan et al., 2015** and displayed in Figure 1.5 (a). Cellulose consists of both crystalline and amorphous domains in varying ratios and depending on the source used. Cellulose nanocrystals (CNCs) are directly extracted from the crystalline

segments under the controlled acid hydrolysis by selectively removing the amorphous domains **(Sullivan et al., 2015; Dhar et al., 2016)**. The aspect ratio and morphology of such crystalline domains can be tuned by simply varying some parameters such as the types of pretreatment, processing parameters, sort of biomass, cellulose polymorph and hydrolysis process, which ultimately contributes towards the mechanical properties. CNCs usually have rod-like morphology with high hydroxyl functionality and tunable aspect ratio which makes it a suitable choice as a reinforcing agent when dispersed in bioplastic such as PLA (**Dhar et al., 2016; Montanari et al., 2008)**. As we know, when CNC is melt-mixed with PLA, it decreases the surface adhesion between the filler and PLA matrix due to hydrophilic tendency of CNC. Due to this, agglomerations of filler take place as well as dispersion of the CNC become difficult especially at higher loading.

- ***Chitosan (CH)***

Chitosan originated from marine resources, is a typical amino based natural polysaccharide prod uced by deacetylation of chitin **(Rinaudo et al., 2006)**, which has been utilized due to its sustainability, antimicrobial nature, biodegradability, bio-compatibility, and non-toxicity **(Wang et al., 2013)**. The structure of chitosan has been adopted from **Pal et al., 2018** and shown in Figure 1.5 (b). Chitosan is the second most abundantly available biopolymer which has gained attention in versatile applications such as wastewater treatment **(No et al., 2000)**, biomedicine **(Jayakumar et al., 2010)**, coating **(Elsabee et al., 2013)**, sensors **(Adlim et al., 2015)**, agricultural **(Zargar et al., 2015)**, food **(No et al., 2007)** and packaging sectors **(Cheung et al., 2015)**. Chitosan have been extensively studied by the researchers due to their good thermo-mechanical properties. Commercially, it is available in many forms such as powder, fiber mesh, film, beads, hydrogels and porous framework etc, based on applications. Recently, the

applications of chitosan have been limited due to its solubility and hydrophilic nature in the packaging sector **(Pal et al., 2016)**. To solve this issue, chitosan has been chemically modified by substituting with hydrophobic oligomer or biopolymer using in situ polymerization **(Pal et al., 2016)** to obtain derivates having increased solubility in aqueous medium and enhanced activity.

- ***Gum Arabic (GA)***

Gum arabic is an edible polysaccharide, branched in nature and exudated from different species of the Acacia tree, main sources are "Acacia Senegal" and "Acacia seyal" at a commercial level. The structure of gum arabic has been adopted from the **Nie et al., 2013** and displayed in Figure 1.5 (c). It has complex chemical compositions of polysaccharides whose backbone consists of 1,3 linked β-D-galactopyranosyl units and its side chains are composed of two to five 1,3 linked β-D-galactopyranosyl units, joined to main chain by 1, 6 linkage **(Nie at al., 2013; Ali et al. 2009)**. Both the main and side chains contain α-L arabinofuranosyl, α-L-rhamnopyranosyl, β-D-glucuronopyranosyl, 4-O-methyl glucuronopyranosyl units. As reported, it is mainly consists of galactose (39-42%) and arabonose (24-27%), rhamnose (12-16%), glucuronic acid (15-16%), protein (1.5-2.6%) **(Triphati et al., 2016)**. It is notified that the chemical compositions of GA are varied based on the source of origin and other factors such age of trees, climates and soil territory. Current literature suggests that it can be widely used as an adhesive, emulsifier, binder, stabilizing agent and enhancing the shelf life in many food applications. It shows versatile applications into a pharmaceutical sector, printing, water color prints, lithography, cosmetics, food and textile industry with appreciable growth into the packaging sector (**Patel et al., 2015; Triphati et al., 2016)**.

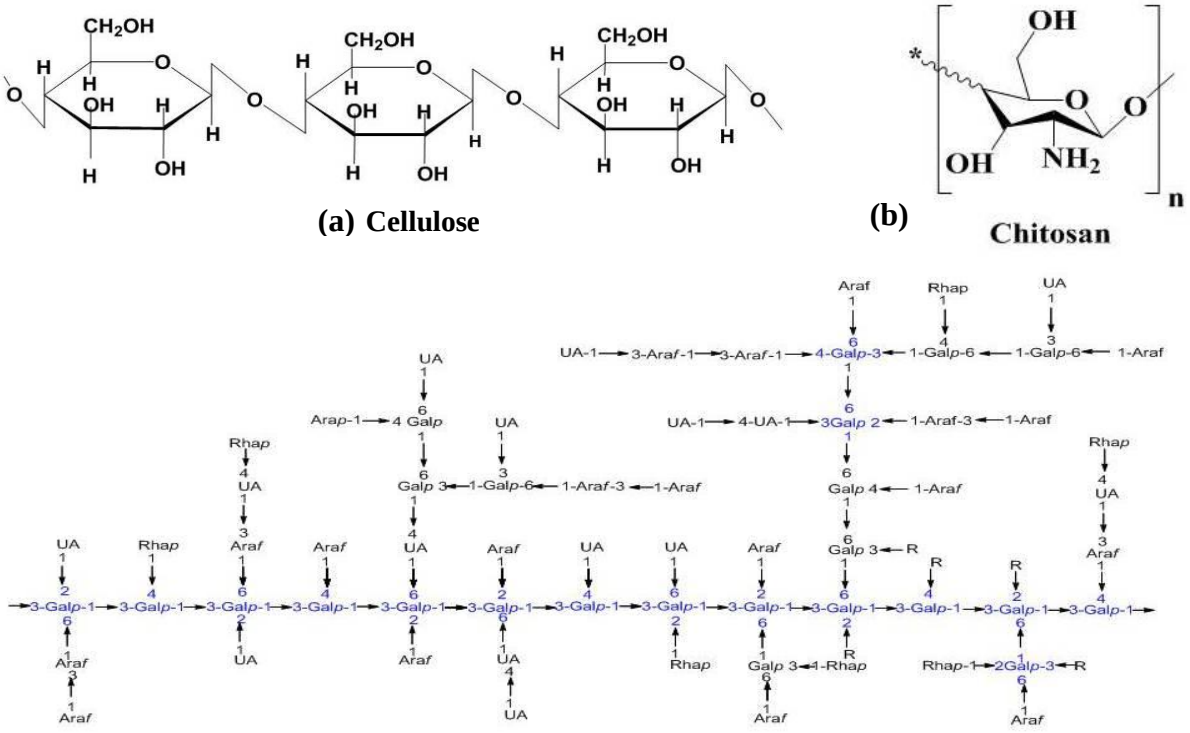

Figure 1.5: Chemical structure of (a) cellulose, (b) chitosan and (c) gum arabic (UA: uronic acid,Ara*f*: arabinofuranosyl, Ara*p*: arabinopyranosyl, Rha*p*: rhamnopyransyl, Gal*p*: galactopyransyl).

1.3 MELT PROCESSING

From the decades, melt processing has been the simple conversion method used for PLA which is similar to that of the petroleum derived thermoplastics. Moreover, this approach avoids the use of organic solvents which impede the substantial changes in the LCA of PLA. It can be processed by existing plastic processing techniques such as extrusion, injection and compression molding and holds promise for versatile application at industrial scale **(Agurrie et al., 2016)**. Many studies have been conducted for the fabrication of PLA/biofiller using the twin screw extrusion process, which can enhance the performance of PLA. Factors affecting the melt processing are granular shape, thermal stability, heat input, flow behavior, cooling rate, crystallization and shrinkage, molecular orientation, processing time and temperature. It is one of

the most established techniques and has own placed in the wide spectrum of manufacturing materials where high production rate of products have to target. As mentioned, the industrial adaptability has allowed a melt-extrusion process to earn broad affirmation and research development in many areas. However, completely dried PLA should be subjected to hopper during extrusion process in order to inhibit the decomposition due to the presence of moisture, which is a possible reason for the deterioration of material properties. Applications of PLA have been limited because of its poor melt strength which makes its responsible to withstand a high shear force and the elevated temperature **(Auras et al., 2010)**. Degradation of polymer is an irreversible process leading to a major change in the structure of a material in which polymer breaks down into smaller pieces due to the external chemical or physical stress **(Pandey et al., 2005)**. The changes include bond dissociations, chemical transformations and the formation of new functional groups. This may cause the deterioration of characteristics such as integrity, molecular mass or structure, mechanical strength and discoloration etc. The material experiences degradation during their production, processing, reprocessing and after its end use. Degradation phenomenon of PLA is a major concern during melt processing which can be facilitated by a trace amount of water, active end sites, surface functional fillers, residual catalyst and residual monomers. Thermal degradation is a major focus of the current research work, impact of molten state need to be addressed properly before adding any fillers or additives during processing.

1.4 REACTIVE COMPATIBILIZATION

Reactive compatibilization in the presence of chain extenders has been postulated as one of the possible solutions to improve the limitation of PLA and their bio-based blend **(Tesfaye et al., 2017; Juntuek et al., 2011)**. Chain extender often contains various types of functionalities and reactive species offering radicals for the generation of free radical on the backbone of the main

chain allowing modification either compatibilization **(Jaratrokamjorn et al., 2011)** or developing more cross-linked/branched sites **(Takamura et al., 2008; Tesfayee et al., 2017)**. The active sites (i.e., peroxide, hydroxyl, carboxylic and isocyanate group) of chain extenders like peroxide can react with the hydroxyl and carboxyl group and easily abstract the H atom from the main chain for radical formation at the back bond **(Nerkar et al., 2015)**. However, if modification involves the free radical sites generation on one component can further react to the second component during melt-mixing, the phases can be linked chemically to modify structure and tailored the properties **(Ji et al., 2014)**. Properties of bionanocomposite have controlled by nature of the chain extender, other polymer or filler composition in the polymeric matrix and processing parameters. Dicumyl peroxide (DCP) has been selected as a free radical initiator at high temperature and possess structural modification to improve compatibility or melt strength of the present system **(Corre et al., 2011)**.

1.5 THERMAL DEGRADATION

Thermal degradation is the molecular deterioration as a result of excessive heating of material. At an elevated temperature, the bioplastic undergoes physio-chemical changes where segments of polymeric chain start to separate and finally react with the one another to change the properties such as physical and mechanical properties **(Carrasco et al., 2013)**. Thermal degradation of bioplastic is affected by the various factors such as macromolecular structure of polymer, environmental condition (heat, UV-light, humidity, temperature, inert medium, presence of oxygen, gas flow rate and so on) and additives (filler, antioxidant, crosslinking agent and stabilizer etc). During the thermal decomposition, molecular chain scission occurs through different routes such as end chain scission, random chain scission and side group eliminations **(Singh et al., 2008; Kopinke et al., 1996)**. Unzipping, as the name indicates, involve sequential

removal of monomeric unit from the backbone ends, resulting in a monomeric unit or some small substituents (Scheme 1.2 a). During random chain scission, bonds in main chain are cleaved at particularly random locations; as a result the molecular weight deteriorates (Scheme 1.2 b). As new free radicals with high reactivity have generated during the depropagation step whereas numerous kind of termination reactions are common such as intermolecular chain transfer, recombination and disproportion termination. The high yield of monomer has received from unzipping mechanism than that of random chain scission **(Su et al., 2008)**. During the random chain scission, main products are oligomers; depending on the structure of a polymer. During the side group elimination reaction, weak substituent groups are stripped off from the side chain before it is broken into smaller fragments because these bonds are weaker than that of main chains (Scheme 1.2 c).

1.5.1 *Thermal degradation in PLA*

In general, PLA is highly susceptible to thermal decomposition during extrusion process which is influenced by processing parameters (at the upper limit of temperature and shear force, long residence time and screw speed, high relative humidity) which leads to depletion in typical properties including reduction in molecular weight, thermal, mechanical and rheological properties of processed components **(Jamshidian et al., 2010; Auras et al. 2010)**. Several other factors such as reactive end groups, unreacted monomer, residual catalyst and impurities have known to enhance the thermal decomposition. Many complex decomposition reactions have been postulated for PLA including inter and intra-molecular transesterification, pyrolytic elimination, moisture or water trace amount of water and oxidative degradation, as displayed in Scheme 1.4 (a)-(d) respectively **(Lim et al., 2000; Kopinke et al., 1996; Oliveira et al., 2016; Nishida et al., 2010; Zho et al., 2016)**.

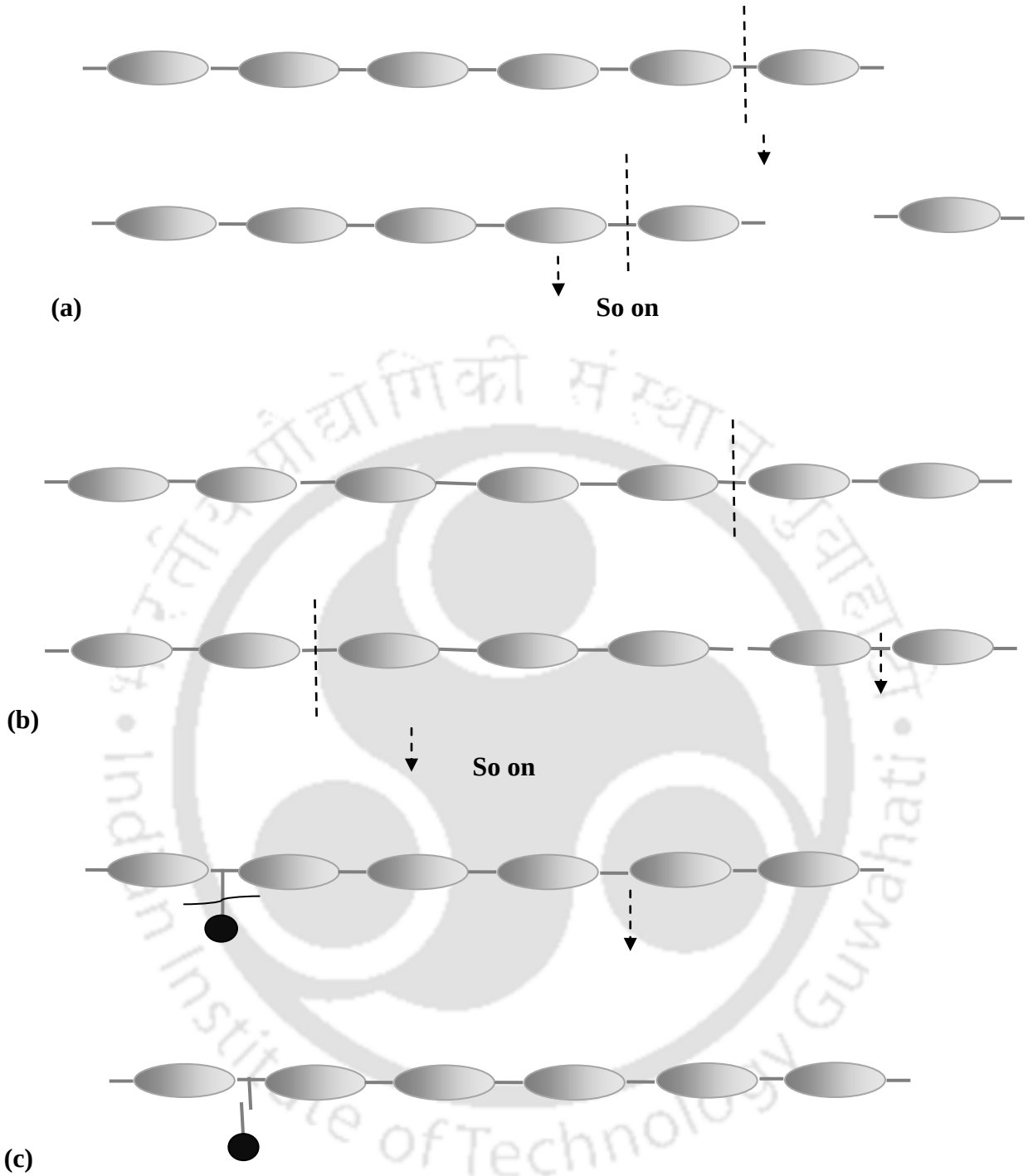

Scheme 1.2: *Routes of thermal degradation (a) sketch of end chain scission, (b) sketch of random chain scission and (c) sketch of side group elimination.*

Wachsen et al., 1997 claimed that the thermal degradation of PLA in the melt has mainly taken

place via the intramolecular transesterification reactions leading to the generation of cyclic oligomers and lactide. Also, recombination of cyclic oligomers with linear polyesters has occurred. Intermolecular transesterification occurs between two ester molecules which exchange their radicals, resulting in the formation of monomer and oligomers esters **(Carrasco et al., 2010)**. Only a few works appraised the intermolecular transesterification as a degradation mechanism under the melt condition which can lessen **(Signori et al., 2009; Jamshidi et al., 1988)** by the incorporation of benzoyl peroxide and other stabilizers **(Sodergard et al., 1994)**. During chain scission (by pyrolytic elimination), the release of acrylic product and acids has observed. PLA is hygroscopic in nature and precisely dried to value below 100 ppm water content to prevent the hydrolysis, as shown in a scheme 1.4 (a) **(Lim et al., 2008; Agurrie et al., 2016)**. At an industrial scale, it has mostly dried less than 250 ppm water. When PLA is exposed to moisture, ester groups of the backbone have been cleaved, resulting in a decrease of molecular weight and soluble products (monomer and oligomers unit) self catalyzed the hydrolysis process. **(Paula et al., 2005; Elsawy et al., 2017; Lyu et al., 2007)**.

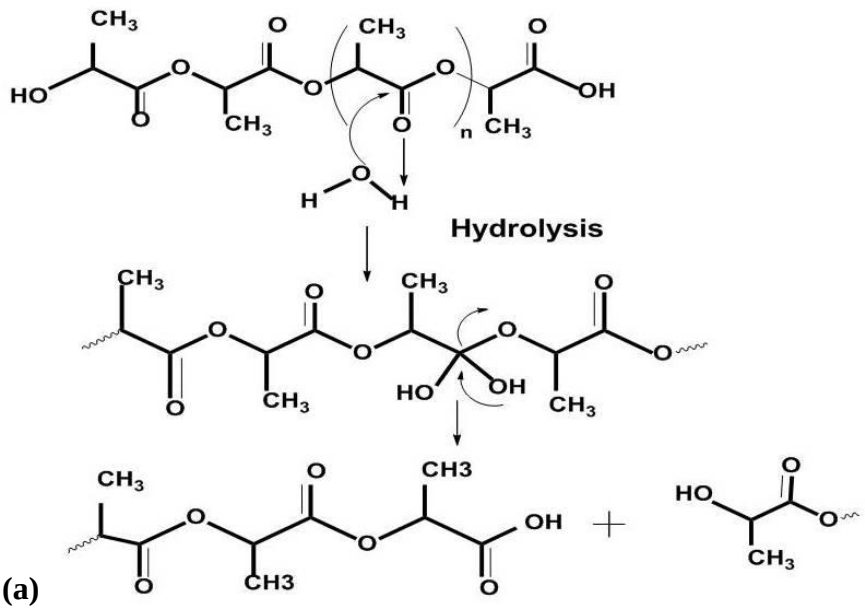

(a)

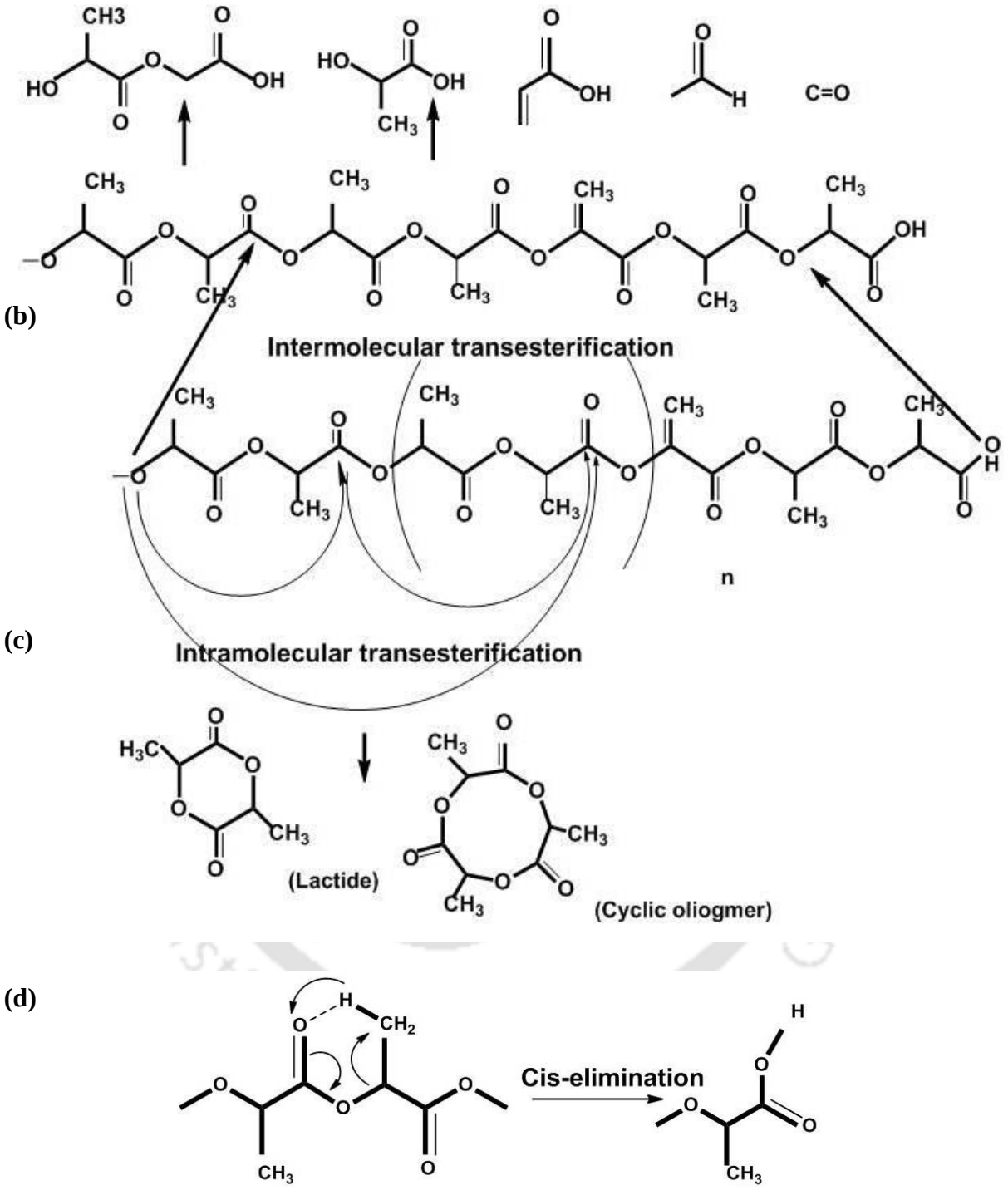

Scheme 1.3: Degradation mechanism of PLA (a) hydrolysis or in presence of trace water, (b) intermolecular transesterification, (c) intramolecular transesterification and (d) cis-elimination.

1.6 KINETIC ANALYSIS

Thermal degradation of polymers is a very complex reaction, the choice of a reliable model or a combination of kinetic models is very important **(Patwa et al., 2018)**. Thermogravimetric analysis (TGA) is one of the most beneficial thermal techniques in which change in mass loss monitored with temperature or time at a specified gas environment and heating rate. Thermal degradation is classified into two categories: Thermal decomposition (thermal degradation in the absence of oxygen) and thermal oxidation (thermal degradation in the presence of heat and oxygen). The main purpose of thermal decomposition is the high temperature effect on the polymer materials without atmospheric condition particularly oxygen and moisture. Actually, a study on thermal decomposition of polymer under inert gas is an ordinary condition for this purpose. However, understanding the thermal behavior of PLA is necessary to optimize its processing and process part qualities. In this regard, thermal degradation kinetic information of polymeric material is crucial for evaluating the times and temperatures associated with the processing, service lifetimes and storage of material.

To investigate the TG kinetics of polymeric system, thermal decomposition process is considered as an irreversible type of reaction. Numerous methods have been selected for investigating the degradation kinetics parameters and mechanism with the help of TGA **(Das et al., 2017)**. These methods have been categorized according to experimental set-up and the computational method carried-out. Experimentally, either isothermal (analysis of weight loss as a function of time at constant temperature) or non-isothermal conditions (analysis of weight loss as a function of temperature) are utilized. Non-isothermal experiments have offered the benefits over isothermal methods to eliminate the error caused by the thermal induction period **(Leroy et al., 2010)**. Computational or analytical mathematical methods are applied to the same set of data to obtain

the kinetic parameters. In general, this kinds of kinetic analysis is divided into linear and non-linear methods. These methods are based on the relationship between heating rate (β); extent of conversion (α) and temperature (T) for calculating apparent activation energies (E_a), pre-exponential factors (A) and reaction order (n) etc. Numerous methods have been developed for analyzing the non-isothermal TGA data; it can be further grouped into two types, model free and model fitting method **(Lorey et al., 2010)**, both displayed in Table 1.2 and also discussed in details elsewhere. The reliability of these parameters depends very much on the actual processes occurring during the thermal degradation of a polymer, and the different assumptions made while applying these methods. General applied methodology for the determination of kinetic parameters and mechanism is shown in a Scheme 1.4.

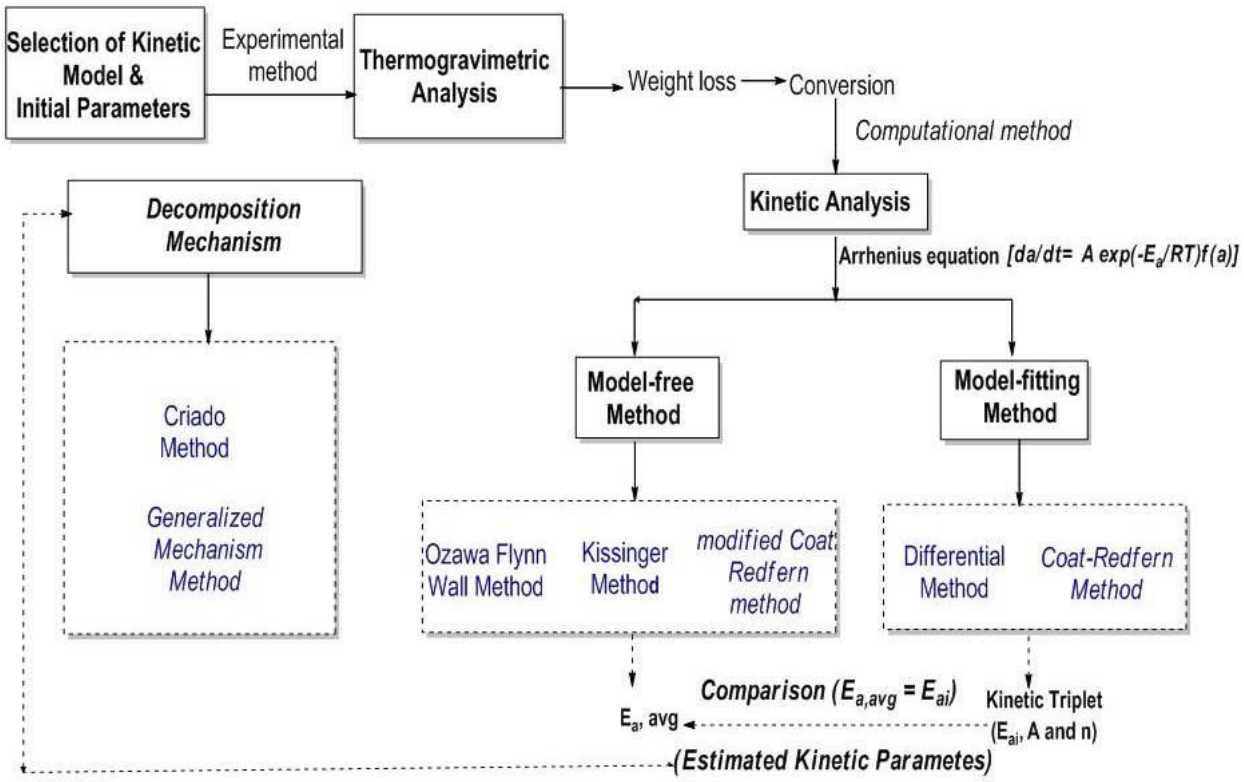

Scheme 1.4: General applied methodology for the determination of kinetic parameters and solid state degradation mechanism.

1.6.1 *Model-fitting methods*

These methods consist of fitting various models to the data (α vs T plots) so that a best statistical fit model may be selected to assist the direct computation of the kinetic triplet (E, A and degradation model) from a single non-isothermal TGA measurement. As it suffers from several issues such as inability to uniquely estimate the reaction model as well as provide high values for kinetic parameters, popularity of these approaches is led to decline in favor of the isoconversional methods (model-free approach) that compute kinetic parameters without modelistic assumptions **(Khawam et al., 2005)**.

1.6.2 *Model-free methods*

This approach is selected to compute the E_a without any prior knowledge of reaction model, as they require multiple TGA curves at various heating rates and unable to direct estimation of A. Although, there are indirect means to estimate A which are not considered the theoretical point of view. In order to evaluate these parameters, models with various assumptions are suggested to simplify the complexity of the decomposition process. Generally, model free kinetic study is selected where the validity of determination of transformation rate is limited or some unreliability over a baseline of TG data exits, as compared to other models. Basically, all model-free methods are isoconversional excluding the Kissinger method (E_a computed at maximum degradation temperature). Isoconversional methods can provide the most reliable approach for the estimation of E_a at progressive values of α **(Valapa et. al., 2014; Chrissafis et. al., 2010)**. Primary assumption is that f(α) is identical at a fixed value of α for a given equation under various conditions. The limitations of these methods are a series of TG run at various heating rate which include the approximately same mass of sample, constant flow rate of inert medium and their fluctuation can cause of errors. The most accurate method is assumed to be the one that

gives E_a closest to that from the obtained from the isoconversional method. This permits one to choose set of models that might otherwise be indistinguishable according to quality of the regression fit alone.

1.6.3 Solid-state reaction mechanism

For many solid-state reaction, the degradation mechanism has been explained by the nucleation and growth, phase boundary controlled reaction, diffusion, random nucleation and random chain scission process. Real crystals have fluctuating local energies due to the presence of intrinsic (for thermodynamic reasons) and extrinsic imperfections (due to foreign atom, surfaces, edges, dislocations, cracks, boundaries, slip and vacancy). It is possible to control the extrinsic imperfection by purification or other ways. Such imperfections are possible sites for nucleation and single or multistep nucleation (N) when the reaction activation energy is reduced at these points. During diffusion (D) models, stepwise migration of atoms from one lattice site to another lattice site is observed at atomic level. Reaction (F) models are the simplest models and closest to those used in homogenous kinetics. In these models, the reaction rate is related to the fraction remaining of reactant raised with the reaction order and concentration. In surface (R) model, the nucleation happens rapidly on the crystal surface. The degradation rate is governed by the resulting reaction interface which shows growth toward the center of the crystal. Random chain scission mechanism is discussed earlier in this chapter. A mathematical form of these reaction mechanisms is described in Chapter 2. For predicting the reaction mechanism, criado or generalized master plots can be used. Generalized mechanism models have the solution for random chain scission analysis.

Table 1.2: Numerous Kinetic model for estimating TGA kinetic parameter

Linear Methods		
Model-free approaches (for multiple heating rate non-isothermal kinetics)		
Methods	**Equation**	**plots**
Kissinger method **(Kissinger et al., 1957)**	$\ln\left(\frac{\beta}{T_m^2}\right) = -\frac{E}{RT_m} + \ln\left(\frac{AR}{E}\right)$	$\ln\left(\frac{\beta}{T_m^2}\right)$ Vs. $1/T_m$
Isoconversional Methods		
Ozawa Flynn Wall method **(Flynn et al., 1983; Zou et al., 2011)**	$\ln(\beta) = \ln\left(\frac{AE}{R\,g(\alpha)}\right) - 5.331 - 1.052\ \frac{E}{RT}$	$\ln(\beta)$ Vs.1/T
Kissinger-Akhaira-Sunose method **(Dhar et al. 2014)**	$\ln\left(\frac{\beta}{T^2}\right) = \ln\left(\frac{AR}{E\,g(\alpha)}\right) - \frac{E}{RT}$	$\ln\left(\frac{\beta}{T^2}\right)$ Vs. 1/T
Modified Coat-Redfern method **(Fischer et al. 1987; Volli et al. 2014)**	$\ln\left(\frac{\beta}{T^2}\right) = \ln\left[\frac{-AR(1 - 2RT/E_a)}{E_a \ln(\alpha)}\right] - \frac{E_a}{RT}$	$\ln\left(\frac{\beta}{T^2}\right)$ Vs. 1/T
Friedman method **(Friedman et al. 1964)**	$\ln\left(\beta\frac{d\alpha}{dT}\right) = \ln A + \ln f(\alpha) - \frac{E}{RT}$	$\ln\left(\beta\frac{d\alpha}{dT}\right)$ Vs.1/T
Model-fitting approaches(for single heating rate non-isothermal kinetics)		
Coat-Redfern method **(Coats et al. 1964; Mallakpour et. al. 2009)**	$\ln\left[\frac{-\ln(1-\alpha)}{T^2}\right] = \ln\left[\frac{AR}{E}\left(1 - \frac{2RT}{E}\right)\right] - \frac{E}{RT}$ for $n = 1$ $\ln\left[-\ln\left\{\frac{1-(1-\alpha)^n}{(1-n)T^2}\right\}\right] = \ln\left[\frac{AR}{E}\left(1 - \frac{2RT}{E}\right)\right] - \frac{E}{RT}$	$\ln\left[\frac{-\ln(1-\alpha)}{T^2}\right]$ Vs. 1/T (in case of n=1) $\ln\left[-\ln\left\{\frac{1-(1-\alpha)^n}{(1-n)T^2}\right\}\right]$ Vs.1/T (in case of n≠1)

Freeman-Carroll method **(Freeman et. al. 1958; Liu et. al. 1999)**	$\frac{-(E/RT)\Delta(1/T)}{\Delta \ln(1-\alpha)} = \frac{\Delta \ln(d\alpha/dt)}{\Delta \ln(1-\alpha)} - n$	$\frac{\Delta \ln(d\alpha/dt)}{\Delta \ln(1-\alpha)}$ Vs. $\frac{\Delta(1/T)}{\Delta \ln(1-\alpha)}$
Van-Krevelen Method **(Mallakpour et. al. 2009)**	$\ln[-\ln(1-\alpha)] = \ln B + \left(\frac{E}{RT_m} + 1\right)\ln T$ for $n = 1$ $\ln\left[\frac{1-(1-\alpha)^{1-n}}{(1-n)}\right] = \ln B + \left(\frac{E}{RT_m} + 1\right)\ln T$ for $n \neq 1$ Where $B = \frac{A}{\beta}\left(\frac{E}{RT_m} + 1\right)^{-1}\left(\frac{0.368}{T_m}\right)^{\frac{E}{RT}}$	$\ln[-\ln(1-\alpha)]$ Vs. $\ln T$ (when n=1) $\ln\left[\frac{1-(1-\alpha)^{1-n}}{(1-n)}\right]$ Vs. $\ln T$ (in case of n≠1)
Differential Method **(Mallakpour et al. 2009)**	$\ln\left[\left(\frac{d\alpha/dt}{f(\alpha)}\right)\right] = \ln A - \frac{E}{RT}$	$\ln\left(\frac{d\alpha/dt}{f(\alpha)}\right)$ Vs. $1/T$
Horwitz Method **(Horowitz et al. 1963)**	$\ln\left[\ln\left(\left\{\frac{W_o - W_f}{W_t - W_f}\right\}\right)\right] = \frac{E_a\theta}{RT_s^2}$ Where $\theta = T - T_S$ where T_s reference temperature	$\ln\left[\ln\left(\left\{\frac{W_o - W_f}{W_t - W_f}\right\}\right)\right]$ Vs. θ
Broido Method **(Briodo et al. 1969)**	$\ln\left[\ln\left(\frac{1}{1-\alpha}\right)\right] = \frac{E_a}{RT} + \ln\frac{ART_m^2}{\beta E}$	$\ln\left[\ln\left(\frac{1}{1-\alpha}\right)\right]$ Vs $1/T$
Model fitting approaches (for multiple heating rate non-isothermal kinetics)		
Augis and Bennett's method **(Mallakpour et al. 2009)**	$\ln\left(\frac{\beta}{T_m - T_o}\right) = -\frac{E}{RT_m} + \ln A$	$\ln\left(\frac{\beta}{T_m - T_o}\right)$ Vs. $1/T_m$
Non-linear methods		
Advanced isoconversional methods **(Vyazovkin et al. 2001)**	$\emptyset(E) = \sum_{i=1}^{n}\sum_{j\neq i}^{n}\frac{I(E_\alpha, T_{\alpha,i})\beta_j}{I(E_\alpha, T_{\alpha,i})\beta_i}$	E_α vs α

1.7 LITERATURE REVIEW

1.7.1 *Poly (lactic acid) (PLA) based Biocomposite*

- ***PLA/Cellulose nanocrystals (CNC) biocomposite***

The influence of CNC polymorphs, i.e. CNC I, CNC II, CNC II-I on the thermal, mechanical and barrier properties of PLA based nanocomposite was investigated by **Dhar et al., 2015**. Various polymorphs of CNC were prepared from bamboo pulp via alkali treatment proceed by acid hydrolysis and its structural, degree of hydrogen bonding, crystal structure and thermal stability are investigated. The different polymorphs derived CNC were well dispersed in PLA matrix using solution casting. Addition of CNC II-I and CNC II remarkably enhanced the young modulus of PLA nanocomposite about to ~ 72 %. Albeit their elongation at break reduced in comparison to CNC I which was probably due to more presence of hydroxyl functional group, shows an entangle H bonded network within the PLA matrix and responsible to enhancement in barrier as well as mechanical characteristics. Mechanical model such as Halpin-Kardos, Ouali and Cox-Krenchel method represented the good association for CNC I, CNC II, CNC II-I. All polymorph CNC has ability to make percolated networks and stability also depends on the type of polymorph. This study suggested the appropriate selection of high performance based PLA/CNC nanocomposite.

The morphological and thermal characteristics of PLA/CNC bionanocompsite were investigated by **Khoo et al., 2016**. CNC was synthesized via acid hydrolysis of microcrystalline cellulose (MCC). PLA/CNC bionanocomposite was fabricated using solvent casting method. The energy filtered transmission electron microscopy (EFTEM) demonstrated that the CNCs have needle like (width ~ 10-20 nm and length ~ 250-200 nm) morphology. DSC data revealed that CNC (upto 5 wt% loading) acts as a nucleating agent for the PLA matrix. TGA result confirmed that the thermal stability of PLA/CNC bionanocomposite was higher than that of neat PLA.

- ***PLA/Gum arabic (GA) biocomposite***

Onyari et al., 2008 studied the biodegradability of PLA and GA in the presence of a microorganism (Lake Bogoria). In this case, samples were fabricated using solvent casting approach with varying wt% of GA (10 to 100 wt %) content. The properties of PLA/GA blends were investigated using Gel permeation chromatography (GPC), differential scanning calorimeter (DSC), thermal gravimetric analysis (TGA), nuclear magnetic response (NMR), thermal mechanical analysis (TMA), and light microscopy (LI). GPC demonstrates the reduction in molecular weight (MW) for biodegradation of PLA. In brief, microorganisms were responsible to increase the rate of biodegradation of PLA. Moreover, diversity of hydrophilic-hydrophobic properties of PLA/GA was useful to fabricate film for different applications.

Lactic acid grafted gum arabic (LA-g-GA) had prepared by one-pot microwave synthesis and its effect on gas barrier, mechanical, thermal and structural properties were observed by **Tripathi et al., 2016**. The PLA nanocomposites with various content of LA-g-GA are prepared by solvent casting method. Oxygen transmission rate (OTR) result indicated that excellent improvement in oxygen barrier of ~ ten folds in case of PLA/OLLA-g-GA bionanocomposite film. Introduction of 5 wt% OLLA-g-GA into the PLA matrix, the value of WVTR was further reduced up to 27%.

- ***PLA/Chitosan (CH) biocomposite***

This nanoamphilic lactic acid oligomer grafted chitosan (OLLA-g-CH) synthesized via in-situ polymerization method and its influence on PLA was investigated by **Pal et al., 2017**. The grafting of OLLA chain conducted on PLA matrix is successfully confirmed by FTIR analysis and it acted as surfactant containing OLLA tails (hydrophobic) with CH head (hydrophobic) with size varying in the range of ~2 to 4 nm. PLA/OLLA-g-CH bionanocomposites were fabricated via solution casting method. From the OTR result, it was observed that the oxygen permeability

reduced up to ~10 folds after addition of OLLA-g-CH into the PLA matrix. This improvement could correlate with high nucleation density of crystal and secondary decreased insolubility of oxygen molecules. Mechanical properties of PLA biocomposite showed remarkable improvement in elongation at break. There was no significant change in onset of thermal degradation (T_{onset}) temperature for PLA bionanocomposite film than that of neat PLA film. DSC results shows that the value of glass transition temperature (T_g) decreased ~18 °C with further increasing the OLLA-g-CH content which suggested the plasticization effect of OLLA-g-CH in PLA matrix. POM result indicated that the spherulites growth of PLA enhanced with the incorporation of OLLA-g-CH.

The bionanocomposite based on PLA and OLLA-g-CH was prepared by the solution casting method and morphological, chemo-mechanical, rheological properties were studied **(Pal et al., 2017)**. The grafting of OLLA chains with CH was confirmed by ^{1}H-NMR analysis. UV spectroscopy showed that transparency reduced increasing the filler loading and had excellent blocking for UV-light. Dynamic mechanical analysis (DMA) data shows the significant decrease in T_g ~ 13°C. The rheological result exhibits that the value of storage modulus (E') is lower than the loss modulus (E'') for PLA and PLA/CH-g-OLLA bionanocomposite. Moreover, Cole-Cole and Han plot suggested the uniform dispersion of CH-g-OLLA in the PLA matrix although it could agglomerate at higher loading of bio filler contents.

1.7.2 *PLA/Poly (butylene succinate) (PBS) based Biocomposites*

PLA/PBS blends with different loading of PBS contents fabricated using melt extrusion at 180°C and its morphological, rheological, thermal and mechanical characteristics were evaluated to explore the worthiness of this blend in the packaging sector **(Bhatia et al., 2007)**. Morphology demonstrates the trend of phase separation based on blend composition. The T_g of the PLA phase

remains almost the same with the loading of PBS, although analysis explained that there was compatibility for PLA/PBS blend up to 20 wt% loading of PBS content. Addition of PBS content in PLA matrix, mechanical properties such as tensile strength, modulus, and elongation at break was dropped down. Moreover, PLA/PBS (80/20) blend followed the rule of mixing. Also, PBS helped to reduce the brittle nature of PLA and indicated the partial compatibility between PLA and PBS phases.

Blend of biopolymers, namely PLA/PBS blend with different blending ratio, was fabricated using melt mixing method to investigate viscoelasticity, interfacial and thermal properties **(Wu et al., 2012)**. The dynamic rheological result shows that the PBS/PLA blend is immiscible with the percolation threshold and narrow co-continuous regime. The viscoelastic response observed with emulsion models such as Palierne and Gramespache & Meissner (G-M) models and it is found that the Palierne displayed better response in comparison to G-M model. The interfacial tension of PLA/PBS blends was computed by several approaches such as deformed drop retraction methods, surface, and rheological properties to observe the compatibility between the two phases. The thermal properties, as well as phase behavior of PBS/PLA blends were investigated to understand the crystallization and melting behavior of the system.

The various loading (5 to 3phr) of wood flour (WF) reinforced into the PLA/PBS (70/30) blend to investigate the mechanical, thermal and morphological characteristics **(Chuayjuljit et al., 2016)**. PLA/PBS/WF biocomposite was prepared using melt extrusion to pelletize and later, a sheet formed with compression molding. It was evident that the justifiable impact strength and maximum elongation at break (ε_b) found after the addition of 30 wt% PBS in PLA. For PLA/PBS/WF biocomposite, thermal stability and mechanical properties (impact, tensile and flexural strength) are reduced with increasing loading of bio based filler. DSC exhibited that the

inclusion of PBS along with WF into PLA matrix had no remarkable change in thermal parameters (glass transition temperature: T_g, melting temperature: T_m) of PLA in the PLA/PBS system with and without WF. In case of PLA/PBS blend and their biocomposites, the computed degree of crystallinity of PLA was higher than that of neat PLA. The PLA/PBS with and without WF degraded is faster than PLA during soil degradation for three months, which was possible due to short degradation time for PBS.

Bourmaud et al., 2016 evaluated the influence of flax on PLA/PBS blend and its biocomposite fabricated using the melt extrusion followed by injection molding process to observe the recycling behavior of biocomposite during successive cycles of injection molding. Authors investigate the fiber length as well as stiffness and hardness after mixing and injection molding. Later, they were focused on the influence of recycling on tensile, thermal and rheological properties. Presented data highlighted the severe evolution of cell wall characteristics and nanoindentation also remained quasi-stable after the first drop. Furthermore, no remarkable changes are observed in mechanical properties after three or four injection cycles. It is noticed that the mechanical performances such as tensile strength and impact strength changed which was due to the decrease in flax length and further enhanced decomposition of PLA. Interestingly, PLA/PBS/Flax biocomposite could be recycled at least three or four injection cycles, which is appropriate for the industry.

1.7.3 *Reactive Extrusion of Aliphatic Polyester and its Composite*

Effect of crosslinking on nanosilk (SNC) grafted PLA bionanocomposite is investigated by **Tesfayee et al., 2017**. All bionanocomposite films are fabricated using reactive melt extrusion technique in the presence of DCP (radical initiator). Successfully grafting of SNC on the PLA matrix was confirmed by ^{1}H-NMR and FTIR investigation. For PLA/DCP system, cross over

point shift to lower frequencies region and remarkable improvement in zero shear viscosities were noticed. For PLA/SNC along with DCP, crystallization rate improved and stable crystal formed during the cooling cycle. Reprocessability of PLA/SNC improved with DCP and also give significant improvement in rheological characteristics than that of branched cum crosslinked PLA during all reprocessing cycles.

Prodyut et al., 2016 successfully fabricated PLA-g-CNC bionanocomposite film using reactive extrusion process in the presence of DCP. PLA-g-CNC based nanocomposite can be successfully recycled multiple times without showing remarkable changes in molecular weight of PLA. Moreover, the PLA grafted chain improved the compatibility and controlled the thermal decomposition due to shielding of the hydroxyl and sulfate group attached to the CNC. Fourier transform infrared (FTIR) and NMR studies showed that PLA chains successfully grafted on CNC confirmed due to the formation of C-C linkage. Mechanical data revealed that young modulus and tensile strength was enhanced by ~490% and 40% respectively. However, MW, crystallization, mechanical and thermal result verified that recycling did not affect the properties significantly.

Wei et al., 2016 worked on the influence of α-cellulose fibers reinforced and grafted PHBV and PHB using the reactive extrusion. The α-cellulose is extracted from the pine wood after removing hemicellulose and lignin and grafted on PHB or PHBV using melt mixing in the presence of DCP acted as a radical initiator. The development of copolymer at the interface of polymer matrix and cellulose behaves as an interfacial coupling agent. It postulates that the reactive extrusion is an effectual method to enhance the characteristics of biocomposites. The grafting of cellulose conducted on the polymer, typically improves the mechanical properties, due to enhancing stress transfer between the two phases. SEM and DMA revealed that there was

good compatibility and interfacial bonding between the interphase of fiber and polymer matrix. In the case of biocomposite, the crystallinity of PHB, PHBV and cellulose was decreased as confirmed by XRD, DSC and FTIR technique.

In the work reported by **Shayan et al., 2015** crosslinked PLA/maleated thermoplastic starch (MTPS) with montmorillonite (MMT) was fabricated to investigate the biodegradation and mechanical properties. Melt-mixing of PLA nanocomposite was done in the presence of DCP along with coagent as triallyl isocyanurate (TAIC) to obtain crosslinked PLA nanocomposites. First of all, thermoplastic grafted with maleic anhydride in an internal mixer to obtain MTPS. Result confirmed that increasing TAIC loading enhances the gel yield, tensile strength, and reduction in elongation at break. With increasing the TAIC content, rate of biodegradation decreased for nanocomposite. After loading of the MTPS, tensile strength reduced while the gel yield and biodegradation increased for nanocomposite. But there was no significant change in gel yield, but tensile strength enhanced after incorporation of nanoclay.

Biobased thermoplastic vulcanizates composed of epoxidized natural rubber (ENR) and PLA with or without DCP is synthesized using dynamic vulcanization method **(Wang et al., 2015)**. SEM result verified the sea-sea continuous phase for PLA/ENR and found good dispersion of crosslinked rubber into the PLA matrix. Addition of 40 wt% of ENR into PLA with DCP, impact strength enhanced and 15 times higher than that of PLA. GPC and DMA result confirmed that crosslinking/branching occurs in the PLA phase.

The influence of lignin (softwood Kraft) on the bacterial Poly (3-hydroxybutyrate-co-hydroxyvalerate) PHBV were successfully prepared with and without DCP act as radical initiator through melt extrusion to understand its effect on morphological, mechanical, structural and thermo-mechanical properties **(Luo et. al., 2016)**. It proved that lignin was successfully

grafted onto PHBV to develop more cross-link sites using FTIR. Gel yield of biocomposite in presence of different amount of DCP was evaluated to get an idea of generated crosslinking/ branching sites. DMA result confirmed that there was a significant improvement in storage modulus (E') and mechanical properties such as young modulus and tensile strength after addition of 2 wt% DCP into PHBV/lignin. For grafted alloy, the degree of crystallinity decreased while crystallization temperature improved which is confirmed by XRD, DSC and FTIR analysis. It is postulated from the polarized optical microscopy (POM) analysis that the spherulites size significantly decreased while nucleation density enhanced for PHBV. Melt strength, thermal stability, and T_g also increased as a result of induced crosslinking.

Kiangkitiwan et al., 2013 applied extrusion during Cassava starch grafted soybean oil maleate (SOMA-g-Starch) with PLA in the presence of DCP. In this case, the soybean oil maleate (SOMA) prepared by grafting soybean oil (SO) with different wt% of maleic anhydride (MA) in addition to DCP. After this, SOMA is used as a surface modifier for starch, producing SOMA-g-Starch with enhancing reactivity. PLA melt mixed with SOMA-g-Starch using twin extrusion and further compress molded to obtain PLA biocomposites. The result confirmed that compatibility, morphological and mechanical characteristics are optimized when 10 and 20 wt% SOMA-g-Starch incorporated into PLA matrix.

The effect of two different crosslinking agents such as triallyl isocyanurate (TAIC) and dicumyl peroxide (DCP) on thermal and mechanical properties of PLA was investigated by **Yang et al., 2008**. FTIR confirmed the crosslinking happened in PLA samples. The tensile modulus and strength improved for crosslinked PLA when compared with the neat PLA. TGA result exhibited higher thermal stability for crosslinked PLA when compared with the neat PLA. It is observed that the crystallinity reduced probably due to crosslinking of PLA begins at the low addition of

DCP or TAIC content.

Sajna et al., 2016 showed that flammability and thermal stability of PLA/silane treated banana fiber (SiB) biocomposite improved by the combined influence of glycidal methacrylate grafted PLA copolymer (PLA-g-GMA) along with nanoclay. Both nanoclay (Cloisite 30B) and PLA-g-GMA were introduced into PLA/SiB biocomposite to enhance the compatibility. First, PLA-g-GMA prepared by radical copolymerization and grafting is detected by FTIR and titration method. The apparent E_a of biocomposite was calculated using Kissinger, FWO and Friedman method using non-isothermal TGA kinetics.

1.7.4 *Reactive Extrusion of Aliphatic Polyester based Blend and its Composites*

Cao et al., 2017 examined the PLA/PBS/microcrystalline cellulose (MCC) (60/30/10) biocomposite compatibilized with chain extender Joncryl ADR to improve the interfacial adhesion and mechanical characteristics. The ADR at the varying amount (0.25, 0.5 and 1 wt %) was applied to PLA/PBS/MCC biocomposite using twin extrusion followed by injection molding. The morphology result showed that the chain extender enhanced the cohesive interfacial forces. FTIR postulated that the chain extender grafted with PLA, PBS, and MCC mainly through end hydroxyl or carboxyl. XRD and DSC represented that the chain extender inhibited the crystallization rate, and these influence were higher when its wt% increased. All composite shows improvement in impact and tensile strength and, it is proportional to the ADR wt %. It found that the elongation at break reduced when ADR above 0.5 wt% added into PLA/PBS/MCC composite. Rheological properties showed that the ADR promoted the increase in complex viscosity, storage and loss moduli of the composite. Consequently, processability and melt strength of the PLA/PBS/MCC biocomposite enhanced after the addition of ADR.

Zhang et al., 2016 investigated the effect of Poly (butylenes succinate) (PBS) grafted cellulose

nanocrystal (CNC) on toughened PLA/PBS (70/30) blend in the presence of dicumyl peroxide (DCP) by melt extrusion at 190°C. PBS-g-CNC synthesized using in situ polymerization whereas its properties were detected using ^{13}C NMR, XPS, FTIR, and GPC technique. The morphological result confirmed that incorporation of PBS-g-CNC along with DCP could reduce size of PBS in the PLA matrix and promotes the dispersion of PBS-g-CNC in both phases, which could be responsible for controlling the mechanical and crystallization characteristics of biocomposites. For the PLA/PBS/PBS-g-CNC biocomposites, the crystallinity of α' phase crystal improved by the incorporation of PBS-g-CNC which subsequently led to the enhancement in percentage crystallinity (% X_c) of biocomposites. It is found that PLA/PBS/DCP shows high impact strength and modulus while it increased by the incorporation of PBS-g-CNC. DMA showed that storage modulus (E') and the glass transition temperature (T_g) increased by the incorporation of PBS-g-CNC along with DCP in PLA/PBS (70/30) system. For DCP treated PLA/PBS blend, there was an enhancement in the thermal stability of composite with the decrement in the crystallinity (% X_c) as well as crystallization temperature (T_c) which was due to crosslinking influence of DCP in PLA/PBS system.

The reactive PLA/PBS (80/20) blends fabricated using DCP (radical initiator) in internal mixer at 180°C and its characteristics such as rheological, morphological, mechanical, gel fractions and crystallization behaviour evaluated **(Ji et al., 2014)**. Rheological and gel fraction data elucidates the development of some branched/crosslinked structures which act as nucleation sites for the PLA/PBS blend. It is found that the isothermal crystallization of PLA improved in case of reactive PLA/PBS blend. The formation of PLA-PBS copolymer in the reactive system could attribute to the improvement of compatibility between the PLA and PBS phase. The tensile test represents the remarkable mechanical result when 0.2 phr DCP into the PLA/PBS system.

Kangwanwatthanasari et al., 2013 used cassava pulp (CP) as bio-filler of PLA/PBS blend with or without PLA grafted glycidal methacrylate (PLA-g-GMA) to investigate the physical properties. First of all, PLA/PBS blend is fabricated with the series of various PBS content (0 to 30 wt %) in an internal mixer. As reported tensile strength and modulus of PLA/PBS decreased as the PBS content increased; however its elongation at break and impact strength improved. In this case, glycidyl methacryate (GMA) was grafted with PLA chains to enhance interfacial adhesion of PLA/PBS blend. Furthermore, the incorporation of PLA-g-GMA increases the mechanical properties of PLA/PBS/CP biocomposite and acts as compatibilizer.

PLA/PBS blend in the presence or absence of DCP fabricated using melt-mixing method and detailed investigation of crystallization behavior was done using differential scanning calorimeter (DSC) **(Ji et al., 2012)**. It is observed that the crystallization ability of PLA matrix remains unchanged after the addition of PBS content probably due to high MW PBS than that of PLA utilized in this study. Although, crystallization ability of PLA enhanced in case of the reactive blend and could ascribe to the formation of some crosslink or graft structure which acted as nucleation sites. When DCP added up to 0.3 phr, crystallization occurred in PBS while the amount of DCP was higher than 0.3 phr, crystallization ability of PBS minimized. PLA started to crystallize whereas crystallization ability of PBS was poor in case of PLA/PBS/0.4DCP. It is concluded that the crystallization ability of PLA and PBS phase in the reactive blend varied according to DCP content.

Toughen PHB/PBS and PHBV/PBS blends with and without DCP had been fabricated using DCP as radical initiator **(Ma et al., 2011)** through in situ compatibilization. After the compatibilization particle size of PBS reduced significantly and improvement in interfacial adhesion between the PBS and PHBV noticed. The elongation at break increased significantly

for PHBV/PBS blend while tensile strength, elongation at break and impact toughness of PHB/PBS blend also enhanced after compatibilization.

Harada et al., 2007 fabricated the PLA/PBS (90/10) blend with and without lysine triisocynate (LTI) using melt extrusion followed by the injection molding process to investigate the compatibility, rheological, mechanical and morphological properties. It is proved that the incorporation of 0.5 wt% LTI in PLA/PBS blend enhanced the impact strength nearly ~ 50 to 70 kJ m^{-2}. It is observed that the isocyanate groups of LTI chemically reacted with both carboxyl and hydroxyl end group of the polymers. Obtained result confirms that the LTI (reactive processing agent) used to improve the compatibility and impact strength of the polymer blend.

Green ternary biocomposites based on PHBV, poly (butylenes adipate-co-terephthalate) (PBAT), epoxidized natural rubber (ENR) and miscanthus fiber (MF) is successfully fabricated via DCP initiated grafting during reactive melt extrusion at 175°C to enhance the interfacial adhesion with balanced properties **(Zhang et al., 2014)**. It is observed that the incorporation of MF into the polymer matrix significantly improved its thermal resistance and stiffness although maintaining the toughness. In addition of 20 wt% MF, high impact strength ~240.5 J/M is obtained. In this work, three different mathematical models such as Tsai-Pagano equation, rule of mixture and inverse rule of mixture are used to estimate mechanical moduli. However, ENR plays a dual role as an impact modifier and coupling agent along with DCP for multiphase blend and biocomposite. Morphological results showed the strong interfacial adhesion among the various phases in green biocomposite which had a significant improvement in toughness and strength of samples. Also for the biocomposite, balanced melt viscosity is achieved which confirms its utility for the wide range of applications.

1.7.5 *Thermal Degradation Kinetic Study of Polymer Blend & its Composites*

Thermal degradation kinetic study of bionanocomposite based on Poly (3-hydroxybutyrate) (PHB)/cellulose nanocrystal (CNC) were evaluated using non-isothermal TGA kinetic study **(Dhar et al., 2014)**. In this work, CNC reinforced PHB biocomposite was prepared by the solvent casting method. Morphological investigation confirmed that interfacial adhesion of PHB/CNC bionanocomposite improved at loading of 3 wt % CNC in PHB matrix. The introduction of 3 wt% CNC resulted in a slight increment in the thermal stability of PHB based biocomposite. TGA kinetics based on the isoconversional method using OFW and KAS methods were applied to predict the activation energy. It is found that E_a was constant throughout with the degree of conversion which indicates the single mechanism. Coat redfern (C-R) method revealed that PHB/CNC bionanocomposite follows the phase boundary controlled mechanism with the random chain scission mechanism.

Novel poly (butylenes succinate) (PBSu) nanocomposite with the addition of two different kind of nanofiller such as strontium hydroxyapatite (SrHNR) and silica nanotube (SiNT) fabricated using melt mixing method **(Papageorgiou et al., 2014)**. Nonisothermal TGA kinetics and degradation mechanism of PBSu nanocomposites were analyzed using TGA and pyrolysis gas chromatography (py-GC/MS) technique in detail. Result revealed that incorporation of SrHNR acted as the catalyst for the initial stage of degradation for PBSu and also during the modified degradation mechanism. On the other hand, addition of SiNT in the PBSu matrix has no noticeable influence on thermal stability as well as degradation mechanism. It is noticed that same type of volatile product was evolved out for neat PBSu and their PBSu/SiNT nanocomposite while in case of PLA/SrHNR, volatile species were slightly varied.

The thermal decomposition behavior of poly (3-hydroxy butyrate) (PHB), poly (ε-caprolactone)

(PCL), polylactide (PLA) was studied via isothermal and nonisothermal TGA analysis **(Aoyagi et al., 2002)**. For non-isothermal TGA kinetics, distribution of E_a with α was estimated using the Ozawa method. Isothermal TGA result directly pointed out that each polyester displays individual profiles for various time-dependent weight loss and degradation mechanism profile reflected by the number average molecular weight (M_n). From the Py-GC-MS and TGA studies, it is inferred that PCL thermally degraded from the hydroxyl end of chains (unzipping mechanism) while PHB is decomposed due to the chain scission (cis elimination) in the random fashion. PLA showed the multistep mechanism because of complex reactions took place simultaneously.

Making of aromatic diacid monomer involved three synthesis steps to produce high purity yield **(Mallakpour et al., 2009)**. Aromatic polyamides (PAs) posed flame retardant characteristic obtained from the various aromatic diamines and diacid monomer using microwave and conventional heating approach. Nonisothermal TGA models such as integral and differential methods are utilized to determine the kinetic parameters (E_a, A) and thermodynamic variables (ΔS, ΔG and ΔH). Further, the kinetic parameters were extensively used to predict the reaction mechanism with the Criado method, half life ($t_{1/2}$) and service life (t_f) of the product.

Thermal decomposition behavior of polymer blend, namely poly benzoxazine and poly siloxane block polyimide were investigated using TGA **(Tiptipakorn et al., 2007)**. Differential thermogram (DTG) data displayed that two and three stages of degradation processed in neat SPI and PBA. For PBA/SPI blend with the varying ratio, DTG showed four stages of thermal decomposition. Kissinger, FWO and CR methods were selected to calculate the E_a of each step. Criado method suggested that neat PBA, SPI and their blend followed the F1 type decomposition mechanism.

Thermal degradation behavior of cellulose derivates reinforced poly ε-caprolactone (PCL) was investigated to analyze the kinetic parameters using the Friedman method **(Ruseckaite et al., 2003)**. PCL was manually mixed with sisal fiber (SF) and microcrystalline cellulose (MCC) to produce the range of mixtures. TGA result indicated that the thermal stability of each component was higher for mixture in comparison to individual biofiller. Friedman result confirmed the complex reaction mechanism for series of mixture and determined value of apparent E_a was in line with the thermal stability.

1.7.6 *Thermal Degradation Kinetic Study of PLA & its Composites*

Fan et al., 2004 purposed the thermal decomposition behavior and degradation mechanism of three different types of stereocomplex (sc)-PLA with various chain ends such as polymerized, purified metal free and precipitated methanol. The decomposition of polymerised sc-PLA followed via unzipping depolymerisation. The range of E_a value was 80 to 100 $kJmol^{-1}$ due to Sn alkoxide chain ends with the zero-order mass loss. On the other hand, decomposition of precipitated sc-PLA is also preceded through zero order weight loss involving of Sn-catalyzed based lactide removal, due to the presence of Sn carboxylate ends group with apparent E_a 100 to 120 kJ mol^{-1}. The decomposition products from polymerized and precipitated sc-PLA were mainly L and D form of lactide. Although, metal free sc-PLA follows the random decomposition process which produced prominently cyclic oligomers and meso lactide.

Carrasco et al., 2013 studied the thermal decomposition behavior of processed PLA using four different types of TGA kinetic methods such as General analytical equation, Kissinger, Horowitz-Metzger and Freeman-Carroll method. PLA pellets processed with and without annealing using two industrial viable techniques: (i) Injection molding and (ii) Extrusion followed via the injection molding technique. By doing that, apparent E_a was approximately 318

kJ mol^{-1} computed from GAE for unprocessed PLA while it was 280±5 $kJmol^{-1}$ for processed PLA. Thermal stability of processed samples was almost similar which was slightly lower in comparison of unprocessed PLA.

Kameno et al., 2016 revealed the multistep kinetic decomposition, types of evolved gaseous products and overall rate behavior of the PLA oligomers (PLAO). It proposed that the thermal decomposition of PLAO containing two partially overlapped mass-loss stages. After melting the reactant, first mass loss stage began with the release of main volatile components such as lactide and after this CO_2, aldehydes, cyclic oligomers were also released with frequent appearance and disappearance of volatile bubbles in the molten PLAO system. During the first stage, mass loss behavior governed by the diffusion mechanism with an E_a of ~ 90 kJ mol^{-1}. It is observed that lactide transferred via diffusion from the reaction sites to the upper surface which was the rate controlling step for molten PLAO. On the other hand, the overall rate of mass loss controlled by bubble phenomena and the estimated value of E_a was ~ 155 kJ mol^{-1}.

Valapa et al., 2014 fabricated the novel sucrose palmitate (SP) reinforced poly (lactic acid) biocompsite for food packaging using the solvent casting approach. TGA results showed that no significant changes are observed in maximum degradation temperature (T_{max}) upto 5 wt % loading of SP which probably due to its protective barrier tendency and finally decelerated the decomposition rate of PLA/SP biocompsite. Further addition of 10 wt % SP in PLA, T_{max} was decreased due to the presence of more acidic sites which was responsible for increasing the degradation rate. The apparent activation energy (E_a) was predicted using the model free approach such as Flynn Wall Ozawa (FWO) and Kissinger method. FWO result suggested that overall decomposition process was complex for PLA and its biocomposite. Apparent E_a determined using Kissinger and FWO methods observed in good agreement for all samples.

Lactic acid grafted hydroxyapatite (LA-g-HA) synthesized using in situ polymerization at 130°C in the presence of stannous octoate acted as the catalyst and PLA/LA-g-HA bio based film prepared by the solvent casting method **(Li et. al., 2009)**. FWO and Invariant kinetic parameters (IKP) method selected to estimate the degradation kinetic parameter for PLA/LA-g-HA bionanocomposite. TGA kinetic study revealed that the addition of LA-g-HA into PLA retards thermal decomposition of the PLA matrix.

Oza et. al., 2014 successfully demonstrated the chemically modified hemp using alkali, acetic anhydride and silane treatment. Moreover, composites prepared to make sandwich a hemp fibers layer between the layers of neat PLA. Influence of chemically surface treated or untreated hemp fibers on PLA matrix to evaluate the thermal degradation behavior. Results showed that acetic anhydride modified hemp based PLA composite had the highest thermal stability and enhanced apparent value of E_a (159-163 kJ/mol) in comparison to other composite due to high bond dissociation energy. Therefore, this research could aid proper selection of modified hemp reinforced PLA composite to explore the decomposition behavior to check the process viability.

Cellulose grafted poly (lactic acid) (CE-g-PLA) was synthesized using ring opening polymerization and degradation study proposed to evaluate the kinetic parameters **(Dia et. al., 2013)**. Friedman, Kissinger and FWO are used to estimate the E_a. Coat red fern method (CR) is selected to determine the probable decomposition mechanism. The trend of E_a of CE-g-PLA gradually increased with increasing the PLA content and obeyed random nucleation with two nuclei on the individual particle (F2 mechanism). Wide angle X ray diffraction (WAXD), nuclear magnetic resonance (NMR) and differential scanning calorimetric (DSC) are conducted to confirm the microstructure and thermal property of CE-g-PLA.

According to **Valapa et al., 2015** PLA/graphene (GR) composite fabricated using solvent casting

method to investigate the influence of GR on thermal degradation and crystallization kinetics of PLA under dynamic heating regime. For crystallization kinetic study, Avrami and Tobin models used to predict kinetic data obtained from the DSC graph. Crystallization kinetic study confirmed the nucleation effect of GR on the PLA system. The Kissing method applied to analyze the TG kinetics of PLA/GR composite. With increasing GR loading, E_a increased which confirmed the increment in thermal stability of PLA/GR composite in comparison to neat PLA. Polarize optical microscopy (POM) is used to analyze the spherulites growth of PLA/GR composite.

Poly (lactic acid) (PLA)/Poly (hydroxybutyrate co valerate) (PHBV) co-continuous blend with or without titanium dioxide (TiO_2) were melt mixed by Brabender plastograph at 170°C **(Mofokeng et al., 2015)**. Morphology observation of PLA/PHBV blend and their nanocomposite confirmed effective dispersion of TiO_2 nanoparticle on the interface of PLA/PHBV blend and also in PLA phase whereas large agglomerates with the tiny amount in PHBV phase. TGA data showed that thermal stability of PLA/PHBV blend improves after the incorporation of TiO_2 nanoparticle. TG kinetic study revealed that the presence of TiO_2 acts as a catalyst in PLA phase could accelerate thermal decomposition process as well as minimize diffusion of volatile species. For PHBV, same influence did not notice, but inhibition of the volatile components could also observe.

Thermal degradation kinetics of poly (lactic acid)/montmorillonite (PLA/OMMT) nanocomposite has been evaluated using the enhanced general kinetic equation **(Carassco et al., 2014)**. PLA nanocomposites containing 0.5 and 2.5 wt% OMMT were prepared using co rotating twin screw extruder. Modified Sestak Berggen equation is selected to analysis TG experimental data which provide the better fit. TGA results confirm those PLA nanocomposites were thermally stable than PLA. Thereafter, obtained kinetic parameters from the modified Sestak

Berggen equation were compared to those estimated using isoconversional and differential methods. Thermal decomposition of PLA is discussed to govern by random chain scission mechanism, for which $f(\alpha) = L(L-1)x(1-x)^{L-1}$ related to random chain scission examined. After optimizing the kinetic parameters, degradation kinetics of PLA-0.5 OMMT, PLA-1.0 OMMT nanocomposite was compared with neat PLA.

Thermal degradation kinetics study of PLA with or without functionalized graphene was investigated to understand the role of functionalizes graphene (FGR) on PLA matrix **(Manafi et al., 2016)**. PLA/functionalized graphene nanocomposite was fabricated using the solution casting method. FGR was synthesized using acid treatment proceeded via grafting PLA on their surface and it was characterized using FTIR, DMTA, Raman and elemental analysis to confirm the functionalization. Onset (T_{onset}) and maximum degradation temperature (T_{max}) improved after the addition of FGR into the PLA matrix which indicated that improvement in thermal stability. Nonisothermal TGA kinetics was studied using FWO and Vyazovkin (VZ) method to calculate the kinetic parameter at four different heating rates (5, 10, 15 and 20°C/min). There was good agreement in apparent E_a acquire from various methods, albeit these method based on different assumptions. Comparison between FWO and VZ suggested that VZ method was much more sensitive to degradation kinetic study.

1.7.7 *Hyphenated TGA-FTIR Techniques to Detect the Release of Volatile Components*

The influence of modified Gum arabic on the thermal properties of PLA biocomposite was examined using non isothermal TGA kinetics and established hyphenated TGA-FTIR technique **(Triphati et al., 2017)**. The lactic acid grafted gum arabic (OLLA-g-GA) was synthesized by one step microwave assist polymerization. Model free and model fitting method utilized for the detailed investigation of TGA kinetic parameters. TGA data revealed that thermal stability

gradually decreases with increasing loading of OLLA-g-GA in the PLA matrix due to the plasticization effect of OLLA-g-GA. It was also noticed that increasing the OLLA-g-GA content alter the decomposition behavior and reduced the E_a with $\alpha \leq 0.6$ conversion. From the result, it concluded that PLA and their biocomposite showed the complex reaction mechanism pathways. The hyphenated TGA-FTIR technique is used to investigate the major gaseous species for PLA/OLLA-g-GA biocomposite such as lactide, aldehydes, cyclic oligomers, N-H containing compounds, cabon di-oxide (CO_2), carbon mono-oxide (CO) and water.

Pal et al., 2016 reported the synthesis of chitosan grafted lactic acid (CH-g-OLLA) using microwave assist condensation polymerization, which was later used to fabricate PLA/CH-g-OLLA biocomposite via the solvent casting method. FESEM image depicted the homogenous dispersion of CH-g-OLLA nanofiller (~ 20 to 150 nm) as spherical aggregates. Kissinger, KAS, OFW and Augis & Benette method is proposed to estimate the apparent activation energy (E_a) for PLA bionanocomposite. For PLA bionanocomposite, decrement in E_a is observed, which subsequently led to enrichment in mobility between chains and intermolecular distance. The volatile species such as CO_2, CO, cyclic oligomers and hydrocarbon detected with hyphenated TGA-FTIR analysis.

This research work is focused on the silk nanocrystal (SNC) stabilized poly (lactic acid) (PLA) based bionanocomposite film to investigate the influence of recycling and non isothermal TGA kinetics **(Tesfaye et al., 2016)**. The PLA/SNC bionanocomposite fabricated using melt extrusion process at screw speed ~100 rpm for 1 min in recycle mode and temperature was set 200°C. FWO and KAS method is used to estimate the kinetic parameter while the Nelder-Mead-Simplex method is further applied to optimize these parameters. For PLA/SNC bionanocomposite, extrus-ion cycles. Hyphenated TGA-FTIR technique is utilized to confirm the release of various types

of gaseous products for the PLA/SNC during multiple recycling.

Thermal degradation study of Poly (lactide-co-propylene carnonate) with various loading of propylene carbonate (PC) unit content investigated by the coupled pyrolysis-gas chromatography-mass spectrometry (Py-GC-MS) and the TGA-FTIR technique **(Huang et al., 2015)**. TGA data indicated that the thermal stability of PLAPC reduced with increasing loading of PC units in the PLAPC chain. TGA kinetic highlighted that improvement in E_a determined using the Kissinger method. At lower temperature main volatile products such as lactide and cyclic propylene carbonate are obtained via the backbiting ester interchanged process as dominated mechanism whereas at the higher temperature beside the propylene carbonate, lactide small yield of acetaldehyde and propenoic acid obtained. The complex reaction mechanism suggested: intramolecular transesterifaction accompanied by chain scission and fragmentation at the higher temperature.

Carboxymethyl starch (CMS) grafted poly (lactic acid) (CMS-g-PLA) copolymer prepared using the solution polycondensation method in the presence of stannous 2-ethyl hexonate [$Sn(Oct)_2$] act as the catalyst **(Tudorachi et al., 2012)**. For PLA, CMS and CMS-g-PLA, release of volatile components detected by hyphenation of TGA and FTIR with mass spectroscopy (TGA-FTIR-MS) where as modification in the structures were characterized by FTIR. TGA study revealed that CMS-g-PLA had lower thermal stability in comparison to CMS, due to the aliphatic behavior of grafted PLA chains, caused by the presence of ester group linkage which responsible for the thermal decomposition. Activation energy (E_a) was computed using three different TGA kinetic methods such as multivariate nonlinear regression (MNLR), FWO and Kissinger method. Distribution of activation energy with the degree of conversion suggested that it proceeded via complex decomposition process and could be distinct at least one or two stages. The major

volatile components that evolved during CMS-g-PLA decomposition were acetic acid, ethanol, methanol, butane, ethane, methane, water and carbon dioxide. It noticed that thermal decomposition of copolymer based on chain homolysis, the hydroxyl end initiated ester interchange process, recombination or hydrogenation reactions and fragmentation occurred at elevated temperature.

Thermal decomposition behavior of flame retardant PLA was investigated using combustion calorimetery, limiting oxygen index, UL-94 and hyphenated TGA-FTIR technique **(Chen et al., 2012)**. PLA/hyper branched polyphosphate ester (HPE) based composite prepared on the two-roll mill at 165°C. Obtained information shows that HPE in the PLA matrix enhanced their flame retardancy. TGA result indicated that HPE improves the char yield. Similar kind of release of gaseous products such as CO_2, CO, aldehydes and aliphatic ester are observed during the thermal decomposition of flame retardant PLA. From the result, it is suggested that HPE catalyzed thermal decomposition of the PLA matrix, and less combustible gaseous products released.

The influence of three different nanoparticles such as fumed silica (SiO_2), montmorillonite (MMT) and multiwalled carbon nanotube (MWCNT) on the thermal decomposition behavior of poly (propylene sebacate) (PPSeb) was studied by **Chrissafis et al., 2012**. All of PPSeb nanocomposites were fabricated using in situ polymerization method. To investigate the influence of nanoparticles on the decomposition mechanism of PPSeb, hyphenated TG-GC-MS and TGA-FTIR technique is utilized to confirm the gaseous products. TGA result demonstrated that incorporation of MMT and MWCNT improved the thermal stability of PPSeb, while it remained same in the case of PPSeb/SiO_2 based nanocomposite. Apparent E_a calculated using the isoconversional approach such as KAS and FWO. It is noticed that the degradation of nanocomposite proceeds via complex routes with the involvement of two types of mechanism.

TGA-FTIR exhibited that similar kinds of products were released which confirms volatile component with related chemical structure was evolved out. From MS, it is detected that major volatile component were sebacic acids, propanol, hydroxypropanol, propenal, allyl, diallyl whereas decomposition proceeded mainly by scission of β-hydrogen bond and also through scission of α hydrogen bond.

Wang et al., 2011 prepared PLA/Starch biocomposite with or without micro encapsulated ammonium polyphosphate (MCAPP) as flame retardant through melt processing and it evaluated using LOI, UL-94 and MCC test to identify that flammability improved. Thermal decomposition and volatile components of PLA/Starch biocomposite with or without MCAPP analyzed with the help of TGA and TGA-FTIR techniques.

Liu et al., 2010 reported the influence of hydrophilic fillers such as starch and wood flour (WF) on the thermal decomposition behavior of PLA. Coupled TGA-FTIR technique was beneficial to detect the influence of volatile species from hydrophilic fillers on the thermal decomposition of PLA. For PLA/WF and PLA/Starch biocomposites, the evolution of major volatile species such as $C_2H_4O_2$, aldehydes, water, CO_2 and CO which acted as chain scissor for PLA system. In the case of PLA/Starch biocomposite, the intensity of IR peak was lower than that of WF during decomposition process which indicated the lower yield of gaseous product. It is found that small particle size of starch was responsible for improving the interfacial interaction between the PLA and starch phases. As compared to WF, addition of starch accelerated the decomposition process of PLA.

In the work, hyphenated TGA-FTIR technique was utilized to investigate the release of major decomposition products of PLA such as CO_2, CO, lactide and acetaldehyde **(Zou et al., 2009)**. Thermal degradation behavior of PLA studied using non-isothermal TGA kinetics whose

interpreted to follow the multistep degradation mechanism. FWO, Friedman and Kissinger methods selected to determine the value of $E_{a.}$ Result confirmed that the estimated E_a by these three methods are found in good agreement.

Hyphenated TGA-FTIR technique was used to observe the main degradation product of PLA, Poly (ε-caprolactone) (PCL) and their blends with Poly (hydroxy butyrate) (PHB) under nitrogen and oxygen atmosphere **(Vogel et al., 2008)**. It is noticed that same kind of major volatile species released such as short chain acids, CO_2, CO and H_2O during decomposition of PLA and PCL in the oxygen atmosphere. It is identified that PLA released to lactide, acetaldehyde, CO_2 and CO, while PCL decomposed to 5-hexconic acid, ε-caprolactone, CO_2, CO in the nitrogen atmosphere. The study revealed that PLA/PHB and PCL/PHB blend decomposed to typical homopolymer with crotonic acid which subsequently released at initial decomposition stage of PHB.

1.8 HYPOTHESIS & CHOICE OF SYSTEM

Here, this PhD thesis work is presented on the following hypothesis:

Ist hypothesis: Different acid hydrolyzed cellulose nano-crystal can be successfully dispersed in PLA using melt extrusion technique in order to significantly improve the thermal stability along with the processibility performance. This study will also provide enough information to select the PLA/acid hydrolyzed CNC based bionanocomposite that are most stable during melt processing without serious decomposition.

2nd hypothesis: DCP generate sufficient free radical sites on PLA chains at elevated temperature and shear force. There is huge possibility that the PLA chains grafted on the active sites of functionalized gum arabic in the presence of DCP to tailor the properties of biocomposites. Such interaction can assist to compatibilizing PLA/FG based system as well as show the impact on

thermal behavior.

3rd hypothesis: Compatibilization of PLA/PBS blend by functionalized chitosan in the presence of DCP was expected to influence the melt behavior of reactive bionanocomposite in the extruder. Furthermore, there are chances that FCH will attack free radical sites of PLA and PBS to form the complex structure including crosslinking/branching sites as well as PLA/PBS copolymer, which may provide stiffness-toughness balance, enhanced crystallization rate and thermal stability along with melt strength of PLA/PBS blend. There is possibility that reactive extrusion is one of the possible ways to minimize or overcome thermal decomposition behavior of aliphatic polyester in the presence of biofiller.

Choice of systems: The present study is framed on the basis of the following systems and characterization techniques.

- Different acid hydrolyzed CNC, functionalized chitosan and functionalized gum arabic used as bio-fillers synthesized as mentioned elsewhere and characterized by FTIR, FESEM or FETEM.
- Haake twin screw extruder preferred for fabrication of bionanocomposite using melt processing to investigate the thermal decomposition behavior in detail. Many characterization techniques are selected to analyze the extruded strips which involves gel permeation chromatography (GPC) to determine molecular weight, crystallization and melting behavior by differential scanning calorimetry (DSC), viscoelastic behavior by rheometer, polarized optical microscope (POM) to understand the spherulites morphology, wettability properties by contact angle analyzer, mechanical properties by universal testing machine (UTM), structural changes by FTIR; morphological changes studied using field electron scanning electron microscopy (FESEM) and field electron transmission electron

microscopy (FETEM).

- Non-isothermal TGA kinetics to estimate kinetic parameters using model free methods such as Flynn-Wall-Ozawa method, modified Coat-Redfern and Kissinger method, thermodynamic variables (Gibb's free energy, entrophy and enthalphy). Criado or generalized method is utilized to predict the reaction mechanism. Hyphenated thermal gravimetric analysis (TGA)-Fourier transform infrared (FTIR) technique is selected to analyze release of volatile species during thermal decomposition.

1.9 AIM & OBJECTIVES

Most researchers have explored either structural aspects of the degradation or changes in properties. The current research work has been undertaken with the following aim and objectives:

***Aim*:** To investigate how molten polymer is processed without serious decompositition in presence of bio-based nanofillers including cellulose nanocrystals, nano-gum arabic and nano chitosan. This research is mainly focused on the enhancement of thermal performance of the polymeric system using the following objectives:

- Investigate the effect of different acid hydrolyzed cellulose nanocrystals (such as sulphuric hydrolyzed CNC, nitric hydrolyzed CNC, phosphoric hydrolyzed CNC and nitric hydrolyzed CNC) on the thermal degradation behavior of PLA matrix.
- Investigate the combined effect of dicumyl peroxide (DCP) and functionalized gum arabic on the structural modifications, compatibility and thermal decomposition behavior of melt processed PLA based reactive bionanocomposite film.
- Investigate effect of DCP content and functionalized chitosan on macromolecular structural changes, thermal decomposition behavior and rheological properties of PLA/PBS blend

during the reactive extrusion process.

- To investigate the volatile product distribution using hyphenated TGA-FTIR techniques.

1.10 PROPOSED THESIS ORIENTATION

***Organization of Chapters*:** The systematic organization of the report is as follows: Chapter 2 highlights the material, characterization techniques, model free methods to predict kinetic parameters and thermodynamic variables, and criado or generalized method to predict degradation mechanism in details. Chapter 3 deals with the thermal degradation behavior of PLA/CNC bionanocomposite films. Chapter 4 and 5 describe the fabrication and thermal degradation study of PLA/*F*G based reactive bionanocomposite films. Chapter 6 and 7 belong to fabrication and thermal degradation study of PLA/PBS/*F*CH based reactive bionanocomposite films. Chapter 8 designates the conclusion and future prospects. This present work has related to basic and applied research analysis which discusses in the following chapters:

Chapter 1: Introduction and literature review

Chapter 2: Materials and methods

Chapter 3: Thermal degradation kinetic study of poly (lactic acid)/different acid hydrolyzed cellulose nanocrystals based bionanocomposite film.

Chapter 4: Effect of dicumyl peroxide on poly (lactic acid)/functionalized gum arabic based bionanocomposite films

Chapter 5: Thermal degradation studies of poly (lactic acid)/functionalized gum arabic based reactive bionanocomposite films

Chapter 6: Effect of dicumyl peroxide poly (lactic acid)/poly (butylene succinate)/ functionalized chitosan based reactive bionanocomposite films

Chapter 7: Thermal degradation kinetic study of poly (lactic acid)/poly (butylene succinate)/

functionalized chitosan based reactive bionanocomposite films

Chapter 8: Conclusion and future prospects.

Chapter 2

Materials and Methods

This chapter demonstrates the details of materials, characterization techniques and experimental protocols for obtaining the desired results. Firstly, the synthesis routes of different biofillers such as different acid hydrolysed CNC, functionalized chitosan and functionalized gum arabic are discussed in brief, as reported earlier **(Dhar et al., 2016; Pal et al., 2016; Triphati et., al 2016)**. After this, the processing of different bio fillers with polymeric systems through melt processing has been discussed. The analytical instrumentation used and experimental procedure followed for the characterization has also been explained in brief. This chapter includes the theoretical modeling approach elaborated to investigate the non-isothermal behavior of the samples to determine the kinetic parameters, thermodynamic variables and solid-state degradation mechanism. Next, the chemical changes thereof at degradation temperatures are evaluated by hyphenated TGA-FTIR technique under set conditions.

2.1 MATERIALS

Commercial poly (lactic acid) (PLA) (grade: 4032D, 98.6 of D-lactic and 1.4 of L-lactic acid unit) with number average molecular weight (M_n~150,000 Da), polydispersity index (PDI~1.3) was purchased from Nature Works (USA). Poly (butylene succinate) (PBS) (grade: 1001MD) with M_n ~ 88,000 Da and PDI~2.2 was supplied by Showa Highpolymer Singapore Pte. Ltd. (Japan). Hydrochloric acid (HCl) (>35%), nitric acid (HNO_3) (>72%), phosphoric acid (H_3PO_4) (>85%) and sulphuric acid (H_2SO_4) (>99%) were purchased from SISCO research laboratories (SRL chemicals, India) and used as hydrolyzing agents for fabrication of cellulose nanocrystals (CNC). Chitosan (degree of deacetylation >70%) was purchased from Sigma Aldrich. L-lactic acid (Sigma Aldrich) was used to synthesize functionalized chitosan. Gum arabic (GA) (G9752) from acacia tree was supplied by Sigma Aldrich, India. Dicumyl Peroxide (DCP, purity > 99.5%), was purchased from Sigma Aldrich (India), used as radical initiator. Whatmann® filter paper (grade: 1) was used to extract the CNC using different acids, functionalized chitosan (*F*CH) and functionalized gum arabic (*F*G). Acetone was supplied by SISCO Research laboratories (SRL chemicals, India). For GPC analysis, HPLC chloroform was purchased from MERCK, India. All the chemicals were consumed without any further purification.

2.2 METHODS

2.2.1 *Fabrication of Different Acid Derived CNC via Different Routes*

Fabrication of CNC from Sulphuric Acid

Chopped filter paper (~2 g) was added to H_2SO_4 (~ 64 weight %) solution and vigorously stirred (~500 rpm) for 2 hr, as per reported paper **(Dhar et al., 2016)**. Excess amount of deionized water was added to stop the hydrolysis process and obtained mixture was cooled down to room temperature. Further, the suspension was centrifuged followed by its dialysis with cellulose acetate membrane (cut of M_w ~14 kDa) obtained from Sigma Aldrich for acid

removal. Finally, the neutralized suspension (pH~7) was centrifuged to precipitate and freeze dried (at ~ –80ºC) to yield CNC in powdered form.

Fabrication of CNC from Phosphoric Acid

Phosphoric acid derived CNC was fabricated by acid hydrolyzing the filter papers (~2 g chopped) with H_3PO_4 (11M, 100 ml) at 100ºC under magnetic stirring (~500 rpm) for 5 hr. After hydrolysis, the pale yellow color product was obtained which was centrifuged and dialyzed to remove the acid until it reached to pH~7. Finally, the suspension was lyophilized into dried CNC powder as per the protocol discussed in the previous section.

Fabrication of CNC from Hydrochloric Acid

Filter paper (~2 g chopped) was reacted with HCl (6M, 120 ml) at a temperature of 120ºC under magnetic stirring of ~500 rpm for 4 hr. The suspension thus obtained was centrifuged and dialyzed to remove the excess acid till the pH of CNC suspension attained ~7 and finally freeze dried as per the reported protocol.

Fabrication of CNC from Nitric Acid

HNO_3 (6M, 50 ml) was used to hydrolyze the filter paper (~2 g chopped) at 40ºC under continuous stirring (~500 rpm) for 4 hr. After the reaction, powder CNC was obtained as per the above protocol.

2.2.2 *Microwave-assisted synthesis of functionalized chitosan (FCH)*

*F*CH was produced using microwave assisted synthesis as reported elsewhere **(**Pal et al., 2016). Both L-lactic acid and chitosan were mixed in the ratio of 3.33:1 (w/w %) in a round bottom flask (RBF) to perform the synthesis of functionalized chitosan. Lactic acid (LA) was mixed manually and completely soaked by hydrophilic chitosan in order to enhance the reaction performance. The soaked mixture was placed inside microwave oven and the inert atmosphere inside RBF was generated by purging N_2 gas. The condenser and ice bath were connected with RBF and placed outside the microwave in such a way that the generated by-

products can easily be collected in the reservoir. The reaction pathway is termed as "condensation polymerization" which was executed at 240 watts, 110°C for 30 min. The microwave was automatically stopped after completion of reaction and the N_2 atmosphere was broken by closing the gas valve. FTIR of *F*CH has displayed in Figure 2.1 S.

A low molecular weight oligomer chain (M_n and M_w values = 1400 Da and 3000 Da respectively) had been attached with chitosan backbone during reaction and finally, a dark brown viscous product was formed as per the mentioned reaction pathway in Figure 2.1.

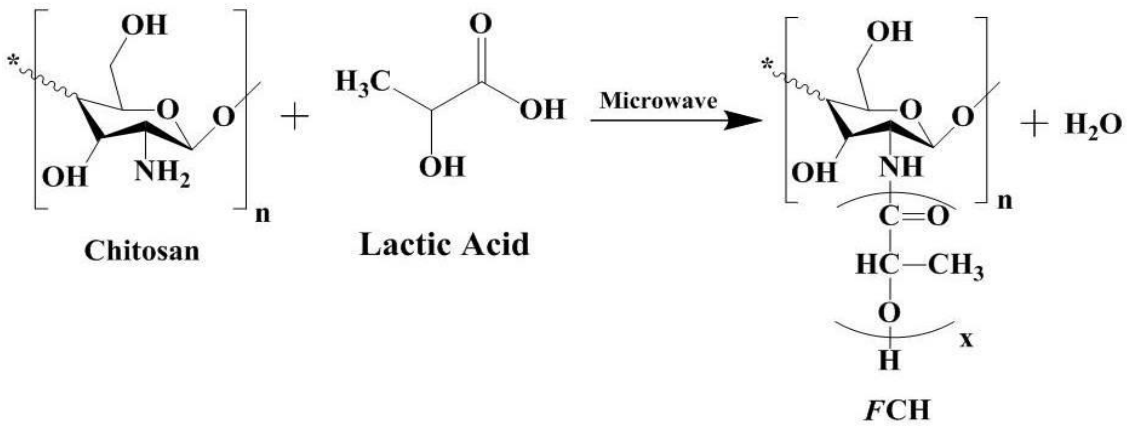

Figure 2.1: *Reaction pathway for the synthesis of functionalized chitosan.*

Thereafter, a fixed amount of *F*CH was dissolved in acetone (20ml), stirred at 1000 rpm for 6 hr followed by vacuum filtration. The supernatant had been discarded and the remaining solution was collected for its use in further experimental work.

2.2.3 *Microwave-assisted synthesis of functionalized gum arabic (GA)*

The functionalized GA was synthesized using microwave reactor and polycondensation reaction occurred between LA with GA **(Triphati et al., 2016)**. Before synthesis, LA and GA were taken in the ratio of ~5:1 (wt/wt) and properly mixed at room temperature in the RBF. RBF was kept inside the microwave reactor and inert atmosphere was applied. The reaction parameters such as temperature, reaction time and power were set to 130° C, 45 minutes and 240 watts. To prevent the condensation of by-products, temperature of the heating belt was

adjusted at 100°C. Finally, the functionalized GA was collected in a sealed bottle. The possible reaction for the synthesis of functionalized GA is displayed in Figure 2.2. FTIR of *F*G has displayed in Figure 2.2 S.Thereafter, a fixed quantity of functionalized GA was dissolved in acetone, magnetic stirred at ~1000 rpm for 6 hours and filtered under vacuum to get the solution which was further utilized.

- ***Possible reaction***

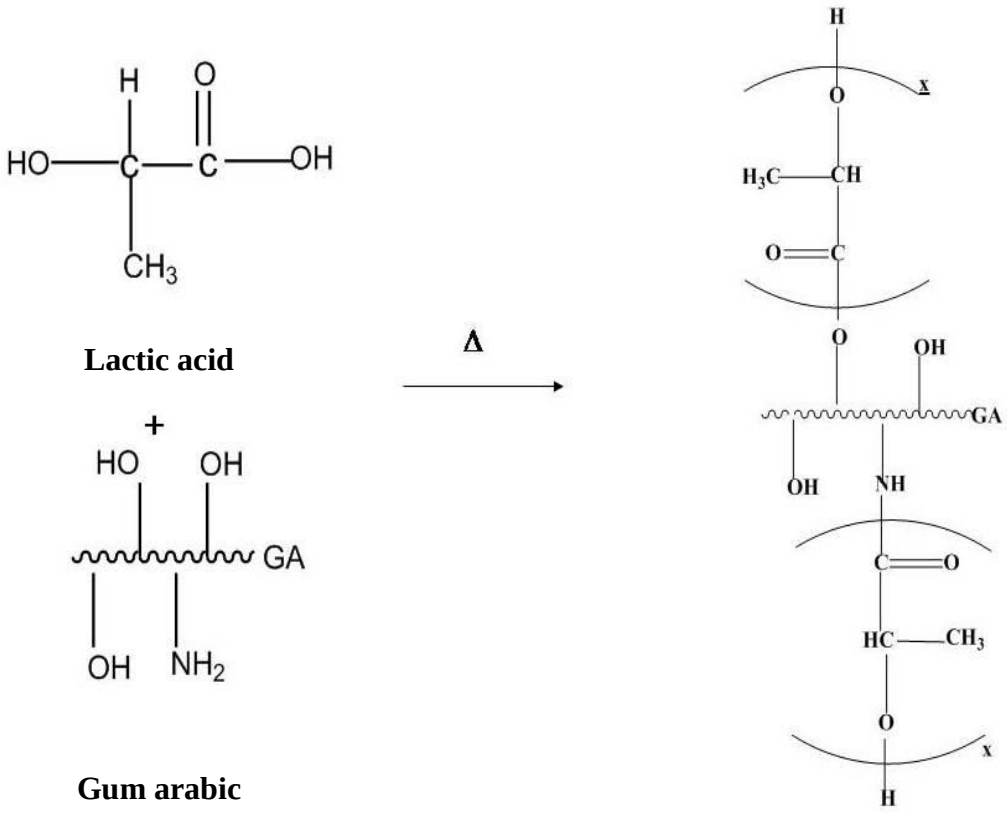

Figure 2.2: *Reaction pathway for the synthesis of functionalized gum arabic*.

2.2.4 *Melt extrusion of PLA/CNC based bionanocomposite films*

PLA (~10g) granules and freeze dried CNC obtained from four different types of acids were pre-mixed at 1 wt % by physical blending and placed in a vacuum oven at 40ºC for ~24 hr to remove the bound moisture. PLA with different acid-hydrolyzed CNC were melt mixed in a twin extruder (Haake Rheomix) which extruded into thin strips at 180ºC, at a screw speed of 50 rpm and 2 min recycle time. Extruded strips with CNC extracted from sulphuric acid

(H_2SO_4), phosphoric acid (H_3PO_4), nitric acid (HNO_3) and hydrochloric acid (HCl) added to the PLA matrix were labeled as PLA-H_2SO_4-CNC, PLA-H_3PO_4-CNC, PLA-HNO_3-CNC and PLA-HCl-CNC nanocomposite.

2.2.5 *Reactive extrusion of PLA/PBS/FCH bionanocomposite films*

PLA and PBS pellets were vacuum dried at a temperature of 40°C overnight to remove the bound moisture. DCP (1 Phr) was dissolved in acetone (10ml) and sprayed on PLA/PBS (80:20wt %) blend. The DCP coated PLA/PBS blend were mixed with filtered *F*CH (1 and 3wt%) and left at room temperature to remove the trapped acetone before processing, followed by drying in a vacuum oven at 60°C. Then PLA/PBS/*F*CH pellets with and without DCP were melt mixed using twin extruder (Haake Mini Lab II, Thermofisher Scientific), processing temperature and screw speed were set at 185°C and 60 rpm respectively for ~5 min. Hereafter, PLA/PBS based bionanocomposite extruded with and without DCP having different loadings of *F*CH (1 and 3wt%) are denoted as PLA/PBS (80/20), PLA/PBS/1*F*CH (80/20/1), PLA/PBS/3*F*CH (80/20/3), PLA/PBS/D/1*F*CH (80/20/1/1) and PLA/PBS/D/3*F*CH (80/20/1/3). Finally, the extruded strips were used for testing.

2.2.6 *Reactive extrusion of PLA/FG bionanocomposite film*

Before the extrusion, PLA pellets were dried in an oven set at the temperature of 40 °C for 24 hr to make sure that bound moisture was removed. DCP was dissolved in acetone and sprayed on PLA and left for drying. After this, *F*G was compounded with DCP coated PLA, followed by vacuum drying in order to remove the trapped acetone for better dispersion of DCP between the PLA and *F*G surface. PLA/FG with and without addition of DCP were melt mixed using Haake Mini Lab II twin extruder (Thermofisher Scientific) at 180°C. The screw speed and recycle time were set at 60 rpm and 240s respectively. DCP amount was fixed at 1 wt % of the total weight of PLA. The ratio of PLA, *F*G and DCP (D) used in the formulation is represented in parentheses, e.g. in the notation PLA (100), PLA/1*F*G (100/1), PLA/3*F*G

(100/3), PLA/D/*F*G (100/1/1) and PLA/D/3*F*G (100/1/3) respectively.

2.3 ANALYTICAL INSTRUMENTATION AND CHARACTERIZATION

2.3.1 *Fourier transform infrared spectroscopy (FTIR)*

IR spectra of samples were collected by Spectrum FTIR (Frontier, Perkin Elmer, and USA) in transmission mode with attenuated total reflectance (ATR) assembly. Extruded strip was placed on zinc selenium (ZnSe) based crystal surface in the wave number range (4000-700 cm^{-1}) with 16 scans at a 4cm^{-1} resolution for the analysis. A background spectrum was collected prior to analysis to compensate the influence of humidity and carbon dioxide presence in air by subtracting the spectra.

2.3.2 *Gel permeation chromatography (GPC)*

The number average (M_n), weight average molecular weight (M_w) and polydispersity index (PDI) of samples were calculated using analytical GPC technique which is calibrated with polystyrene (PS) standards. The GPC apparatus (UFLC, SCHIMADZU, Japan) is equipped with a refractive index (RI–10A) detector, at set injection volume of sample (40 µL) and eluent flow rate of ~1mL min^{-1}. The fixed amount of sample was dissolved in 1.5 mL of HPLC Chloroform for 24 hr and filtered through a non-sterile polytetra fluoroethylene (PTFE, pore size 0.25 µm) syringe filter.

2.3.3 *Gel content (%)*

HPLC grade chloroform was used for the removal of unreacted part, since it is considered as a good solvent for PLA, PBS and *F*CH but not appropriate for crosslinked structure. The amount of gel from the extruded strips was obtained by washing it in excess chloroform for ~12 hr, after that suspension was vacuum filtrated and gel washed several times to remove the unreacted portion. Finally, the gel was collected and vacuum dried at ~40°C to remove the chloroform. The gel content (%) was calculated using the Equation 2.1:

$$\text{Gel content (\%)} = (W_{gel}/W_o)X\ 100 \qquad (2.1)$$

where W_{gel} is the weight of gel after vacuum drying and W_o is the initial weight of strips.

2.3.4 *Field electron scanning electron microscopy (FESEM)*

FESEM (ZEISS, USA) was used to examine the fractured behavior of the extruded strips at an accelerating voltage (~2−5 kV). After tensile testing, the cross-section of the film strips were mounted on a stub using carbon tape and sputter coated with thin layer of gold for ~180 sec under vacuum before analysis.

2.3.5 *Field electron transmission electron microscopy (FETEM)*

FETEM (JEM-2100, JEOL, USA) was used to evaluate the phase morphology at 200KV. The samples were prepared in chloroform (grade HPLC) followed by magnetic stirring for minimum 2 hr to obtain uniform dispersion. The solution was filtered and casted on grids (Tedpell, USA) in droplet form and dried for ~24 hr at 60 °C and then characterized.

2.3.6 *Wide angle X-Ray diffraction (XRD)*

Wide angle XRD measurements were carried out using diffractometer (D8 Advance, Burker, Germany) equipped with Ni−filtered Cu−Kα radiation (λ=0.1541 nm). The operating sources (receiving & diverging slits) were set at 40 kV and 40 mA at scan rate ~2 sec step^{-1} in the 2θ range of ~3−50°. Film strips were annealed at 60 ^{o}C for 6 hr prior to analysis. The diffractogram inbuilt software was used to deduct the peaks. Crystallinity indexes (I_{CR}) of polymer composites were determined using the following Equation 2.2:

$$I_{CR} = \left(\frac{A_c}{A_C + A_a}\right) X\ 100 \qquad (2.2)$$

Where A_c and A_a represent the area of crystalline and amorphous peak.

2.3.7 *Differential scanning calorimetric (DSC)*

The calorimetric measurement of sample was subjected to DSC (NETZSCH, Germany) equipped with a liquid nitrogen cylinder required for cooling. Indium was used to check the calibration according to the standard before the sample analysis. For PLA/*F*G based reactive

bionanocomposite, heating and cooling scan rate was 5°C min^{-1} during DSC experiments. The strips were heated from 25 to 180 °C, held for 3 min to remove the previous thermal history followed by cooling to 25 °C. Then the specimens were reheated from 25 to 180°C. For PLA/PBS/*F*CH based reactive bionanocomposite, sample was kept in platinum crucible and heated from – 50 °C to 200 °C at a scanning rate of 10 °C min^{-1} under nitrogen (50 ml min^{-1}) atmosphere, held in the isothermal state for 2 min at 200 °C to erase the thermal history. Sample was then cooled to −50 °C with the same scan rate to understand the crystallization behavior. Then, it was heated again to 200 °C with the scan rate as that of first heating cycle. The reported data was obtained from the first cooling and second heating cycle. The crystallization temperature (T_c), melting temperature (T_m) and cold crystallization temperature (T_{cc}) were determined from endothermic and exothermic peaks. The heat of fusion (ΔH_f) and crystallization enthalpy (ΔH_c) were calculated from the area of melting and crystallization peak. For calculating the percentage of crystallinity (% X_c), the used standard heat of fusions (ΔH_m^o) for pure PLA and PBS are 93.0J g^{-1} and 110.0 J g^{-1} respectively.

2.3.8 *Universal testing machine (UTM)*

The mechanical properties (elongation at break, tensile strength and modulus) of the strips were measured using UTM KIC 2-050-C (Kalpak Instrument, India) equipped with load cell (500 N) at a speed of 5mm min^{-1}. The dimension of the specimens was set 50 mm in length and 5 mm in width according to ASTM D 882. Three specimens were tested for each sample and average value was reported with the standard deviation.

2.3.9 *Contact angle (CA) analyzer*

Hydrophobicity quantification was performed using CA analyzer (Kruss DS 25, Germany). The sessile drop method used to measure the static contact angle by depositing a drop of mili pore water on the film substrate at various locations. Measurement of each samples (~2 x 2 cm^2) repeated at least three times and sufficient time was provided for the drop to get settle

before angle measurement.

2.3.10 *UV-Visible spectrophotometer*

Optical transmittance of samples (25 x 15 mm^2) was measured using a UV-visible spectrophotometer (Lambda 25, Perkin Elmer, and USA) over the wavelength range 250-1100 nm. The transmittance spectrum was analyzed in presence of air as reference medium.

2.3.11 *Polarized optical microscopy (POM)*

POM analysis was carried out to investigate the growth rate and nucleation density of PLA crystals with POM eclipse (LV100N POL, Nikon Co., Japan) instrument. The film samples (~ 0.3 mg) were sandwiched between two glass slides to make thin film at 190 °C. For PLA/FG reactive bionanocomposite, the samples were first melted by hot stage (Linkam TST350, Linkam scientific instrument, UK) at 190 °C with 50 °C min^{-1} and held for three minutes. The morphologies of the prepared films were observed at three different temperatures of 120, 130 and 140 °C respectively. In case of PLA/PBS/*F*CH based reactive bionanocomposite, samples were first melted by hot stage at 185 °C with 50 °C min^{-1} and held for three minutes. After this, the samples were cooled rapidly to different temperature (i.e. 126 °C and 140 °C) with same rate and placed at isothermal conditions on a hot stage for 20 min.

2.3.12 *Rheological investigation*

Rheological properties were determined using an interfacial rheometer (Anton Par MCR 301), a parallel plate (diameter 25 mm) at 190 °C. The experiments were performed in the linear viscoelastic region, and strain rate (~5%) was applied. For PLA/PBS blend and their nanobiocomposites, the measurements were performed using dynamic frequency sweep mode (frequency range ~ 0.1 to 600 rad s^{-1}). The space between the parallel plates was maintained at 0.1 mm and a constant temperature of 190 °C was fixed for approximately 10 min, to eliminate the thermal history of polymer prior to the analysis. Polymer melt was uniformly

dispersed between the plates without any trapped air bubbles. Dynamic strain sweep tests were performed to observe the linear and nonlinear viscoelastic region of polymer melt.

2.3.13 *Thermogravimetric analyzer (TGA)*

Thermal stability of the samples was calculated by TGA **(**4000 Perkin Elmer, USA) in order to acquire knowledge about its thermal behavior. The measurements were carried out in the temperature range of 30° to 600 °C at 10 °C min^{-1} under N_2 inert atmosphere. Non isothermal TGA kinetic study of film samples was determined by TGA 4000 (Perkin Elmer, USA) in order to get more insight into its decomposition behavior. The measurement was performed at various heating rates of 5, 10, 15 and 20 °C min^{-1} under N_2 atmosphere.

2.3.14 *Hyphenated TGA-FTIR*

TGA system coupled with Frontier FTIR (Perkin Elmer, USA) spectrometer was used to evaluate the thermal decomposition of gaseous product from the IR spectra. The spectra were collected at same temperature range at 10 ºC min^{-1}, and the gaseous products were transferred to FTIR by transfer line TL 8000 maintained at flow rate of 50 ml min^{-1}. FTIR cell window and transfer line were heated at a constant temperature of 260 ºC to avoid condensation of gaseous products and the spectra were scanned from region 4000 cm^{-1}- 450 cm^{-1} with 4 cm^{-1} resolution.

2.4 THERMAL DEGRADATION KINETICS AND CALCULATIONS

Thermogravimetric analysis (TGA) is a beneficial thermal technique to investigate the degradation kinetics parameters and mechanism **(Papageorgiou et al., 2014)**. To investigate the TG kinetics of polymeric system, thermal decomposition process was considered as irreversible type of reaction. For the systematic investigation, nonisothermal kinetic modeling helped for the better understanding of the decomposition behavior of all the systems and conducted a quantitative result from the TGA data. For this, TGA data at dynamic heating regime had been analyzed using model-free kinetic approach to speculate the effect of

biofiller on polymeric system. TGA is the most accepted tool for calculating the thermal stability, degradation kinetic triplets such as activation energy (E_a), rate constant (k) and pre-exponential factor (A). Generally, the kinetics practice of polymer decomposition can be demonstrated using the following rate Equation 2.3 which was mentioned by **Dhar et al., 2014**:

$$\frac{d\alpha}{dt} = k(T)\, f(\alpha) = A \exp\left(\frac{-E_a}{RT}\right) f(\alpha) \quad (2.3)$$

where α means the extent of conversion, $\frac{d\alpha}{dt}$ indicates the decomposition rate, k(T) expressed the temperature based rate constant and f(α) denoted the typical differential expression of various kinetic model functions, which relied on specific decomposition mechanism. A indicates the pre-exponential factor (s^{-1}), T denotes the absolute temperature (K), R for the universal gas constant (J mol^{-1} K^{-1}) and E_a denotes the activation energy (kJ/mol). It can be defined by the given expression in Equation 2.4:

$$\alpha = \frac{(w_o - w_T)}{(w_o - w_f)} \quad (2.4)$$

where w_o was the initial weight, w_t was the weight at temperature T and w_f was the final weight of the samples.

For non-isothermal TGA kinetic study, substituting the heating rate (β_i = dT/dt) and rearranging the Equation (2.3), one can get the Equation (2.5) in which the temperature-dependent degradation rate defined as follows which was shown by Ref. **(Manafi et al., 2015)**:

$$\left(\frac{d\alpha}{dT_i}\right) = \frac{A}{\beta_i} \exp\left(\frac{-E_a}{RT_i}\right) f(\alpha) \quad (2.5)$$

and

$$g(\alpha) = \frac{A}{\beta_i} \int_0^T \exp\left(\frac{-E_a}{RT_i}\right) dT \quad (2.6)$$

Equation (2.5) incapable to solve using analytical solution and it can be rewritten as:

$$g(\alpha) = \frac{AE}{R\beta_i}\left[\exp\frac{(-x)}{x} - \int_x^{\infty}\exp\left(\frac{-x}{x}\right)\,dx\right] = \frac{AE}{R\beta_i}\,p(x) \qquad (2.7)$$

where x (= E_a/RT) was the reduced activation energy. The function p(x) can be changed by different approximations. Thermal degradation of the polymer nanocomposite was a complex reaction phenomenon, since the appropriate selection of a kinetic model or combination of models was crucial parameter to get reliable information. Thermal degradation kinetic information of polymeric material was crucial for evaluating the times and temperatures associated with processing, service lifetimes, and storage of material. In order to evaluate these parameters, models with various assumptions had been suggested to simplify the complexity of the decomposition process. Generally model free kinetic study was selected where the validity of determination of transformation rate was limited or where some unreliability over baseline of the TG data exits, as compared to other models. Model free (Flynn-Wall-Ozawa: FWO, modified Coat-Redfern: CR and Kissinger) methods can provide the most reliable approach for the estimation of E_a of polymeric system.

2.4.1 *Flynn Wall Ozawa (FWO) method*

FWO was an integral isoconversional method which quantifies the distribution of E_a as α without prior comprehension to decomposition mechanism **(Onus et al., 2011; Valapa et al., 2015)**. This method was utilized for TGA kinetic interpretations of complex degradation mechanism. Using Doyle's approximation ($lnp(x) \cong -5.3305 - 1.025x$), this data can be integrated and solution of integration after logarithms was represented in Equation (2.8) which was valid for $(20 \leq x \leq 60)$ (Fan et al., 2004).

$$\log\beta_i = \left\{\log\frac{AE_a}{g(\alpha)R} - 2.315\right\} - \frac{0.457E_a}{RT_i} \qquad (2.8)$$

The distribution of Ea with α can be estimated based on the slope (-0.457 Ea/RTi) of the

straight line.

2.4.2 *Modified Coat–Redfern (CR) method*

Modified CR has both the features of the Friedman (Papageoriou et al., 2014) and Coats-Redfern (CR) **(Yildirim et al., 2012)** method for analyzing the data series at several heating rates using the Equation 2.9 **(Volli et al., 2014)**. The plotting of $\ln\left(\frac{\beta_i}{T_\alpha{}^2}\right)$ versus $-1/T_\alpha$ provide a series of straight linear fits for each α to obtained E_a from the slope. Also, A can be determined from the intercept by simply putting known value of E_a for each α.

$$\ln\left(\frac{\beta_i}{T_i{}^2}\right) = \ln\left[\frac{-AR(1-2RT_i/E_a)}{E_a\ \ln(\alpha)}\right] - \frac{E_a}{RT_i} \tag{2.9}$$

2.4.3 *Kissinger Method*

Kissinger method was based on model free approach with no necessity to determine E_a for each α in order to easily obtain triplet kinetic parameter (E_a, A and n) and thermodynamic variables (ΔG, ΔH and ΔS) **(Chrissafis et al., 2011; Baloch et al., 2011)**. This method was based on the fact that the reaction rate, dα/dt reached maximum at the T_m to calculate activation energy. Kissinger method relied on the following Equation 2.10:

$$ln\left(\frac{\beta_i}{T_m^2}\right) = \left[\ln\frac{AR}{E_a} + \ln\{n(1-\alpha_m)^{n-1}\}\right] - \frac{E_a}{RT_m} \tag{2.10}$$

where n was the reaction order, T_m was the temperature at which the maximum weight loss occurs and α_m was the value of conversion degree at this point of the thermal decomposition curves. Making assumption according to Kissinger $\ln\{n(1-\alpha_m)^{n-1}\}$ was independent of the heating rate. So the following Equation (2.11) was obtained:

$$\ln\left(\frac{\beta_i}{T_m^2}\right) = \ln\frac{AR}{E_a} - \frac{E_a}{RT_m} \tag{2.11}$$

The apparent E_a was obtained from the slope of $\ln(\beta_i/T^2_m)$ against $-1/T_m$ (= E/R) at multiple heating rates for each conversion.

2.4.4 Thermodynamic parameters

Entropy of activation (ΔS) is specified as the difference between of the entropy of activated complex and the sum of entropies of the reactants in chemical reaction. Entropy of activation energy is calculated using the following Equation 2.21 (Nair et al., 2007).

$$\Delta S = R\left[\ln\left(\frac{Ah}{kT_m}\right)\right] \quad (2.21)$$

Where k ($1.38x10^{-23}$ m^2 kg/ s^2 K^1) and h ($6.626x10^{-34}$ m^2 kg/s) are Boltzmann constant and Planck's constant respectively, T_m is the temperature at which maximum weight loss occurs in the DTG curve. The remaining thermodynamic parameters **(Mallakpour et al., 2009; Pan et al., 2016)** Gibbs free energy (ΔG) and enthalpy of activation (ΔH) are estimated using Equation (2.22) and Equation (2.23) respectively.

$$\Delta G = \Delta H - T_m \Delta S \quad (2.22)$$

$$\Delta H = E_a - RT_m \quad (2.23)$$

2.5 PREDICTION OF DEGRADATION MECHANISM

2.5.1 *Criado method*

Kinetic (E_a, A) parameters calculated by Kissinger method were used in Criado method to predict the solid state reaction mechanism of samples. Equation (2.12) was used for obtaining the experimental plots as a function of α is driven by **Criado et al., 1989**:

$$Z(\alpha)_{exp} = \frac{E_a}{R}\frac{d\alpha}{dT_\alpha} e^{E_a/RT_\alpha} p(x) \quad (2.12)$$

Where p(x) was the typical form of temperature integral (see Equation 2.13). It was well described using a 4th order rational expression given by Senum and Yang which showed error lower than 10^{-5} % (x>20) **(Tiptipakorn et al., 2007)**.

$$p(x) = \frac{e^{-x}}{x}\left(\frac{x^3+18x^2+86x+96}{x^4+20x^3+120x^2+240x+120}\right) \quad (2.13)$$

The master $Z(\alpha)$ versus α plots of various degradation mechanisms listed in Table 2 **(Pilawka et al., 2014)**, were obtained according to Equation (2.14),

$$Z(\alpha)_{\text{theortical}} = \frac{\beta}{A}\, g(\alpha) \frac{d\alpha}{dT_\alpha} e^{\frac{E_a}{RT}} \tag{2.14}$$

Comparing experimental $Z(\alpha)$ plot with the master plots lead to precise determination of the mechanism involved during the thermal degradation process

2.5.2 *Established master plots*

The established kinetic equation proposed by Ozawa **(Ozawa et al., 1965)** was utilized to interpret the master plots that showed validity for the experimental plots obtained under any heating rate **(Gotor et al., 2000)**. Thus, reduced time (θ) **(Ozawa et al., 1986)** was defined by Equation 2.15:

$$\theta = \int_0^t \exp\left(-\frac{E_a}{RT_\alpha}\right) dt \tag{2.15}$$

While considering the integral of Equation 2.2, it can be mentioned that θ indicated the time required for attaining a specific value of α at infinite T and the following expression can be obtained by differentiating Equation 2.15:

$$\frac{d\theta}{dt} = \exp\left(-\frac{E_a}{RT_\alpha}\right) \tag{2.16}$$

After a combination of Equation (2.3) and Equation (2.16), the following Equation (2.17) got

$$\frac{d\alpha}{d\theta} = Af(\alpha) \tag{2.16}$$

This can be rearranged, as described in Equation 2.18,

$$\frac{d\alpha}{d\theta} = \frac{d\alpha}{dt} \exp\left(-\frac{E_a}{RT_\alpha}\right) \tag{2.18}$$

Where $\frac{d\alpha}{d\theta}$ denotes the generalized reaction rate

According to the differential form of the generalized kinetic equation, the relationship between the experimentally obtained data and generalized kinetic rate can be accomplished, using α at 0.5 (reference point), from Equation 2.19:

$$\frac{d\alpha/d\theta}{(d\alpha/d\theta)_{0.5}} = \frac{d\alpha/dt}{(d\alpha/dt)_{0.5}} \frac{\exp(E_\alpha/RT_\alpha)}{\exp(E_\alpha/RT_{0.5})} \quad (2.19)$$

Thus, $T_{0.5}$ denoted the reaction temperature when α=0.5.

The master plots of degradation mechanisms listed in Table 2.1, can be determined according to Equation 2.20:

$$\frac{d\alpha/d\theta}{(d\alpha/d\theta)_{0.5}} = \frac{f(\alpha)}{f(0.5)} \quad (2.20)$$

Thereafter, the master plots have been compared with the experimental plot for obtaining the mechanism of the decomposition process under any heating rate, Equation 2.20 should be reliable for the analysis of TG data. Further, it was independent of the temperature profiles under which they were obtained **(Sanchez-Jimenez et al., 2010)**. As displayed in Table 2.1, the algebraic expressions that showed the degradation mechanism of polymers divided into five categories: nuclei formation and growth (A_n), reaction mechanism controlled by the surface (R_n), diffusion phenomena depend on heat transfer (D_n), random degradation of nuclei (F_n) and random chain scission (L_n) for thermal decomposition process **(Sanchez-Jimenez et al., 2010; Khawam et al., 2006)**.

Table 2.1: Algebraic expressions for f (α) and g (α) for the most widely used mechanism of the solid state process.

Mechanism-Solid State Processes	***f*(α): differential form**	***g*(α): integral form**
A2-Nucleation and growth (Avrami–Equation 1)	$2(1-\alpha)[-\ln(1-\alpha)]^{1/2}$	$[-\ln(1-\alpha)]^{1/2}$
A3-Nucleation and growth (Avrami-Equation 2)	$3(1-\alpha)[-\ln(1-\alpha)]^{2/3}$	$3(1-\alpha)[-\ln(1-\alpha)]^{2/3}$ $[-\ln(1-\alpha)]^{1/3}$
A4-Nucleation and growth (Avrami-Equation 3)	$4(1-\alpha)[-\ln(1-\alpha)]^{3/4}$	$[-\ln(1-\alpha)]^{1/4}$
R2- Phase boundary controlled reaction (Contracting Area)	$2(1-\alpha)^{1/2}$	$[1-(1-\alpha)^{1/2}]$
R3- Phase boundary controlled reaction (Contracting Volume)	$3(1-\alpha)^{2/3}$	$[1-(1-\alpha)^{1/3}]$
D1 - One dimensional diffusion	$1/2\alpha$	α^2
D2-Two dimensional diffusion (Valensi equation)	$[-\ln(1-\alpha)]-1$	$[(1-\alpha)\ln(1-\alpha)]+\alpha$
D3-Three dimensional diffusion (Jander equation)	$3(1-\alpha)^{2/3} / [2(1-(1-\alpha)^{1/3})]$	$[1-(1-\alpha)^{1/3}]^2$
D4-Three dimensional diffusion (Ginstling-Brounsthein equation)	$[1-(2/3)\alpha] -(1-\alpha)^{2/3}$	$(3/2)[1-(1-\alpha)^{1/3}]^{-1}$
F1- Random nucleation with one nucleus on the individual particle	$(1-\alpha)$	$-\ln(1-\alpha)$
L=2 minimum chain length of polymer during the random Chain scission	$\alpha(1-\alpha)$	No symbolic solution

Chapter 3

Thermal Degradation Kinetics of Poly (lactic acid)/ Different Acid Hydrolzed Cellulose Nanocrystals based Bionanocomposite Films

This chapter demonstrates the thermal decomposition behaviour of poly (lactic acid) (PLA) and different acid hydrolyzed cellulose nanocrystals (CNC) based bionanocomposite films. As we know that CNC presents rod like morphology with tunable aspect ratio, high hydroxyl functionality which makes its ideal choice as reinforcing filler. Introduction of different acid hydrolyzed CNC in PLA matrix shows the enhanced phyiso-chemical properties. In general, PLA and hydrophilic CNC based bionanocomposites are susceptible to thermal decomposition at high temperature during melt mixing. Hence the influence of CNC on the thermal properties of PLA based bionanocomposite films are important to investigate the thermal stability, kinetic parameters and decomposition mechanism in details to confirm its suitability for packaging application without showing serious thermal decomposition process.

The work in this chapter is published as:

Monika, Dhar, P. & Katiyar, V. (2017) *Thermal degradation kinetics of poly (lactic acid)/acid fabricated cellulose nanocrystals based bionanocomposites. International Journal of Biological Macromolecules, 104, 827-836. DOI:10.1016/j.ijbiomac.2017.06.039.*

ABSTRACT

Cellulose nanocrystals (CNC) are fabricated from filter paper (as cellulosic source) by acid hydrolysis using different acids such as sulphuric (H_2SO_4), phosphoric (H_3PO_4), hydrochloric (HCl) and nitric (HNO_3) acid. The resulting acid derived CNC are melt mixed with polylactic acid (PLA) using twin screw extruder at 180°C. Thermogravimetric (TGA) result shows an increase in 10% and 50% weight loss (T_{10}, T_{50}) temperature for PLA-CNC film fabricated with HNO_3, H_3PO_4 and HCl derived CNC which are found to have improved thermal stability in comparison to H_2SO_4-CNC. Non isothermal kinetic studies are carried out with modified-Coats-Redfern (C-R), Flynn-Wall-Ozawa (FWO) and Kissinger method to predict the kinetic and thermodynamic parameters. Subsequently the prediction of these parameters leads to the proposal of thermal induced degradation mechanism of bionanocomposite film using Criado method. The distribution of E_a calculated from FWO model are (PLA-H_3PO_4-CNC: 125-139 kJ mol^{-1}), (PLA-HNO_3-CNC: 126-145kJ mol^{-1}), (PLA-H_2SO_4-CNC: 102-123 kJ mol^{-1}) and (PLA-HCl-CNC: 140-182 kJ mol^{-1}). This difference among E_a for the decomposition of PLA-CNC bionanocomposite is probably due to various acids used in this study. The E_a calculated by these two methods are found in consonance with that observed from Kissinger method. Hyphenated TG-Fourier transform infrared spectroscopy (FTIR) result shows that gaseous products such as CO_2, CO, lactide, aldehydes and other compounds are given off during the thermal decomposition of PLA-CNC bionanocomposite films.

Graphical Abstract

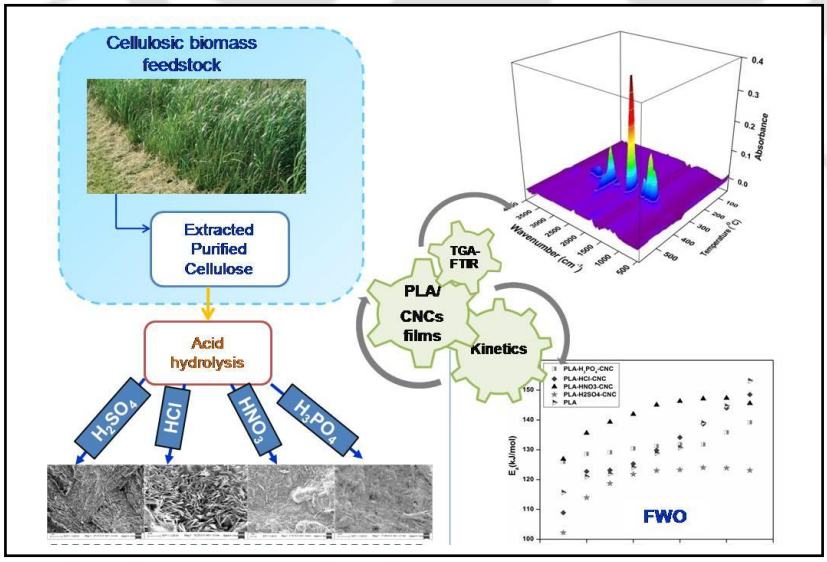

Scheme 3.1 : *Schematic representation of thermal decomposition behavior of PLA/CNC bionanocomposite.*

3.1 INTRODUCTION

Increasing consumer demands, environmental and economic concerns have lead manufacturers and scientists to replace the conventional petrochemical based synthetic polymers with renewable bio-based materials **(Wu et al., 2005)**. So far, the synthetic polymers derived from fossil feedstock can be replaced by bio based and biodegradable polymers such as poly (lactic acid) (PLA), poly (butylene succinate) (PBS), poly (hydroxybutyrate) (PHB) and poly (ε-caprolactone) (PCL) at industrial level **(Nerantzaki et al., 2014)**. However, PLA is one of the representative bio-plastics which have been commercialized in the market because of its relatively high strength, high modulus, good biocompatibility and easy processability **(Kamal et al., 2015)**. It is an aliphatic polyester derived from renewable plant resources such as corn, sugarcane and sugar beet etc. Various industries are focusing on the development of sustainable packaging technologies for manufacturing of renewable biofiller based PLA products (for e.g. Cellulose, Starch etc) to make it cost effective in comparison to conventional petrochemical based polymers **(Yang et al., 2009)**. PLA has low thermal stability, slow degradation rates and poor toughness, which limits its potential use in the packaging field. In order to attain these objectives, incorporation of bio-based nanofillers into the PLA matrix may lead to the development of sustainable packaging along with significantly amended properties of the PLA bionanocomposites.

Among various bio-based nanofillers, the potential of cellulose nanocrystals (CNCs) as a reinforcement material in the PLA matrix has been explored over a few decades **(Goffin et al., 2011; Sullivan et al., 2015)**. CNCs have rod-like structures **(Dhar et al., 2016)** that are obtained from native cellulose by isolating the crystalline domains which have high degree of crystallites. CNCs are obtained from most abundant renewable biomass resources and exhibit exceptional characteristics such as unique physical, chemical properties, renewability, biodegradability and sustainability **(George et al., 2015)**. Various routes for fabrication of

CNC included acid hydrolysis, enzymatic hydrolysis and hydrolysis assisted by ultrasound as well as high pressure homogenization **(Filson et al., 2009)**. Among them, acid hydrolysis is the most widely used method to remove the amorphous segment which is usually carried out under controlled conditions. Morphology and physiochemical characteristics of CNC can be affected by some crucial parameters such as acid type, process time, temperature, variation in acid concentration and acid to solid ratio during acid hydrolysis **(Peng et al., 2011; Habibi et al., 2010)**. Therefore, these parameters must be optimized and controlled in order to achieve the desired and targeted properties of CNC such as tuned morphology, aspect ratio, physico-chemical and structural properties. During the past few decades, significant efforts have been made towards reinforcing PLA with CNC using different processing methodologies such as solvent casting **(Petersson et al., 2007)** blow molding, melt spinning **(Garcia et al., 2016)** and extrusion **(Bondson et al., 2017)**. However, in the solvent casting process utilization of the large volume of solvent during bionanocomposite preparation increases the environmental concern and limits its commercialization potential. In addition, it is known that the incorporation of CNC in small loading fraction into the PLA matrix leads to the production of bio-based composites having high performance including improved transmittance and heat deflection temperature (HDT) **(Spinella et al., 2016)**. Although, processing of PLA-CNC by melt extrusion is a promising technique for nanocomposite fabrication at large scale, uniform dispersion of hydrophilic CNC into hydrophobic PLA matrix still remains a challenging task **(Habibi et al., 2008; Barun et al., 2012)**. In general, PLA is susceptible to thermal decomposition at the elevated temperature during the extrusion which leads to the decrease in properties such as molecular weight reduction. At elevated temperature, segments of the polymer chains start to separate and react with one another to change the physical and mechanical properties of the material **(Carrasco et al., 2013)**. Hence the effects of different acid hydrolyzed CNC on the thermal properties of PLA bionanocomposites are important to

understand the processing of PLA. It is important to note that processing of PLA should be carried out without serious thermal degradation in order to make the bionanocomposite suitable for packaging application with enhanced properties **(Gotor et al., 2000; Perinovic et al., 2010)**. In this study, CNCs have been fabricated using sulphuric acid (H_2SO_4), nitric acid (HNO_3), phosphoric acid (H_3PO_4) and hydrochloric acid (HCl) after the hydrolysis of native cellulose derived from filter paper. CNC from various types of acids have quite divergent characteristics such as morphology and aspect ratio. Both these parameters have a significant role in improving the dispersion as well as tuning the thermo-mechanical properties of the PLA matrix.

The current work focuses on the degradation kinetics of the fabricated PLA-CNC bionanocomposite films using TGA measured at the different heating rates. The influence of different acid hydrolyzed CNC on degradation mechanism of PLA based bionanocomposite is determined using Criado approach. Hyphenated TGA-FTIR is carried out to quantify the release of the volatile gaseous products during thermal decomposition **(Huang et al., 2015)**. Furthermore, this study provides enough information to choose the PLA-acid hydrolysed CNC based bionanocomposites that are the most stable during melt processing without suffering significant decomposition during extrusion.

3.2 RESULTS AND DISCUSSION

- ***FESEM of PLA/different Acid Hydrolyzed CNC based bionanocomposite films***

CNC fabricated using different acid sources such as sulphuric, nitric, phosphoric and hydrochloric acid leads to the modification of its hydroxyl group with respective anionic moieties of acids during hydrolysis process at different relative weight fractions. The degree of protonation of acids depend on their dissociation constants, thereby altering the extent of degradation of amorphous segments, extracting the crystalline domains of cellulose with comparatively different physiochemical and morphological characteristics **(Dhar et al.,**

2016). As shown in Figure 3.1, CNCs fabricated from sulphuric acid have rod-like morphology with distinct needle structures with the morphological dimension of L=1100±80 nm and D=30±11 nm and aspect ratio~36. CNCs with small rod morphology i.e. L=210±25 nm and D=15±4 nm with lower aspect ratio ~14 are formed when hydrochloric acid used as a hydrolyzing agent. CNC fabricated from the phosphoric acid is found to have rice-grain morphology with dimension of L=940±65 nm and D=21±5 nm and aspect ratio of ~44. Thin fibrils like CNC with L=520±45 nm and D=24±12 nm of aspect ratio ~21 are formed when nitric acid is used as hydrolyzing acids. Therefore, CNC fabricated using different acids leads to a significant variation in its morphology as well as physico-chemical properties which leads to variation in their thermal properties as discussed in the subsequent sections.

- ***Thermogravimetric analysis (TGA) of PLA/different acid hydrolyzed CNC based bionanocomposite films***

Thermal stability of PLA-CNC bionanocomposite films with different acid hydrolyzed CNC have been evaluated by TGA. TGA and derivative thermogravimetric (DTG) curves for all samples at 10 ^{o}C min^{-1} are shown in Figure 3.2 (a) and (b) respectively. The profiles of mass loss versus temperature show single stage degradation for all bionanocomposite films **(Yuzay et al., 2010)**. It is clear from the figure that CNC derived from different acids significantly affects the thermal decomposition of the PLA matrix. To better understand the thermal decomposition behavior of samples, the 10% weight loss temperature (T_{10}), 50% weight loss temperature (T_{50}) and 90% weight loss temperature (T_{90}) have been summarized in Table 3.1. These parameters are important as basic fundamentals to predict the effects of different acid derived CNC on PLA decomposition. The T_{10} (340 ^{o}C), T_{50} (358 ^{o}C) and T_{90} (369 ^{o}C) for PLA are taken as reference points. For PLA-HNO_3-CNC and PLA-H_3PO_4-CNC bionanocomposite, T_{10} and T_{50} increase which might be due to the substitution of the hydroxyl groups with anionic moieties from acid CNC leading to tunable surface properties.

These results indicate that PLA-H_2SO_4-CNC bionanocomposite are least thermally stable which might be due to the presence of sulphate groups (SO_4^-) onto the CNC that have a catalytic effect on the bionanocomposite chain of PLA leading to the increase thermal decomposition rate **(Henriquea et al., 2015)**. Improved thermal stability of different acid derived CNC follows the order of CNC-HNO_3 > CNC-H_3PO_4 > CNC-HCl > CNC-H_2SO_4 as reported earlier **(Dhar et al., 2016)**. It is suggested that the reason for the improved thermal stability of the different acid fabricated CNC due to stable bond formation between the carbon and substituted anion (for e.g. bond strength C-N > C-P) or thermal behavior of the substituted anion (for e.g. thermal stability Cl^- > SO_4^-) on the CNC surface (Dhar et al., 2016; Espinosa et al., 2013.Thus, the thermal stability trend for PLA based bionanocomposite follows the order of PLA-HNO_3-CNC > PLA-H_3PO_4-CNC > PLA-HCl-CNC > PLA-H_2SO_4-CNC. It is therefore assumed that the inherent thermal behavior of different acid derived CNC is responsible for variation in thermal properties of PLA-CNC bionanocomposite film.

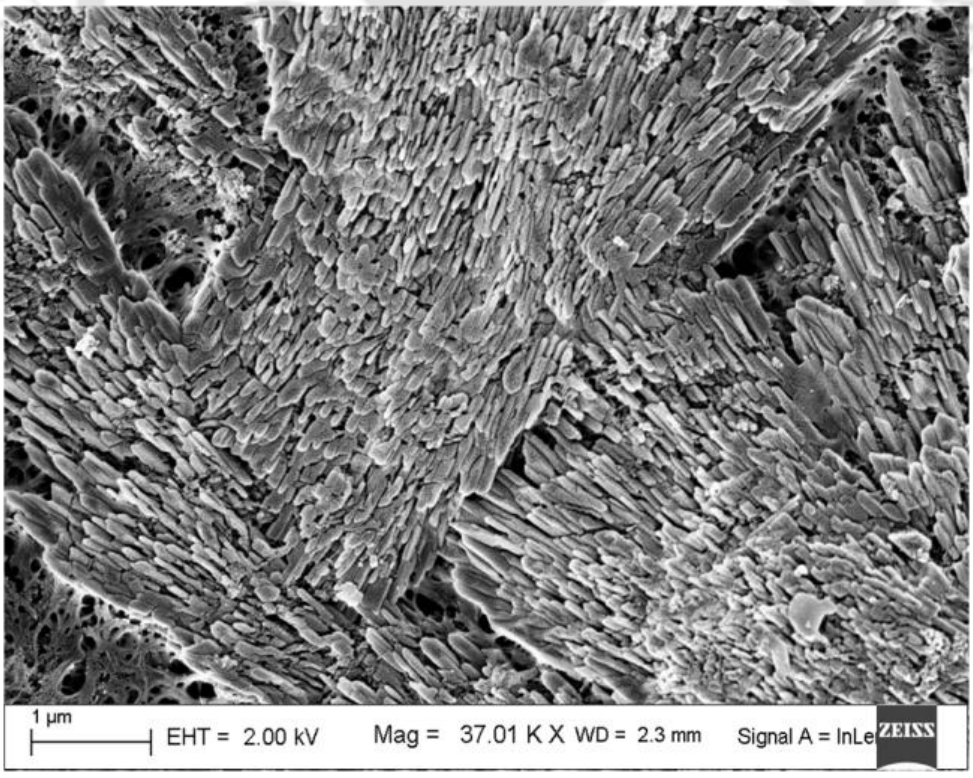

(a)

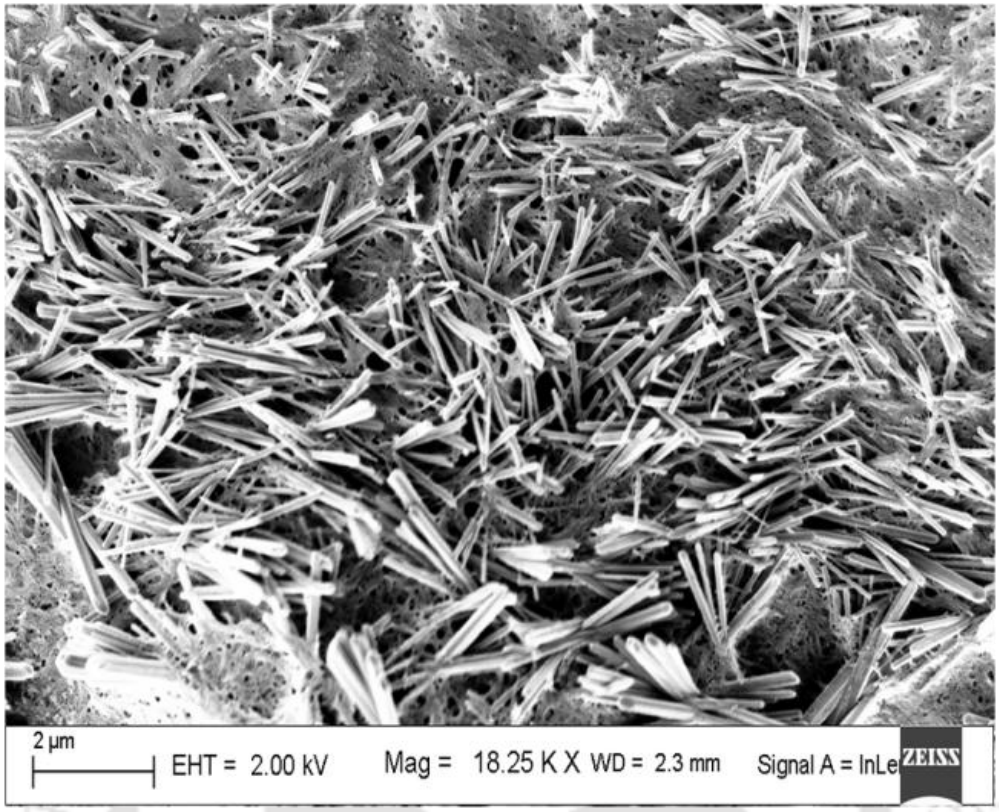

(b)

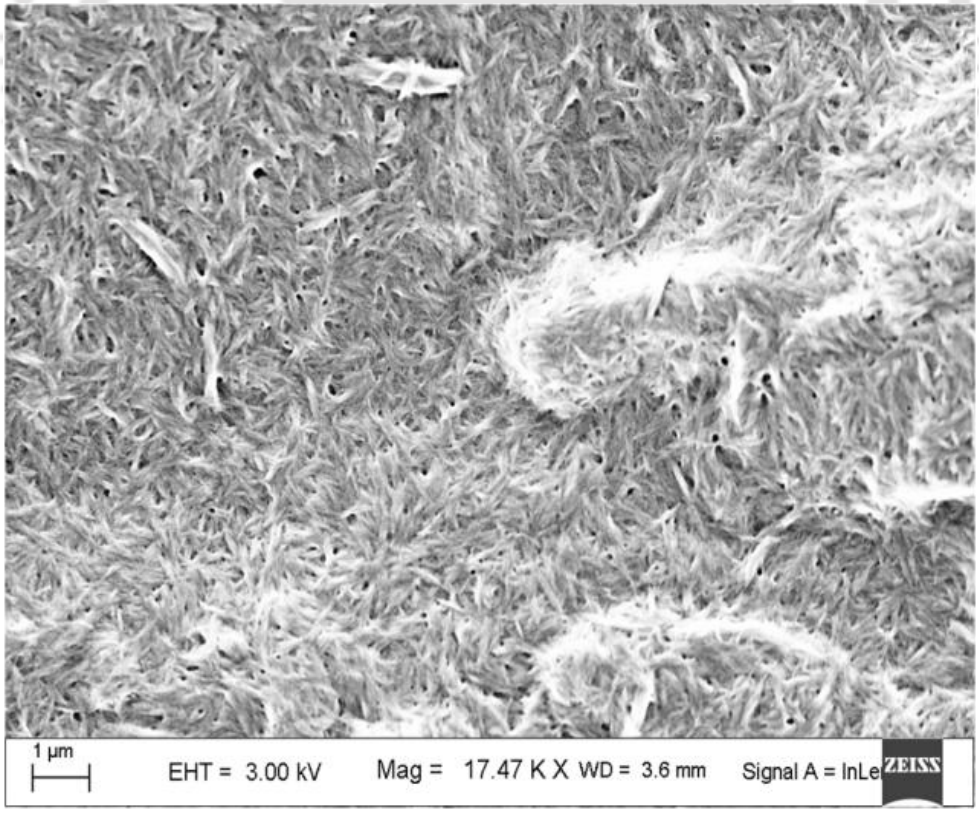

(c)

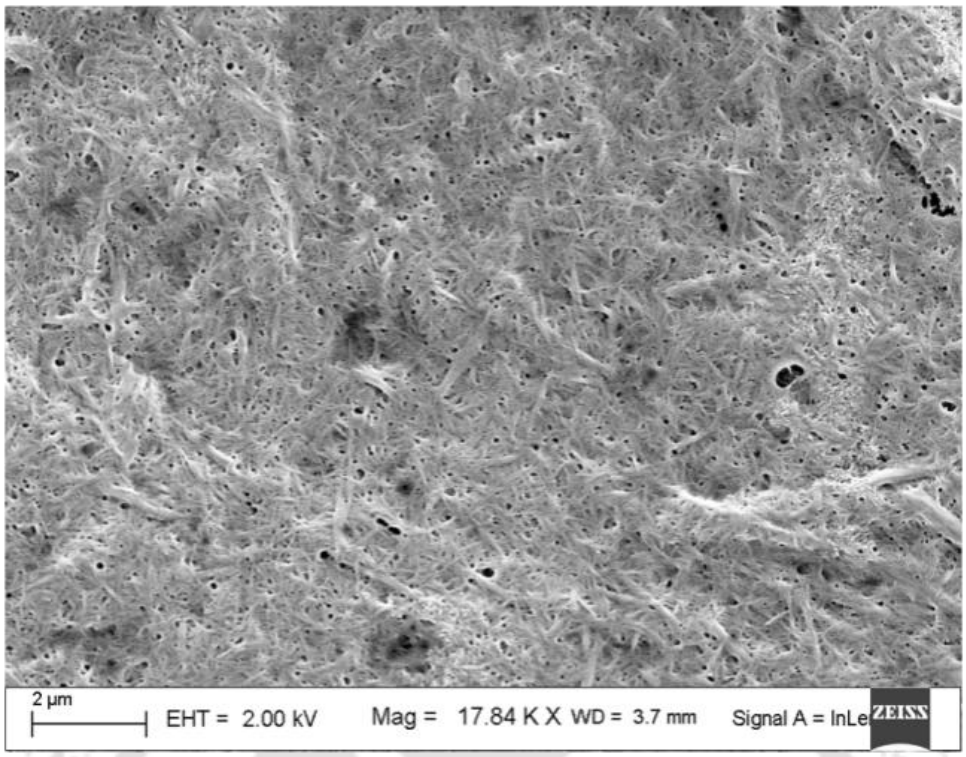

(d)

Figure 3.1: *FESEM micrograph of the CNC after hydrolysis with (a) sulphuric acid (b) hydrochloric acid (c) phosphoric acid (d) nitric acid.*

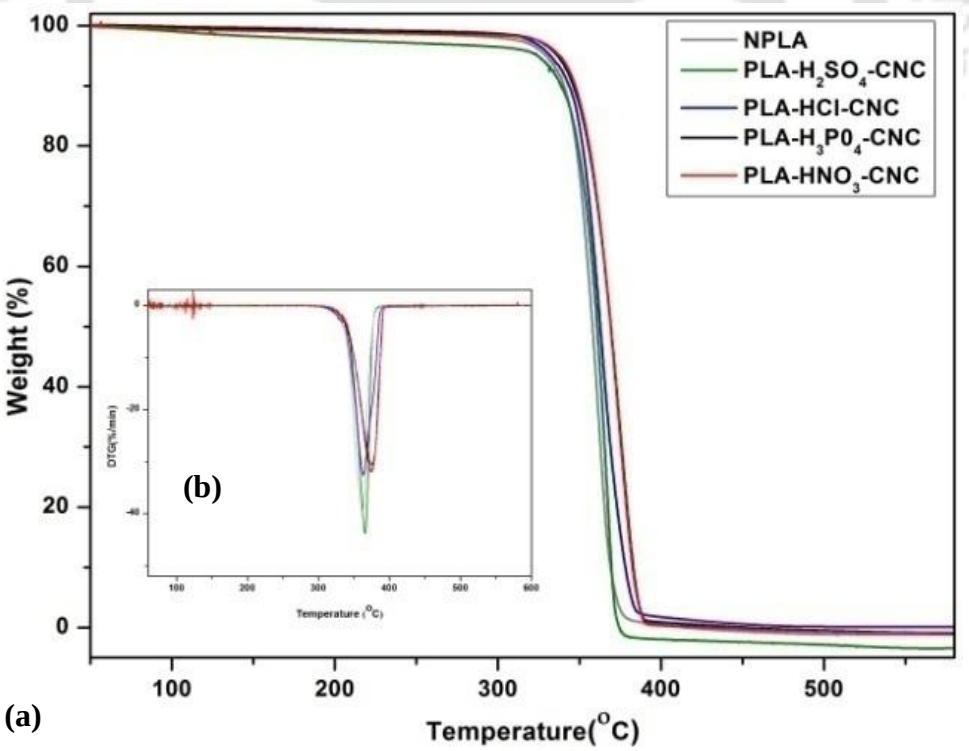

Figure 3.2: *(a) TGA and (b) DTG profiles of PLA with different acid hydrolyzed CNC bionanocomposite films at 10°C min^{-1}.*

Table 3.1: *10% weight loss (T_{10}), 50% weight loss (T_{50}) and 90% weight loss (T_{90}) temperature of PLA-CNC bionanocomposite films at 10°C min^{-1}.*

Sample	T_{10} (°C)	T_{50} (°C)	T_{90} (°C)
PLA	340	358	369
PLA-HNO_3-CNC	347	370	382
PLA-H_3PO_4-CNC	346	368	382
PLA-H_2SO_4-CNC	338	360	368
PLA-HCl-CNC	343	362	378

- ***Nonisothermal degradation kinetics analysis of PLA/different acid hydrolyzed CNC based bionanocomposite films***

TGA is always essential to quantify the weight loss (%), apparent activation energy (E_a), pre-exponential factor (A) and the rate constant (K) of fabricated PLA-CNC bionanocomposite films. In order to systematically investigate the thermal degradation kinetics of PLA-CNC bionanocomposite, we have selected dynamic method under nitrogen atmosphere. Moreover, the thermal degradation kinetic parameter is computed using three different analytical methods such as Flynn wall Ozawa (FWO), Kissinger and modified Coat-Redfern (CR) method. The TGA and DTG plots of PLA and PLA with different acid hydrolyzed CNC based bionanocomposite films at four different heating rates of 5, 10, 15 and 20ºC min^{-1} are illustrated in Figure 3.3. The TGA graphs reveal the various decomposition profiles relying on different heating rate and type of acid utilized. It can be observed from Figure 3.3 (a)-(e) that for all the samples, TGA plots shifted to higher temperature with increasing heating rate which could be attributed to the short time provide for bionanocomposite to attain a specific temperature **(Yuzay et al., 2010; Aboulkas et al., 2008)**. From DTG, it is clear that peak temperature and rate curve shift to higher temperature range with increasing heating rate

because of the faster release of gaseous products (Kan et al., 2016). PLA-5, PLA-10, PLA-15 and PLA-20 means PLA samples are run at 5, 10, 15 and 20ºC/min, respectively.

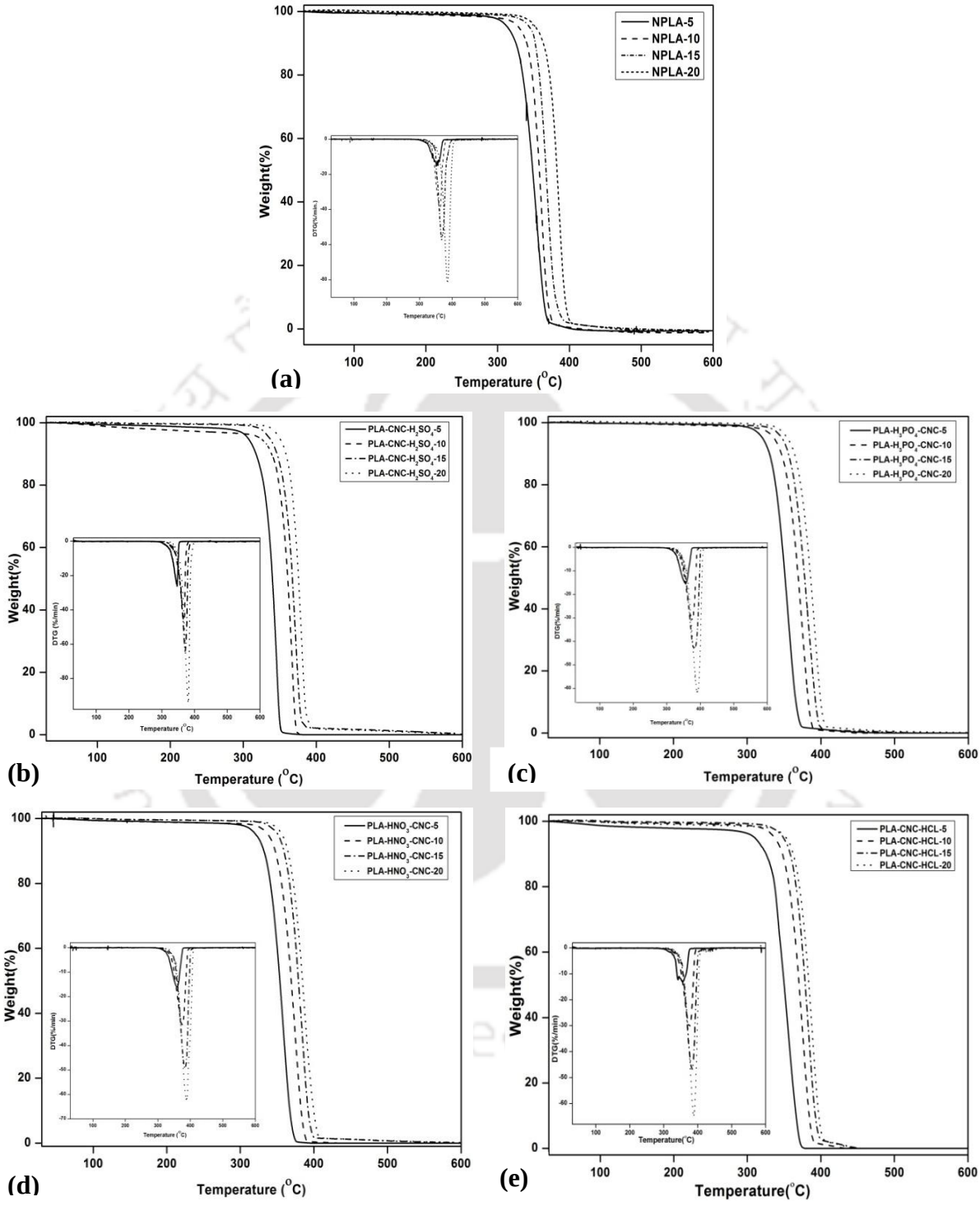

Figure 3.3: *TGA and DTG profiles of samples a) PLA (b) PLA-H_2SO_4 –CNC (c) PLA-H_3PO_4-CNC (d) PLA-HNO_3-CNC and (e) PLA-HCl-CNC bionanocomposite films at different rates of 5, 10, 15 and 20ºC min^{-1}.*

The main step observes the thermal decomposition behavior of PLA and PLA/different acid hydrolyzed CNC bionanocomposite films to estimate the apparent E_a according to the method represented in theoretical approach. The linear fits derived from the graphs using FWO (log β with respect to -1000/T) and modified CR (log β against $-1000/T^2$) method are also displayed in Figure 3.4 (a)-(e) and Figure 3.5 (a)-(e) respectively. It is noticed that straight-lines obtained at conversion ranges (0.1-0.9) are nearly parallel in both the cases. FWO and modified CR methods are well applicable to explore the degradation kinetics of these systems at all level of extent of conversion **(Sinha et al., 2013)**. Table 3.2 has summarized the apparent Ea distribution with conversion (α), correlation coefficient (R^2) using FWO and modified CR for PLA, PLA-H_2SO_4-CNC, PLA-H_3PO_4-CNC, PLA-HNO_3-CNC and PLA-HCl-CNC bionanocomposite films.

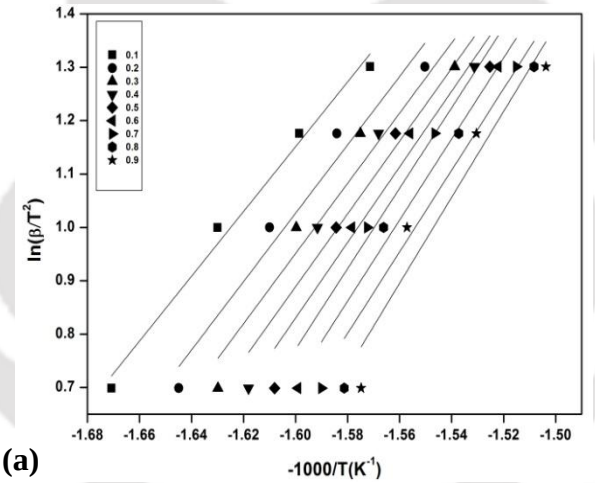

(a)

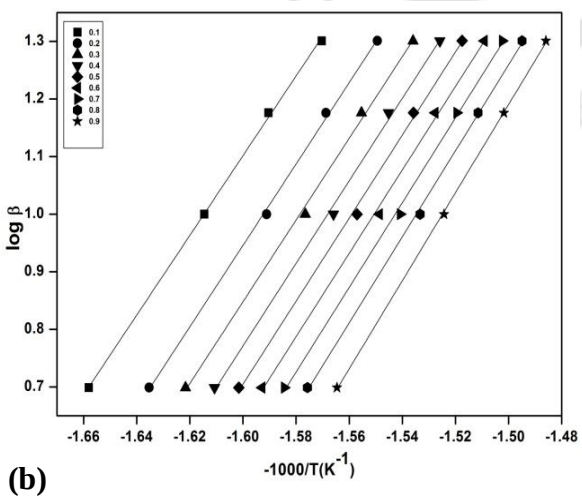

(b)

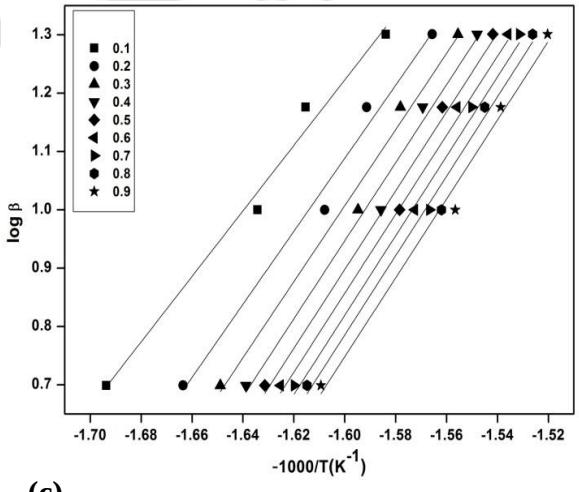

(c)

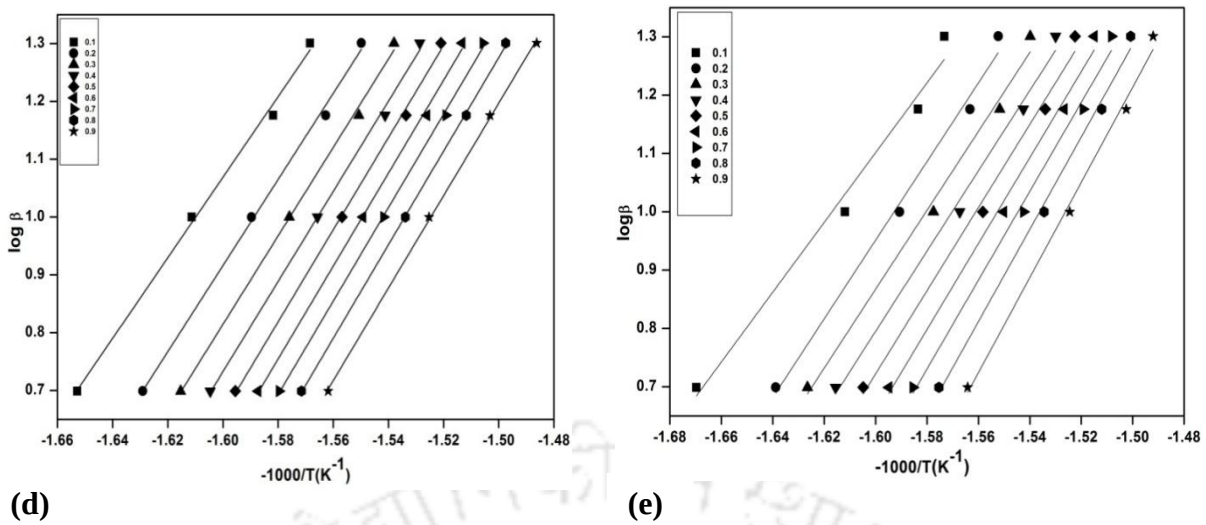

Figure 3.4: *FWO plots for thermal decomposition of (a) PLA, (b) PLA-H_2SO_4-CNC, (c) PLA-H_3PO_4-CNC, (d) PLA-HNO_3-CNC and (e) PLA-HCl-CNC bionanocomposites.*

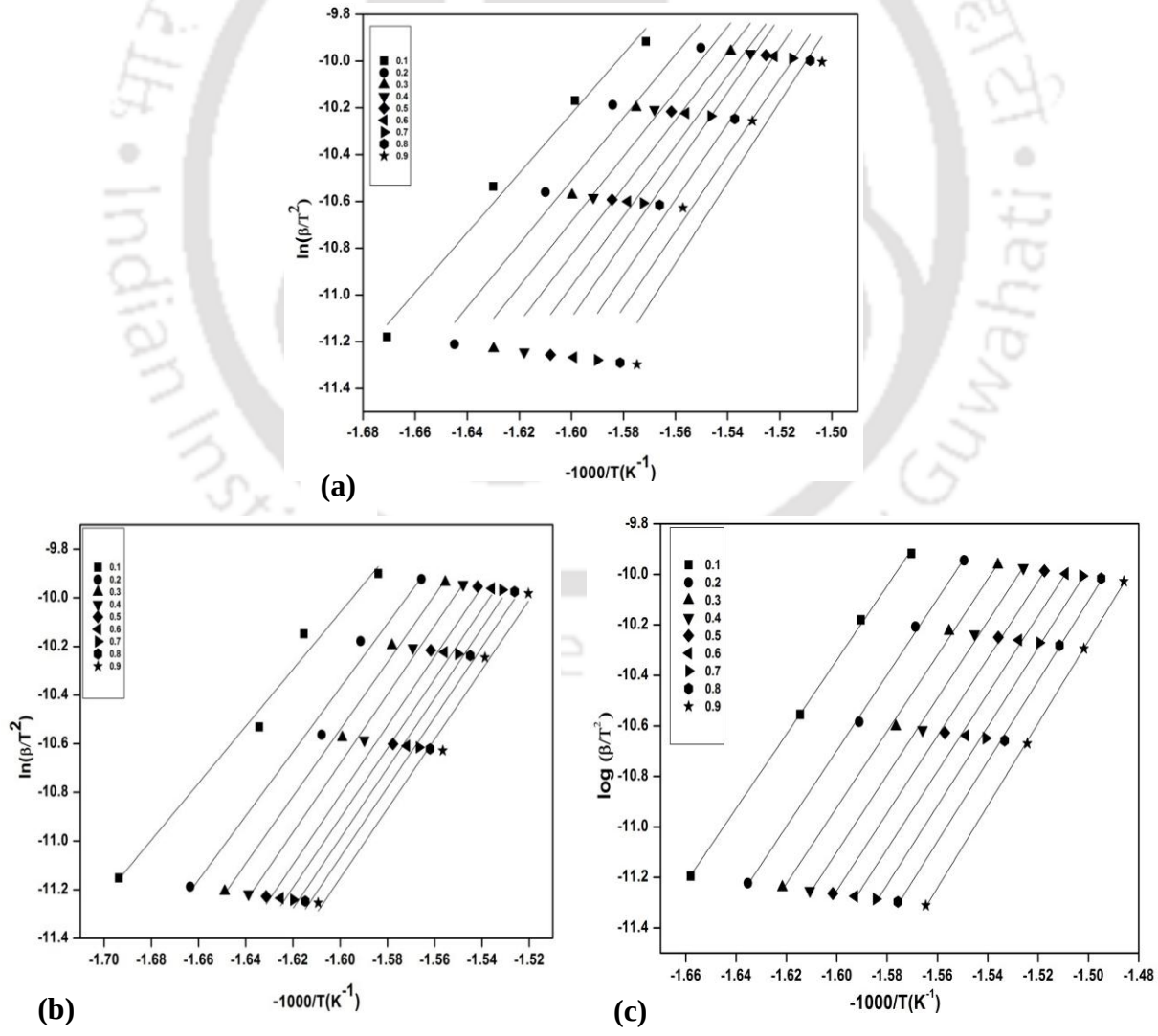

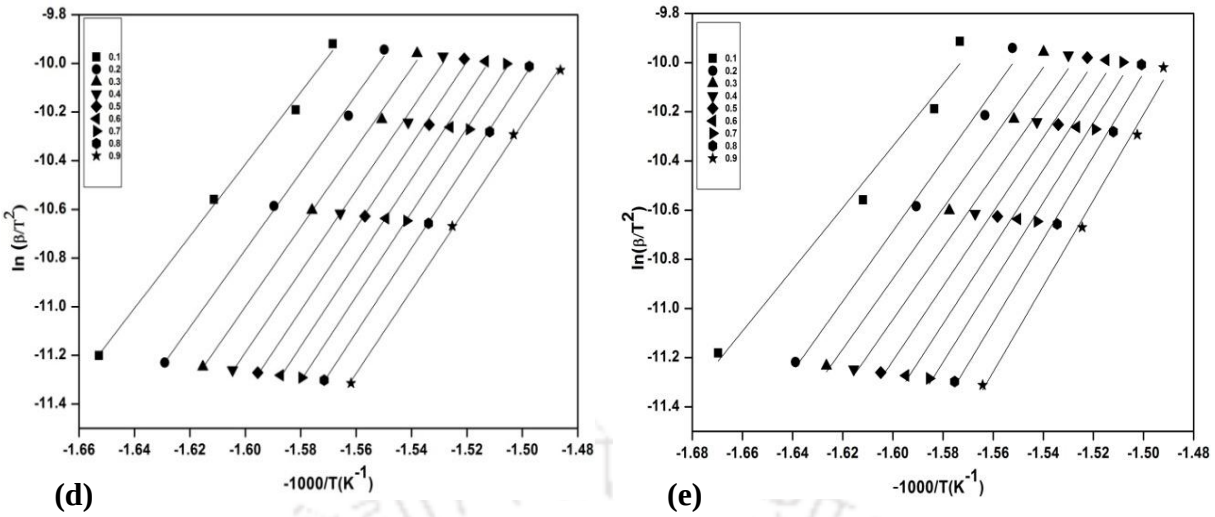

Figure 3.5: *Modified CR plots for thermal decomposition of (a) PLA, (b) PLA-H_2SO_4-CNC, (c) PLA-H_3PO_4-CNC (d) PLA-HNO_3-CNC and (e) PLA-HCl-CNC bionanocomposite films.*

- ***Estimation of activation energy (kJ mol $^{-1}$) for PLA/different acid hydrolyzed CNC based bionanocomposite films***

Figure 3.6 (a)-(b) gives relationship of apparent E_a as a function of mass conversion α obtained by the isoconversional (FWO and modified CR) methods for different acid hydrolyzed CNC with the PLA matrix. For all systems, the variation in the E_a with α has been seen through the thermal decomposition process. This proves that the decomposition process of the nanocomposite is quite different from each-other and not proceeded through the simple way **(Chen et al., 2007)**. For neat PLA apparent E_a has increased gradually with conversion range (0.1-0.9) and similar behavior has also been reported earlier **(Tesfaye et al., 2016)**. This finding confirms that the thermal decomposition of PLA has a complex mechanism including depolymerization, random scission, inter and intra molecular transesterification and cis-elimation **(Valapa et al., 2014)**. As seen in Figure 3.6, apparent E_a are ~102 kJmol^{-1} (α=0.1) for PLA-H_2SO_4-CNC bionanocomposite. It means less energy is required to break bond at the initial level due to the presence of more acidic sites. When $0.1 < \alpha > 0.4$, slight increment in E_a has observed that implies the possible decomposition process of backbone

chain at primary level. When α > 0.3, determined E_a remains almost unchanged which informs that the same type of bond breaks, thereby leading to presence of single-process reaction **(Zong et al., 2005)**. In case of PLA-HNO_3-CNC bionanocomposite, a gradual change in E_a with α noticed. This result confirms that it promotes the complex reaction mechanism **(Dhar et al., 2014)**. It has observed that the value of E_a is the highest in this case because the energy is required for breaking the stable C-N in HNO_3 hydrolyzed CNC. For PLA-H_3PO_4-CNC bionanocomposite, the dependence of E_a on α can be distinct in three regions. In first region (I), ~ 0.2, a slight increment of the E_a is noticed. In the second (II) region (0.2 <α <0.7), E_a is considered to have a constant value, while in the third region (III), for α >0.8, a small changes in E_a is noticed. Such a variation of E_a with α is an evidence of complex process with the participant of at least two different mechanisms **(Huang et al., 2012)**. For PLA-HCl-CNC bionanocomposite, it has noticed that there is a possibility of complex reaction process involving at least two types of mechanisms.

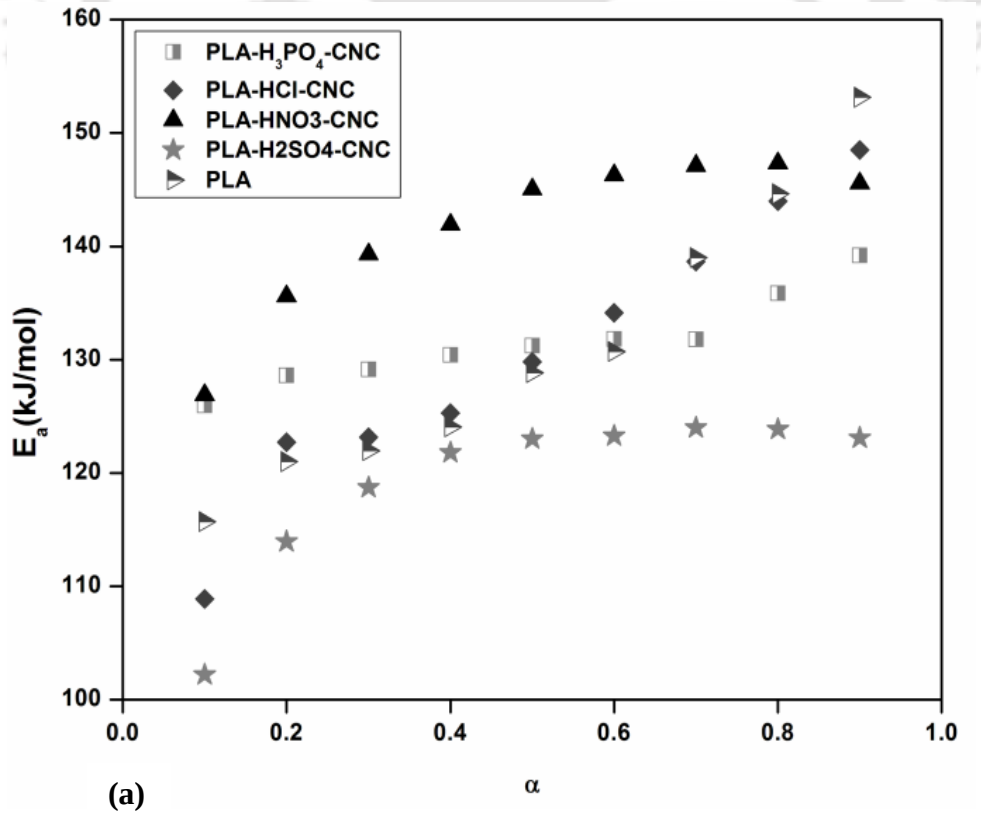

(a)

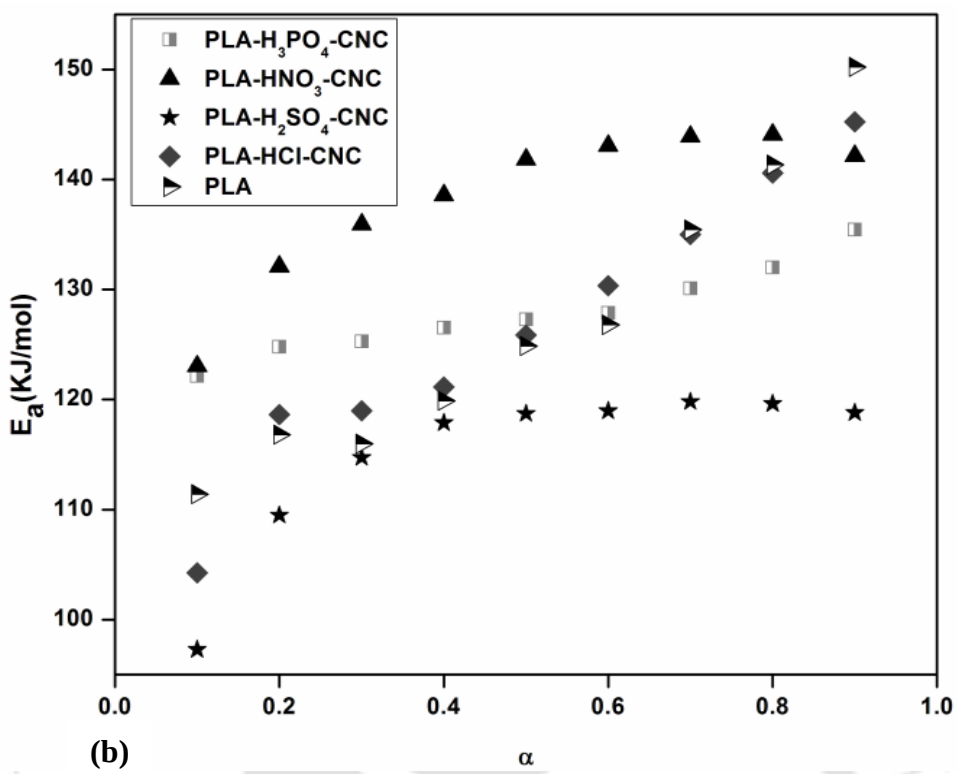

Figure 3.6: *Distribution of E_a (kJ mol^{-1}) vs. α plots for PLA/different acid hydrolyzed CNC based bionanocomposite films using (a) FWO, and (b) modified CR methods.*

Table 3.2: *Apparent activation energy distribution with conversion (α) for all the different acid derived CNC with PLA matrix calculated by FWO and modified CR methods.*

Samples	α	FWO		modified CR	
		E_a (kJ mol^{-1}) (0.1-0.9)	R^2	E_a (kJ mol^{-1}) (0.1-0.9)	R^2
PLA	(0.1-0.9)	115-153	0.928	111-150	0.917
PLA-HNO_3-CNC	(0.1-0.9)	126-145	0.998	123-142	0.997
PLA-H_3PO_4-CNC	(0.1-0.9)	125-139	0.998	122-135	0.998
PLA-HCl-CNC	(0.1-0.9)	108-148	0.992	104-154	0.991
PLA-H_2SO_4-CNC	(0.1-0.9)	102-123	0.986	97-118	0.986

In case of Kissinger method, graph of ln (β/T^2_m) versus -1000/T_m indicates the linear fit as displayed in Figure 3.7 for all PLA-CNC bionanocomposite films. The smooth linear fitted

lines confirm the feasibility of the Kissinger method for PLA-CNC bionanocomposite. Table 3.3 includes the resulting kinetic parameters (E_a, A) and thermodynamic variables (Δ G, ΔH and ΔS), as calculated at T_m for the degradation of the PLA and different acid hydrolyzed CNC based PLA bionanocomposite films.

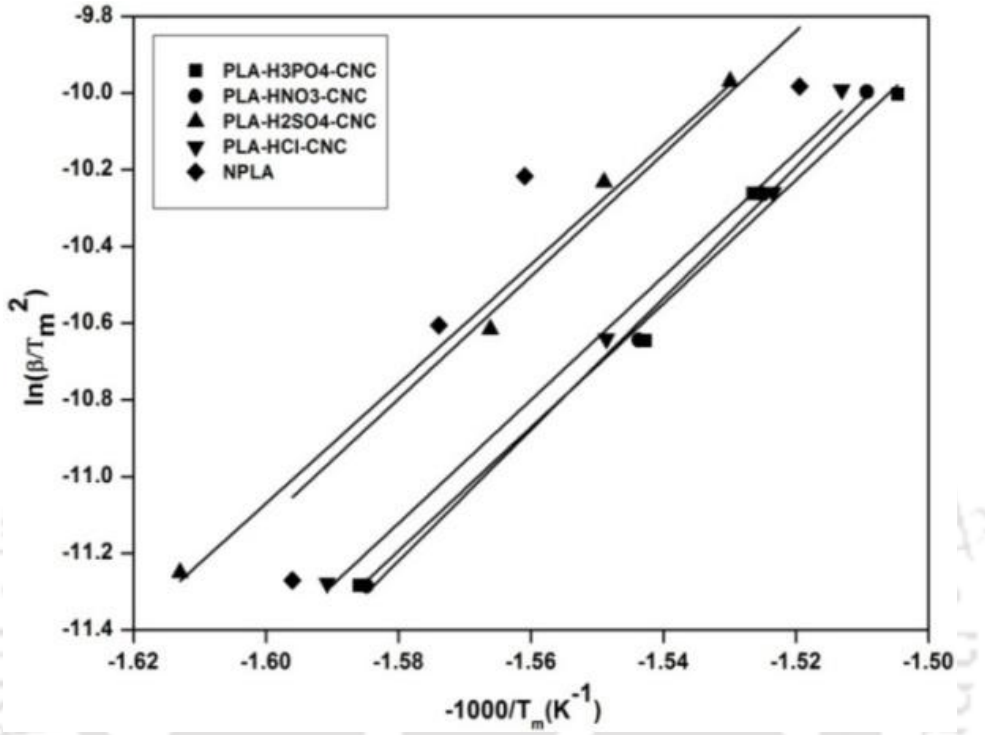

Figure 3.7: *Kissinger plots for thermal decomposition of (a) PLA, (b) PLA-H_2SO_4-CNC, (c) PLA-H_3PO_4-CNC, (d) PLA-HNO_3-CNC, and (e) PLA-HCl-CNC for bionanocomposite films.*

Table 3.4 indicates that the average E_a is estimated from these three methods in good agreement for PLA with the incorporation of different acid hydrolyzed CNC. Increment in the average E_a after the addition of H_3PO_4 derived CNC, HNO_3 derived CNC and HCl derived CNC in the PLA matrix in comparison to H_2SO_4 derived CNC is observed. Different acid hydrolyzed CNC (excluded sulphuric acid derived CNC) have improved thermal stability of the PLA matrix. Results indicate that PLA-H_2SO_4-CNC bionanocomposite has the lowest thermal stability because many hydroxyl (OH) group of CNC are replaced by SO_4 groups **(Teixeira et al., 2010)** to assist thermal degradation of the PLA matrix and it has lead

to the decrement in E_a. The difference in E_a for all samples may be due to the various types of acids employed to hydrolyze the CNC. This finding confirms that PLA-HNO_3-CNC bionanocomposite is more suitable to be used as nano filler as it controls the thermal decomposition of the PLA matrix.

Table 3.3: *Kinetic parameters and thermodynamic variables for the degradation of different acid derived CNC with the PLA matrix using Kissinger method.*

Samples	Kinetic Parameters			Thermodynamic variables		
	E_a ($kJmol^{-1}$)	R^2	A (s^{-1})	ΔG ($kJmol^{-1}K^{-1}$)	ΔH ($kJmol^{-1}$)	ΔS ($kJmol^{1}$)
PLA	132	0.836	1.73E+11	186.5	127.7	-0.0938
PLA-HNO_3-CNC	142	0.997	1.28E+11	233.8	137.0	-0.1534
PLA-H_3PO_4-CNC	133	0.991	2.48E+10	234.0	128.6	-0.1670
PLA-HCl-CNC	133	0.992	1.18E+11	193.7	128.1	-0.9660
PLA-H_2SO_4-CNC	129	0.991	1.62E+10	230.04	124.3	-0.1704

Table 3.4: *Comparison of E_a estimated by FWO, modified CR and Kissinger method.*

Samples	FWO E_a ($kJmol^{-1}$)	Modified CR E_a ($kJmol^{-1}$)	Kissinger E_a ($kJmol^{-1}$)
PLA	131	127	132
PLA-HNO_3-CNC	141	138	142
PLA-H_3PO_4-CNC	131	128	133
PLA-HCl-CNC	130	126	133
PLA-H_2SO_4-CNC	119	115	129

- ***Estimation of thermodynamic variables of PLA/different acid hydrolyzed CNC based bionanocomposite films***

For the different acid hydrolyzed CNC based PLA nanocomposite, an estimated value of ΔG, ΔH has positive sign and ΔS shows negative sign. The negative sign of ΔS confirms that activated complex is formed at elevated temperature when polymer segment undergoes some

chain alignment and degree of product disorder is found lower than the initial degree of disorder of the reactants **(Turmanova et al., 2011)**. The positive values of ΔH suggest that the processes of bond dissociation are found endothermic in nature for all cases **(Mallakpour et al., 2009)**. During the endothermic process, energy of products is always higher than reactants energy and dissociation of bonds increased with ramping temperature. ΔG value for all systems is positive which indicates that dissociation processes are nonspontaneous **(Ramukutty et al., 2014)**.

- ***Degradation mechanism for PLA/Different Acid Hydrolyzed CNC based Bionanocomposite Films***

E_a is calculated by Kissinger method and evaluated thermal decomposition mechanism of PLA bionanocomposite proposed by Criado method. Figure 3.8 (a)-(e) displays the master and experimental curves of PLA-CNC based film. It has shown that the degradation mechanism of PLA follows F3 at conversion range (0.1-0.6). When $\alpha > 0.6$, it tends towards the F2 mechanism.

For PLA-H_2SO_4-CNC bionanocomposite, it proceeds via A2 at conversion range (0.1-0.6). In A_n type mechanism, decomposition has started from the development of nuclei sites that acts as growth centre to propagate the thermal degradation. At $\alpha > 0.6$, mechanisms has changed from A2 to A3 and followed D1 at $\alpha \sim 0.9$. This can promote an acceleration of decomposition by 1-D diffusion which involves heat propagation at the higher temperature.

The degradation mechanism of PLA-HCl-CNC bionanocomposite can be followed either by F2 or A2 at lower α value. When $\alpha > 0.3$, it proceeds via F2. In case of PLA-H_3PO_4-CNC and PLA-HNO_3-CNC bionanocomposite, the thermal decomposition proceeds via A_n type mechanism. The degradation process follows A2 at conversion range (0.1-0.6) and shift towards A4 when $\alpha > 0.6$.

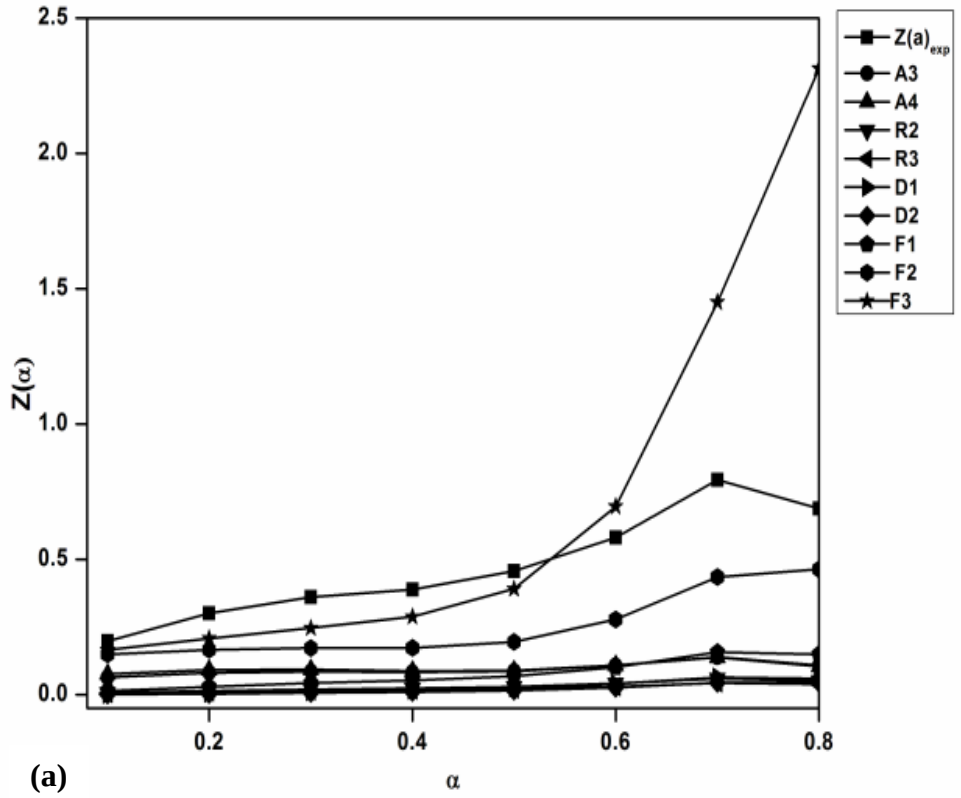

(a)

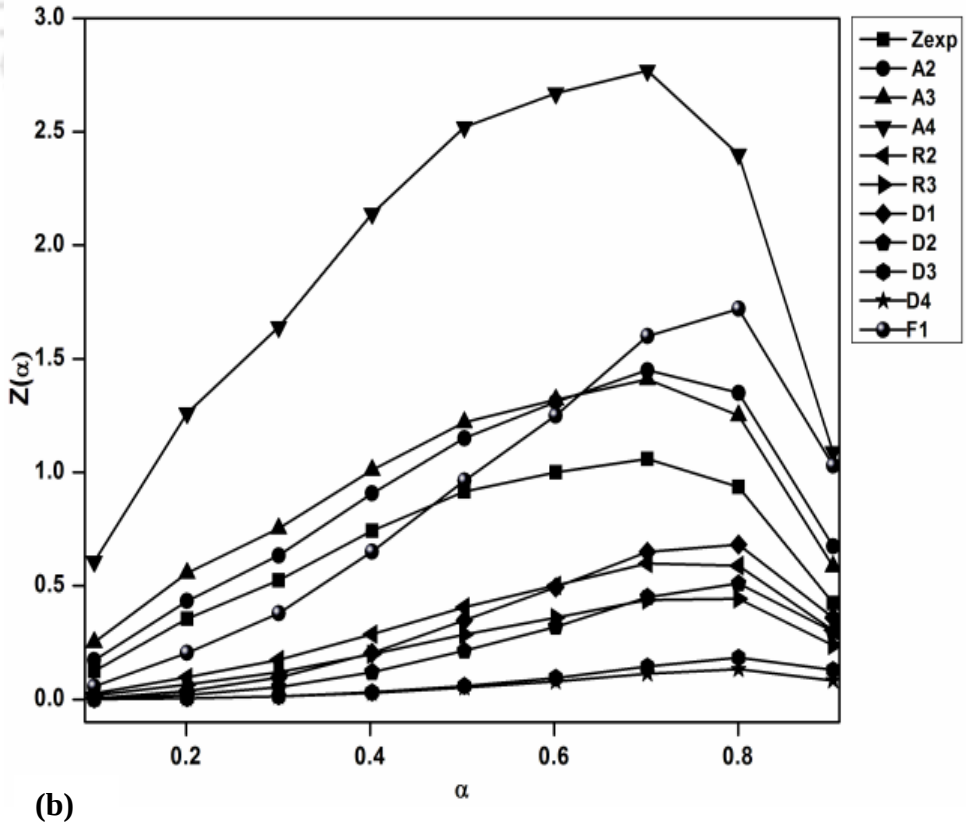

(b)

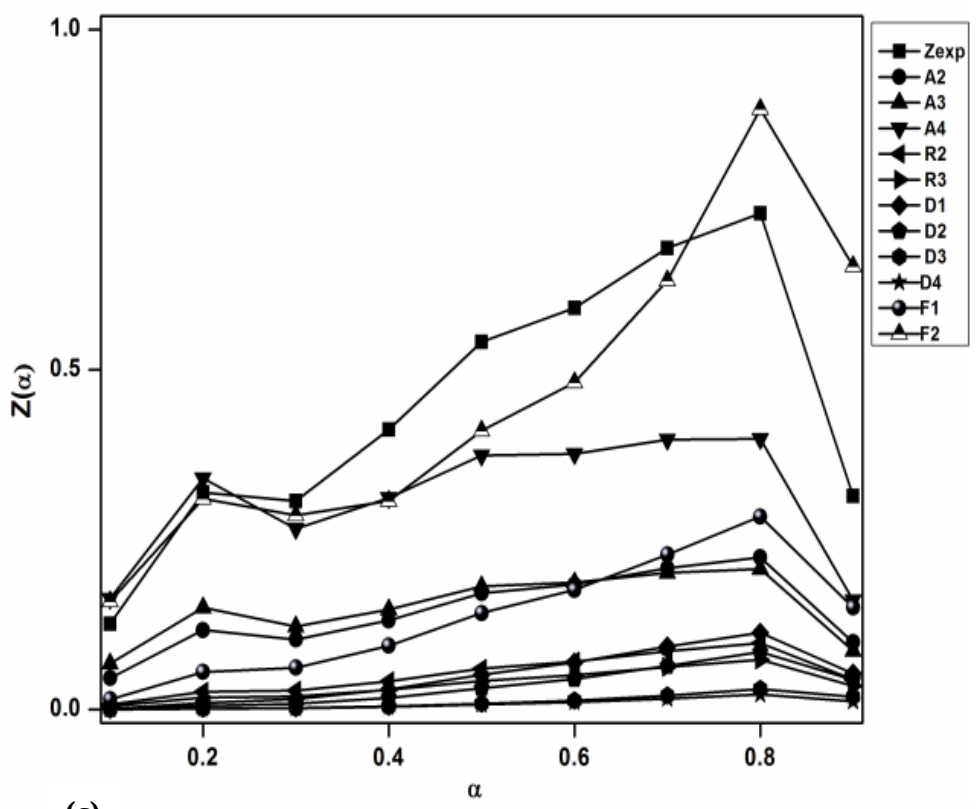

(c)

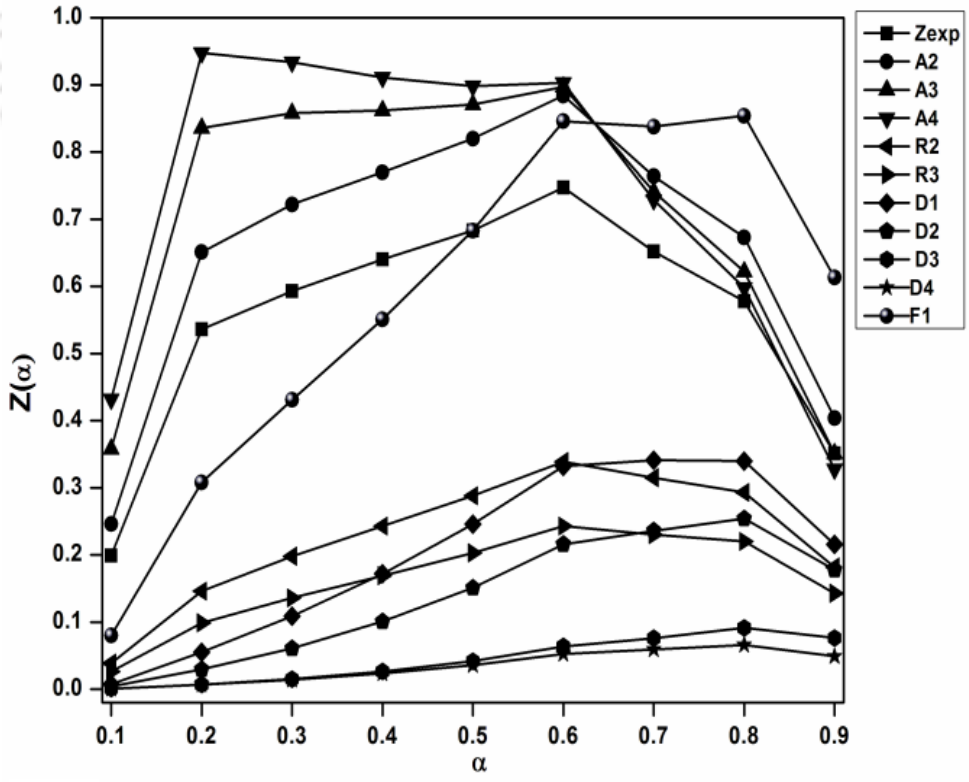

(d)

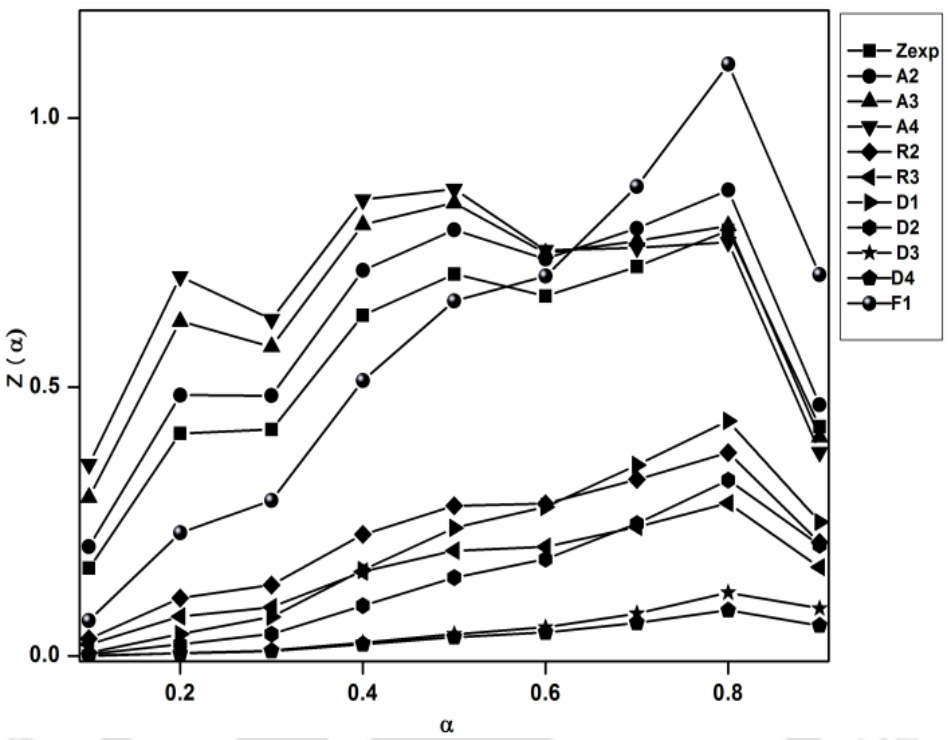

(e)

Figure 3.8: *Criado plots for (a) PLA (b) PLA-H_2SO_4-CNC (c) PLA-HCl-CNC (d) PLA-H_3PO_4-CNC and (e) PLA-HNO_3-CNC based bionanocomposite films.*

3.2.5 *Hyphenated TGA-FTIR Analysis of PLA/Different Acid Hydrolyzed CNC based bionanocomposite Films*

TGA system coupled with Fourier transform infrared (FTIR) spectrometer is a powerful analytic technique that can be beneficial for identification of volatile components released during thermal treatment of polymer nanocomposite **(Zhu et al., 2001; Huang et al., 2015)**. Therefore, TGA-FTIR is utilized in this study to accumulate detailed information to elucidate the reaction mechanisms. In hyphenated TGA-FTIR system, the height of IR peak indicates concentration variation of volatile species.

- ***Release of volatile products from PLA-H_2SO_4-CNC bionanocomposite film***

Figure 3.9 (a) illustrates the 3D and (b) 2D stacked IR spectra for PLA-H_2SO_4-CNC bionanocomposite using TGA-FTIR respectively. Releasing of volatile components is mainly observed at the temperature range of 343 – 470 ºC during decomposition process, which

relates well with TGA data in Figure 3.2. It is noticed that weak band of CO_2 produced due to breakdown of carbonyl group when temperature is above 340 ºC. At 384 ºC, the specific wave numbers of the IR absorption peaks of the main volatile species for H_2SO_4-CNC with PLA matrix have listed as the following **(Vogel et al., 2008; Tudorachi et al., 2012)**: CO_2 at 2358-2309 cm^{-1} (O=C=O asymmetric stretching), 669 cm^{-1}(O=C=O bending), CO at 2178-2108 cm^{-1}(C-O bending), H_2O at 3500-3750 cm^{-1} for (O–H stretching), cyclic oligomer at 935 cm^{-1}, formation of lactide confirmed due to bands located at 3001 cm^{-1}(C-H stretching), 2956 cm^{-1}(C-H asymmetric stretching)-2893 cm^{-1}(C-H symmetric stretching) of CH_3 group, characteristic band at 1792 cm^{-1} (C=O stretching), 1242 and 1106 cm^{-1} (C–O–C stretching). Band at 1456-1375 cm^{-1}(C-H bending) of CH_3 group, high intensity of band at 1762 cm^{-1}(C=O stretching), 2738 cm^{-1}(C-H=O stretching), 2822 cm^{-1}(stretching of C-H) has assigned to acetaldehyde. In this case additional band at 1509 cm^{-1} are related to the aromatic compound. The new advent peaks for ethanol are detected at 1118 cm^{-1} and 1064cm^{-1} related to (stretching of O-H) and (stretching of C-OH) respectively **(Yang et. al., 2007)**. Small release of methanol is confirmed by the presence of a weak band at 1033 cm-1. Result indicates that it follows a random chain scission analysis.

- ***Release of volatile products from PLA-H_3PO_4-CNC bionanocomposite film***

Figure 3.10 (a) represents the 3D and (b) stacked IR spectra for the main degradation process of PLA-H_3PO_4-CNC bionanocomposite from 330 to 470 ºC intervals respectively. Moreover, similar kinds of degradation products have been produced during thermal degradation of PLA-H_3PO_4-CNC bionanocomposite without release of aromatic compound and methanol in this case. This reaction will continue until degradation is finished and confirms the higher amount of lactide monomer released **(Mofokeng et al., 2015; Chianga et al., 2011)**. We believe that deploymerization has dominated reaction route which involves bond rupturing and formations of the new chemical bonds than random chain scission.

- ***Release of volatile products from PLA-HNO_3-CNC bionanocomposite film***

From Figure 3.11 (a)-(b), it is clear that there is no release of gaseous species up to 330ºC. Similarly, lactide, acetaldehyde, CO_2, CO, cyclic oligomers and the small amount of water have been detected at 385 ºC during the thermal degradation of PLA-HNO_3-CNC bionanocomposite film. In this case, it s suggested that decomposition mechanism of PLA has favored by random chain scission.

- ***Release of volatile products from PLA-HCl-CNC bionanocomposite film***

In similar fashion, lactide, acetaldehyde, CO_2, CO, cyclic oligomers and small amount of water have also been detected during thermal decomposition of PLA-HCl-CNC bionanocomposite film. These results confirm that decomposition process governs using depolymerization because the intensity of peak 1792 cm^{-1} (C=O stretching) assigned for lactide is the higher than band located at 1762 cm^{-1} (C=O stretching) for carbonyl compound in this case.

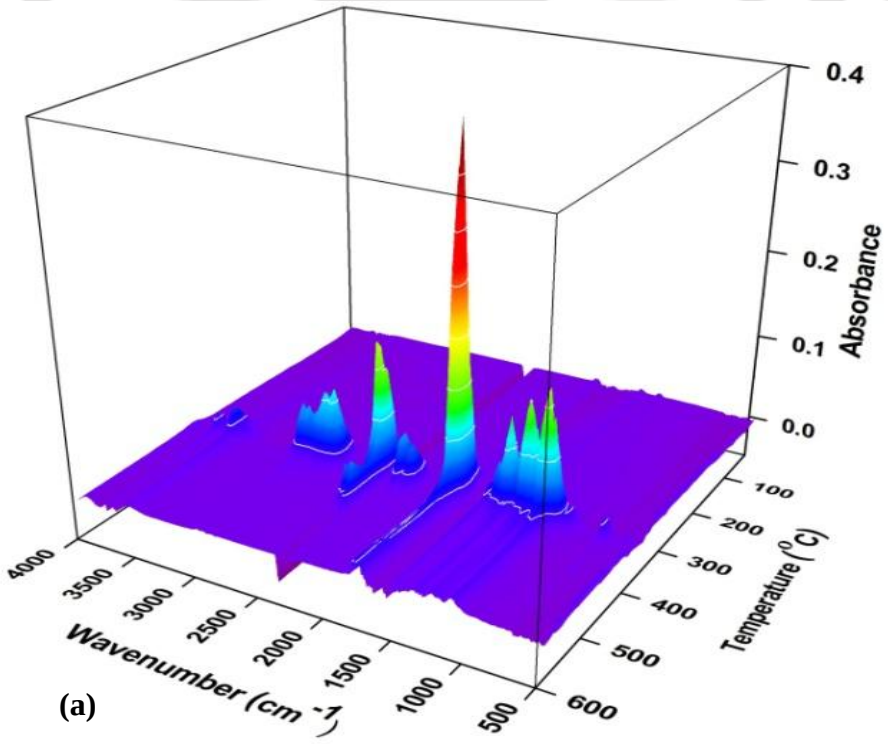

(a)

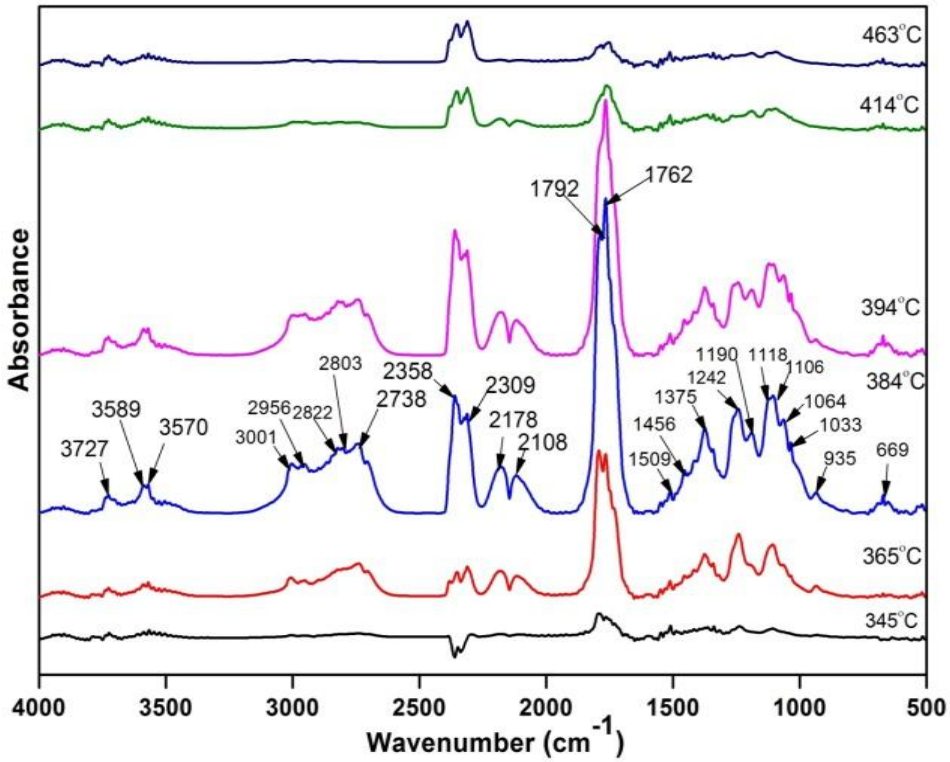

(b)

Figure 3.9: *(a) 3D FTIR and (b) 2D-stack plots of IR spectra of gaseous products after thermal decomposition of PLA-H_2SO_4-CNC bionanocomposite film at different temperature.*

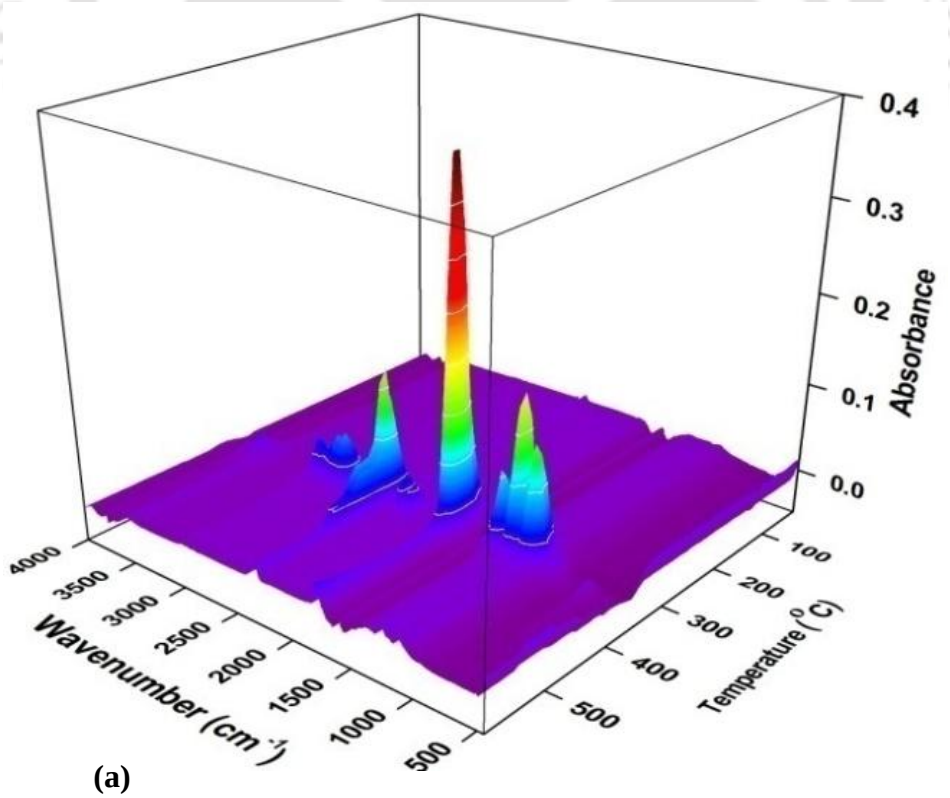

(a)

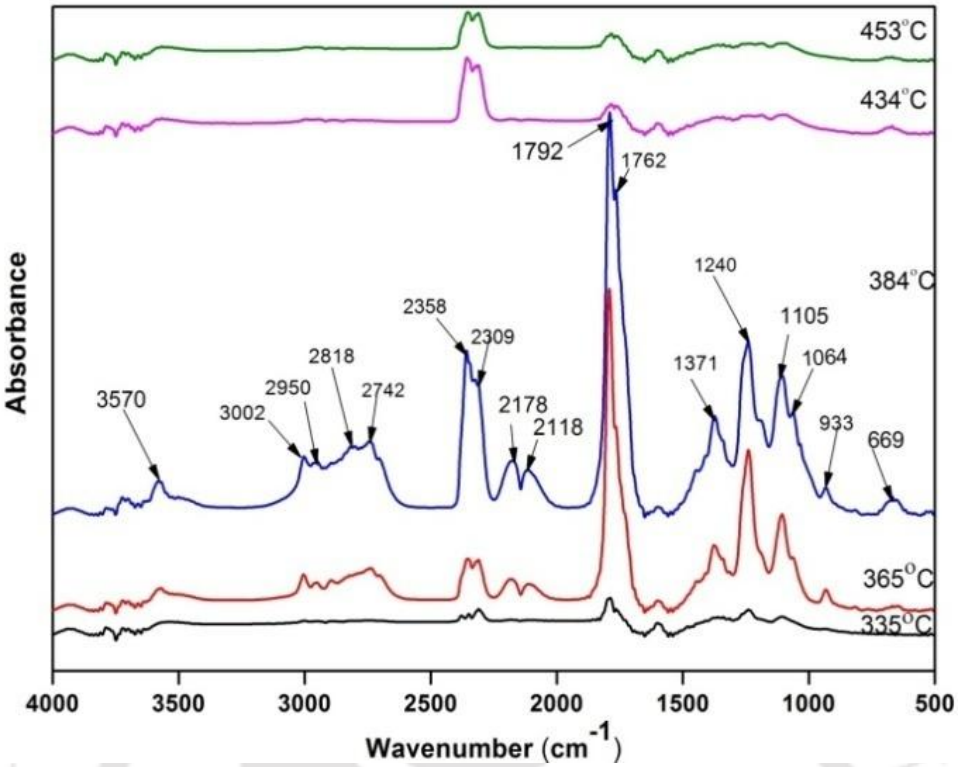

(b)

Figure 3.10: *(a) 3D and (b) 2D-FTIR stack plots of IR spectra of gaseous products after thermal decomposition of PLA-H_3PO_4-CNC bionanocomposite film at different temperature.*

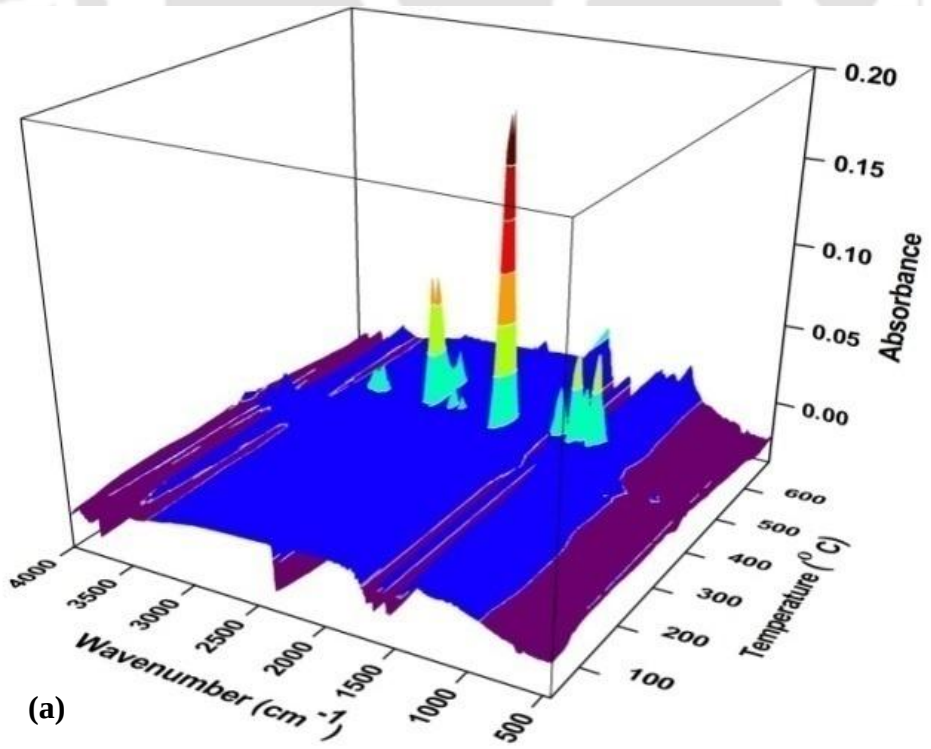

(a)

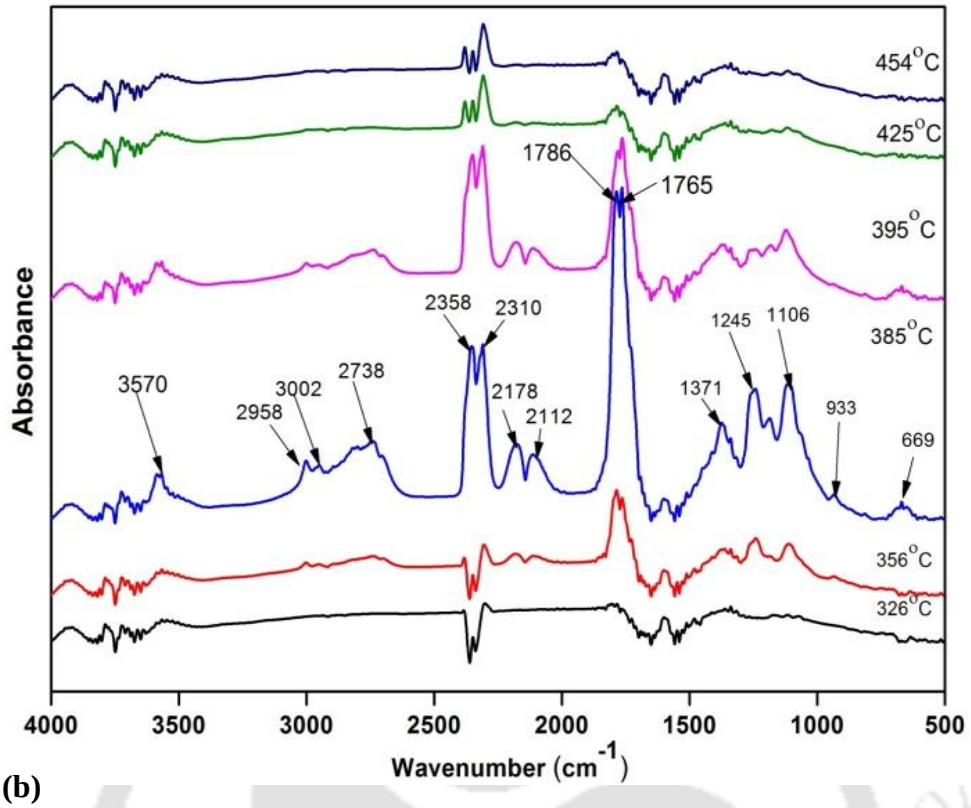

(b)

Figure 3.11: *(a) 3D and (b) 2D-FTIR stack plots of IR spectra of gaseous products after thermal decomposition of PLA-HNO_3-CNC at different temperature.*

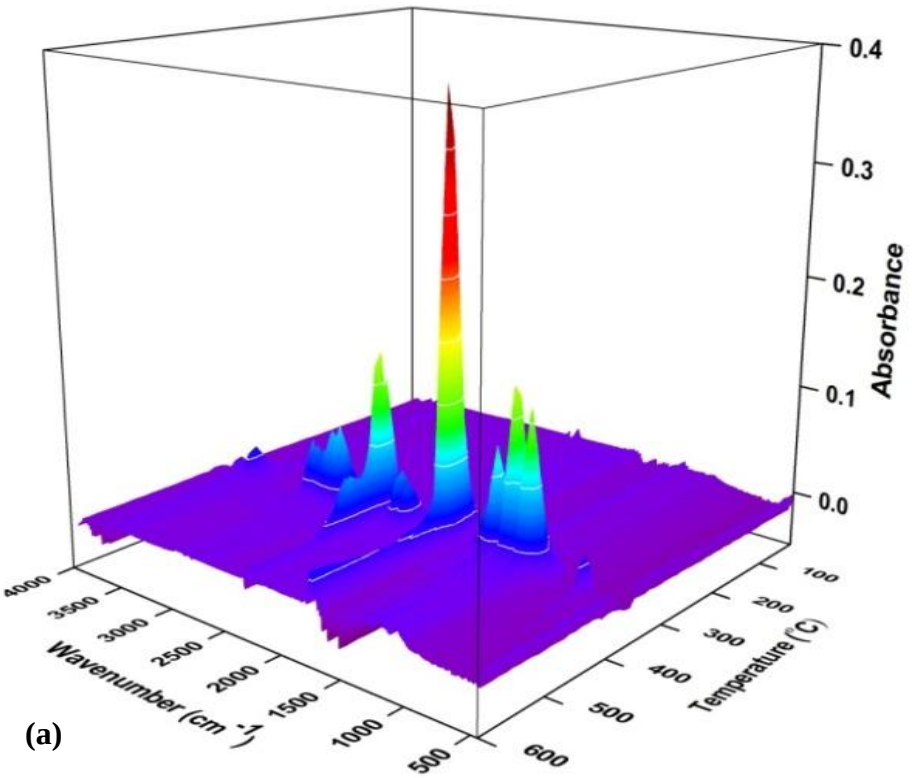

(a)

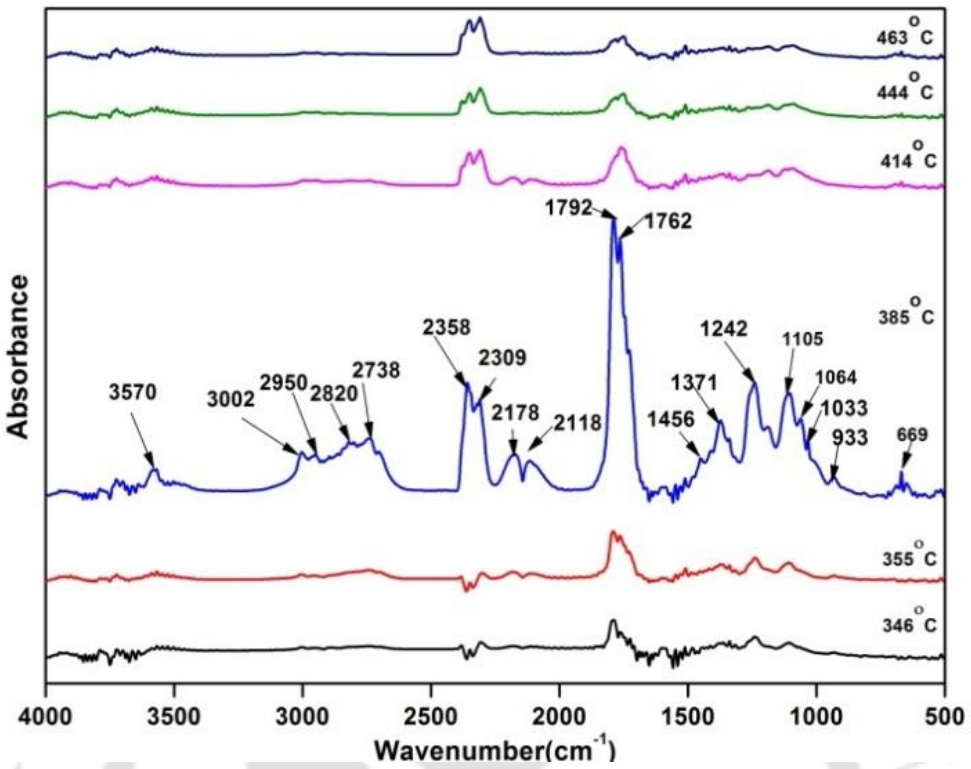

(b)

Figure 3.12: *(a) 3D and (b) 2D FTIR stack plot of IR spectra of gaseous products after thermal decomposition of PLA-HCl-CNC at different temperature.*

Absorption peaks of the released volatile species for PLA-CNC bionanocomposites are shown in Table 3.5 and Figure 3.13 (a)-(e). In all cases, the absorption related to various volatile species has increased gradually with increasing the temperature and intensity drop after the maximum degradation temperature is achieved. Results confirm that those peaks corresponding to CO_2 are present till the end of the process but having a lower yield. Maximum yields of CO_2, CO and aldehyde (CHO) compounds are noticed in case of PLA-H_2SO_4-CNC nanocomposite so it is little environmental friendly than other PLA nanocomposites. In case of PLA-HNO_3-CNC nanocomposite, small emission of CO_2, CO, CHO containing compounds has observed in comparison to other acid derived CNC into the PLA matrix. It is the most thermally stable among all prepared nanocomposite and also retard thermal decomposition of the PLA matrix. Therefore, HNO_3 derived CNC with the PLA

matrix is one of the best choices and used as promising filler for fabrication of the eco-friendly packaging product. From the comparison of FTIR profiles of the major volatile components, it is noticed that the total amount of gaseous species from the HNO_3 derived CNC-PLA nanocomposite is lower than others. Intensity of main peaks of evolved volatile products with bonds of C=O and C-O-C, CO_2 is the highest in case of PLA-H_3PO_4-CNC nanocomposite which confirms the maximum release of carbonyl product from others. During the thermal decomposition of PLA-H_2SO_4-CNC nanocomposite, evolved gaseous products such as CO and CHO has released in the major amount.

3.3. CONCLUSIONS

TGA analysis is inducted in this article to investigate the thermal performance of different acid derived hydrolyzed CNC based PLA bionanocomposites. TGA study reveals that the PLA-HNO_3-CNC has the highest thermal stability. HNO_3 derived CNC has strong interaction with the PLA matrix, which enhances the thermal stability of biocomposite. The E_a is the highest for PLA-HNO_3-CNC nanocomposite while E_a is the lowest in the case of PLA-H_2SO_4-CNC nanocomposite. In case of PLA-HCl-CNC, E_a increases with increasing conversion and remains constant after reaching a certain conversion value in case of PLA-H_3PO_4-CNC and PLA-H_2SO_4-CNC. Results indicate that E_a calculated by three methods are found in good agreement. The difference in E_a for all samples may be due to various types of acid employed and changes in morphology. This finding confirms that PLA-HNO_3-CNC bionanocomposite is most suitable to be use as a nano-filler since it controls the thermal decomposition of the PLA matrix. For PLA-HNO_3-CNC bionanocomposite, the lowest intensity of volatile products is released during TGA-FTIR confirms the small release of volatile products such as CO_2, CO and aldehydes. The detailed thermal degradation study may assist to choose the appropriate PLA-CNC bionanocomposite for packaging applications.

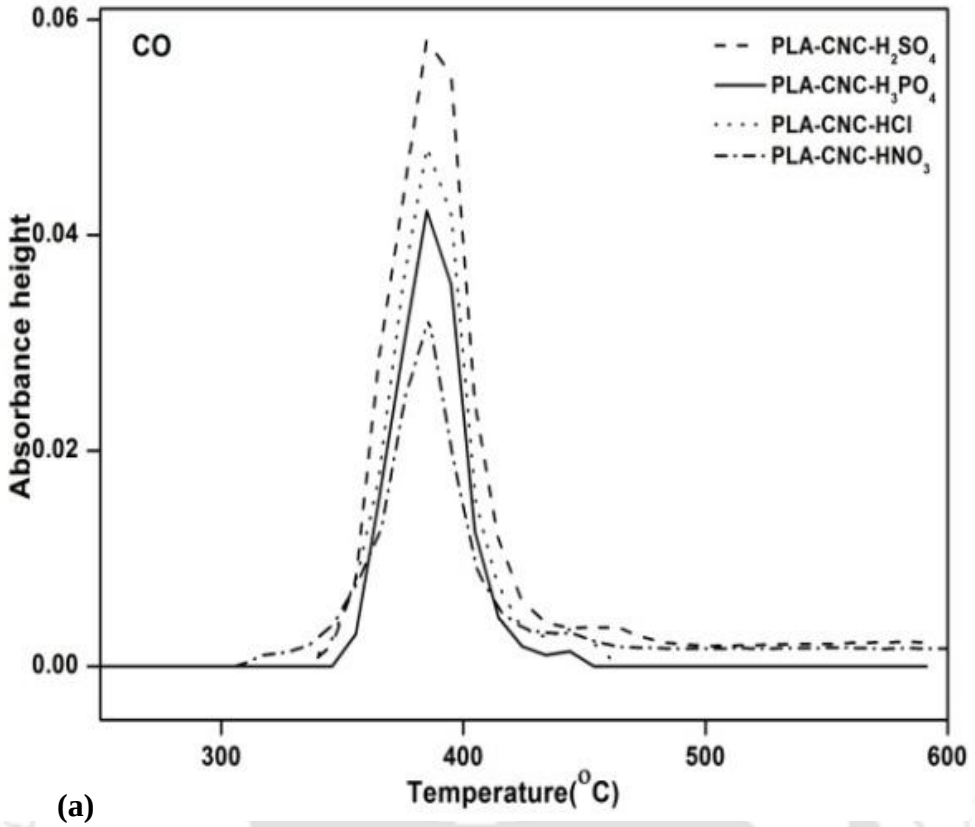

(a)

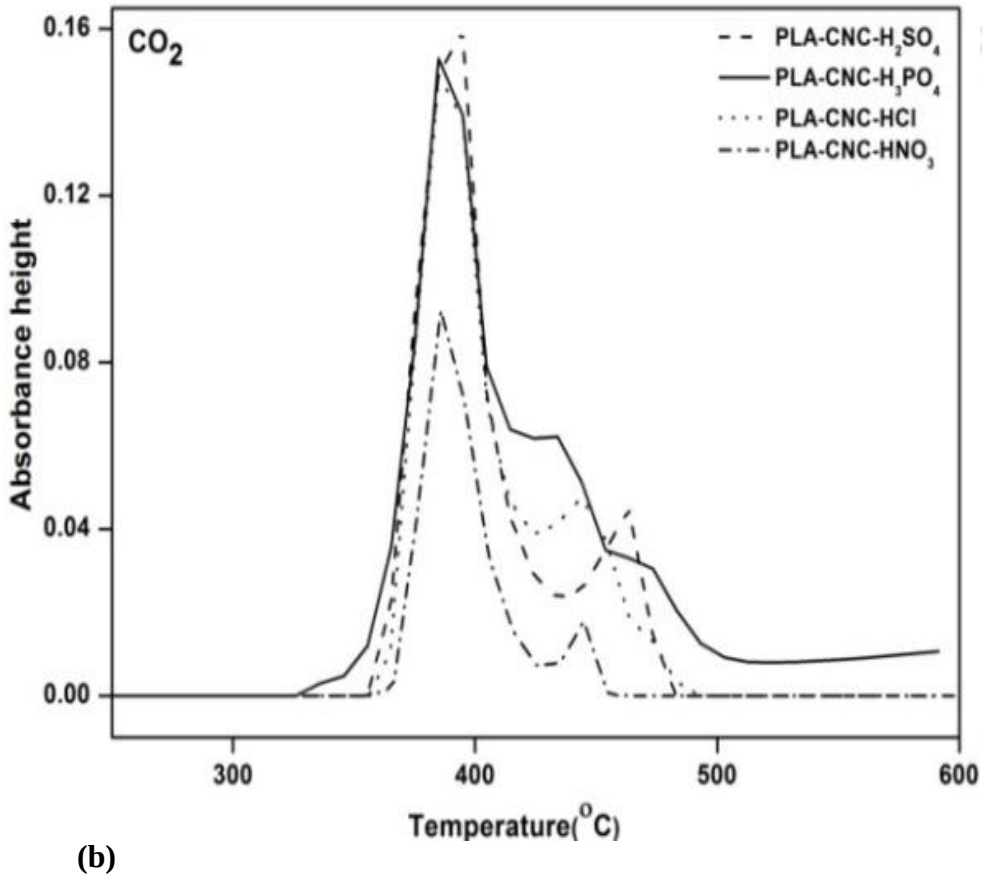

(b)

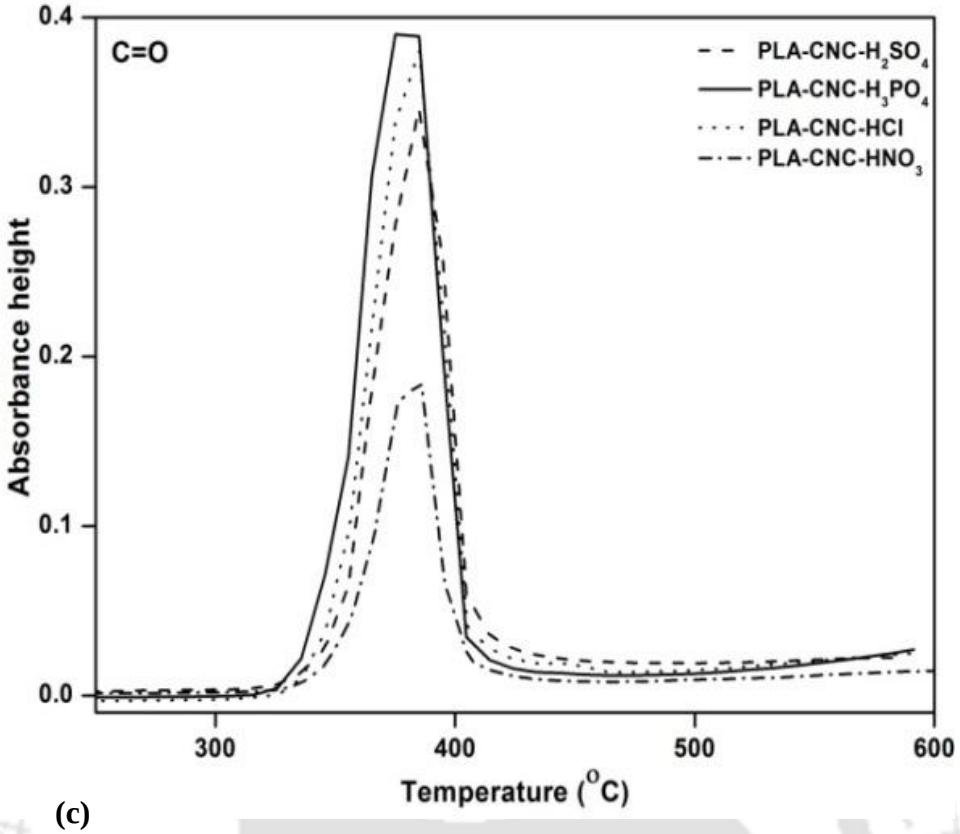

(c)

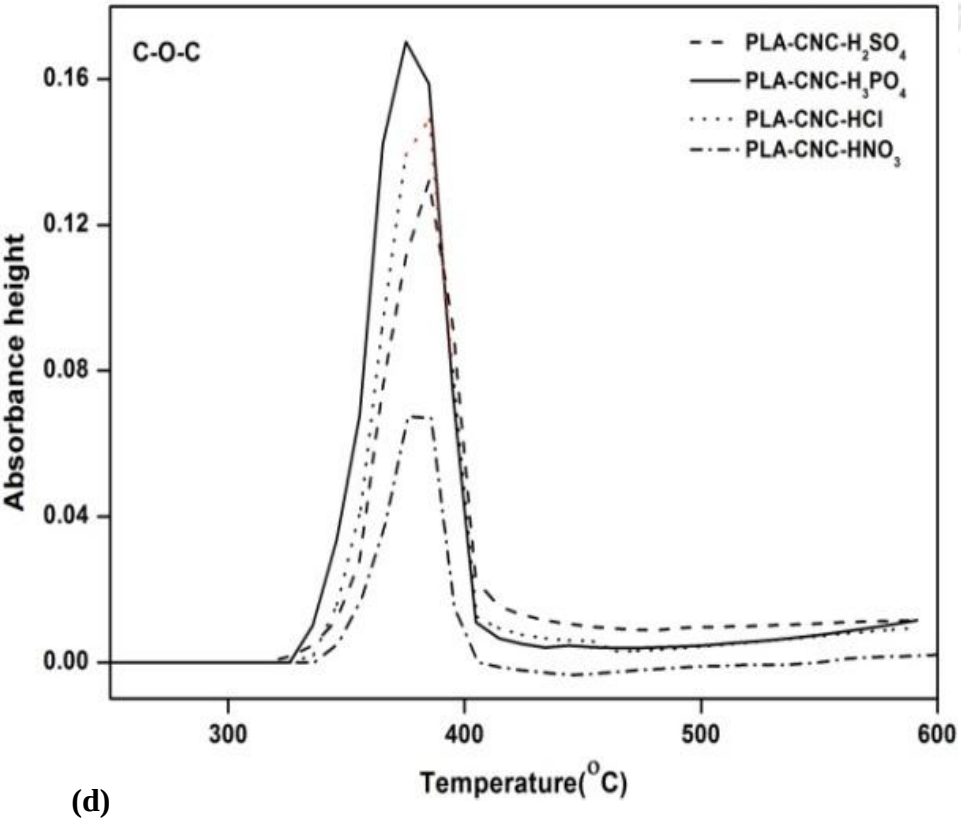

(d)

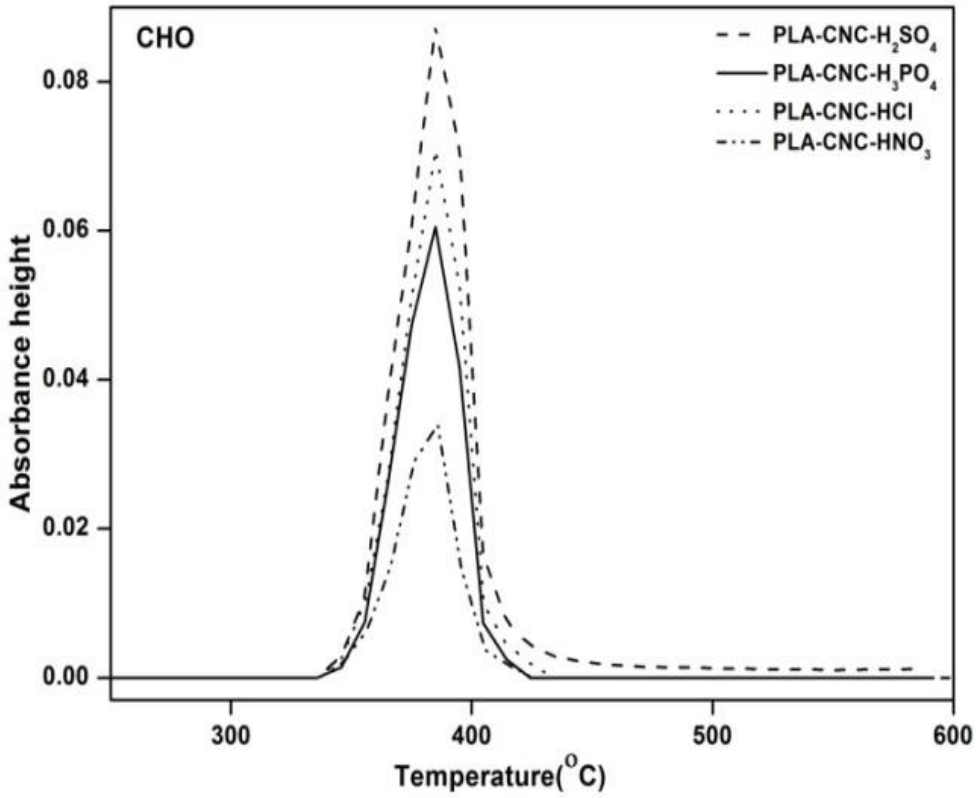

(e)

Figure 3.13: *FTIR profiles of volatile species released from the four components during thermal degradation.*

Table 3.5: *Absorption peaks of the evolved gaseous product detected by TGA-FTIR (at 384 ºC) for different acid derived CNC with PLA matrix at 10 °C/min.*

Wave number for PLA-H_2SO_4-CNC	**Wave number for PLA-HCl-CNC**	**Wave number for PLA-H_3PO_4-CNC**	**Wave number for PLA-HNO_3-CNC**	**Assignment (bond)**	**Products**
3500-3700	3570	3570	3570	υ_{as} O-H	H_2O
2358-2309, 669	2358-2310, 669	2358-2309, 669	2358-2310, 669	υ_{as}C=O δC=O	CO_2
2178-2108	2174-2118	2178-2118	2178-2112	υ C-O	CO
3001	3002	3002	3002	υ C-H	Lactide
2956	2950	2950	2958	υ_{as} C-H	
1792	1792	1792	1786	υ_s C=O	
1456	1456	-	-	δC-H	
1242	1242	1240	1245	υ_{as} C-O-C	
1106	1106	1105	1106	υ_s C-O-C	
935	933	933	933	Ring skelton	Cyclic oligomer
1118	-	-	-	υ_s C-O	Acetaldehyde
1375	1372	1371	1371	δ C-H	
1765	1762	1762	1765	υ C=O	
2738	2738	2738	2738	δ (-C-H=O)	
2822	2820	2818		υ C-H	
1106				υO-H	Ethanol
1064	1062	1064	-	υC-OH	
1033	1033	-	-	υ C-OH	Methanol
1509	-	-	-	C-C	Aromatic structure

Chapter 4

Effect of Dicumyl Peroxide on Poly (lactic acid)/ Functionalized Gum Arabic based Bionanocomposite Films

The motivation of this chapter is to observe the influence of functionalized gum arabic (FG) on the properties of poly (lactic acid) (PLA) based reactive bionanocomposite films in presence of dicumyl peroxide (DCP). PLA/FG based reactive bionanocomposite films have been produced using industrially viable techniques, i.e. twin screw extrusion technique. In this chapter, the research studies have been carried out for possible utilization of reactively extruded PLA/FG based bionanocomposite films in the packaging sector. Addition of FG along with DCP in the PLA matrix shows the fabrication of sustainable packages with enhanced compatibility, UV barrier properties and mechanical properties.

The work in this chapter is to be communicated:

Monika, Mehmood, K. & Katiyar, V. "Compatibilized PLA/Functionalized Gum Arabic based Bionanocomposite Films with Dicumyl Peroxide (DCP): A Reactive Extrusion Approach (Status: To be communicated in Polymer Bulletin)."

ABSTRACT

Blending of poly (lactic acid) (PLA)/functionalized gum arabic (*F*G) in presence of dicumyl peroxide (DCP) presents a simple process to produce films using melt extrusion process (recycle time ~ 4 min, screw speed ~60 rpm) at 180°C with tailored characteristics. The FTIR investigation shows that grafting of PLA chains on *F*G leads to the formation of new C–C linkage. Properties of fabricated films such as morphological, mechanical, UV barrier and contact angle have been examined to develop the films with improved interfacial interaction, elongation at break (~28%), UV–C blocking effect (~95%) and hydrophobicity (~14%). Polarized optical microscopy (POM) revealed that PLA/*F*G with and without DCP has more nucleation density as compared to PLA. This reactive extrusion permits the formation of biocomposite film via a straightforward technique. The biocomposite has a great potential when modified with DCP in packaging application.

Graphical Abstract

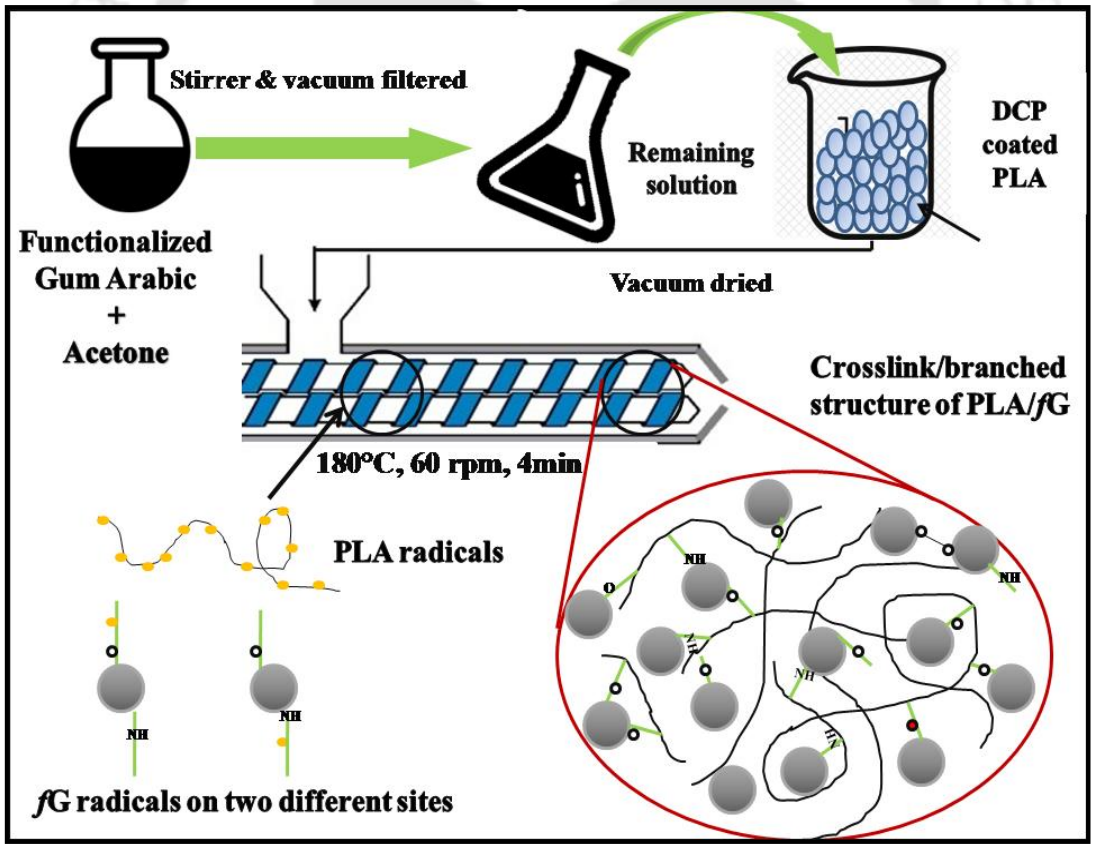

Scheme 4.1: *Schematic* illustration *of possible pathways of mechanism for PLA/FG in the presence of DCP during reactive extrusion.*

4.1 INTRODUCTION

The research on the development of environmental friendly packaging based on biopolymers such as polyesters, polysaccharides (cellulose, chitosan, chitin and gum) and their structural complexes has been modified to large extent, to fulfil the requirements of sustainable society. In this context, keeping in mind the necessity of industrial area and consumer needs, the addition of biopolymer with nano–functional biofillers is compelling alternative to conventional plastic packaging **(Foutunati et al., 2013)**. In response to bionanocomposite made from biopolymer, and nano–functional biofiller are further visualized as one of the alternative options to gain profits such as biodegradability, renewability and balanced properties **(Zhang et al., 2014)**.

Poly (lactic acid) (PLA) is known for its biocompatibility, biodegradability and hydrophobic behaviour, which has comparable mechanical performances with conventional plastics such as polystyrene (PS) and polyethylene terephthalate (PET), and derived from renewable resources such as corn and sugar feedstock **(Zhang et al., 2015; Yang et al., 2017 and Martin et. al. 2001)**. PLA is acknowledged as the leading aliphatic bio–derived polyester and the prospect polymer for the utilization at industrial production. Apart from the versatile applications, span of PLA is confined due to the narrow processing window, poor crystallization rate, poor barrier properties and low thermal stability **(Nerkar et al., 2015)**.

Polysaccharide gum is therefore, one of the most recommended biopolymer for many wide sectors applications due to its biodegradability, renewability and non-toxicity. Gum Arabic (GA) has attracted much attention, which is abundantly available in nature and it can be further used as a polymer matrix as well as biofiller. It is type of complex polysaccharide which is derived from Acacia trees (i.e. *Acacia seyal* and *Acacia Senegal*) **(Ali et al. 2010)**. GA is mainly composed of 90% arbinogalcatan, and 10% arbinogalctan protein and 1% glycol-protein **(Wang et al., 2014)**. It is nontoxic, hydrophilic in nature and has the potential

to be grafted on to the polymeric chain on bio filler which leads to certain modifications in structural characteristics. According to United States Food and Drug Administration, it is considered as a safe food additive. Therefore, it can be utilized as biofiller in food packaging.

It is a well known fact that the limited interfacial compatibility between the PLA matrix and bio based filler; causes a poor dispersion of the filler into matrix which may be responsible to worsen the final performance of film i.e. mechanical characteristics **(Haque et al., 2017)**. According to **Tripathi et al., 2016** *F*G can be used as a biofiller for improving several characteristics of PLA based packaging film such as barrier properties. Although, melting process of PLA with functionalized GA would be a challenging task due to the presence of short OLLA chains attached with GA. PLA undergoes thermal decomposition at an elevated temperature and due to the shear action, finally shows reduction in melt strength. To compete these challenges, reactive extrusion of bionanocomposites is carried out either in the presence of chain extender or radical initiator which leads to the enhancement in melt strength with wide range of processing window. This technique can be widely used at the industrial level. Recently, various research articles have been published on PLA based bionanocomposites with the different kind of chain extender and radical initiators which assist to improve the melt strengthen or compatibility **(Yang et al., 2008; Wei et al., 2015; Dhar et al., 2016)**. **Prodyut et al. 2016** fabricated PLA grafted cellulose nano crystals (CNC) on backbone through radical grafting using reactive extrusion. This led to a remarkable improvement in the tensile strength (41%) of PLA/CNC bionanocomposite films. Similarly, the reactive extrusion of PLA/Silk nanocrystals (SNC) bionanocomposite films in presence of radical initiator leads to an enhancement in the rheological characteristics **(Tesfaye et al., 2017)**. In this work, DCP acts as an initiator to enhance compatibility between PLA and functionalized GA through reactive extrusion process. The morphology, thermal, mechanical, and FTIR have done to investigate the influence of *F*G with DCP on the phase interaction, crystallization process,

strength and modification in structural properties of film. The wettability and UV sensitivity of samples are detected by contact analyzer and UV spectroscopy. The growth of spherulites and nucleation of PLA crystal is analyzed using POM technique. All the film samples are further characterized to understand the viability of films in packaging application.

4.2. RESULTS AND DISCUSSION

- ***Plausible reaction mechanism of reactive extruded PLA/FG bionanocomposite films in the presence of DCP***

Based on the FTIR analysis, formation of new C–C linkage between PLA and *F*G bionanocomposites in presence of radical initiator (DCP) has been presented in Scheme 4.1. It is well documented that the abstraction of the hydrogen (H) from the PLA backbone facilitates the radical sites onto the PLA chains **(Takamura et al., 2008)**. In case of filler, free radicals have generated due to the abstract of hydrogen from the available weak sites during the reactive extrusion process. These radical sites generated on PLA have two possibilities to react with *F*G: (i) developed free radicals on OLLA chains attached to NH_2 group of gum arabic (ii) generated free radicals on OLLA attached to OH group of gum arabic, to form crosslinked/branched structure in macromolecular chains. Other possibilities are formation of PLA/PLA, *F*G/*F*G interaction in presence of DCP during the melt extrusion **(Ma et al., 2012)**.

FTIR analysis is carried out to investigate the possible interaction between the PLA and *F*G in presence of DCP, as depicted in Figure 4.2 (a). For PLA, the transmittance band at 2996, 2923 and 2853 cm^{-1} are related to the C–H stretching, asymmetric stretching of CH_3 and symmetric stretching of CH_3. IR peaks at 1382, 1452 and 1359 cm^{-1} are attributed to the symmetric bending of CH_3, deformation of C–H, asymmetric bending of CH_3. The peak at 1749, 1180, 1128, 1078, 1041, 954, 868 and 753 cm^{-1} are assigned to C=O stretching, asymmetric C–O–C stretching + asymmetric rocking CH_3, symmetric rocking CH_3, symmetric

stretching C–O–C, stretching C–CH_3, rocking CH_3 + stretching C–C, stretching C–COO & also attribute to amorphous region of PLA phase and bending C=O in PLA due to its crystalline phase **(Dhar et. al. 2016; Tesfaye et. al. 2017; Pal et. al. 2016)**. It is noticed that there is no significant change in the spectra of PLA/*F*G based bionanocomposites except the height of bands located at 2920 and 2853 cm^{-1} is increased as increasing the filler content. Therefore, it can be predicted that there is only electrostatic interaction between the PLA and *F*G. When DCP is introduced into PLA/1*F*G, a new peak at 2962 cm^{-1} is found while the peaks at 2923 and 2853 cm^{-1} are also shifted to 2920 and 2850 cm^{-1} respectively as represented in Figure 4.2 (b). The peak height at 2996 cm^{-1} for asymmetric stretching of –CH group and 1358 cm^{-1} for deformation of C–H group from PLA also weakens and assists the radical initiated abstraction of hydrogen. It indicates the possible chain modification by grafting, long chain branching/crosslinking occurs between the –CH of PLA and the *F*G, which reduced the CH groups present in PLA. It is found that the intensity of peak decreases at 1240–1000 cm^{-1} which is ascribed to C–O–C stretching. A typical peak at 799 cm^{-1} (some new C–C linkage) appears due to the development of branching/crosslinking which influences the intensity of the ester group as mentioned in Figure 4.2 (c) **(Tesfaye et al. 2017)**. Also, the intensity of the band at 753 cm^{-1} is reduced which corresponding to C–COO bond and leads to high branching in modified structures. These FTIR data set represent the successful branching/crosslinking of *F*G with PLA chains.

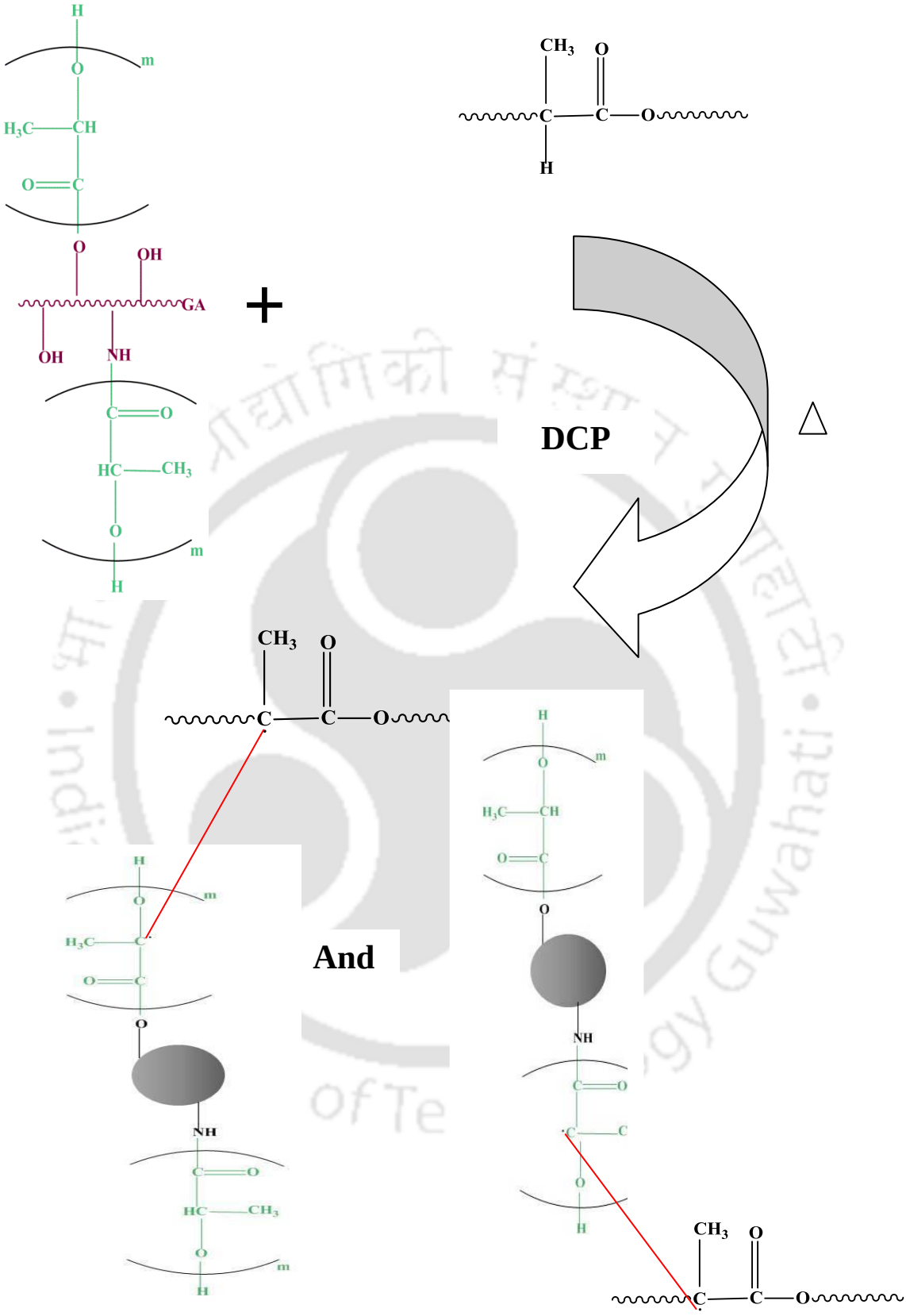

Figure 4.1: *Plausible reaction mechanism of PLA/FG based reactive bionanocomposite films in the presence of DCP.*

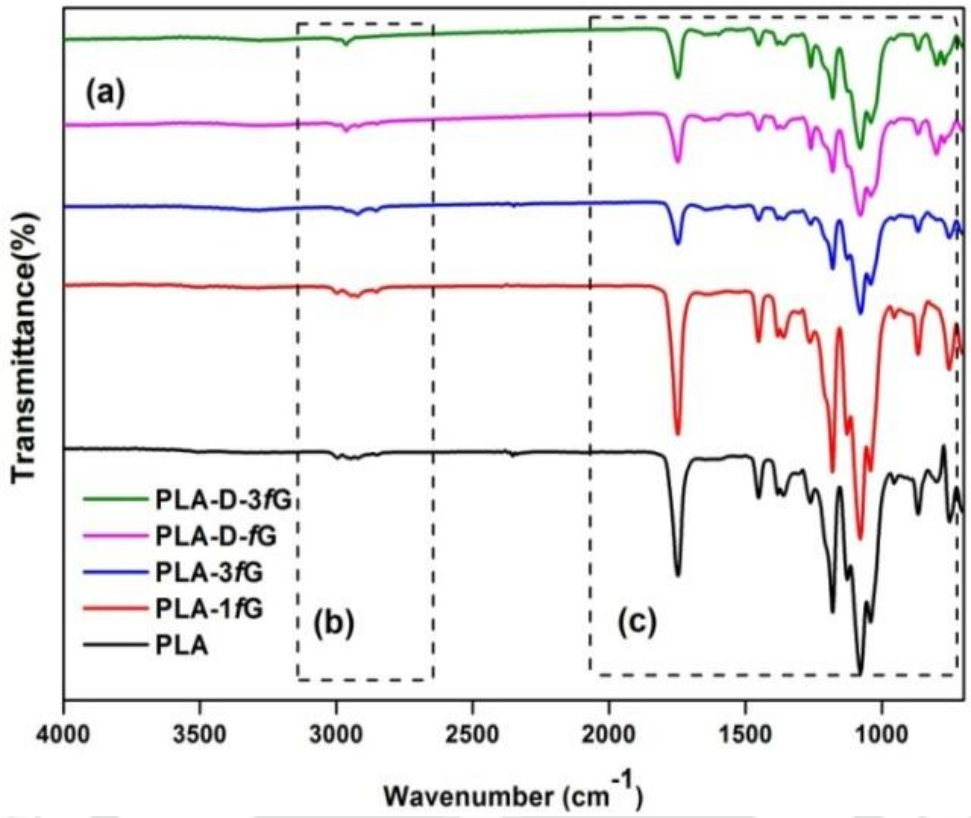

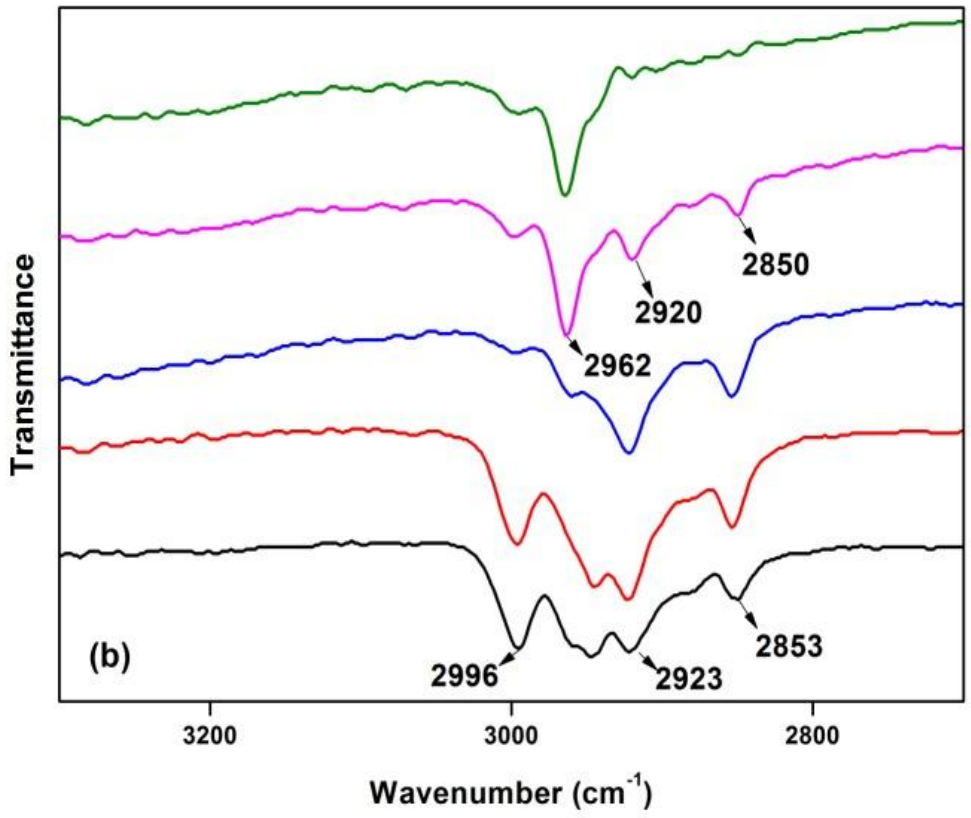

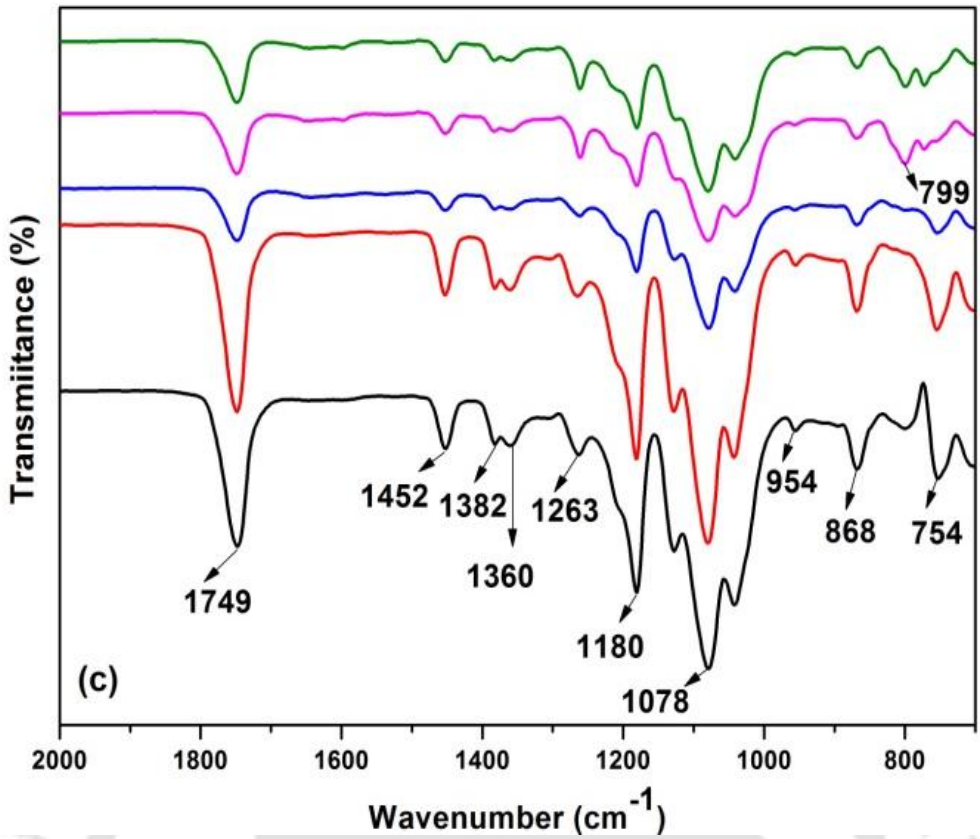

Figure 4.2: *Chemical structural analysis of PLA and their PLA/FG bionanocomposites with and without DCP using FTIR in (a) Full range (4000-700 cm^{-1}), (b) C–C stretching fitted band (range: 3300-2700 cm^{-1}), (c) Carbonyl group, C–O–C, C–C and C–H fitted band (range: 2000-700 cm^{-1}).*

- ***Morphological investigation of the reactively extruded PLA/FG bionanocomposite films with and without DCP***

The morphological investigation of the tensile fractured surface of the selected bionanocomposite films are assessed through FESEM (Figure 4.3). Fractured surface of the PLA/1*F*G displayed a smooth surface due to the dispersed *F*G in the PLA matrix. This result reveals that the addition of the DCP content enhance the compatibility between the PLA and *F*G dispersed phase; and assists to improve the adhesion of *F*G and PLA since *F*G remains intact with the PLA and successfully shows termination of crazing **(Huang et al., 2017)**.

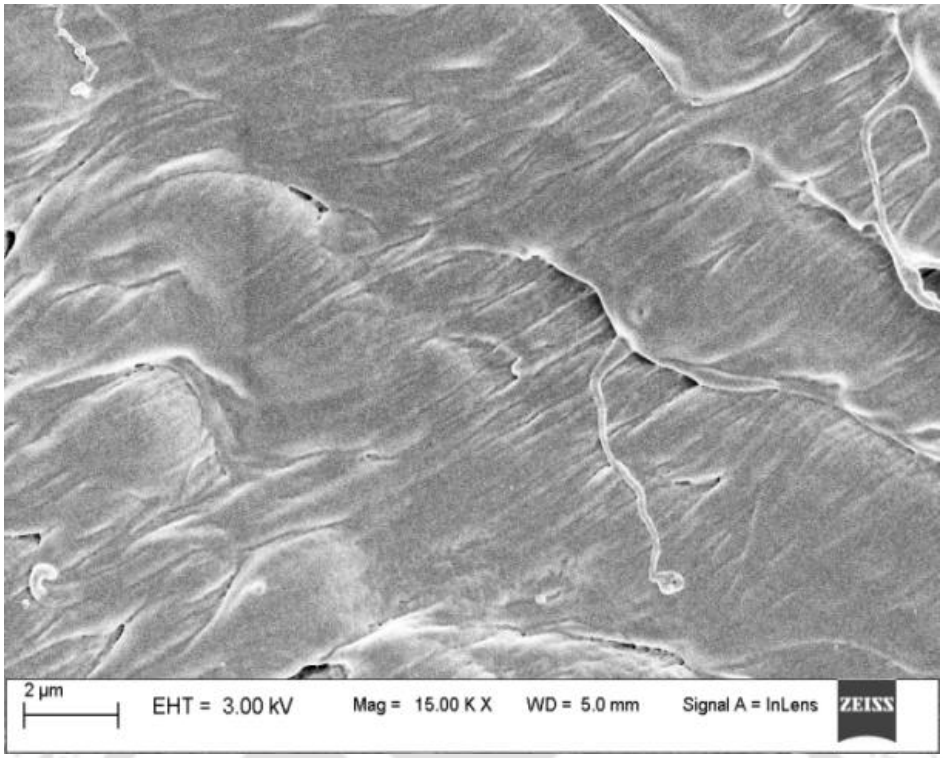

(a)

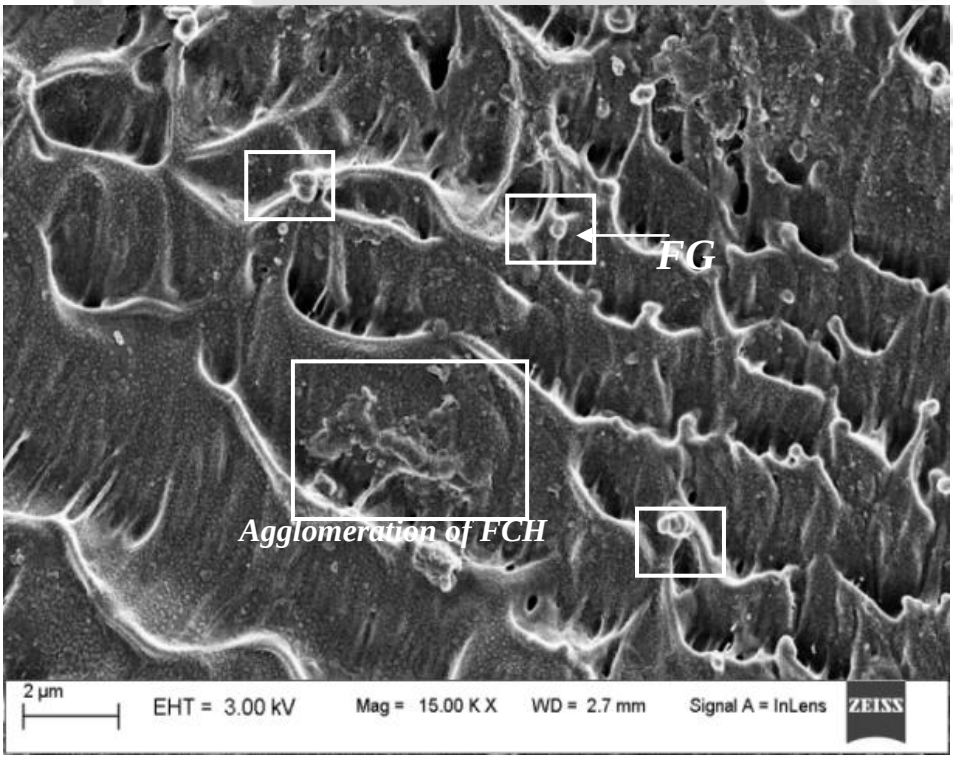

(b)

Figure 4.3: *FESEM micrograph for the tensile fratcure surface of the samples (a) PLA/FG, (b) PLA/D/1FG bionanocomposite films.*

- ***Crystallization study of the reactively extruded PLA /FG bionanocomposite films with and without addition of DCP***

The influence of reactive modification on the DSC second heating curves of PLA/*F*G bionanocomposites are displayed in Figure 4.4; the key data of thermal characteristics are summarized in Table 4.1. From the second heating cycle, glass transition temperature (T_g) is observed at 61.5 °C for PLA. After reactive grafting of *F*G with PLA, insignificant change in T_g is found which subsequently led to restricted motion of PLA chains due to grafting. The slight decrement in T_{cc} upto ~ 3 °C is noticed for PLA with 3 wt% *F*G, as compared to neat PLA at 111°C. In addition, the broadness of T_{cc} peak is clearly enhanced and moved to lower temperature side in the presence of *F*G content which suggest the formation of more irregular structure **(Tripathi et al., 2016)**. DCP modified samples induce a restricted crystallization of PLA in melt state, which could be associated with the development of branching/crosslinking sites as compared with PLA/*F*G bionanocomposite films **(Xu et al. 2017; Zhang et al. 2016)**. For PLA/*F*G bionanocomposite (without DCP), there is an insignificant change in terms of T_m (170 °C) while a slight reduction in T_g (~2 °C) observed. However, the main melting transition with shoulder peak is noticed which could be due to the presence of more perfect crystalline structure (T_{m1} = 170 °C at high melting temperature) and less perfect crystalline (T_{m2}= 164 °C at lower temperature). This bimodal melting peak of PLA is well reported in published article **(Dhar et al. 2016; Frone et al. 2013)**.

It is noticed that all the DCP treated PLA/*F*G samples have lower value of T_m than those of the PLA and physical blend, i.e. PLA/D/3*F*G had a T_m of 167 °C which is 3 °C lower than that of the PLA. The possible reason for the lowering of T_m is that the branching/crosslinking sites which broadened the molar-mass distribution of PLA and restricted the packing perfection of PLA chains **(Xu et al., 2017; Wei et al., 2015)**.

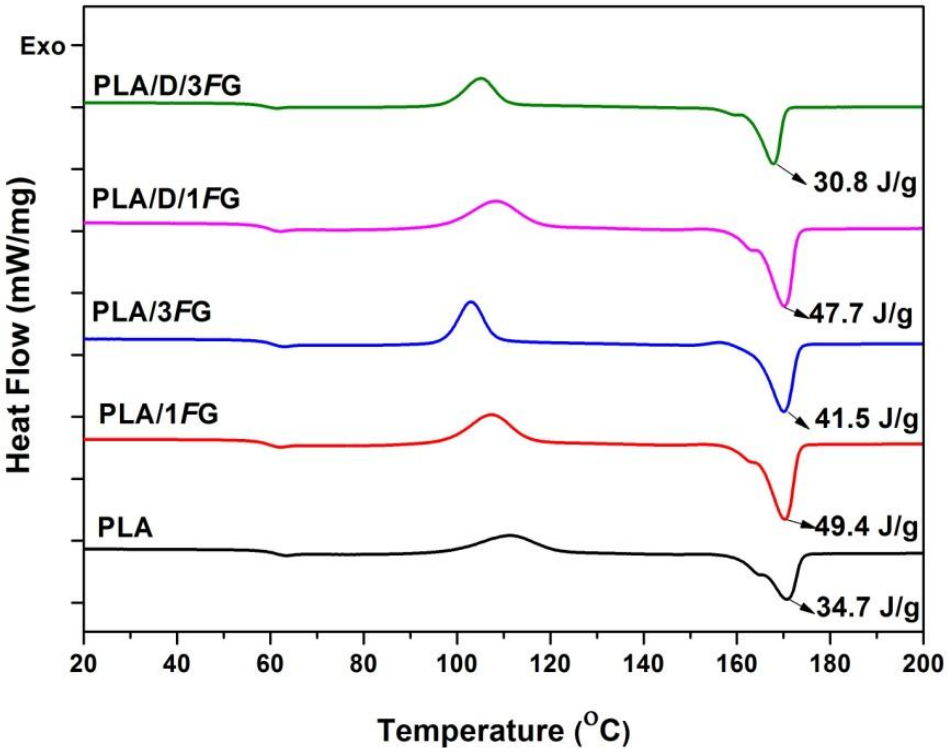

Figure 4.4: *DSC thermograms (second heating cycles) of PLA, PLA/FG and their reactive modified bionanocomposite films*

Table 4.1: *Thermal characterstics and the percentage crystallinity of extruded PLA and their bionanocomposite films.*

Samples	T_g (°C)	T_m (°C)	T_{cc} (°C)	ΔH_m (J/g)	ΔH_{cc} (J/g)
PLA	61.5	170.7	111.6	34.7	28.8
PLA/1*F*G	59.7	170.3	107.4	49.4	35
PLA/3*F*G	59.2	168.5	103.1	41.5	31.5
PLA/D/1*F*G	60	169.1	108.2	47.7	40.4
PLA/D/3*F*G	60	167.8	105.2	30.2	23.1

Glass transition temperature (T_g) calculated from the inflection mid-point of heating curve, melting peak temperature (T_m), cold crystallization peak temperature (T_{cc}), cold crystallization enthalpy (ΔH_{cc}), melting enthalpy (ΔH_m).

- ***Mechanical properties of the reactively extruded PLA/FG bionanocomposites films with and without addition of DCP***

Mechanical properties (tensile strength and % elongation at break) are evaluated and displayed in Figure 4.5. PLA exhibits a typical nature of brittle polymer which has high strength (48.1±2.3 MPa) and modulus, with poor elongation at break below 9.08±1.41%. Moreover, PLA has limited applications in packaging sector due to its brittleness. There is no significant change in the tensile strength (47.83±1.10 MPa) observed for PLA/1*F*G due to improve dispersion, as compared to PLA (48.1±2.3 MPa), respectively. Such reduction in the tensile strength 47.83±1.10 to 45.1±2.5 MPa is also noticed for PLA/1*F*G and PLA/3*F*G films, respectively. This result implied that the presence of more OLLA chains attached with gum arabic may have contributed to the limited interfacial interaction between *F*G and PLA **(Triphati et al., 2016; Pal et al., 2016)**. However, PLA/FG bionanocomposite shows slight improvement in elongation, i.e. 10.07±1.2% for PLA/1*F*G, as compared to PLA. Hence it should be noted that the flexibility of chains increase due to plasticizing influence of OLLA chains attached to Gum Arabic. At high *F*G content (3wt %), value of elongation at break is decreased (9.07±1.4%) because the filler has a tendency to aggregate in PLA matrix. In relation to the tensile strength and elongation at break, for reactive bionanocomposite, DCP modified samples presents no significant change in tensile value (46.3±2.06 MPa) while the elongation at break increase slightly (11.7±1.3%) for PLA/D/1*F*G, in comparison with PLA/1*F*G. This is because that the incorporation of DCP into PLA/1*F*G contributes to slightly improved interfacial adhesion between the PLA and *F*G due to the presence of some branching/crosslinking sites across the interphase in this system **(Ma et al., 2014)**. PLA/D/3*F*G shows further deterioration of mechanical characteristics which is probably due to the decrease in efficiency of branching/crosslinking structure.

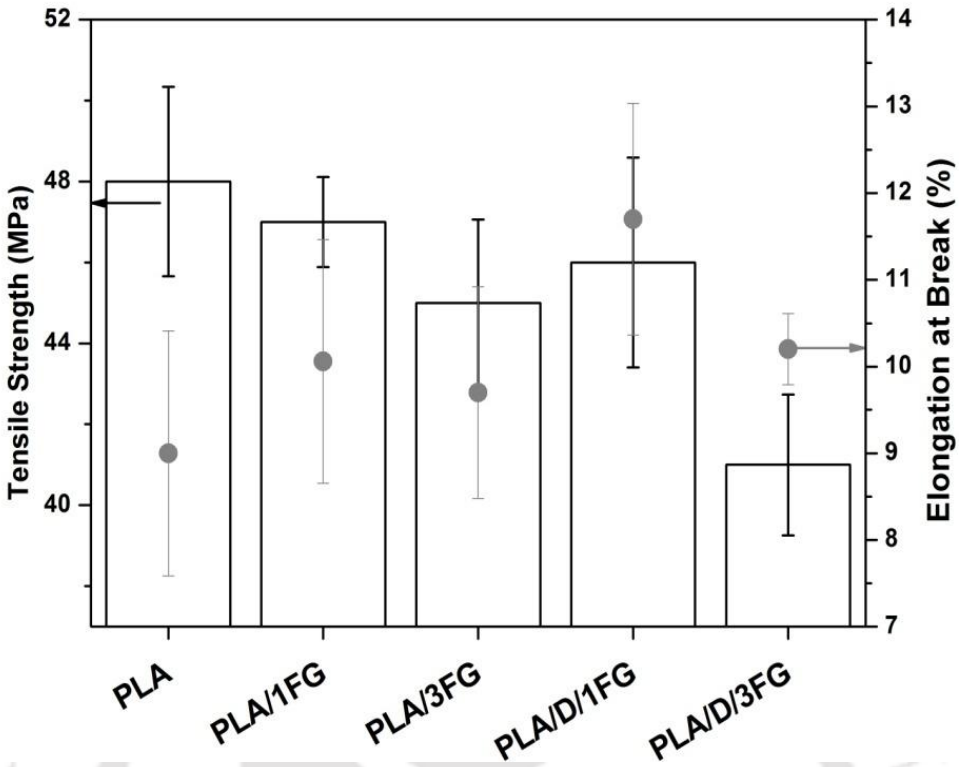

Figure 4.5: *Mechanical properties such as tensile strength and elongation at break (%) of PLA, PLA/FG and their reactive modified bionanocomposite films.*

- ***Wettability properties of the reactively extruded PLA/FG bionanocomposite films with and without addition of DCP***

Surface wettability plays a vital role in food packaging to protect the food stuff from the humidity during primary stages (handling, storage, transportation) to consumption stage. The contact angle (θ_c) test is essential for the material characterization intended for food packaging which determines the wettability of solid substrate by depositing water on the film surface. In fact, $\theta_c > 65°$ imply hydrophobic surface and $\theta_c < 65°$, is typical hydrophilic surface. In the entire scenario, value of θ_c is higher than 65° as shown in Figure 4.6 (a) – (e) which confirms the poor association of water to the polymeric films and makes it beneficial in the packaging. After addition of *F*G into PLA matrix, value of θ_c is significantly increased up to ~ 10°. The possible reason for this behavior may be the replacement of the polar groups (hydrophilic) of GA with the ester group (hydrophobic) of OLLA chains, which has tendency

to influence the surface characteristics, finally responsible to enhance the hydrophobicity of PLA/*F*G samples. We can note that on addition of DCP into PLA/*F*G based bionanocomposite, value of θ_c is significantly increased (~14%) as compared to PLA. This result implies that the nucleation of polymer bionanocomposite contributes to the reduction in polarity of chains. Also, increase in surface roughness assists improvement in hydrophobicity of PLA bionanocomposite. Hence, these results are impressive to the potential use of film in packaging.

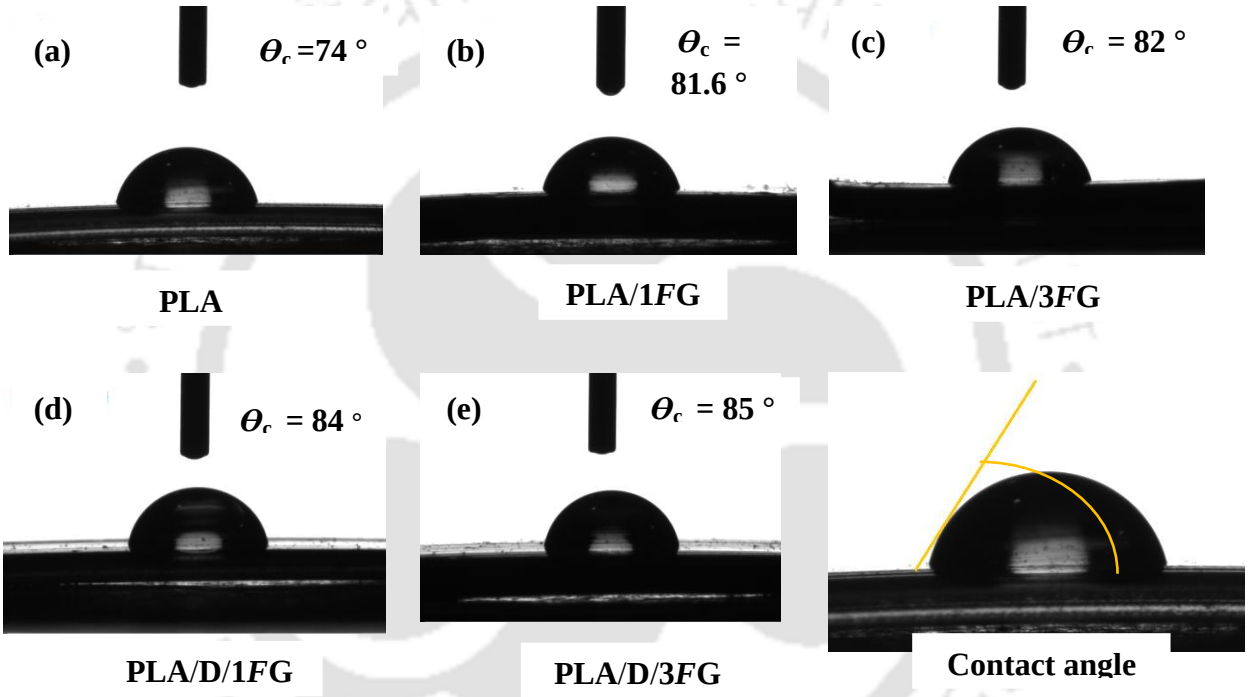

Figure 4.6: *Determination of static contact angle (at 25 °C) to confirm wettability of (a) PLA, (b) PLA/1FG, (c) PLA/3FG, (d) PLA/D/1FG and (e) PLA/D/3FG bionanocomposite films.*

- ***UV transmittance of the reactively extruded PLA/FG film with and without addition of DCP***

UV blockage of the light (< 315 nm) is a crucial parameter which should be considered for the packaging film, especially for preventing the oxidation of light sensitive items **(Auras et al., 2004; Frone et al., 2013)**. As we know that PLA has poor UV barrier properties and atten

-tion is required for its utilization in the packaging area. The UV transmittances (%T) for PLA, PLA/*F*G with and without DCP are well reported in Figure 6.8 (a)-(b) respectively. The estimated value of %T of PLA, PLA/1*F*G, PLA/3*F*G, PLA/D/1*F*G and PLA/D/3*F*G is ~68%, ~38%, ~30%, ~18% and 30%, respectively, at 700 nm (visible region). From the result, it is confirmed that %T is decreased continuously for all physical blend film with and without DCP, as compared to PLA. After addition of *F*G into PLA matrix, the transparency is drastically reduced by ~ 44%, ~55% (at 700 nm) for PLA/1*F*G and PLA/3*F*G respectively. Similar type of behaviour is noticed in UV region (400-200 nm) where value of %T is markedly decreased by 61%, ~71% (at 275 nm). This is probably due to two major reasons (i) the brownish colour imparted by the *F*G and (ii) presence of *F*G granules in PLA which could diffract the visible lights because of the size domain of dispersed phase **(Pal et al., 2017; Bher et al., 2018)**. Also, uniform dispersion of *F*G in the PLA matrix is responsible for UV blocking. Reactive samples show lower %T than the PLA/*F*G based films. For PLA/D/1*F*G, it is observed that transparency is further decreased by ~73% in visible region. This behaviour could be attributed due to better distribution and compatibilization of the *F*G into the PLA, and 95% of UV blocking effect as compared to PLA **(Bher et al., 2018)**. Therefore, the UV blocking is the most pronounced effect in case of DCP treated PLA/1*F*G.

- ***Polarized optical microscopy investigation of reactively extruded PLA/FG bionanocomposite films with and without DCP***

The spherulites morphology for the PLA, PLA/FG bionanocomposite films with and without DCP have been discussed in detail. The morphological evolution for the PLA, PLA/1*F*G, PLA/3*F*G, PLA/D/1*F*G and PLA/D/3*F*G samples is investigated at three different temperatures of 120, 130 and 140°C respectively using POM analysis. All samples displayed a maltese cross pattern, the size and nucleation density are totally distinct from each other. For all the samples, the spherulites display negative birefringence which is found in

agreement with literature (Vasanthakumari et al., 1998; Quero et al., 2012). At 120°C, PLA has weak nucleation ability, but the spherulites grow faster, leading to the formation of large and distinct non-banded spherulites **(Quero et al., 2012)**. It is also difficult to observe the spherulite growth rate for PLA/*F*G nanobiocomposites with and without DCP as many crystal nuclei are grown with a decrease of the induction period. The appeared POM micrographs at the same temperature clearly show that the PLA/1*F*G (Figure 4.8) exhibit the strongest nucleation density and covers the bulk area which is probably due to the presence of grafted points which acted as primary nucleation points. Also, large spherulites are found which are responsible for the improvement in the mobility of chains **(Jia et al. 2017)**. According to **Nofar et al., 2011**, the grafted points in PLA function as nucleation sites during the crystallization process. In concrete, the micrographs revealed that the spherulitic growth rate is gradually increased with the incorporation of 1 and 3 wt% *F*G. Because the short–chain of OLLA associated with *F*G favours the folding of polymeric chains and enhances the spherulites size. Pal et al., 2016 has reported the similar type influence of oligo-L lactic acid grafted chitosan (OLLA–g–CH) on nucleation of PLA and they observed that the spherulitic growth rate of PLA/OLLA–g–CH bionanocomposite is higher than that of PLA, which is found in agreement with our result. Interestingly, the spherulites exhibit entirely disturbed ring pattern (Hsieh et al., 2013) at 120 °C which is probably due to lamellae twisting and on further increasing the temperature from 120 to 140 °C, transition from ring pattern to non ring pattern are observed in case of PLA/3*F*G. **Xu et al. 2005**, suggested that incorporation of second amorphous polymer persuade the lamellar twisting. While nucleation took place slowly in case of DCP treated PLA/*F*G in comparison of PLA/1FG; however, once the crystallites begins to grow, the nucleation growth rate is the highest. Compared to PLA/1*F*G, large spherulites are noticed in PLA/D/1*F*G in smaller quantities.

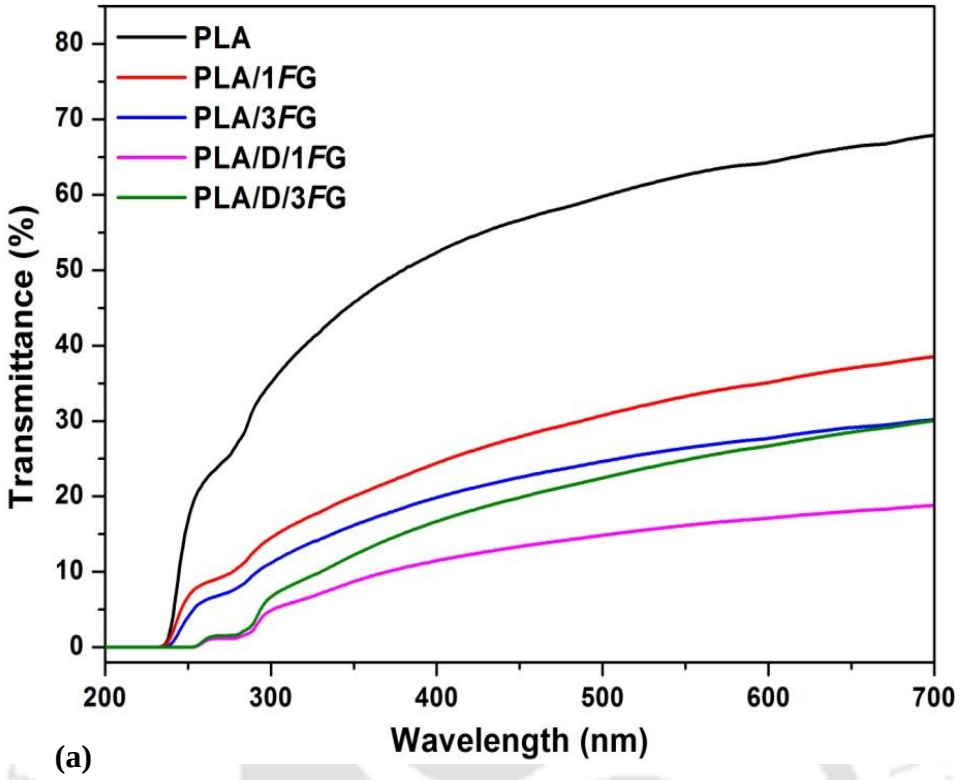

(a)

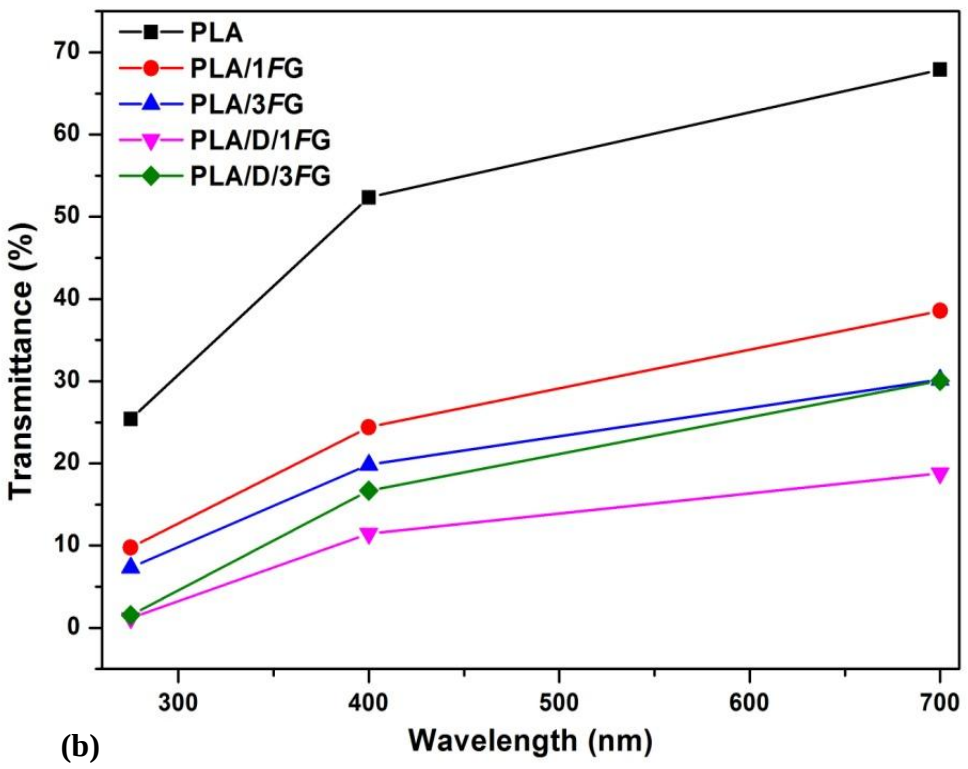

(b)

Figure 4.7: *(a) UV visible spectra (b) in range (700-200 nm), (c) Comparison of % transmittance at 700, 400 and 275 nm of PLA, PLA/FG and their reactive modified bionanocomposite films.*

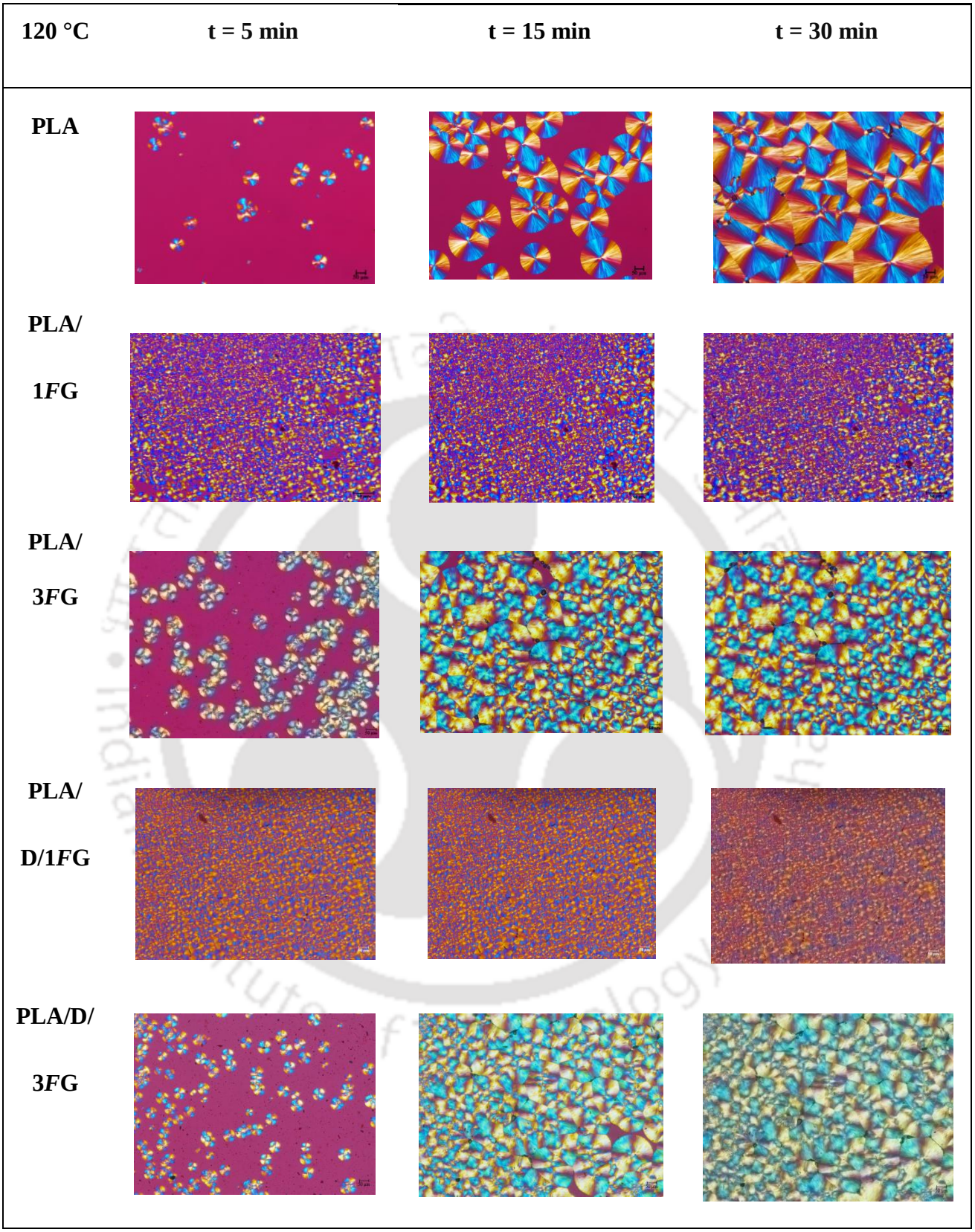

Figure 4.8: *Selected POM images of PLA, PLA/FG and their reactive modified bionanocomposite films at 120°C temperatures.*

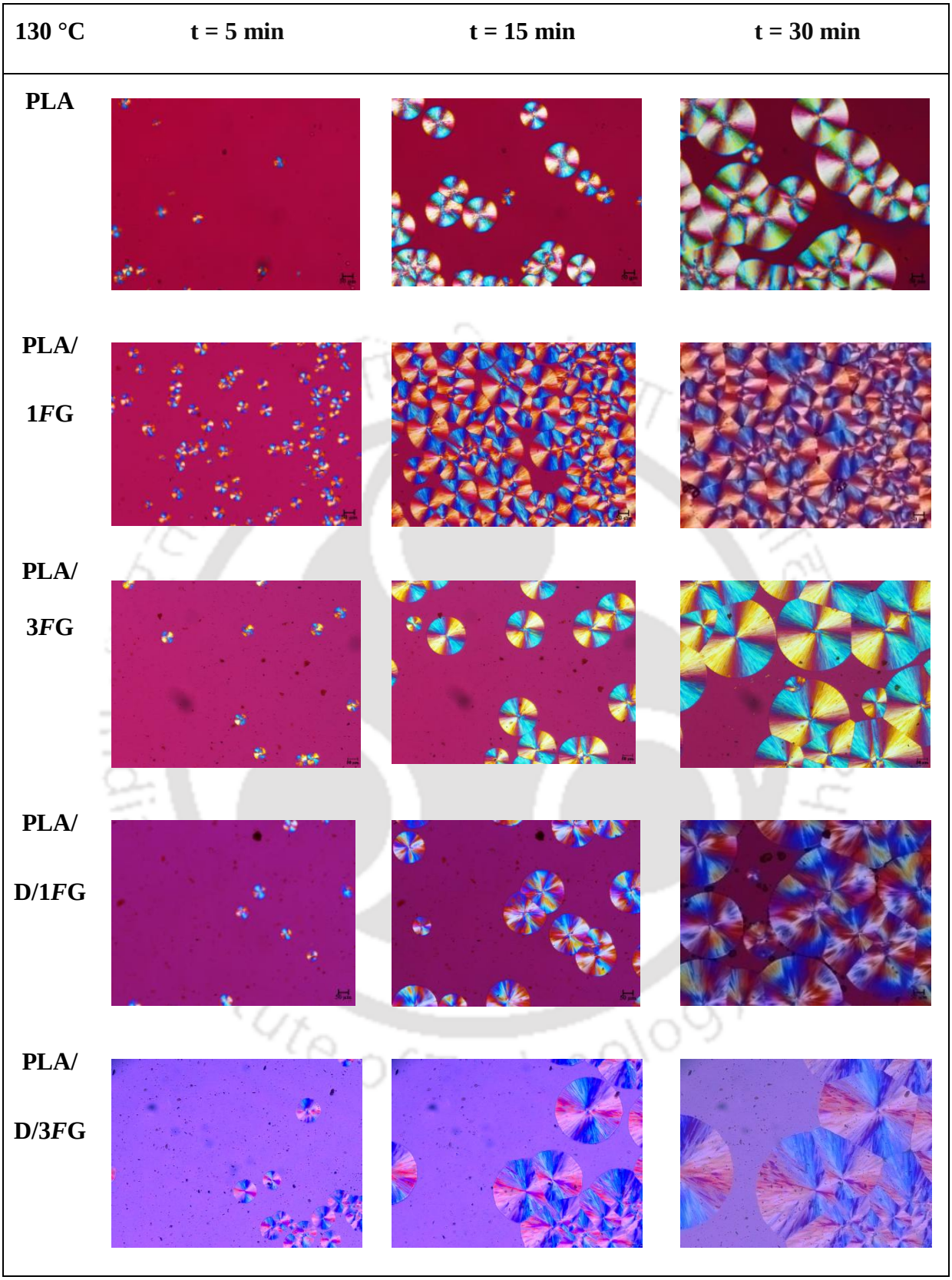

Figure 4.9: *Selected POM images of PLA, PLA/FG and their reactive bionanocomposite films at 130 °C.*

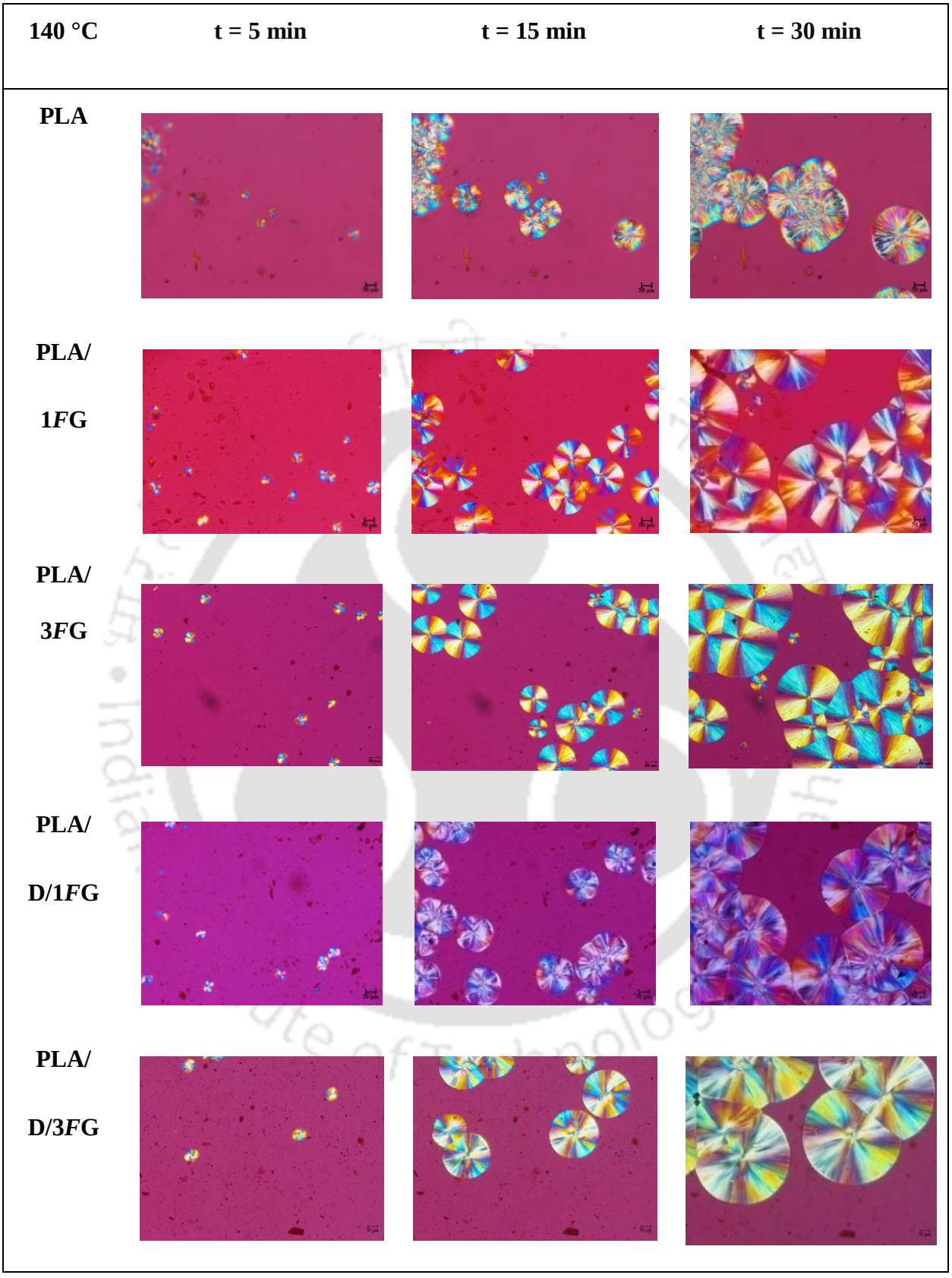

Figure 4.10: *Selected POM image of PLA, PLA/FG and their reactive bionanocomposite films at 140 °C.*

The effect and the difference between the blended PLA/*F*G with and without DCP is clearly noticed at 130 and 140 °C respectively. It is clearly observed from the Figure 4.9 (a) at 130 and Figure 4.10 (b) at 140 °C, that PLA/1*F*G has the strongest nucleation ability. The morphology of the PLA, PLA/1*F*G, PLA/3*F*G, PLA/D/1*F*G and PLA/D/3*F*G bionanocomposite films, especially the spherulites radius (µm) as function of time is investigated at 130 and 140 °C respectively. The growth rates (µm min^{-1}) can be estimated from the slope of the fitted lines until solidification is aborted due to the impingement on neighbouring spherulites whereas the nucleation density is estimated from the number of spherulites per unit area **(Xu et al. 2005; Bai et al. 2014)**. Thus, the growth rate and nucleation density are estimated for all the samples at 130 and 140°C are summarized in Figure 4.11 (a)-(d). For semi crystalline polymers, the G plot has established bell-pattern temperature based, as mentioned by many authors **(Xu et al. 2005)**. After attaining a maximum value of G at particular crystallization temperature, value of G is further decreased on increasing the temperature. For all the samples, the rate of spherulites growth are maximum at 130°C slightly decreased as the temperature increases from 130 to 140°C, which indicates that nucleation becoming slightly difficult at elevated temperature. For neat PLA (grade 4032 D), this observation is consistent with published article **(Xu et al., 2005)**. These results indicate that the crystallization rate is significantly accelerated after addition of *F*G which is associated with an increment in the number of nuclei and the spherulites growth of PLA. In contrast, crystallization rate is slightly slowing down in case of DCP treated PLA/*F*G nanobiocomposites which is probably due to insignificant change in the spherulites growth and slight reduction in number of nuclei, as compared with PLA. This finding is also supported by the DSC result, as summarized in Table. 4.1. After addition of DCP, compatibility between the PLA and *F*G has improved instead of nucleation. This is probably due to insignificant generation of crosslink density which will not produce sufficient

nucleation sites. Figure 4.11 (d) indicates that the nucleation density for PLA/1*F*G is the highest at the temperature of 130 and 140°C, respectively. In addition, the nucleation density is decreased with increasing temperature and increased with increasing degree of grafting sites.

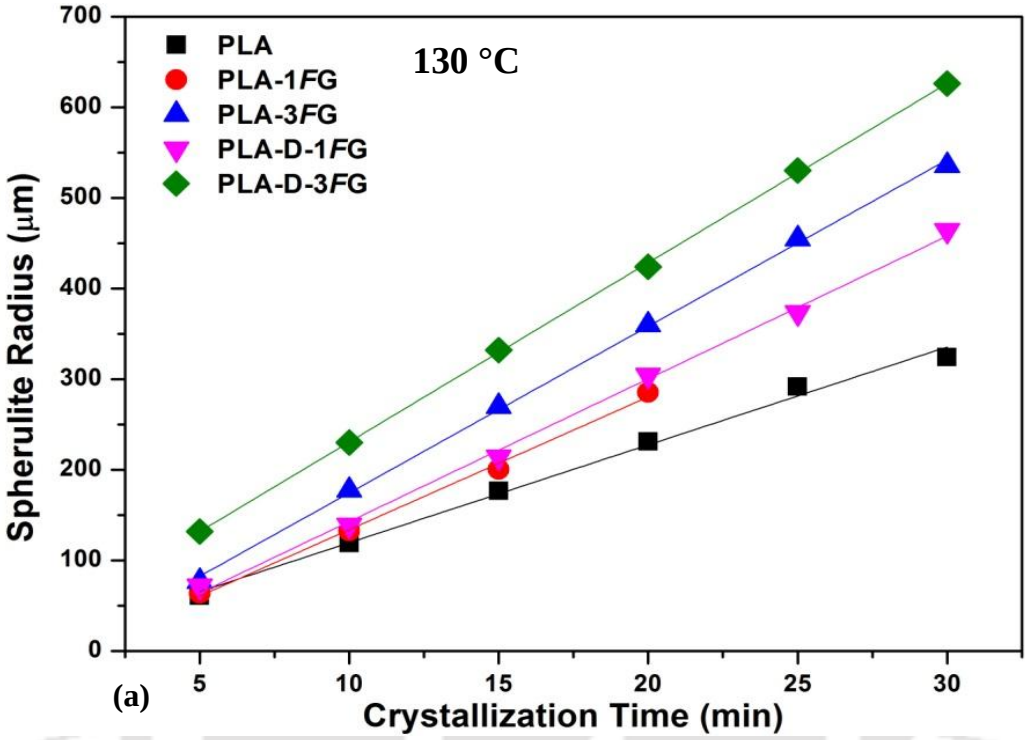

(a)

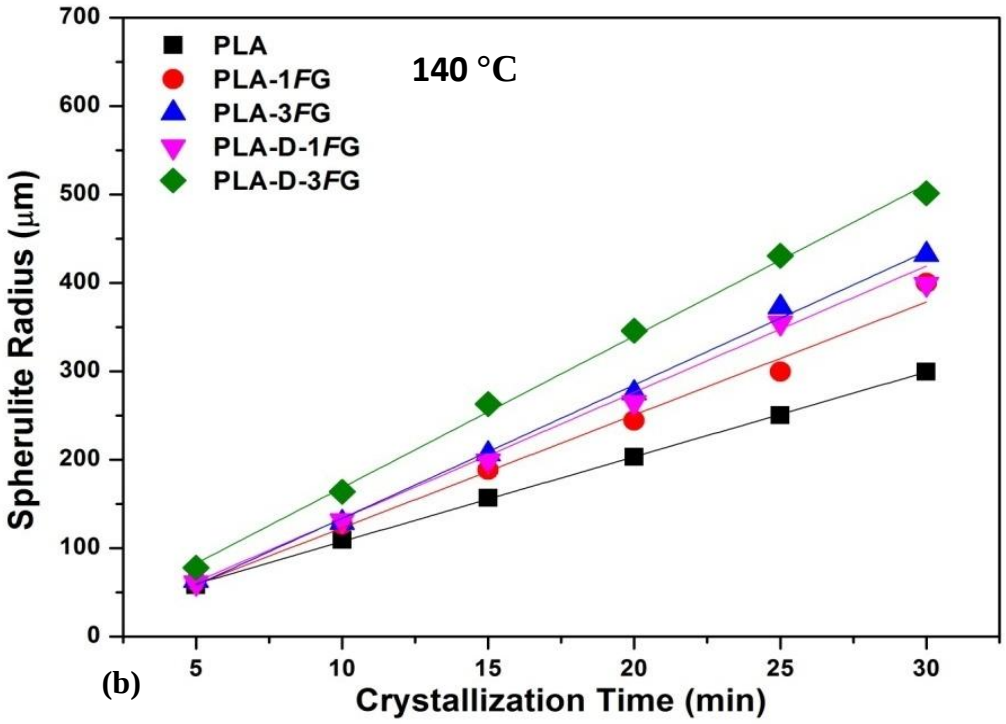

(b)

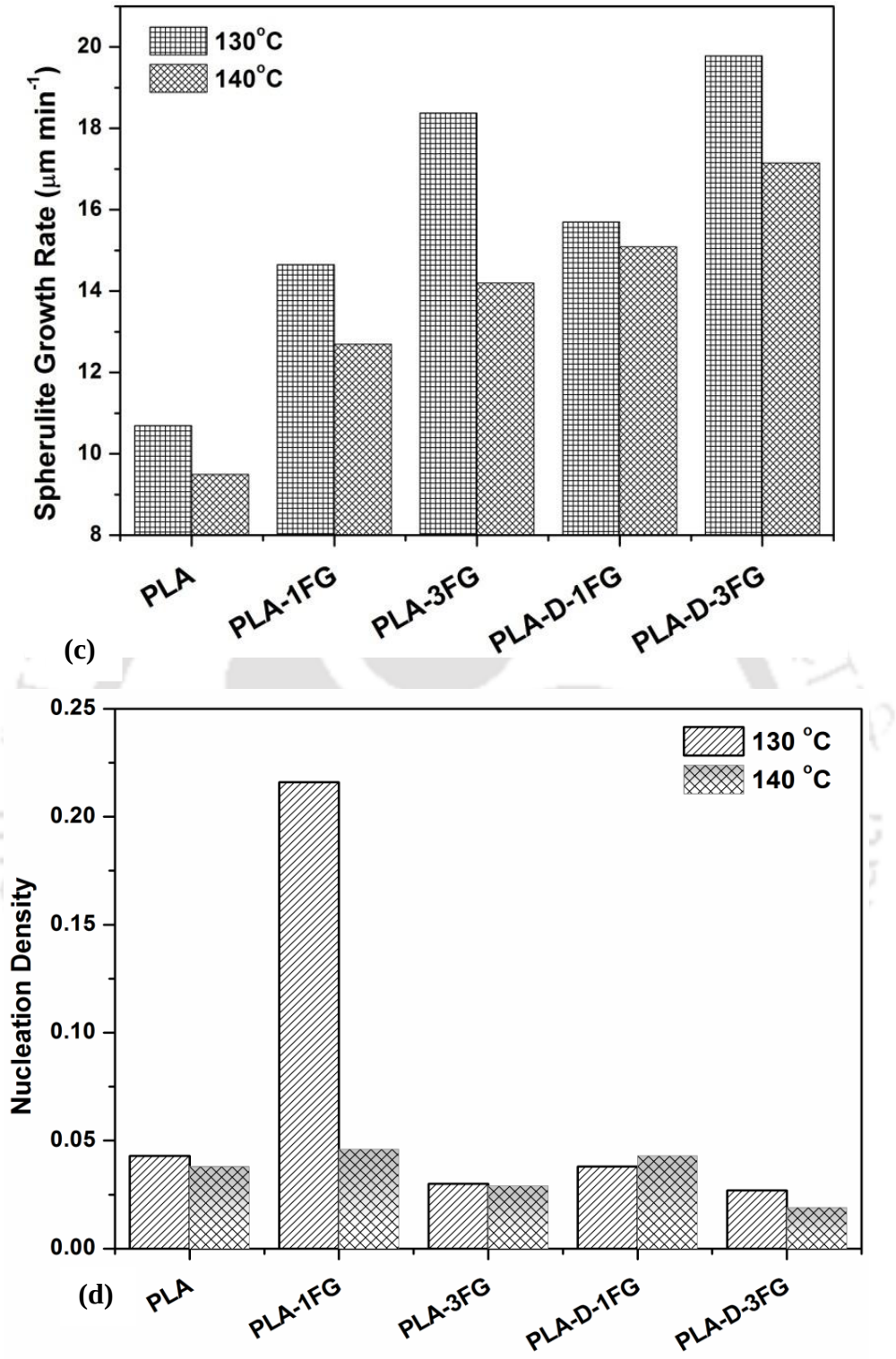

Figure 4.11: *Plot of spherulites diameter as function of time at (a) 130 and (b) 140°C, comparison of growth rate of spherulites (c) and nucleation density (number of spherulites cm^{-2}) in case of PLA, PLA/FG and their reactive modified bionanocomposite films.*

4.3 CONCLUSIONS

In this work, reactively extruded PLA/*F*G based bionanocomposite was fabricated with DCP and modification in structural properties is investigated using the FTIR technique. Addition of *F*G with DCP exhibits strong effect on the morphological, crystallization, UV barrier as well as mechanical characteristics. Reactive modification shows an improvement in interfacial compatibility between the PLA and *F*G in presence of DCP. Furthermore wettability of PLA/D/1*F*G is observed to be as high as ~14%. POM results indicate that the FG with and without introduction of DCP behaves as a nucleating agent. For PLA/D/1*F*G, UV–C blocking influence is the most pronounced (~95% improvement) which is utilized for packaging of UV sensitive items. The ultimate tensile strength is slightly decreased (~4%) with combined effect of 1 wt% *F*G along with DCP, but the elongation at break is enhanced up to ~28%. Therefore, it can be concluded that the reactive extrusion strategy of PLA/*F*G leads to the crosslinked structure with balanced performances. These findings assist the potential application of the developed film in the packaging applications.

Chapter 5

Thermal Degradation Studies of Poly (lactic acid)/ Functionalized Gum Arabic based Reactive Bionanocomposite Films

The current chapter focuses on the determination of thermal decomposition behaviour of the reactively extruded PLA/FG bionanocomposite films, wherein the change in weight loss as function of temperature was measured using thermogravimetric (TGA) analysis under dynamic heating regime to estimate the kinetic parameters such as apparent activation energy and pre-exponential factor. In this subsequent section, the predictions have been made on the possible decomposition mechanism using the generalized methods with feasible explanations. Hyphenated TGA-FTIR technique is utilized to detect the volatile components released from gum arabic, functionalized gum arabic and reactively extruded PLA/FG based bionanocomposite films.

The work in this chapter is published as:

Monika & Katiyar, V. (2018) Non-Isothermal Degradation Kinetics of PLA-Functionalized Gum Arabic based Bionanocomposites with Dicumyl Peroxide (DCP). Journal of Thermal Analysis & Calorimetry, 1-16. *DOI: 10.1007/s10973-019-08231-7*

ABSTRACT

The effect of functionalized gum arabic (*F*G) on the thermal decomposition behaviour of poly (lactic acid) (PLA) in presence of dicumyl peroxide (DCP) has been investigated from the thermogravimetric analysis (TGA) and coupled TG–Fourier transform infrared spectroscopy (FTIR) techniques. A series of *F*G compatibilized PLA films in presence of DCP have been fabricated using reactive extrusion at the set processing parameters, i.e. temperature and speed of screw are maintained at 180 °C and 60 rpm respectively. As compared to PLA, the thermal stability is reduced with the increase of the *F*G content. The addition of DCP could assist to maintain the thermal stability of PLA/1*F*G based bionanocomposite films. The activation energy (E_a) is evaluated using the model free approach, i.e. (i) modified Coats-Redfern (CR) (ii) Flynn Wall Ozawa (FWO) and (iii) Kissinger method that rely on a set of dynamical TGA experiments. The value of E_a is determined using Kissinger method is 158 (PLA), 143 (PLA/1*F*G), 125 (PLA/3*F*G), 154 (PLA/D/1*F*G) and 140 $kJmol^{-1}$ (PLA/D/3*F*G) respectively. The generalized mechanism methods suggest that the mechanism change A2 (2D nucleation and growth) to R3 (3D Phase boundary controlled reaction) for PLA, PLA/1*F*G, shift A2 to A4 (4D nucleation and growth) for PLA/3*F*G and A2 to R2 (2D Phase boundary controlled reaction) in case of DCP treated PLA/*F*G bionanocomposites. The release of the decomposed products for gum arabic, *F*G, PLA/*F*G based reactive bionanocomposite are investigated using TGA–FTIR technique.

GraphicalAbstract

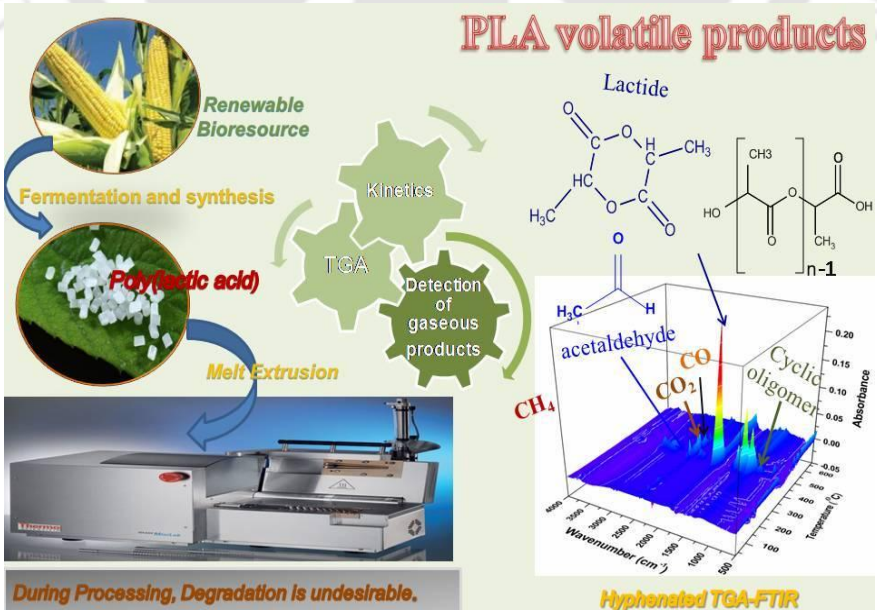

Scheme 5.1: *Schematic representation of thermal decomposition behaviour of PLA/FG bionanocomposite films.*

5.1 INTRODUCTION

Fossil fuels based plastics are widely used in diversified are such as packaging due to low cost, good barrier and mechanical properties. These conventional petro-plastics are non-biodegradable and have a short-lived after the use in case of packaging application and, therefore inevitably go to the ecosystem for decades causing serious environment and health issues. There is burgeoning interest in the plastic industry to replace the conventional petro-plastic from the bio-plastic **(Carassco et al. 2017)**. As we know that packaging materials easily get contaminated by the direct contact of food items or chemicals and, therefore discarding the plastic debris by incineration or landfill. However, incineration of plastic can release of hazardous volatile species into the environment and landfills can cause serious ground and water contamination. In this prospect, fully bio based plastic is one of the promising solution for solving environmental issues as well as provide a greener image to make it highly desirable for the packaging sector **(Carassco et al. 2017; Nair et al. 2018)**. Among various bio-plastics, poly (lactic acid) (PLA) has a great potential to substitute the commodity plastics due to its good mechanical and processing characteristics in the industrially viable applications such as packaging. It is thermoplastic polyester which is biodegradable and derived from various bioresources such as beet sugar, corn and sweet potato **(Song et al., 2012)**.

Gum arabic (GA), is a natural polysaccharide which mainly consists of arabinose, glucuronic acid, rhamnose, galactose and proteinaceous molecules, obtained from exudates of Acacia Seyal and Senegal trees **(Tripathi et al., 2017; Nayak et al., 2012)**.GA can be divided into three major fractions: (i) arabinogalactan (ii) arabinogalactan–protein (iii) and glycoprotein (GP) which contains different protein content (%) and molecular mass. It has been widely utilized in various applications such as pharmaceutical, cosmetics and food industry etc. It is also reported that, by using in situ polymerization to modify chemical structure of GA

attaching some other hydrophobic polymer as a side chain, it may possible to utilize in food packaging applications **(Tripathi et al., 2016)**. Such modifications not only helpful to promote the growth of bioplastics at commercial level but also encourage the depletion of petroleum based commodity plastics. It is necessary to observe the thermal decomposition behaviour of PLA based biocomposite to make it feasible at commercial level **(Yoshikawa et al., 2014; Dhar et al., 2016)**.At an elevated temperature, polymers start to undergo physicochemical changes due to the bond redistribution and formation of volatile products **(Dhar et al. 2016; Das et al. 2017)**. Thermal degradation includes the bond cleavage which subsequently leads to a rapid decrease of molecular weight that affects the final properties of materials, such as thermal and mechanical properties. From the literature it is observed that the thermal decomposition of PLA is due to depolymerization, transesterification reactions, random chain scission and oxidative degradations **(Valapa et al. 2014; Signori et al. 2009)**. Moreover, various factors such as type of filler, oligomer, unreacted monomers, residual catalyst, and specified conditions in the decomposition environment, molecular weight and its distribution have been reported to enhance the decomposition rate of PLA **(Borkotoky et al. 2018)**. Commonly, necessary attempts are required to prevent the decomposition of PLA in the melt state. Thermogravimetric analysis (TGA) is an efficient tool to understand the pathways to estimate the microscopic kinetics of these process.TGA is the most common technique to investigate the decomposition kinetics of PLA and its bionanocomposites. The data obtained from non-isothermal TGA profiles is helpful to understand the decomposition kinetics of the polymeric system. It is postulated that the thermal decomposition of plastic is a complex phenomena; also the choice of a reliable model or combination of kinetic models is very important. The kinetic modelling of the degradation behaviour of polymers has been widely investigated to evaluate the time and temperature associated with the processing and service lifetimes. In this work, mathematical methods based on model-free approach are

widely accepted for thermally activated reaction due to its potential to find apparent E_a as a function of α without knowledge of f(α) **(Valapa et al., 2014)**. In solid state kinetics, apparent E_a means that the least energy is required to break the chemical bond at a specific temperature. Since the E_a obtained from a kinetic model is the average of the E_a of physical process and chemical reactions, it known as apparent E_a. Isoconversional methods are utilized to confirm the complexity found in the thermal decomposition of polymeric system **(Chrissafis et al., 2010)**.

The present work focuses on the thermal decomposition kinetics of PLA; PLA/*F*G based reactive bionanocomposites to investigate the molten PLA processes without serious thermal decomposition under melt extrusion. Model-free methods i.e. isoconversional (FWO and modified Coat Redfern) and Kissinger method are selected to estimate the apparent E_a. Moreover, thermal degradation mechanism of the system is explained using the generalized master plots for PLA/*F*G with and without DCP. In addition, the evolved gases are investigated using the coupled TGA-FTIR technique at higher temperature to observe the decomposition process.

RESULTS AND DISCUSSION

- ***Molecular weight analysis of reactively extruded PLA/FG bionanocomposite films***

The molecular weight and the molecular weight distribution of PLA affects various properties associated with the mechanical strength, processability, and degradation of the polymer. Figure 5.1 illustrates the number average molecular weight (M_n), weight average molecular weight (M_w) and polydispersity index (PDI) of PLA and PLA/*F*G based bionanocomposite films. For PLA/1*F*G bionanocomposite, the area of peak associated with high molecular weight (at retention time ~11.5 min) is slightly reduced while the peak area of low molecular weight (at retention time ~16.5 min) is increased. Finally, no significant change in M_n (~12%) and M_w (~4%) is detected. In case of PLA/3*F*G, M_n and M_w are gradually decreased

with ~13% and ~10% respectively due to further reduction in the area of high molecular weight peak (~2%) whereas a remarkable increase in the area of low molecular weight peak (~46%) is observed with increasing the *F*G (~3 wt%) content. It has been suggested that the existence of OLLA chains functionalized with GA or agglomeration of *F*G at higher content (~3 wt %) is responsible for the faster degradation of PLA at elevated temperature during melt processing. Also, a small peak with shoulder at low molecular weight fraction region is noticed due to the PLA chain scission. With the incorporation of DCP into PLA/1*F*G, Mw is found to improve (~9%) and polydispersity index (PDI) increases from 1.6 (PLA) to 2.2. There is a possibility that the *F*G radicals developed by the decomposition of the *F*G chains would be able to further interact with PLA radicals which leads to the improvement in M_w of reactively extruded PLA/*F*G as compared to PLA. It is worthwhile to mention that the area related to low molecular weight fractions of PLA/D/1*F*G is lower (retention time ~ 16.6) than that of PLA. From this observation, it can be comprehended that DCP is responsible for enhancing the efficacy of compatibility between the matrix and filler (newly formed C-C linkage) which leads to the enhancement in molecular weight via propagation reactions. Other possibility is that decomposing species would possibly be interacting with PLA and *F*G (Yuzay et al., 2010). For PLA/D/3*F*G biocomposite, the extent of compatibility is dropped due to the agglomeration of *F*G at higher loading (~3 wt %) and further reduction in molecular weight is observed which indicates that the material experiences thermal decomposition during the extrusion process **(Dhar et al. 2016)**. The reactive modified bionanocomposite films reveal the molecular weight distribution in a broader fashion.

- ***Thermal performance of the reactively extruded PLA/FG bionanocomposite films***

Thermal stability of PLA, PLA/*F*G with and without DCP and the parameters are summarized in Figure 5.2 and Table 5.1 respectively. A single step degradation pattern is noticed from differential thermogram (DTG) at various heating rates. PLA/*F*G

bionanocomposites represent a reduction in the thermal stability with the increment in the amount of filler. This behaviour is noticed due to the presence of short oligomer (OLLA) chains attached with gum arabic in PLA/*F*G bionanocomposites, which are responsible for increasing the thermal decomposition process **(Tripathi et al., 2017; Kumar et. al., 2017)**. No significant changes are observed in the thermal stability with the incorporation of DCP into PLA/1*F*G as compared to PLA. For PLA/D/3*F*G, the value of thermal parameters such as 10% wt loss (T_{10}), 50% wt loss (T_{50}) and maximum degradation temperature (T_{max}) are further reduced by ~6°C. Therefore, it can be inferred that the increase in the number of shorter chains due to chain scission, leads to the decrease in thermal stability of PLA/D/3*F*G bionanocomposite.

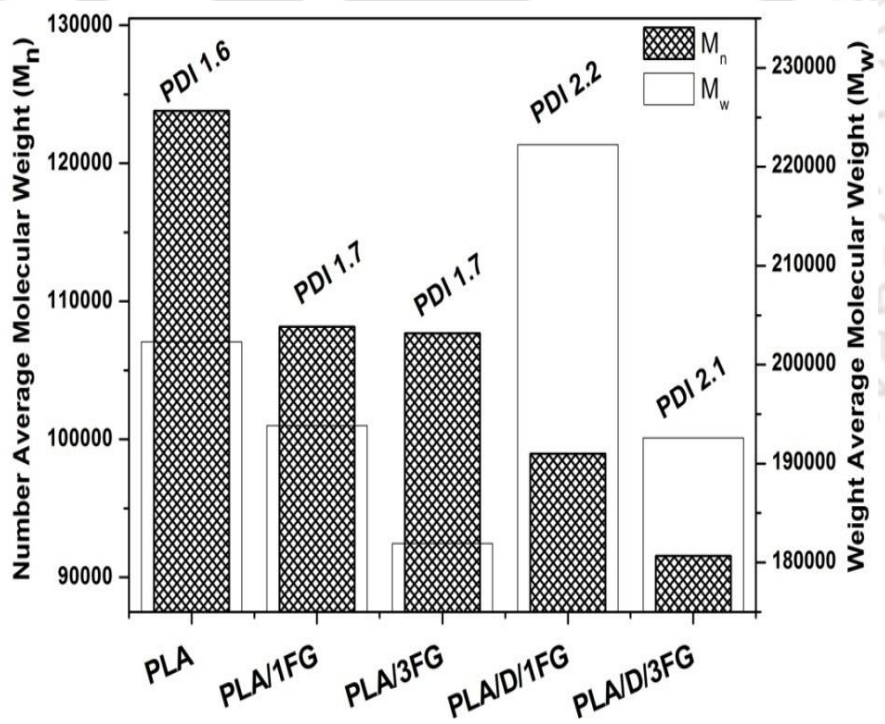

Figure 5.1: *Determination of number average (M_n),weight average molecular weight (M_w) and polydispersity index (PDI) of PLA, PLA/FG and their reactive modified bionanocomposite films.*

- ***Nonisothermal TGA data for the reactively extruded PLA/FG based bionanocomposite***

The TGA and differential thermogram (DTG) plots of neat PLA, PLA/*F*G and their reactive

bionanocomposite film at multiple heating rates (β) as: 5, 10, 15 and 20 °C min^{-1} respectively, are illustrated in Figure 5.3 (a) – (e). As expected, the degradation curves are shifted to the higher set value of representative temperature as β is raised from 5 to 20°C min^{-1}, which confirms that the less time is required to attain a given temperature at higher β **(Yuzay et al., 2010)**.

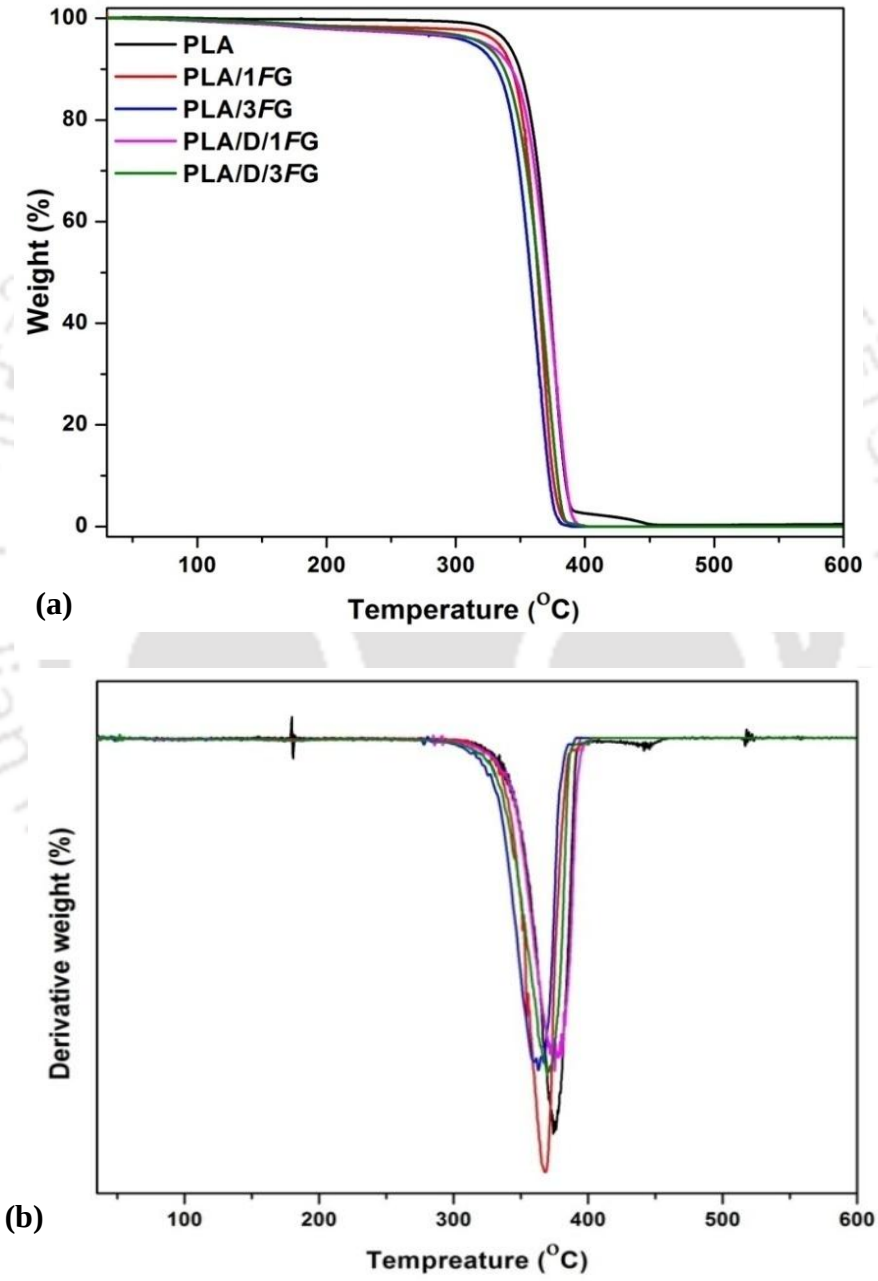

Figure 5.2: *(a) TGA (b) DTG profiles for PLA, PLA/FG and their reactive modified bionanocomposite films at 10 °C min^{-1}.*

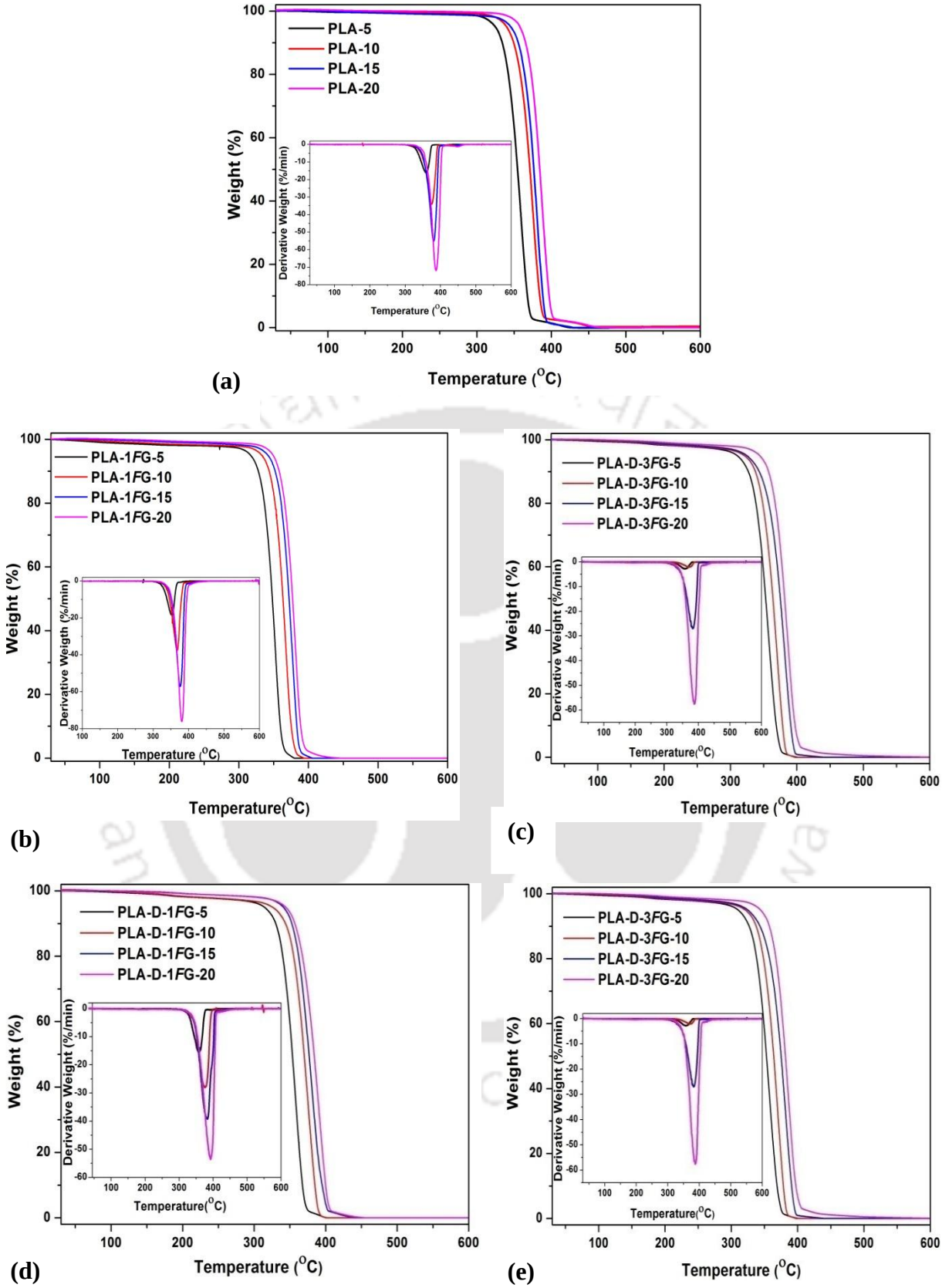

Figure 5.3: *TGA and DTG profiles for (a) PLA, (b) PLA/1FG, (c) PLA/3FG, (d)PLA/D/1FG, and (e)PLA/D/3FG at different heating rates such as 5, 10, 15,20 °C min^{-1}.*

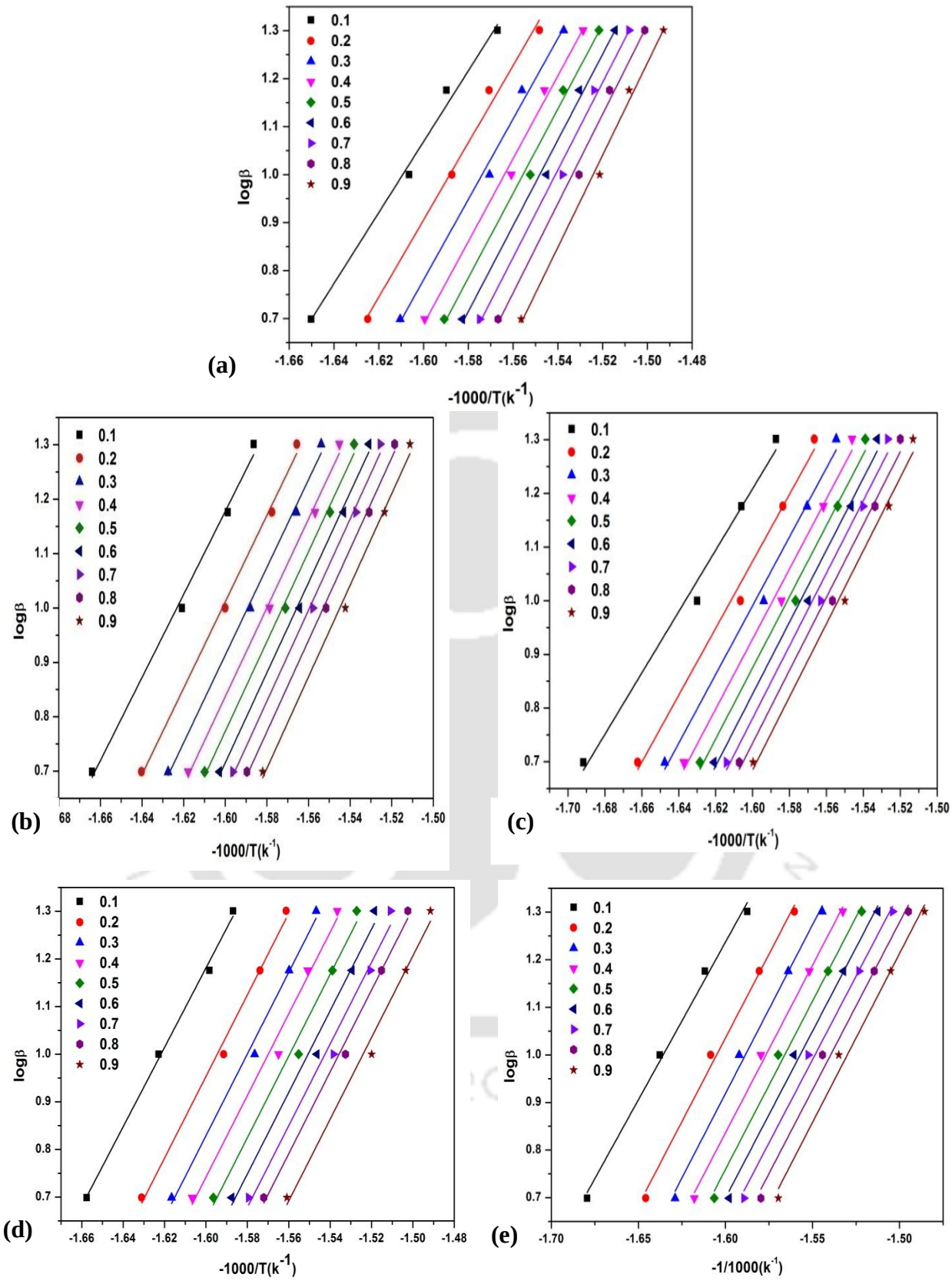

Figure 5.4: *FWO plots for (a) PLA, (b) PLA/1FG, (c) PLA/3FG, (d) PLA/D/1FG, and (e) PLA/D/3FG bionanocomposite films.*

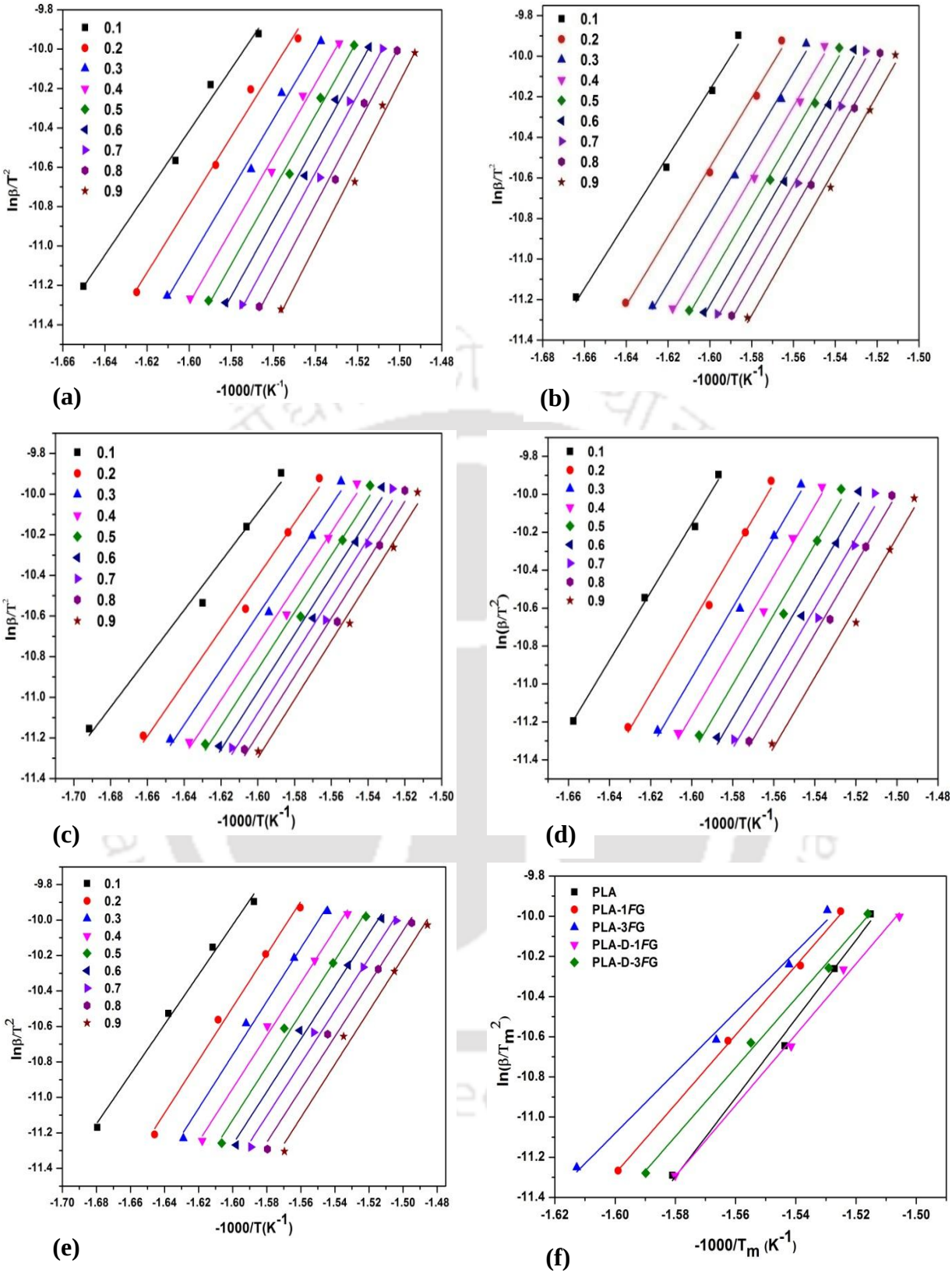

Figure 5.5: *Modified CR plots for (a) PLA, (b) PLA/1FG, (c) PLA/3FG, (d)PLA/D/1FG, (e) PLA/D/3FG and (f) Kissingerplots for PLA, PLA/FG bionanocomposite films with and without DCP.*

These two isoconversional (FWO and modified CR) methods offer straight linear fit to the experimental data. Figure 5.4 (a)-(e) & Figure 5.5 (a)-(e) confirm the applicability of these two methods for all bionanocomposites. Kissinger method is used in Equation 2.1 for fitted plots of ln β/T_m^2 (Y-axis) versus -1/T_m (X-axis) and E_a is obtained from the slope of a linear fit. Moreover, it is found that estimated value of E_a by Kissinger's method coincides with the FWO and modified CR method and comparisons of E_a with regression coefficient (R^2) are also summarized in Table 5.2.

- ***Distribution plots of E_a (kJ mol^{-1}) for the reactively extruded PLA/FG bionanocomposite films using FWO and modified CR method***

Distribution of E_a for PLA, PLA/*F*G bionanocomposite films with reactive extrusion is estimated using the FWO and modified CR methods to get deeper insights on the influence of *F*G with DCP to the PLA. For all the samples, E_a is the lowest at the low α (0.1) which is probably due to the existing weak linkage in the polymeric chains end. These weak sites are generally responsible to initiate the degradation process. In case of PLA based film, E_a is observed as 158 kJ mol^{-1}, similar finding is reported by **Tesfaye et al., 2016**. As seen in Figure 5.6 (a) – (b), a gradual variation in E_a vs α is an indication of complex mechanism for PLA film. Similar behaviour has been reported by **Valapa et al., 2014** suggesting that the decomposition of PLA follows the decomposition mechanism, i.e. cis-elimination, inter and intra molecular transesterification, random and unzipping depolymerisation. Addition of 1 wt% *F*G into PLA leads to the reduction in the value of E_a which is lower than that of the PLA in the range $0.2 \leq \alpha \leq 0.9$. As compared to PLA, the difference in estimated E_a is greater at high α (0.9) than that of low α (0.1) which indicates that *F*G might responsible to vary the decomposition route of PLA. From Table 2, the estimated E_a represents the similar decreasing trend further increasing the loading of *F*G (3 wt %) content in PLA at an entire α range. Therefore, PLA/3*F*G shows a significant reduction in E_a with the representative values

of α and the lower value of the E_a indicates the faster decomposition. It can be attributed that the presence of OLLA functionalized GA generates the weak link sites in the PLA matrix by improving the segmental mobility in polymeric chains as well the enhancement in the intermolecular distance due to the short chains segment of the bio-filler **(Tripathi et al., 2017)**. These weak sites are responsible for enhancing the decomposition rate.

It is also noticed that the incorporation of DCP in the PLA/1*F*G has stabilized the value of E_a withthe range (0.1–0.9), which also suggest the similar types of bonds are breaking during the decomposition process. However, the difference of E_a in case of PLA/D/1*F*G is found to increase by ~15 kJ mol^{-1} at low α (0.2) and almost close at high α (0.9), as compared to that of PLA/1*F*G. This result indicates that the decomposition route of DCP treated PLA/1*F*G is almost similar to PLA/1*F*G at high α. As observed in Figure 5.5 (a), E_a is highest at the low α (≤0.4) which subsequently led to the improved compatibility for *F*G grafted PLA samples (due to the formation of new C–C linkage), as compared to PLA. The incorporation of DCP into PLA/3*F*G significantly reduces the E_a, as compared to PLA/D/1*F*G. The decrement in E_a is possibly due to decrease in crosslinking/branching sites which are due to the agglomeration of *F*G at higher loading. This confirms that the chain dissociation accelerates the thermal decomposition of PLA/*F*G bionanocomposites.

- ***Degradation mechanism for reactively extruded PLA/FG bionanocomposite films***

Figure 5.7 (a)–(e) represents the comparison of the master plots with the experimental plots which is supposed to predict the accurate mechanism at 10ºC min^{-1} heating ratefor all the samples. The estimated values of E_a using Kissinger method are selected to solve the Equation 2.19 and Equation 2.20 respectively. It is observed that the decomposition profile of PLA film obeys the nucleation model (A2 mechanism) till α~0.8 and finally shifts towards the R3 mechanism (phase boundary controlled reactions, at α~0.9) corresponding to the thermal decomposition of sample which proceeds through the volatilization from the surface

towards the centre of the sample **(Badia et al., 2010; Tesfaye et al., 2016)**, as shown in Figure 5.7 (a).These type of kinetic models are generally observed during the crystallization process, but sometimes it is also noticed in case of the thermal degradation of polymers. These studies deal with the controversy of the correlation between the solid-state mechanism and the mathematical models **(Badia et al., 2010)**. Meanwhile, a physical approach of the effect of thermal decomposition on the PLA, PLA/*F*G bionanocomposite with and without reactive modification has been employed from estimated kinetic parameters. In case of PLA/1*F*G, it follows the A2 type mechanism up to 0.8 conversion and slightly shifts to R3 when α is 0.9, as depicted in Figure 5.7 (b). This possibly means that thermal decomposition starts from the active zone (nuclei), which is further responsible for the activation and growth of gas bubbles in the polymeric system during the melt state. In case of PLA/3*F*G, it follows the A_n type mechanism, as noticed in Figure 5.7 (c). There is gradual variation from A2 (α~0.1 to 0.3) to A3 (α~0.4), then to A4 (α~0.5 to 0.9) mechanism. Figure 5.7 (d) exhibitsthe experimental curve of PLA/D/1*F*G bionanocomposite which is almost consistent with the A2 mechanism up to α~0.9. As it can be seen in Figure 5.7 (e), it follows the A2 mechanism in case of PLA/D/3*F*G.

- ***Detection of evolved volatile components using hyphenated TGA–FTIR technique***

The evolved volatile components are analysed using hyphenated TGA–FTIR technique with the aim of observing the decomposition behaviour of GA, *F*G, PLA/*F*G with and without addition of DCP at elevated temperature **(Materazzi et al., 1997)**. The IR bands at several sets of temperatures during decomposition stages investigate the mechanism of the gaseous species evolved out. In case of TGA–FTIR, the intensity of IR spectra corresponding to different gaseous products is found to enhance with raising the temperature and are dropped off after achieving the temperature at which the decomposition rate is maximum **(Mili et al., 2017)**.3D–IR stack plots of the released volatile components for gum arabic, *F*G, PLA/1*F*G

and PLA/D/1*F*G are displayed in Figure 4.1S (a)-(d) in the supplementary section and wave number assignment for IR bands are listed in Table 5.3.

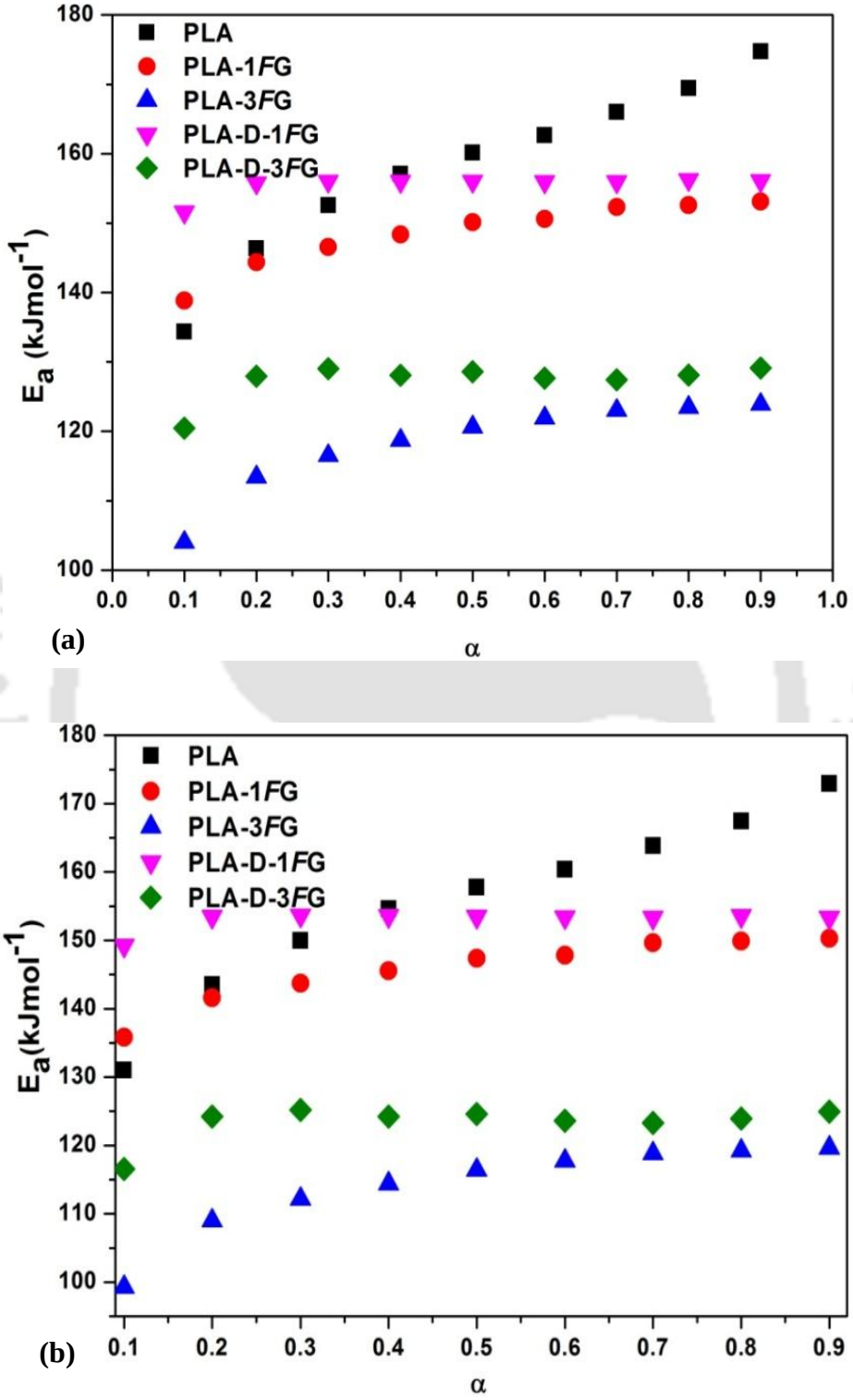

Figure 5.6: *Distribution of E_a with α using (a) FWO and (b) modified CR method for PLA, PLA/FG and their reactive bionanocomposite films*

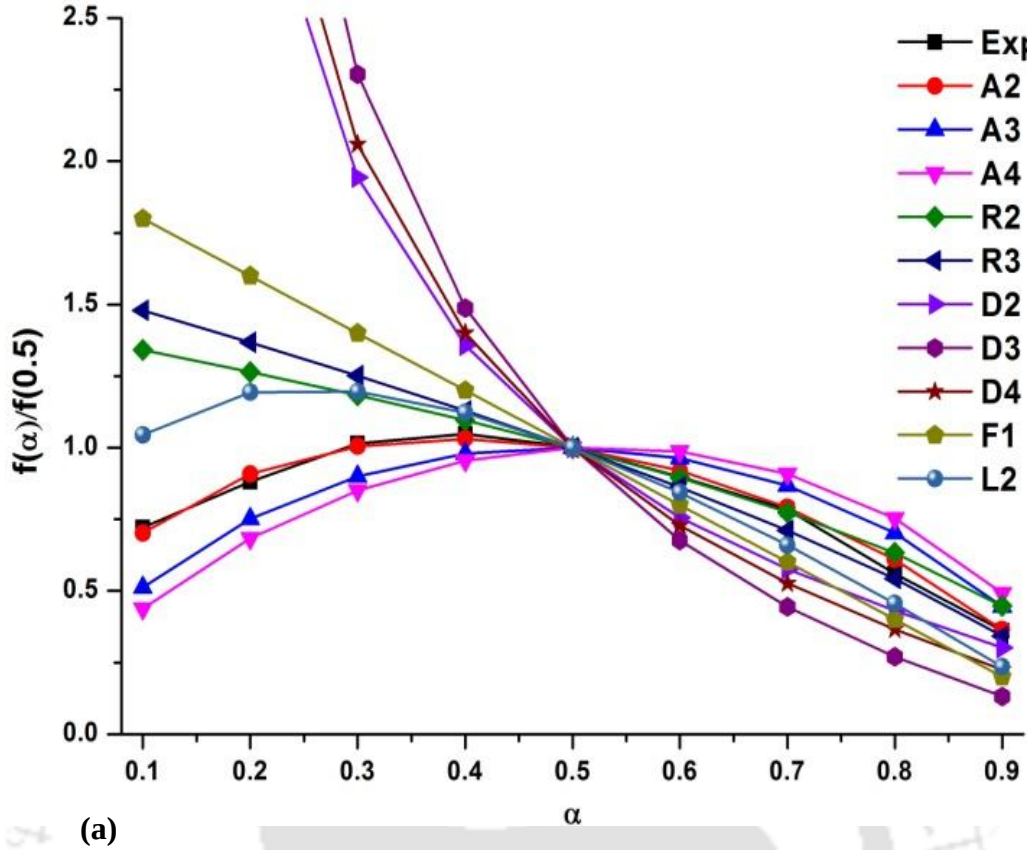

(a)

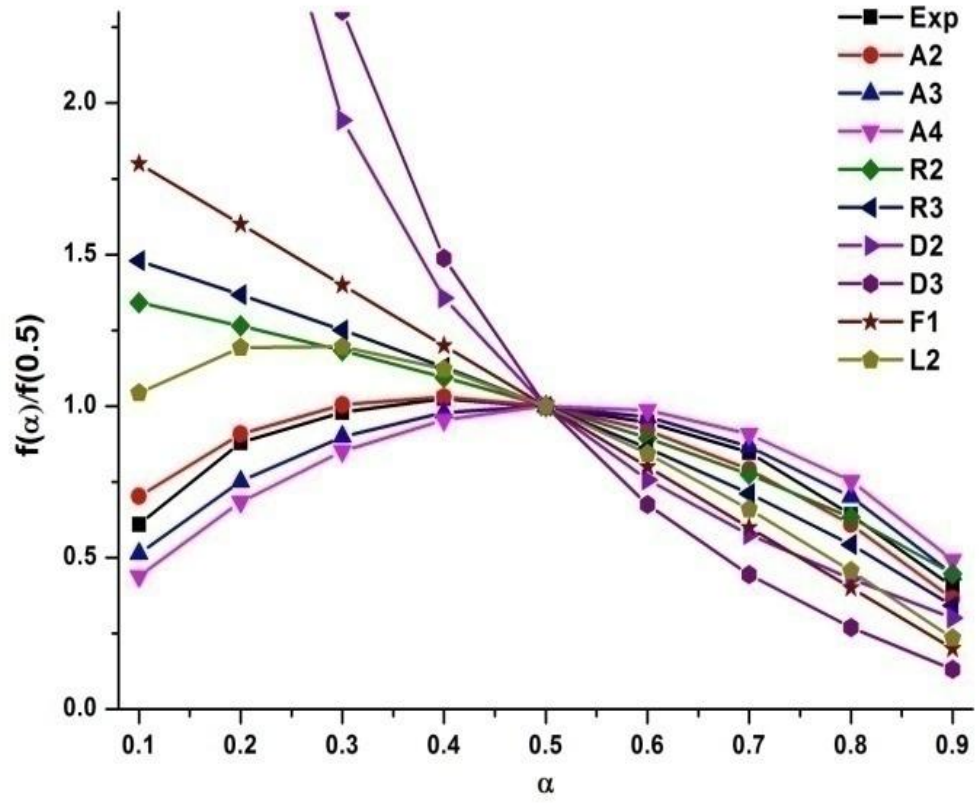

(b)

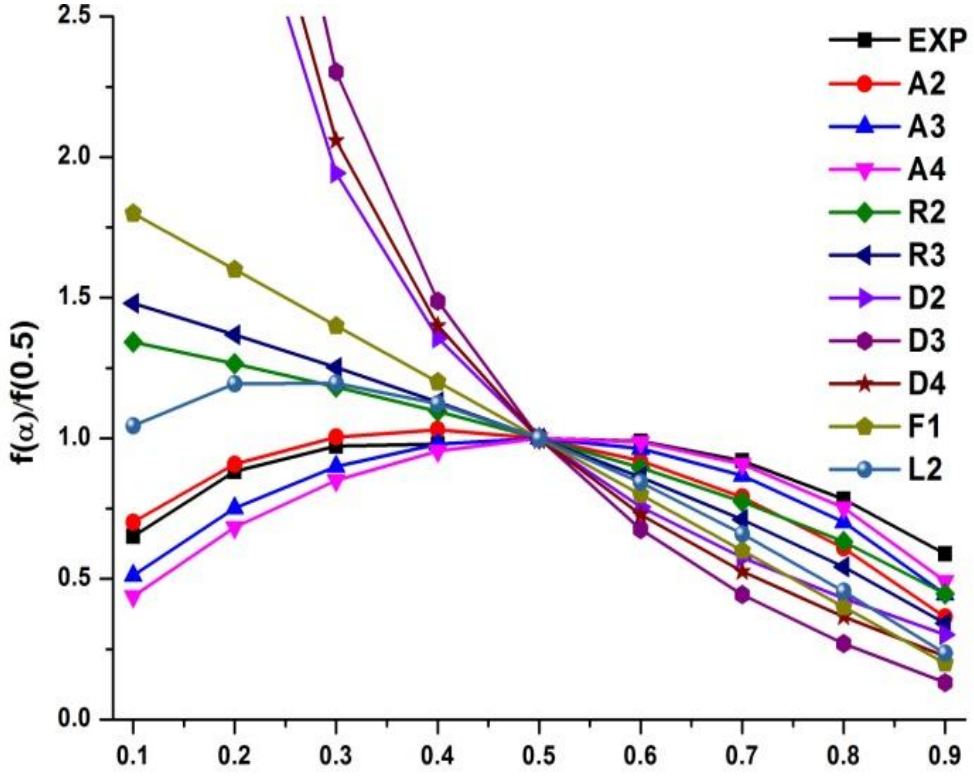

(c)

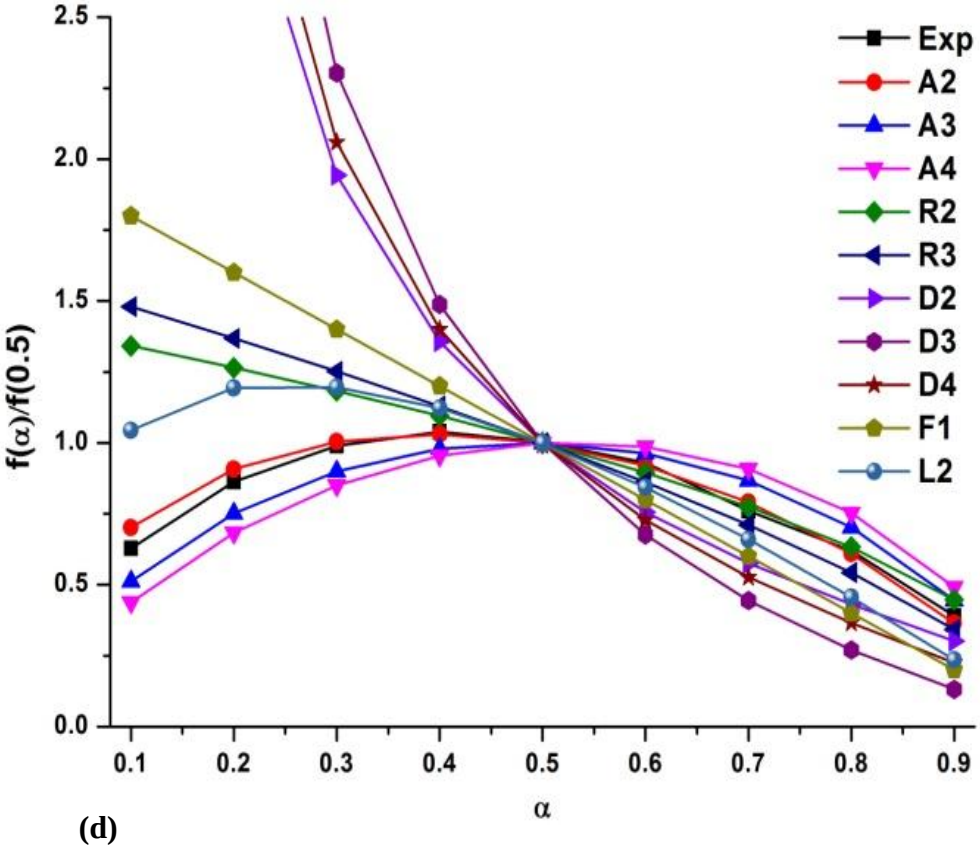

(d)

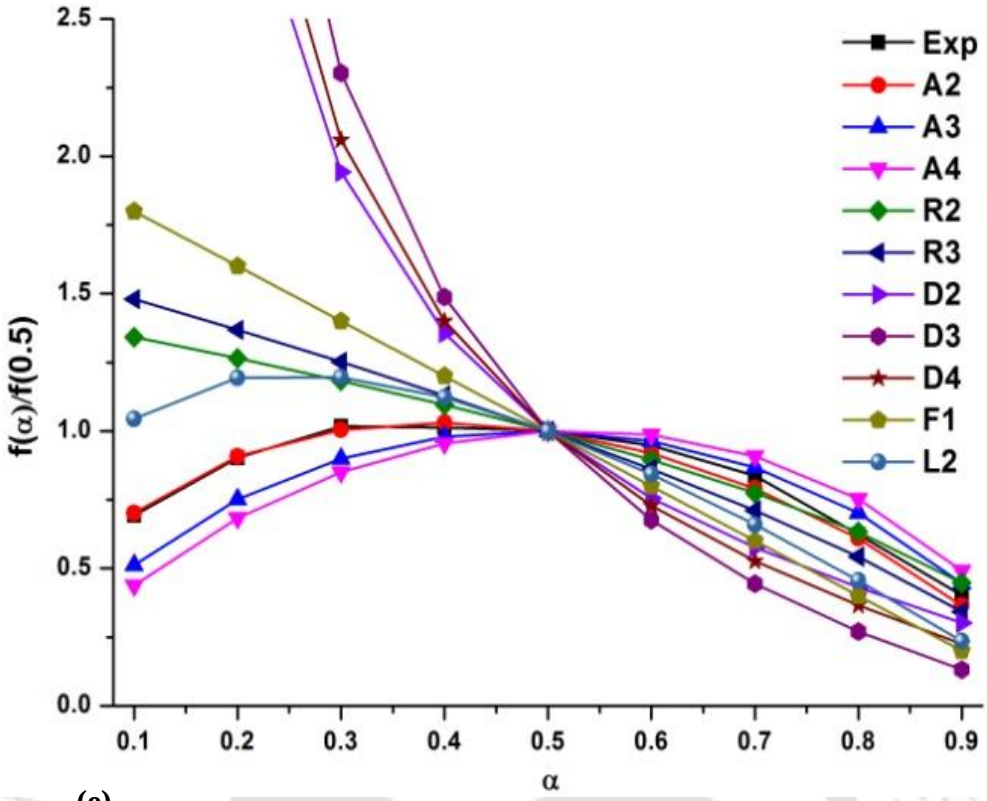

(e)

Figure 5.7: *Generalized mechanism plots for (a) PLA, (b) PLA/1FG, (c) PLA/3FG, (d) PLA/D/1FG, (e) PLA/D/3FG bionanocomposite films.*

- ***Gum arabic (GA)***

The IR spectra at several typical temperatures during decomposition process are collected to detect the evolved products. Figure 5.8 (a)–(b) exhibit the stacked plot of the volatile components by the thermal decomposition of the GA and the IR spectra at 327 °C respectively. At 327 °C, the characteristic bands of CO_2 are noticed at 2352–2309 and 669 cm^{-1}, and a double apex of CO at 2180–2115 cm^{-1} **(Patwa et al., 2018)**. The major bands are the following **(Gonc et al., 2014; Shen et al., 2009)**: O–H (3500–3700cm^{-1}), C–H (2800–3000 cm^{-1}), C=O (1802, 1783, 1765 and 1727 cm^{-1}), N–H (1598 cm^{-1}), C–C (1374 cm^{-1}) and C–O (1174–1104 cm^{-1}). In addition, a band at 1509 cm^{-1} appears for aromatic group containing species. The presence of functional groups is due to the release of the products such as water, methane and other substances that are produced such as ester, acid, aldehydes and alkanes

during the thermal decomposition of the polysaccharides. When the temperature is above 400 °C, the higher yield of CO_2 is generated by the secondary reaction of polysaccharides in the charring stage. It is also produced by the secondary reaction of gaseous product which may be dominated in this case. In all the cases, the formation of CO_2, CO and different carbonyl compounds in the IR spectra confirm the scission of the glycosidic linkage which subsequently leads to the cleavage of C–C bond in the backbone of polysaccharides **(Liu et al., 2014)**. The presence of large number of hydroxyl groups and the dehydration reaction are responsible for the production of carbonyl components. A small quantity of CO is generated in the main decomposition stage, which is due to the cracking of C=O group. Therefore, CO is classified as a primary product of thermal decomposition of polysaccharides. While the release of anhydride containing component is affirmed by the IR peak located at 1802–1778cm^{-1},the two sharp absorbance peaks at 1783, 1765 cm^{-1} assigned to C=O stretching which confirms the release of carbonyl components in the decomposition of GA.

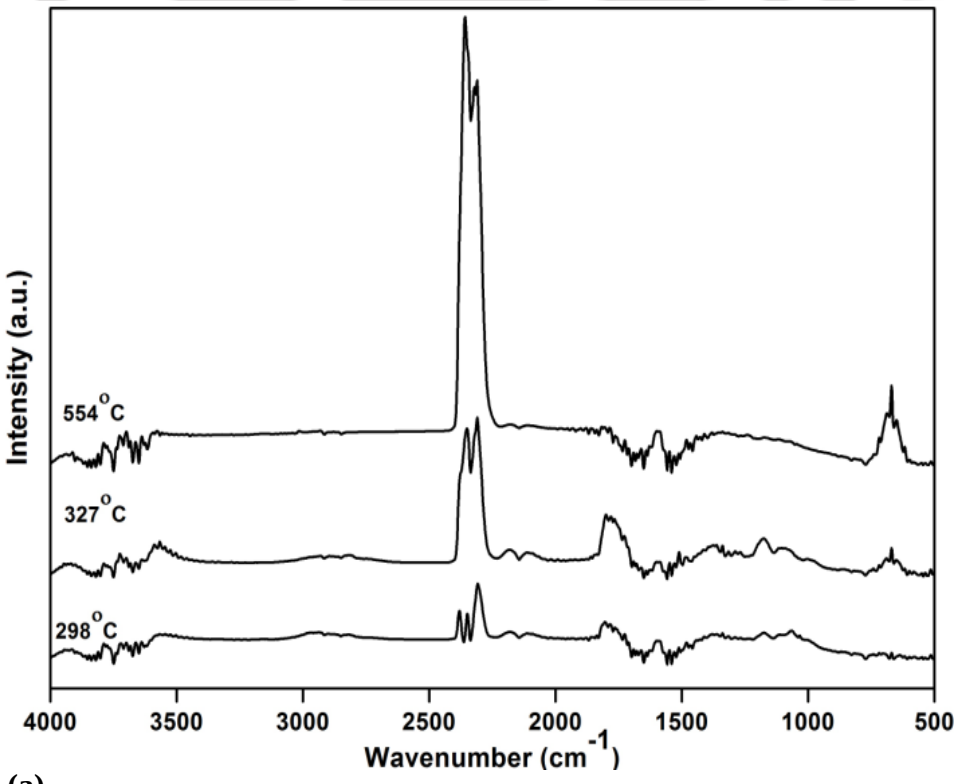

(a)

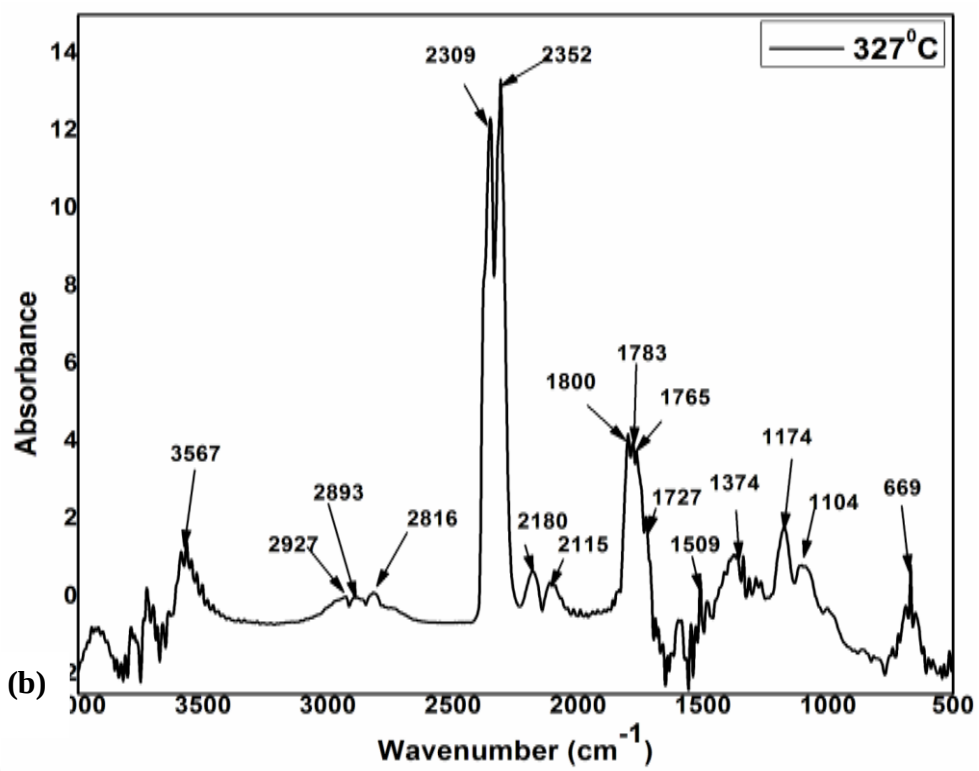

Figure 5.8: *2D-stacked graph of the evolved volatile species obtained at (a) selected temperature interval from 250−600 °C and (b) FTIR spectra obtained at 327°C during the thermal decomposition of gum arabic.*

Functionalized gum arabic (FG)

Figure 5.9 displayed the 2D stacked plot of the volatile components by the thermal decomposition of the *F*G. At 200 °C, the bands at 1788 with 1792 cm^{-1} (C=O), 1241-1113 cm^{-1} (C–O–C), 2358-2309 cm^{-1} (CO_2) confirm the formation of acid, cyclic oligomers or lactide and CO_2 respectively. When the temperature rises up to 330 °C, the characteristics bands of CO_2 (2352–2309, 669 cm^{-1}) and CO (2180–2115 cm^{-1}) are noticed. Moreover, the major IR bands are the following **(Triphati et al. 2016; Vogel et al., 2008)**: O–H (3500–3700cm^{-1}), C–H (3008cm^{-1}), $–CH_3$ (2952–2894 cm^{-1}), C=O (1792cm^{-1}) for lactide or cyclic oligomers, N–H (1598 cm^{-1}), $–CH_3$ (1452–1380cm^{-1}), C–O–C (1240–1109 cm^{-1}), ring skelton (933cm^{-1}). The presence of IR bands for O–H (3500–3700 cm^{-1}) and aromatic C–C (1509 cm^{-1}) confirm the formation of water and aromatic compounds.

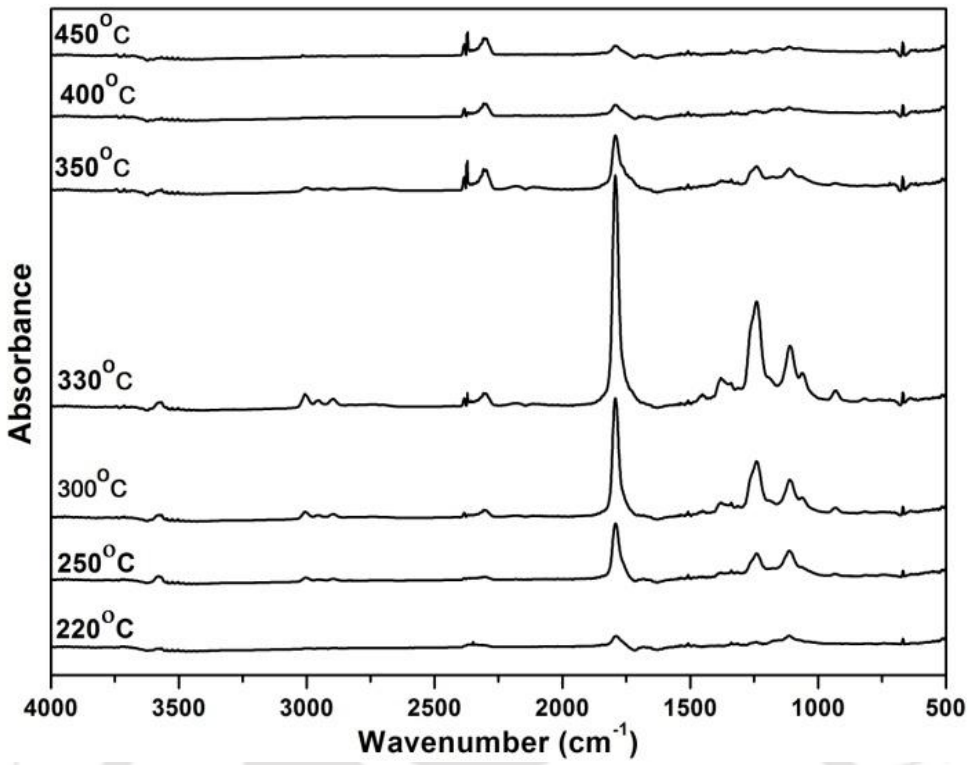

Figure 5.9: *2D-stacked graph of the evolved volatile species obtained at selected temperature intervals from 220−450°C during the thermal decomposition of functionalized gum arabic.*

Comparison of PLA/FG bionanocomposite films with and without DCP

Figure 5.10 (a) – (b) illustrates the total IR spectra plots in absorbance mode for main decomposition profiles of PLA/1*F*G bionanocomposite with and without incorporation of DCP. It is noticed that almost similar type of volatile components are released from the DCP treated PLA/1*F*G, as compared to PLA/1*F*G such as carbon dioxide, carbon monoxide lactide or cyclic oligomers, acetaldehyde, acetic acid, esters and acrylates respectively, as mentioned in Table 5.3. **(Vogel et al., 2008; Marechal et al., 1987)**. In case of DCP treated PLA/*F*G bionanocomposite, IR absorbance of lactide or cyclic oligomers are increased in a remarkable way, as shown in Figure 4.1S (d). In this case, the evolved products and DCP are responsible for enhancing the radical reaction **(Zhao et al., 2014)**. Hence, these results confirm that the formation of C=O compounds are more favourable at the higher temperature in case of DCP

treated PLA/*F*G.

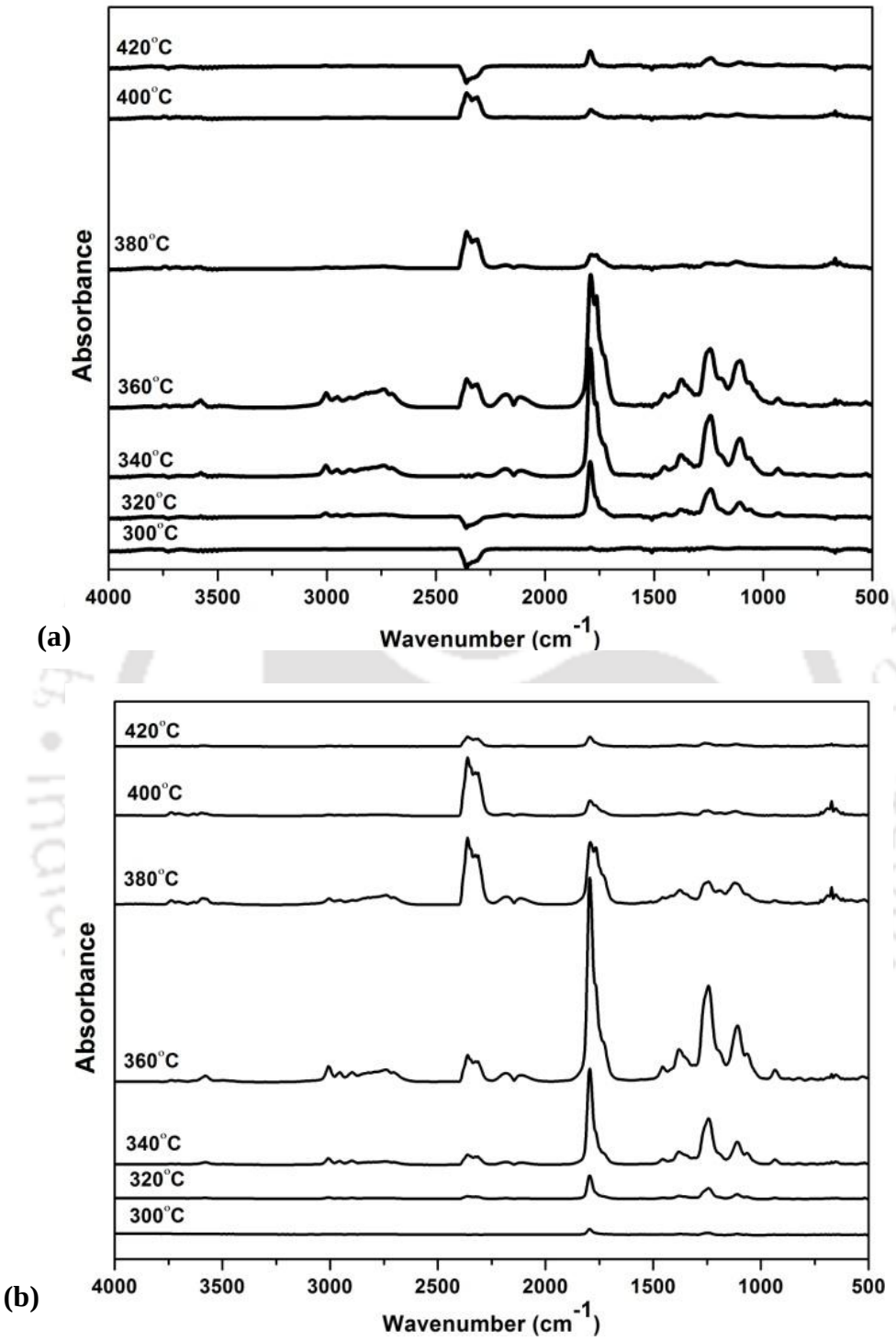

Figure 5.10: *2D-stacked graph of the evolved volatile species obtained at a selected temperature interval from 300−450°C during the thermal decomposition of (a) PLA/1FG and (b) PLA/D/1FG bionanocomposite films*

5.2 CONCLUSIONS

In this chapter, it has been found that the thermal stability is significantly improved for DCP treated PLA/1*F*G as compared to PLA/*F*G but it is lower than PLA. Meanwhile, the thermal stability is decreased after addition of *F*G into PLA matrix. TGA kinetic study confirms that E_a is enhanced for PLA/D/1*F*G, as compared to PLA/1*F*G. From the distribution E_a plot, it is found that PLA/*F*G proceeds through a different decomposition process than that of PLA. Moreover in comparison to PLA/*F*G, decomposition behaviour is observed at high α for the DCP treated PLA/*F*G. Results obtained from the generalized mechanism shows that PLA and PLA/1*F*G followed A2 and R3 mechanism while it changing from A2 to A4 in case of PLA/3*F*G bionanocomposite. DCP treated PLA/*F*G bionanocomposites proceed A2 to R2 type mechanism. Based on the coupled TG–FTIR technique, it is concluded that the scission of the typical glycosidic linkage and C–C bond is responsible for initiating the decomposition of GA. In case of *F*G, the decomposition starts due to the cleavage of the ester group, C–C and C–O bond of OLLA functionalized with GA. Furthermore, lactide, cyclic oligomers, acetaldehyde, acetic acid, esters and acrylates are produced at high temperature for DCP treated PLA/*F*G.

Table 5.1: *Thermal parameters of PLA, PLA/FG with and without addition of DCP.*

Samples	T_{10} (°C)	T_{50} (°C)	T_{90} (°C)	T_{max}(°C)
PLA	344	368	382	374
PLA/1*F*G	343	363	375	368
PLA/3*F*G	340	361	372	363
PLA/D/1*F*G	343	369	384	375
PLA/D/3*F*G	337	363	377	369

Table 5.2: *Comparison of E_a (kJ mol^{-1}) and regression coefficient (R^2) deduced from the FWO, modified CR and Kissinger methods.*

Samples	FWO E_a (R^2)	modified C-R E_a (R^2)	Kissinger E_a (R^2)
PLA	158 (0.992)	155 (0.992)	158 (0.994)
PLA/1*F*G	148 (0.996)	145 (0.995)	143 (0.998)
PLA/3*F*G	118 (0.991)	114 (0.990)	125 (0.994)
PLA/D/1*F*G	155 (0.991)	152 (0.990)	154 (0.996)
PLA/D/3*F*G	127 (0.994)	123 (0.993)	140 (0.990)

Table 5.3: *IR peaks of the volatile products confirmed by hyphenated TGA–FTIR for PLA/1FG with and without DCP at 380°C.*

Wave number for PLA/1*FG*	Wave number PLA/D/1*FG*	Assignment (bond)	Vibration	Products
3577	3579	O–H	asymmetric stretching	Hydroxyl and water
2310–2358, 669	2310–2358, 669	C=O	asymmetric stretching	CO_2
2110–2180	2110–2180	C–O	stretching	CO
930	930	Aromatic C–H (ring skelton)	stretching	For Cyclic oligomer
1795	1795	C=O group	asymmetric stretching	Lactide/ Cyclic oligomer
3002	3002	C–H group	stretching	
2950	2950	CH_3	asymmetric stretching	
2889	2892	CH_3	symmetric stretching	
1452–1380	1452–1380	C–H_3 group	bending	
1242–1104	1242–1104	C–O–C group	stretching	
1764	1764	C=O group	stretching	Acetaldehyde
2738	2738	–C–H	bending	
2820	2820	C–H	stretching	
1370	1370	C–H	bending	
1788	1788	C=O	stretching	Acetic acid
3580	3580	O–H	stretching	
1390	1390	C–H	Bending	
1745	1745	C=O	stretching	Lactic acid ester
1728	1728	C=O	stretching	(ester, acrylate)

Chapter 6

Effect of Dicumyl Peroxide on Poly (lactic acid)/ Poly (butylene succinate)/Functionalized Chitosan based Bionanocomposite Films

Chitosan (CH) is known to have poor dispersion in hydrophobic bio based aliphatic polyester due to its hydrophilic nature. Hence, the strategic functionalization of oligo-L lactic acid (OLLA) chains onto chitosan has been demonstrated in this chapter in order to improve the compatibility of CH with the hydrophobic bio based polyester matrix. PLA/PBS blends have been reactively modified in melt condition, using dicumyl peroxide (DCP) as an initiator in presence of the functionalized chitosan (FCH) to produce high molecular weight crosslinked/branched structures with improved properties of PLA/PBS/FCH based bionanocomposite films. Moreover, the fabricated films show balanced mechanical properties, improved melt strength, thermal performance and UV barrier properties, making them adequate for the packaging of UV sensitive material for commercial scale with a great potential to replace the fossil based conventional plastics.

The work in this chapter is published as:

Monika, Pal, A., Bhasney, S., Bhagbhati, S. & Katiyar, V. ***(2018)*** *Effect of Dicumyl Peroxide on a Poly(lactic acid) (PLA)/Poly(butylene succinate) (PBS)/Functionalized Chitosan based nanobiocomposite for packaging: A reactive extrusion study, ACS Omega, 3, 13298-13312.DOI:10.1021/acsomega.8b00907*

ABSTRACT

Bionanocomposites with balanced mechanical characteristics have been fabricated from poly (lactic acid) (PLA)/Poly (butylene succinate) (PBS) blends in the weight ratio (80/20) by varying the concentration of functionalized chitosan (*F*CH) through the reactive extrusion at a temperature of 185 ºC. The combined effect of *F*CH and dicumyl peroxide (DCP) shows an insignificant change in the tensile strength with a remarkable increase in % elongation at break (~ 45%) values. Addition of DCP leads to an increase in the molecular weight (Mw ~ 22%) of PLA/PBS/D/1*F*CH bionanocomposite which may be attributed to cross-linking/branching effect of *F*CH on the polymers. The interfacial polymer-filler adhesion is also improved, which is observed the morphological image of PLA/PBS/D/1*F*CH. For PLA/PBS/D/1*F*CH, the crystallization rate and nucleation density of PLA are found to increase due to formation of cross-linked/branched structures, which possibly act as nucleating sites. Therefore, the present work facilitates a simple reactive extrusion processing with a combination of balanced thermal and mechanical properties, improved hydrophobicity (7°) and UV-C blocking efficiency, which draws the possibilities for the utilization of the ecofriendly bionanocomposite films in the packing of UV sensitive material on a commercial level.

Graphical Abstract

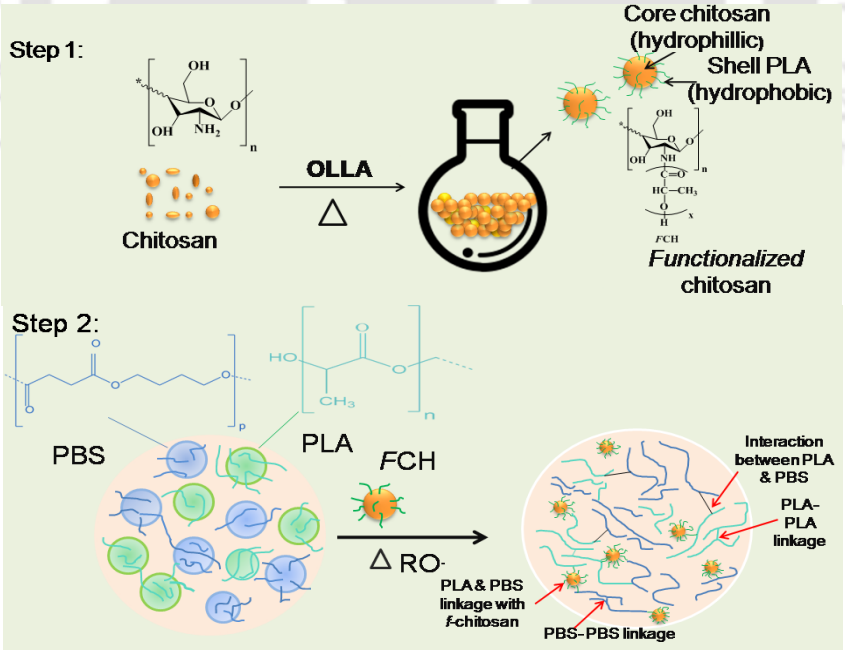

Scheme 6.1: *Schematic illustration of possible mechanistic pathways for PLA/PBS blends in the presence of FCH along with DCP during reactive extrusion.*

6.1 INTRODUCTION

The recent trends have focused on the consumption of bio-plastics in developing novel processes for the fabrication of eco-friendly polymeric materials and for solving the fossil-oil crisis associated with conventional synthetic polymers **(Wu et al., 2005)**. Poly (lactic acid) (PLA), a biomass based thermoplastic polyester, is generally produced from renewable resources (tapioca roots, sugar beet and sugar cane), which is the most sustainable alternative to the conventional synthetic polymers as compared to other biopolymers **(Drumright et al., 2000)**. Among those bio-plastics, PLA has drawn a considerable interest due to its competitive mechanical properties, biocompatibility, and easier processability **(Kamal et al., 2015)**. However the application of PLA on industrial scale is limited because of its brittle nature, high glass transition temperature (T_g ~ 55 ºC), slow crystallization rate, poor melt strength and inferior barrier properties **(Nerkar et al., 2015)**.

From this view point, the modification of PLA by copolymerization or physical blending, loading of nano-fillers or plasticizers are economic and effective approaches to overcome these limitations. The primary role of blending PLA with flexible biopolymers that exhibits lower T_g values such as poly (butylene succinate) [PBS, (T_g ~ -32 ºC)], poly (butylenes succinate-co-adipate) [PBSA, (T_g ~ -45 ºC)] and polycaprolactone [PCL, (T_g ~ -60 ºC)] to maintain the biodegradability with tuned T_g, which resolves the brittleness problem and finally improve the toughness **(Shibata et al., 2006; Jiang et al., 2006)**.

Melt polycondensation allows the synthesis of PBS by the reaction of 1, 4-butanediol with succinic acid, which can also be derived using monomers from fossil feedstock or renewable bioresources **(Cherykhunthod et al., 2015; Bahari et al., 1998)**. PBS is a bio based polyester with high flexibility, impact strength, and chemical resistance which is similar to polypropylene (PP). Thus, PBS has attracted much attention as a promising eco-friendly bio-plastic and could be an appropriate choice to melt mix with PLA. Nevertheless, applications

of PBS are limited because of its poor gas barrier (OTR) properties, water vapor transmission rate (WVTR), and melt viscosity (η) properties which are essential in the packaging sector.

In fact, PLA/PBS system is one of the best choices because the combination of two gives desired properties of each polymer. One polymer has potential to tailor the mechanical characteristics (e.g. toughness and elongation at break) of the blend to control the physiological environment by varying the blend ratio and the other polymer provides stability to molecular properties of the two components system **(Jiang et al., 2006; Bhatia et al., 2007)**. Many researchers have reported about PLA/PBS, and claimed that the PLA/PBS (80/20) blend has shown better compatibility in comparison to other blend ratios **(Bhatia et al., 2007)**. However, the properties of PLA/PBS system are not significantly enhanced by melt processing probably due to the poor interfacial adhesion and the phase separation between the PLA and PBS domains.

Chitosan (CH) is a cationic polysaccharide produced by deacetylation of chitin, which is an extremely recommended biopolymer for packaging applications due to its biodegradability, biocompatibility, excellent oxygen barrier, anti-oxidant, antifungal, antimicrobial characteristics and most importantly film forming ability **(Pal et al., 2016)**. It is the second most abundant biopolymer in nature after cellulose and can be used as a polymer matrix as well as bio-filler. On the other hand, chitosan has poor dispersion in the PLA matrix due to its hydrophilic nature. According to **Pal et al., 2016** hydrophobic functionalized chitosan (*F*CH) can solve the dispersion problem of chitosan in the hydrophobic PLA matrix. It is also worth mentioning that *F*CH has a great potential to be used as a bio bio-filler in the food packaging applications with enhanced barrier properties.

As mentioned above, PLA, PBS and *F*CH are one of the most promising candidates and play vital roles in contributing towards the marketing of bio-plastics designed for sustainable packaging. None of these three components can fulfill the demand for almost all structural

materials in packaging application when used alone. For food packaging applications, barrier to UV light is also one of the essential characteristics to inhibit the decomposition of packed food stuff **(Pal et al., 2018)**. It is a well known fact that UV light is responsible for damaging the vitamins and fatty acids which are found in food items. Therefore, this demand should be fulfilled for its benefits in the food packaging applications. The evolution of bionanocomposite with requisite melt-strength, thermal performance and stiffness-toughness balance, is still a challenging task. In comparison to binary system, a multicomponent polymer system usually shows more balanced performance in terms of physicochemical and thermal properties. Recently, investigating the properties of multicomponents based polymeric system formed by the combination of three or more components has attracted the attention from both the commercial and the academic sectors **(Zhang et al., 2012)**. To the best our knowledge, PLA/PBS/*F*CH based bionanocomposites in the presence and absence of DCP has not been evaluated so far. To consider the promising tailored characteristics of PLA, and PBS, we have investigated the influence of *F*CH and DCP (as compatibilizing agent) on various analytical properties of PLA/PBS system. The reactive extrusion technique is utilized to prepare bionanocomposite with balanced performance and different characteristics such as surface morphology, structural, thermal and mechanical properties in order to determine its feasibility of production in a continuous manner. These complementary properties of PLA/PBS/*F*CH with the addition of DCP are very important, the most important being tailored mechanical properties, melt strength and thermal performance.

6.2 RESULTS AND DISCUSSION

- ***Plausible reaction mechanism of reactively extruded PLA/PBS/FCH bionanocomposite in presence of DCP***

The plausible reaction mechanism of bionanocomposites in the presence of DCP during melt state under high shear action has been illustrated in Scheme 6.1. When DCP is decomposed

into free radicals during elevated temperature, it facilitates the extraction of the H's from the PLA and PBS chains to generate free radicals on the backbone of PLA, PBS component which is the result of propogation of radical reaction to form crosslinked/branched structure between the PLA and PBS **(Takamura et al., 2008; Ji et al., 2014)**. PLA generates free radicals on tertiary C atoms which gets readily stabilized during reactive extrusion **(Nerkar et al., 2015; Ji et al., 2014)**. It is well reported that PBS contains many secondary hydrogen's (H) atoms which provide easy abstraction of hydrogen's (H) by peroxide radicals in comparison to PLA. On the other hand, free radicals are formed on lactic acid oligomer (OLLA) chains attached to *F*CH. It is noteworthy to mention that there are possibilties for the formation of a strong covalent (C–C) chemical linkage via a combination of PLA/*F*CH, PBS/*F*CH, PLA/PBS, PLA/PLA, PBS/PBS, PLA/PBS/*F*CH and PLA/*F*CH/PBS. This may result in the formation of more complex products, which included crosslinking/branching of PLA and PBS with *F*CH, and PLA-g-PBS copolymers and the resulting reaction will be more complicated **(Nerkar et al., 2015; Formela et al., 2018; Ma et al., 2012)**. In a nutshell, it is assessed that the crosslinked/branched structures in the bionanocomposites played a vital role modifying the properties of the reactive bionanocomposites in a controlled fashion. With the help of literature we have put forwarded a plausible reaction mechanism in Figure 6.1.

FTIR–attenuated total reflectance (ATR) technique is used to identify the structural modification taking place during the chemical reactions among PLA, PBS and *F*CH in the presence of DCP, as shown in Figure 6.2. The characteristic infrared bands of all the samples are tabulated in Table 6.1. The representative characteristic peaks of PLA are as follows: 2996 (corresponding to asymmetric CH_3 stretching, 2946 (symmetric CH_3 stretching), 2880 (C–H stretching), 1748 (C=O stretching), 1382 (symmetric bending of CH_3), 1381-1358 (symmetric bending of CH_3), 1452 (asymmetric bending of CH_3), 1180 (asymmetric C–O–C asymmetric rocking CH_3), 1128 (symmetric rocking CH_3), 1080 (symmetric stretching

C–O–C), 1041 (stretching C–CH_3), 868 (stretching C–COO & also attribute to amorphous region of the PLA phase), 954 (rocking CH_3 + stretching C–C) and 753 cm^{-1} (bending C=O in PLA due to its crystalline phase) **(Kister et al., 1998; Maio et al., 2015; Silva et al., 2015)**. However, PBS shows band at 2880 cm^{-1} (–CH_2 stretching) in the PLA/PBS blend. For PLA/PBS/1*F*CH spectra, transmittance band at 1646 cm^{-1} also confirms the presence of amide linkage in *F*CH. It is noticed that the intensity of bands at 2996, 2946 and 2880 cm^{-1} decreased, whereas the band at 2964 (–CH_2 vibration) is more intense than that of the PLA/PBS blend. However, a new chemical bond is not formed after the addition of *F*CH into then PLA/PBS blend which indicates merely an electrostatic interaction of *F*CH with the PLA/PBS system **(Martino et al., 2015)**.

After addition of DCP into PLA/PBS/1*F*CH, it is observed that the band at 2996 cm^{-1} has shifted slightly to 2992 $cm^{-1}$and the band at 1748 cm^{-1} is shifted to 1746 cm^{-1} due to the change in structure. The peak at 2880 cm^{-1} is absent, and two new peaks at 2918 cm^{-1} (asymmetric stretching CH_3) and 2850 cm^{-1} (symmetric stretching CH_3) have been found. Further the modification in chain due to the branching/cross-linking through the formation of new band at 805 cm^{-1} (C–C bond) is detected, which influences the intensity of ester linkages **(Tesfaye et al., 2017)**. While chain modification in PBS chains has confirmed through the presence of doublet which is attributed to the twisting of CH_2 at 1338-1312 cm^{-1}, C=O at 1712 cm^{-1} and band at 917 cm^{-1} assigned to C–OH bending in carboxylic group **(Ishak et al., 2013; Yao et al., 2017; Pallathadka et al., 2017)**. It may be attributed to the evident interaction of PLA, PBS and *F*CH in the presence of DCP existed upon reactive modification at elevated temperature.

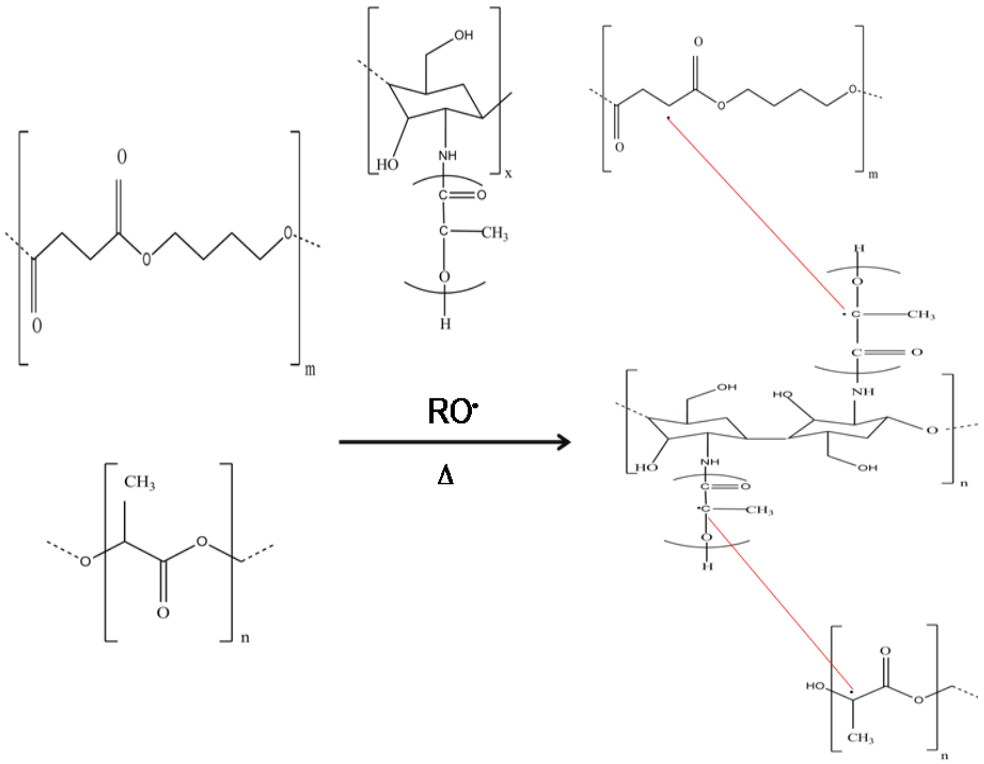

Figure 6.1: *Plausible reaction mechanism of PLA/PBS/FCH based reactive bionanocomposites in the presence of DCP.*

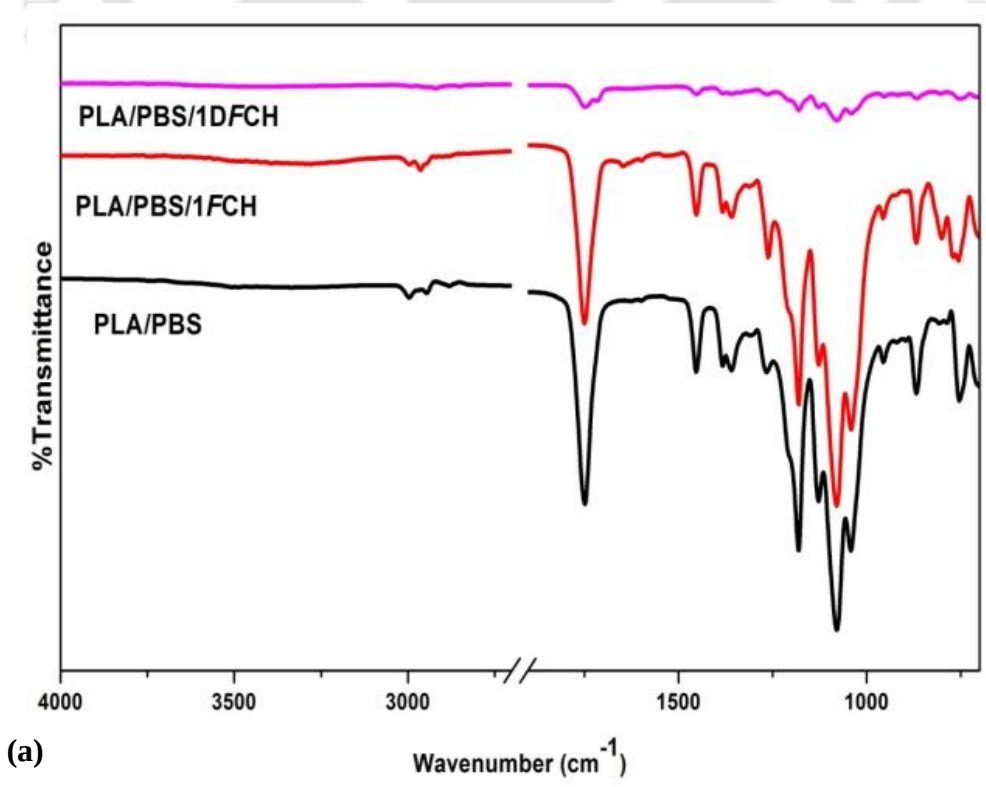

(a)

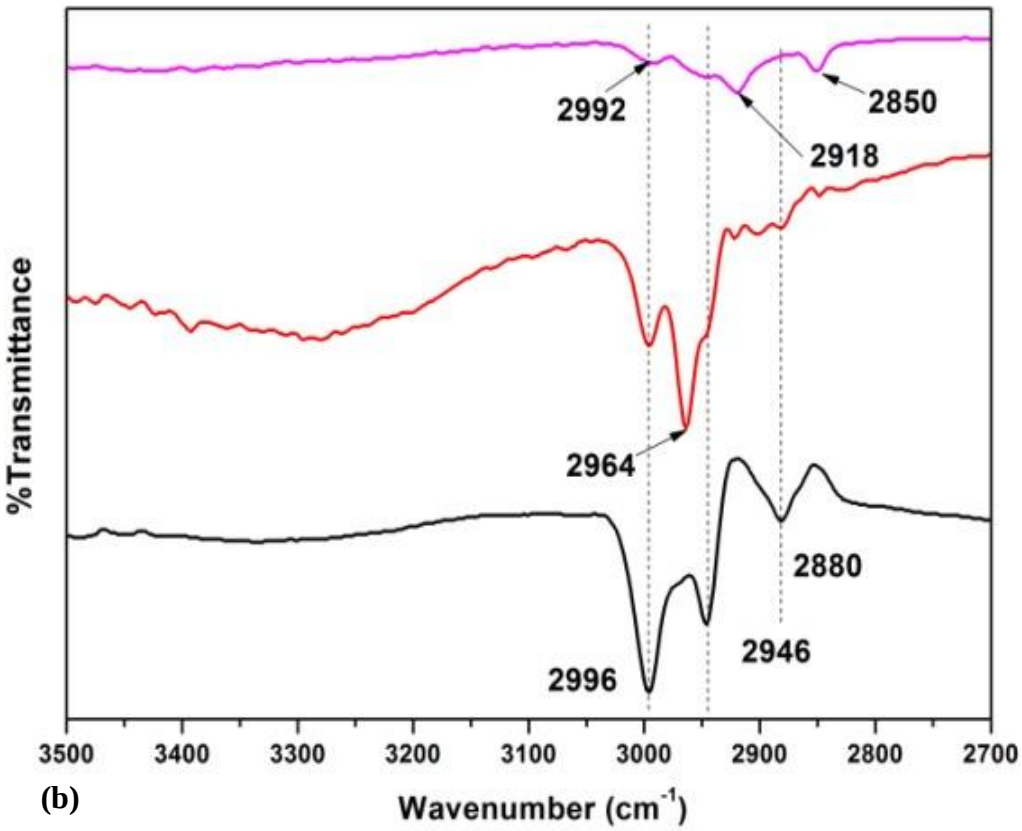

(b)

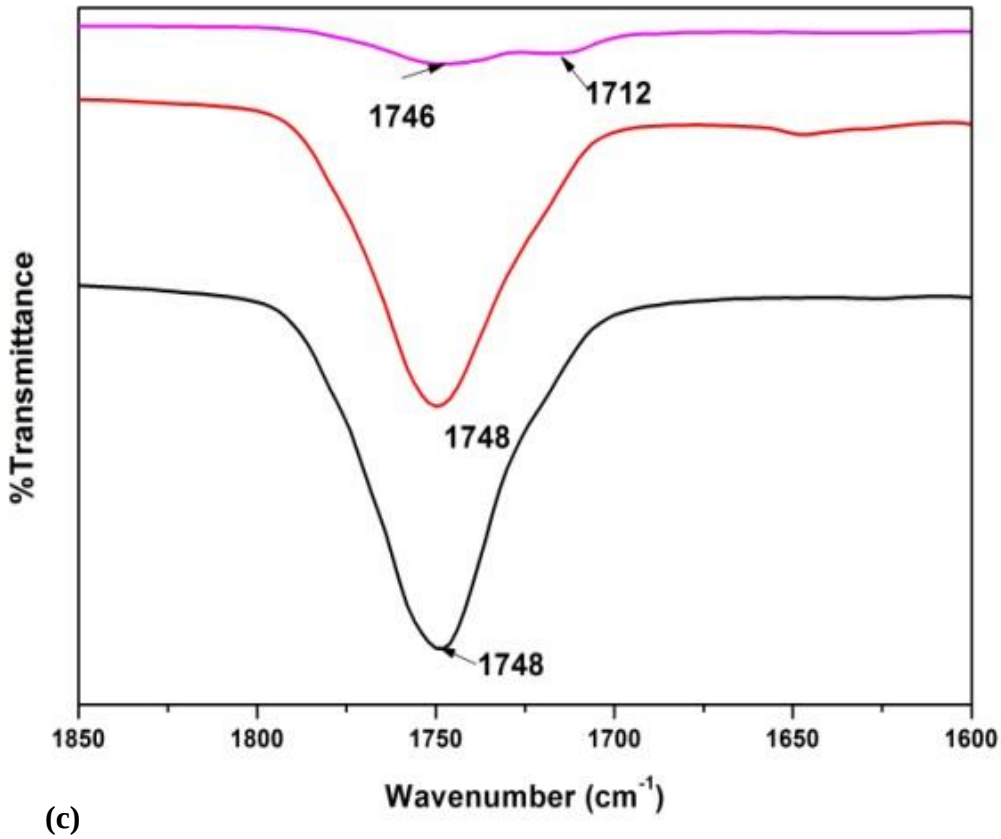

(c)

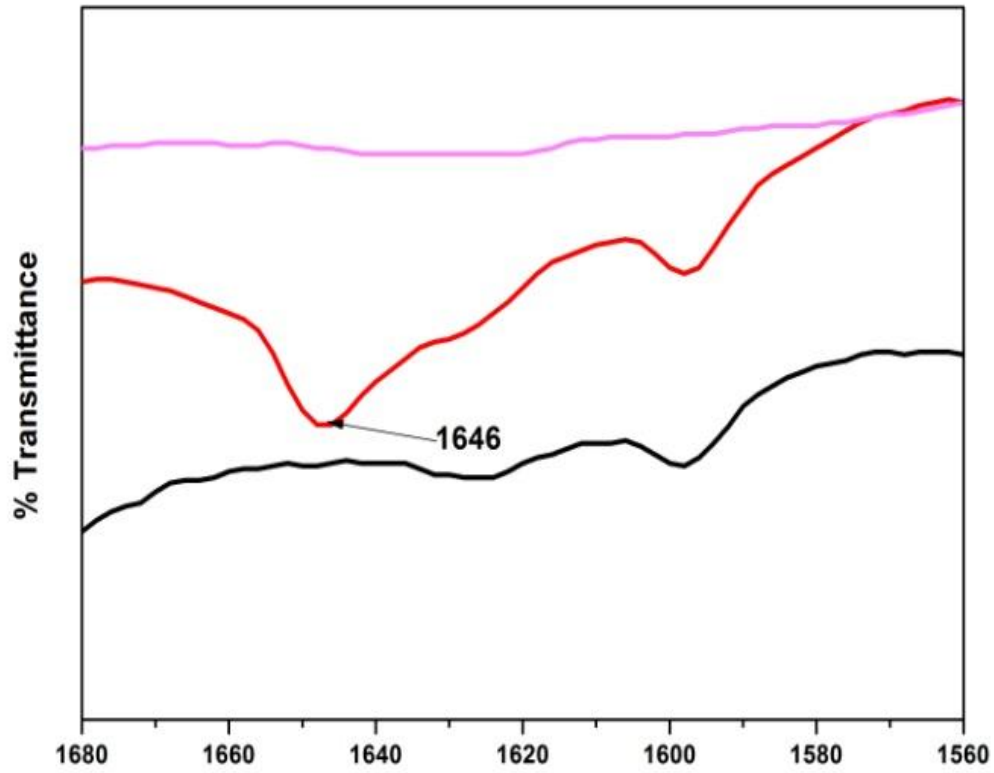

(d)

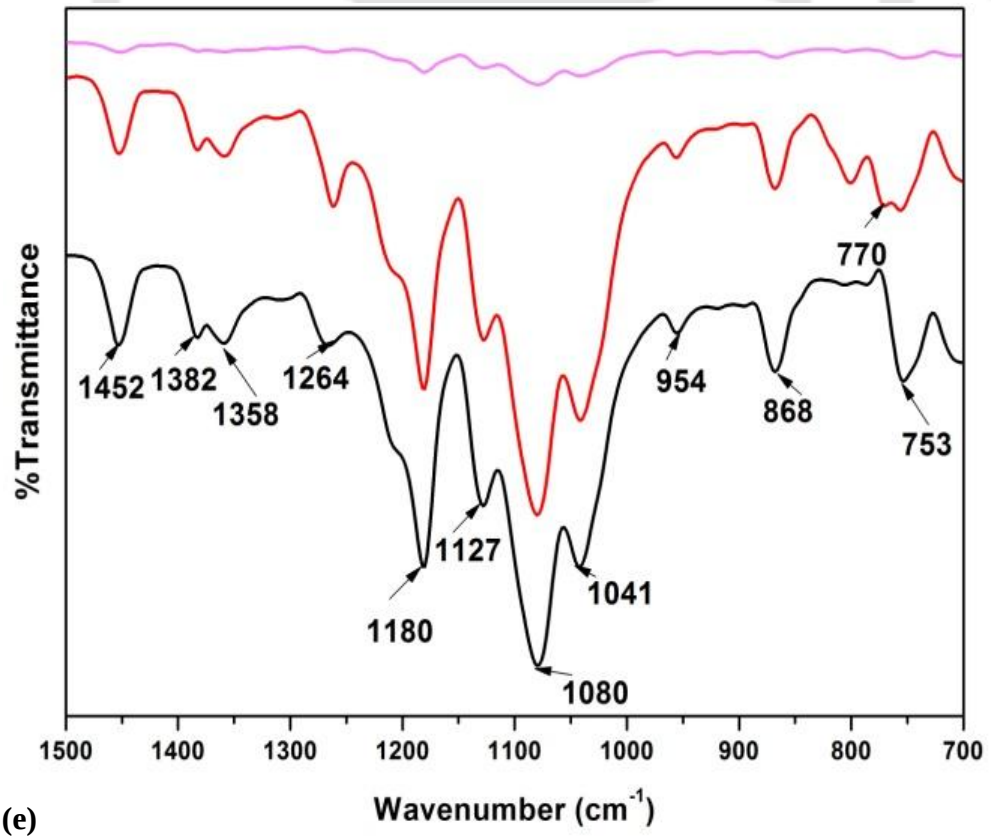

(e)

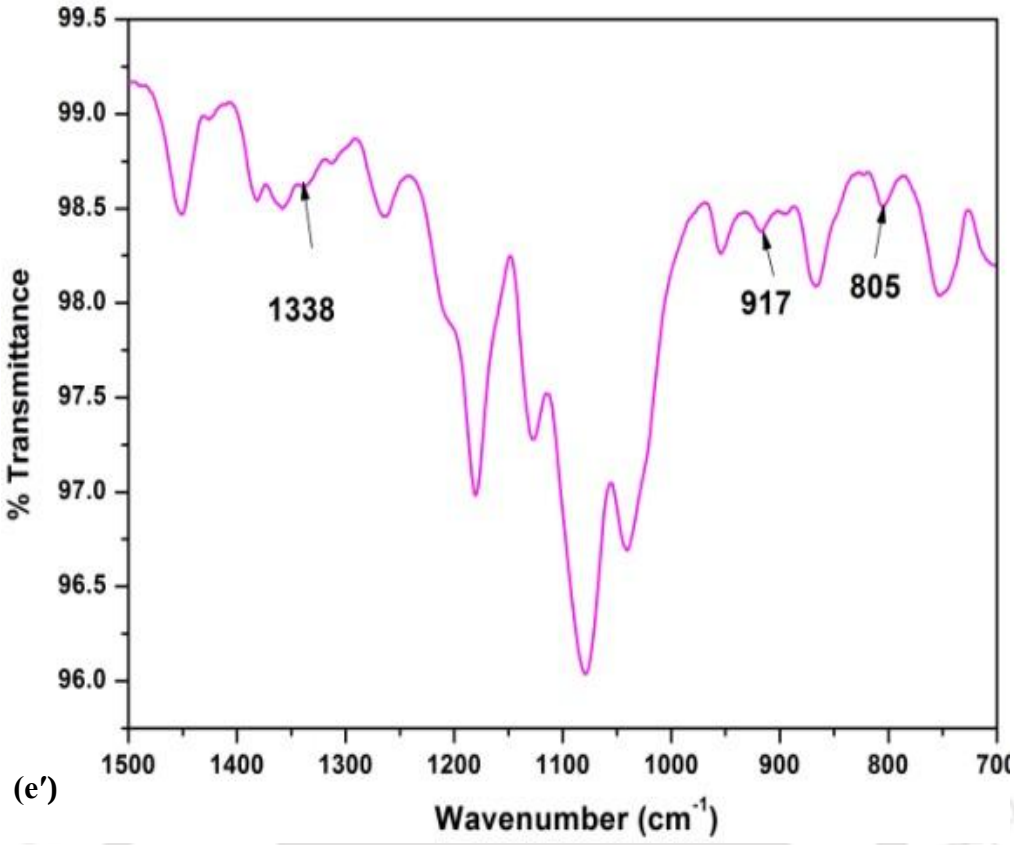

(e′)

Figure 6.2: *Chemical structural analysis of PLA/PBS blend, PLA/PBS/FCH and their reactive bionanocomposite films using FTIR in (a) Full range (4000-700 cm^{-1}), (b) 3500-2700 cm^{-1}, (c) 1850-1600 cm^{-1}, (d) 1680-1560 cm^{-1} (e) 1500-700 cm^{-1} and (e') enlarge image of PLA/PBS/D/1FCH from 1500-700 cm^{-1}.*

- ***Gel content and molecular weight analysis***

As mentioned in the schematic of the reaction mechanism, PLA/PBS/*F*CH based bionanocomposite system with DCP content exhibit a complex type of reactions through the formation of crosslinked/branched structure as well as copolymerization of PLA and PBS in the presence of DCP. The gel content of PLA/PBS, PLA/PBS/*F*CH bionanocomposite at various *F*CH loading (1 and 3 wt %) in presence of DCP has been determined based on an extraction process. It is found that the gel fraction of PLA/PBS/D/1*F*CH bionanocomposite is significantly improved in comparison to PLA/PBS blend as shown in Figure 6.3 (a). The reason behind such high gel content is due to the development of cross-linking sites within all

the three components. With the fixed amount of DCP, the gel fractions of PLA/PBS with *F*CH composites are approximately inversely proportional to the *F*CH quantity. It is observed that the calculated gel fraction is lower than 10% when *F*CH is 3 wt% in the presence of DCP. This is probably due to the reduction in crosslinking efficiency which subsequently leads to the thermal decomposition of a polymeric system due to the agglomeration of *F*CH at higher loading (3 wt %) **(Dhar et al., 2016)**.

Figure 6.3 (b) and (c) represent the distribution of molecular weight and polydispersity index (PDI) for PLA, PLA/PBS based bionanocomposite with or without DCP as a function of *F*CH content. As compared to processed PLA, depletion in the M_w and M_n values of PLA/PBS blend by ~22% and ~10% respectively indicate that it has experienced thermal degradation during its processing at elevated temperature. Interestingly, the reactive extrusion of PLA/PBS/D/1*F*CH bionanocomposites show an increase in both M_n and M_w by ~16% and ~51% respectively and this can be ascribed to the formation of some cross-linking/branching sites, which is also referred to improved value of gel content as mentioned in the previous section. This is probably due to the reactive processing, which helps to inhibit thermal decomposition in the presence of 1phr DCP. However, PLA/PBS/D/3*F*CH bionanocomposite underwent decrease in M_n and M_w with slightly high PDI ~ 2.4 and noticeable reduction in the gel content which supports possible agglomeration.

When *F*CH is added into PLA/PBS, it displays small reduction in the values of M_n and M_w, as compared to PLA/PBS blend. Therefore, it can be inferred that *F*CH has minor effect on thermal decomposition of the PLA/PBS blend. After addition of DCP, the crosslinking as well as the degradation occur simultaneously in the reactive modified bionanocomposite which enhances both high and low molecular weight region, resulting in the improvement of PDI (broadening molecular weight distribution) index. From Figure 6.3 (d), the presence of crosslinked/long chain branched linkage is confirmed due to the appearance of new shoulder

peak in the high molecular weight (MW) population in case of PLA/PBS/D/1*F*CH **(Tesfaye et al., 2017)**. Also, this fact should be considered that hydrodynamic volume is highly influenced by the chain topology; as the determination of molar mass distribution using only GPC is not preferable.

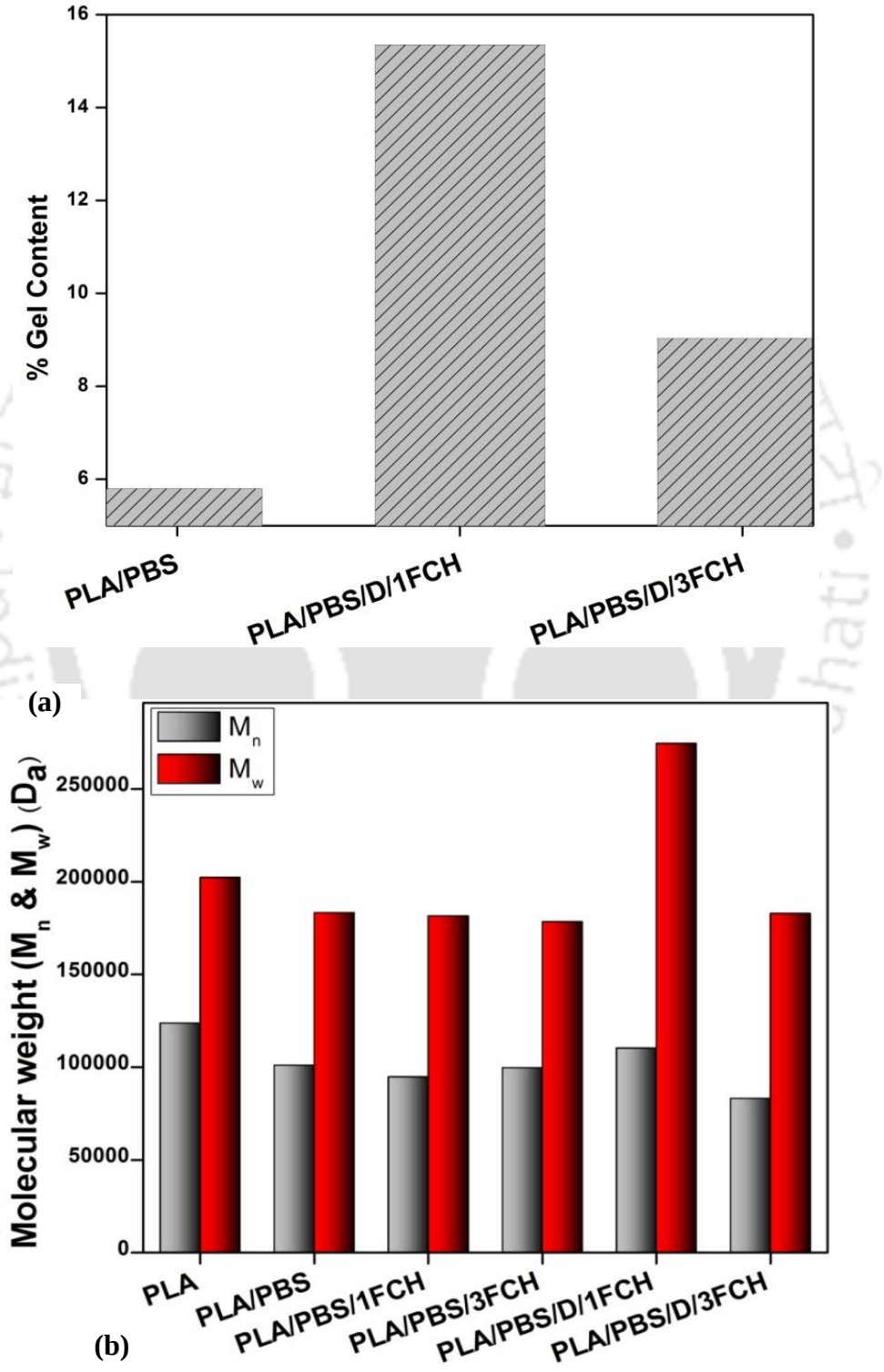

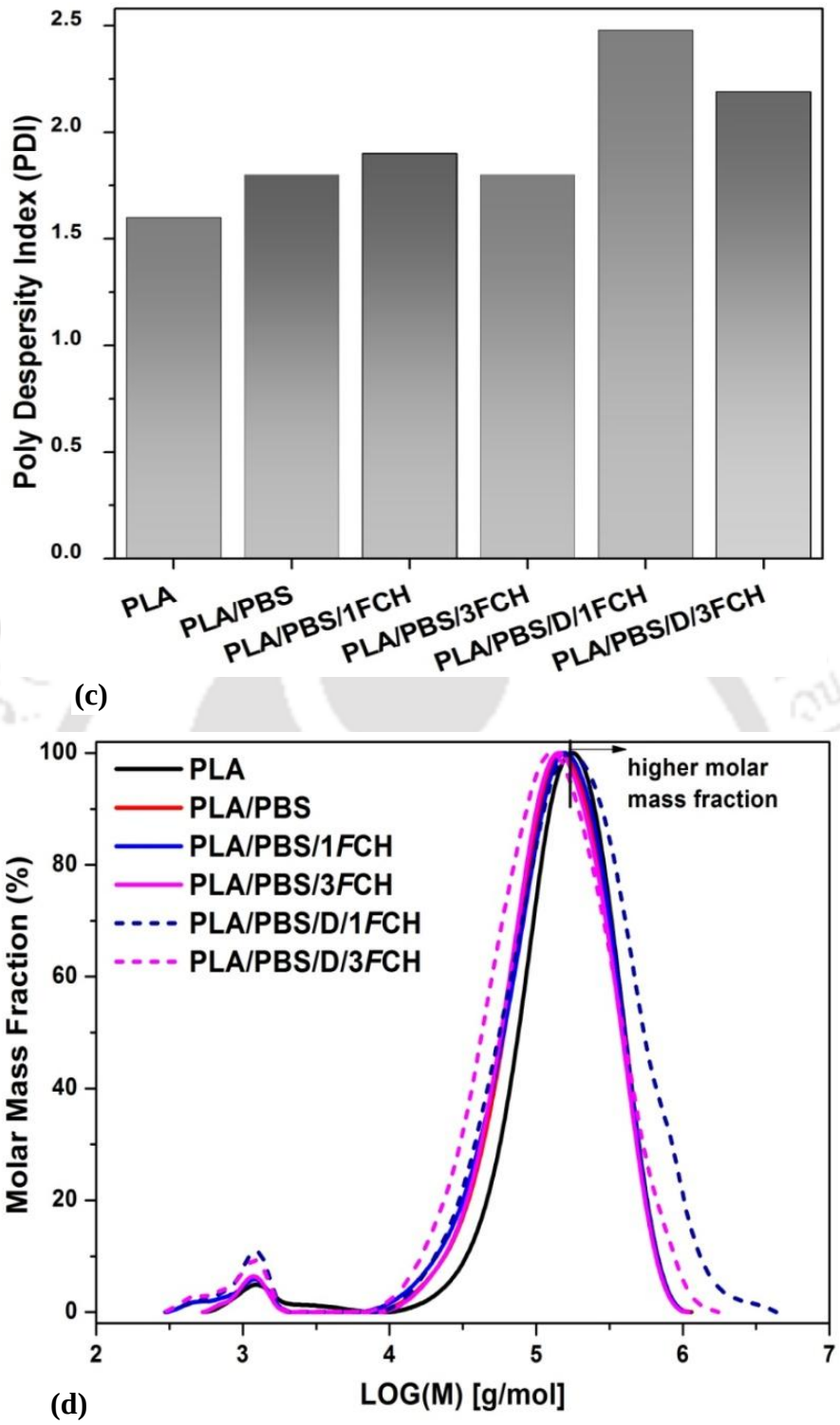

Figure 6.3: *(a) Gel content (%) of PLA/PBS/FCH based bionanocomposites in presence of DCP (b) Number average (M_n) and weight average (M_w) molecular weight distribution and (c) Polydispersity index (PDI) and (d) Molar-mass fraction of PLA, PLA/PBS blend,PLA/PBS/FCH and their reactive bionanocomposite films.*

- ***Morphological investigation of reactively extruded PLA/PBS/FCH bionanocomposite films with and without DCP***

As known that PLA and PBS are semicrystalline polymers; their thermal resistance and mechanical characteristics are mostly affected by two important factors such as solid state morphology and % crystallinity **(Zhang et al., 2016)**. Fractured morphology of all the bionanocomposite films as well as PLA/PBS film have been observed using FESEM analysis. For polymer blends, the moderate interfacial adhesion between the two phases is favorable for the enhancement of mechanical properties, particularly toughness, whereas too weak or too strong interfacial adhesions suppress the stress through the interfacial debonding or induce complete phase separation between dispersed and matrix phase. FESEM micrographs of the fractured surfaces of the PLA/PBS, PLA/PBS/DCP, and PLA/PBS/*F*CH with or without DCP are displayed in Figure 6.4 (a) – (d). It has been reported earlier that PLA and PBS are compatible partially with each other **(Ji et al., 2014)**. As seen in Figure 6.4 (a), PBS is poorly embedded with the PLA matrix and the interfacial adhesion between PLA and PBS phase is weak which is evident from the oval cavities found after the tensile deformation **(Wu et al., 2012)**. In case of a PLA/PBS reactive blend, no dispersed phase of PBS has been noticed due to the reduction in PBS size **(Ji et al., 2014)**. Moreover, the presence of voids between the PLA and PBS has also been observed. These could assist as stress concentrators' during tensile stress, which are responsible to level off the mechanical properties such as tensile strength in Figure 6.4 (b). For PLA/PBS/1*F*CH bionanocomposite, *F*CH has been dispersed into the PLA/PBS phase as displayed in Figure 6.4 (c). After the addition of DCP in PLA/PBS/1*F*CH, the morphology of the bionanocomposite film is found to be uniform as clearly demonstrated in Figure 6.4 (d). Moreover, *F*CH nanoparticles nicely adhere to PLA and PBS phase in presence of DCP and no voids are noticed after the tensile fracture, indicating an improvement in the interfacial adhesion between PLA and PBS phase

which is again attributed to the development of copolymer or crosslinked network at the interface. Consequently, it could control the mechanical properties significantly. It also has the potential to prevent the stress concentration when the external force has been applied to composite in the tensile mode **(Wu et al., 2012)**. Therefore, a synergistic influence of *F*CH with DCP could enhance the compatibility of PLA and PBS in the studied bionanocomposite.

(a)

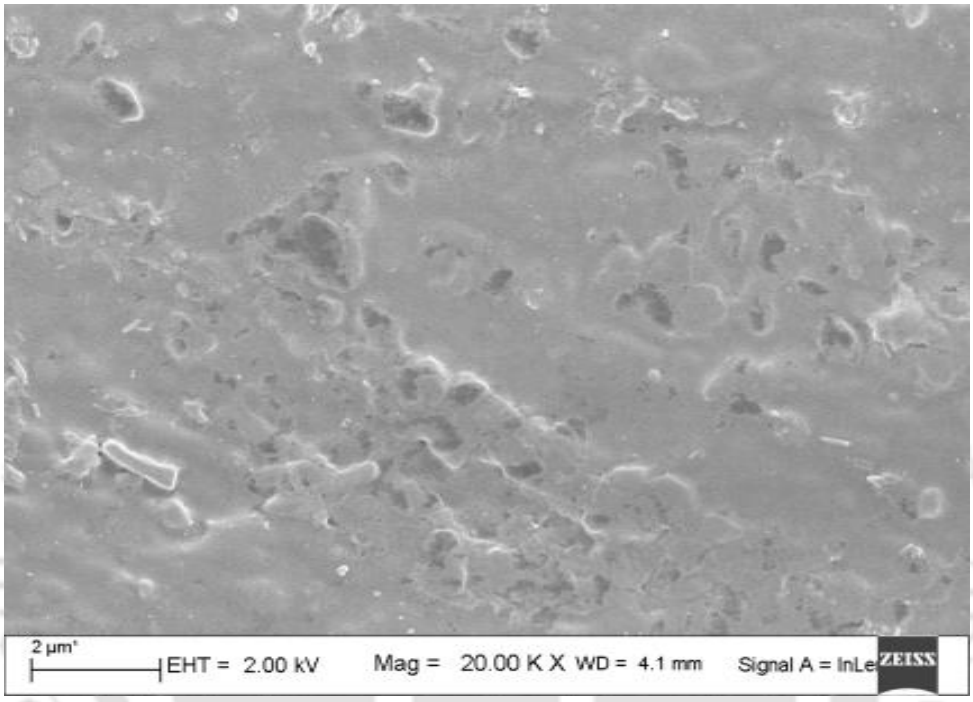

(b)

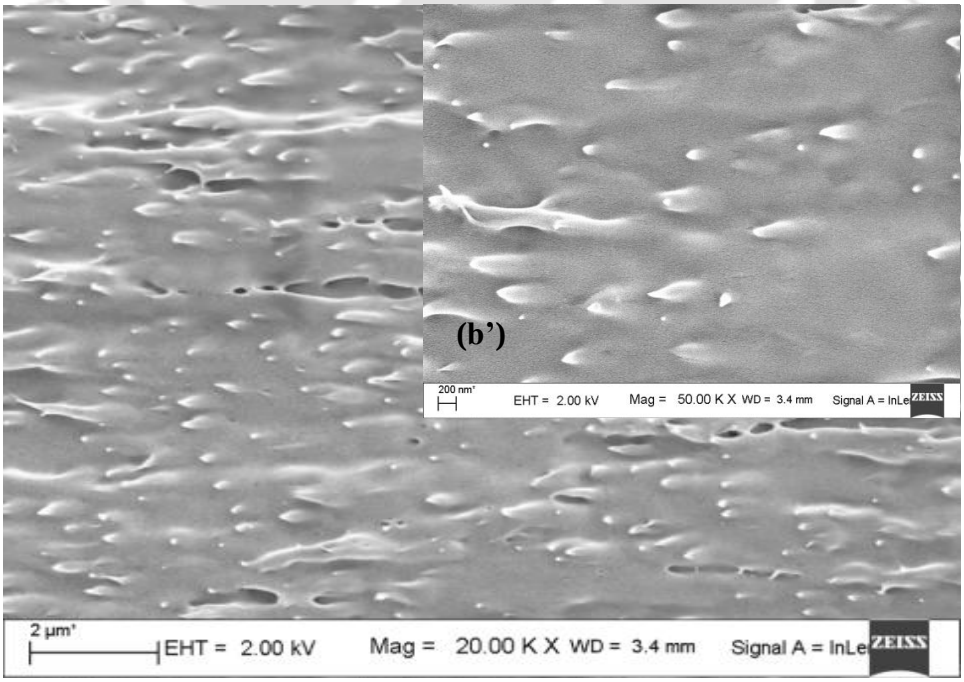

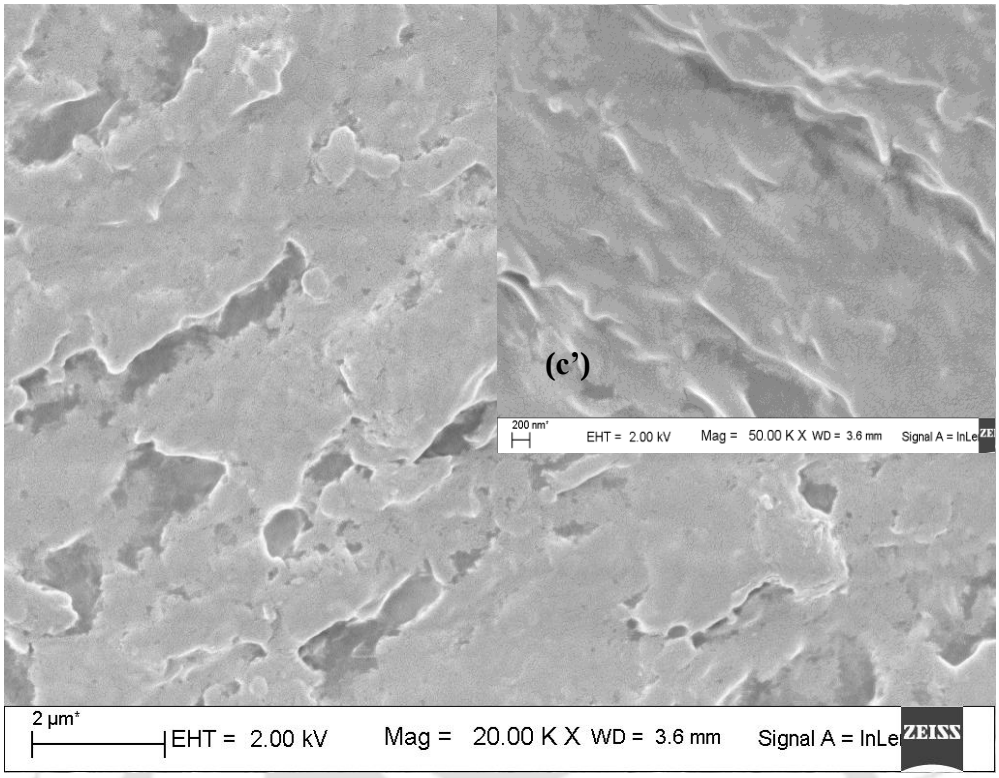

(c)

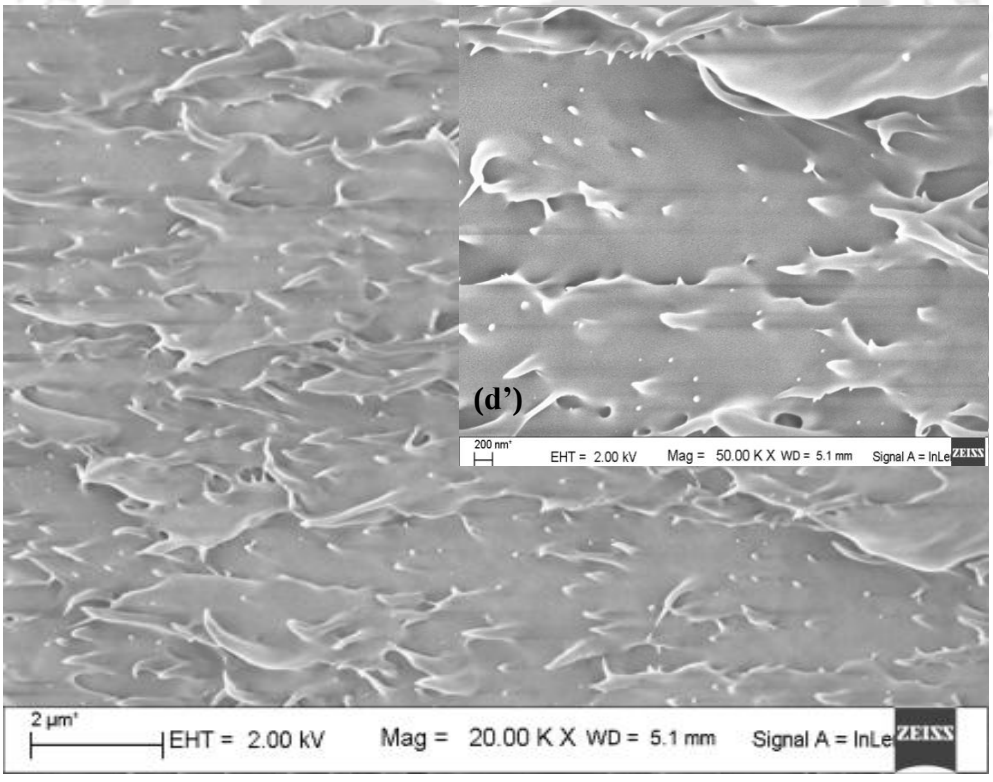

(d)

Figure 6.4: *FESEM micrograph fot the tensile fratcure surface of the film samples (a) PLA/PBS blend, (b)-(b') PLA/PBS/1DCP, (c)-(c')PLA/PBS/FCH and (d)-(d') PLA/PBS/D/1FCH.*

- ***Crystallization study of the reactively extruded PLA/PBS/FCH bionanocomposite films with and without addition of DCP***

Crystal structures of PLA/PBS/*F*CH based bionanocomposite have been verified to observe the influence of crosslinking/branching by utilizing wide angle XRD technique. The diffraction peaks positioned at Bragg angles of 16.4º (2 0 0)/(1 1 0) and 18.6º (1 1 0) have been assigned to α′ phase crystal of PLA in PLA/PBS and their bionanocomposites; as mention in Figure 6.5 (a) **(Zhang et al., 2016; Kawai et al. 2007)**. It represents the orthorhombic crystal unit cell of PLA which is confirmed by reflection pattern (2 0 0). The peaks appear at 22.5º (1 1 0) which contribute to PBS. When 1 wt % *F*CH is added with DCP in PLA/PBS blend, it represents an increase in the peak height at 16.4º which indicates the growth of α′-crystal of PLA. From Figure 6.5 (b), it is noticed that the addition of *F*CH into PLA/PBS gradually decrease the relative crystallinity of (X_c) of PLA in PLA/PBS/*F*CH based bionanocomposites. The X_c of PLA/PBS/D/1*F*CH bionanocomposite is significantly increased upto 33%. Further, it is concluded that the incorporation of *F*CH with DCP in PLA/PBS not only improves the X_c of bionanocomposite but also contributes to the growth of α′ crystal of PLA phase.

DSC analysis is carried out to understand the crystallization and melting behavior of fabricated PLA/PBS blend and its bionanocomposites with and without DCP. In the present investigation relating thermal properties of bionanocomposites, it is necessary to study the effect of *F*CH on the thermal parameters of a PLA/PBS system with and without DCP. The second heating and cooling curves of PLA/PBS based reactive system and the corresponding melting and crystallization parameters have also mentioned in Figure 6.5 (c)-(d). For PLA, the second heating scans show a glass transition temperature (T_g) at 60 ºC and cold crystallization temperature (T_{cc}) at 115 ºC. The crystallization (T_c) temperature has not been identified during the first cooling scan (at 10 ºC min^{-1}), which gives the confirmation that

neat PLA shows slow crystallization property due to is amorphous nature **(Chaiwutthinan et al., 2015)**. This finding is in consonance with the wide angle XRD result also. Further, neat PLA exhibits double melting peaks and can be explicated by the similar type of crystal structure which melted at various temperatures due to lamellar divergence **(Xiong et al., 2013; Najafi et al. 2013)**. For the PLA/PBS blend, the T_g and T_m of PLA is unchanged, indicating that both are thermodynamically incompatible **(Teamsinsungvon et al., 2013; Eng et al., 2013)**. However, broad T_{cc} of PLA phase has been shifted to lower temperature as blended due to the dispersed molten PBS content or the presence of contamination in PBS. Therefore, it can perform as nucleation sites for PLA system **(Yokohara et al. 2008)**. The T_m of PBS is found at 110.9 ºC and the T_{cc} of PLA component is around 100.9 ºC which attributed to the partly overlapping of the melting peak of PBS with the cold crystallization peak of PLA. On the other hand, mobility of PBS segments would be strongly constrained by PLA chains and inhibited the PBS crystallization. Therefore, no peak has been noticed for crystallization of PBS during the cooling run. For PLA/PBS/*F*CH based bionanocomposites, the melting peak of PBS is not clearly observed because it is masked by the cold crystallization region of the PLA. Subsequently, due to the confinement effect the crystallization of PBS is restricted as mentioned before. Moreover the presence of *F*CH shows no significant change in T_g and T_{cc} of PLA in the PLA/PBS based ternary system in comparison to PLA/PBS blend. Similarly, T_m of both PLA and PBS have not been affected after incorporating *F*CH, but their melting enthalpy values have been reduced with increasing *F*CH loading up to 3 wt% due to the reduction in volume fraction of polymer **(Muthuraj et al., 2017)**. For the PLA/PBS/D/1*F*CH, it has noticed that T_g is not clearly visible, and the relative temperature at this inflection (T_g) point has been found at 60 ºC. The results show that the melting peak related to PBS phase become clear and reduction in T_m of PLA is observed due to generation of imperfect crystals in PLA. For DCP treated PLA/PBS/1*F*CH,

the decrease in value of T_m of PLA is probably due to the broad molar mass distribution of the polymeric matrix which probably due to the developed crosslinking sites between the chains **(Ambrosio-Martín et al., 2018)**. It has been observed that the shapes of the melting endotherms slightly vary when 1 Phr DCP content has been added to PLA/PBS/*F*CH. These data reveal a decrease of $\Delta H_{m,\ PLA}$ after incorporating DCP in PLA/PBS/*F*CH. It also exhibits a notable T_c with the absence of T_{cc} for PLA phase, indicating an increment of crystallization ability of amorphous part of PLA from melt state to cooling state. It is probably explained from the interface due to the phase-separation where favorable nucleation sites are formed for the crystal growth **(Zhang et al., 2012; Kim et al., 2001)**. Other researchers have reported when the T_c of PLA > 126 °C, indicates that it crystallizes as the α-form **(Li et al., 2015)**. At higher loading of *F*CH (~ 3 wt %), a decrease in T_c of PLA demonstrates that the unreacted part of PLA chains have rearranged along with the essential energy to overcome the reaction barrier, and finally crystal has been formed at lower temperature **(Dhar et al., 2016)**. These data indicates that the value of ΔH_c is also increased which confer the higher portion of unreacted PLA chains undergo rearrangement to form crystal. The percentage crystallinity of both PLA and PBS domains are determined and their values in bionanocomposites as summarized in Table 6.2. PLA/PBS blend depicts percentage crystallinity (X_c) of 24.86 % for PLA and 15.72 % for PBS phase, respectively. It could be considered that PBS is more efficient in assisting the crystallization of PLA phase. However, the X_c (%) of PBS is slightly reduced in presence of PLA content. It is attributed that crystallization of PBS is compromised by PLA phase. Table 4.2 reports that the addition of 1wt% *F*CH in PLA/PBS blend, X_c of PLA content is slightly enhanced, while X_c of PBS is decreased. It is found that the X_c of PLA is further reduced after incorporation of *F*CH especially at higher loading (~ 3 wt %), while the crystallinity of PBS phase remain unchanged. Conversely, *F*CH has a tendency to suppress the crystallization of PBS phase. With the aid of 1phr DCP content,

value of crystallinity of both PLA and PBS are increased from ~ 27.15 to 49.01 % and ~0.6 to 4.15 % respectively in PLA/PBS/D/1*F*CH bionanocomposite. For PLA/PBS/D/3*F*CH bionanocomposite, it is clear that the X_c of PBS content does not alter significantly, while PLA crystallinity is slightly reduced to 43.23 %. This implies the low molecular segment mobility during crystallization.

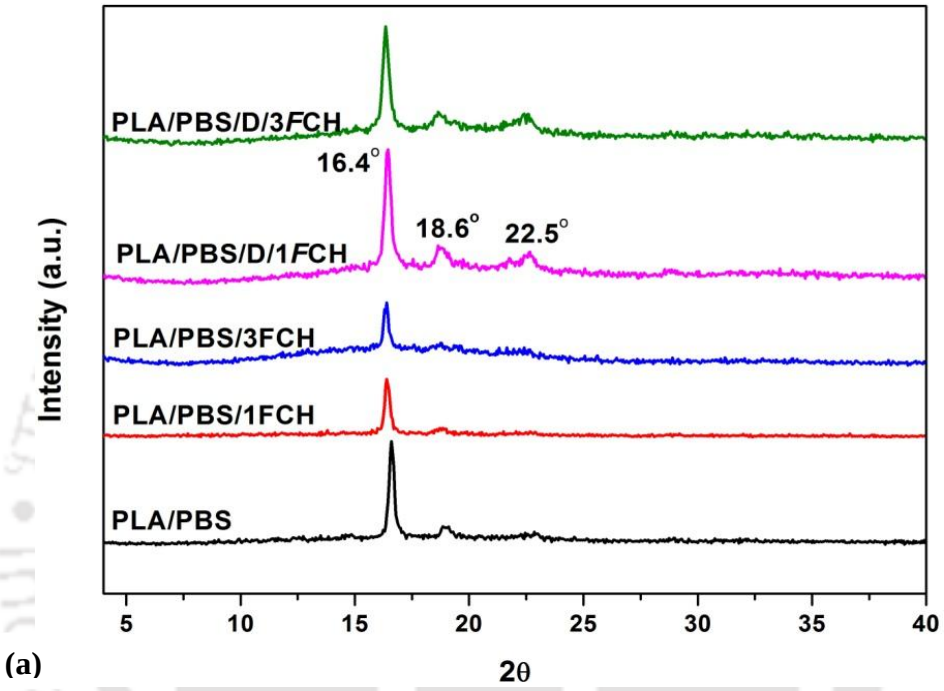

(a)

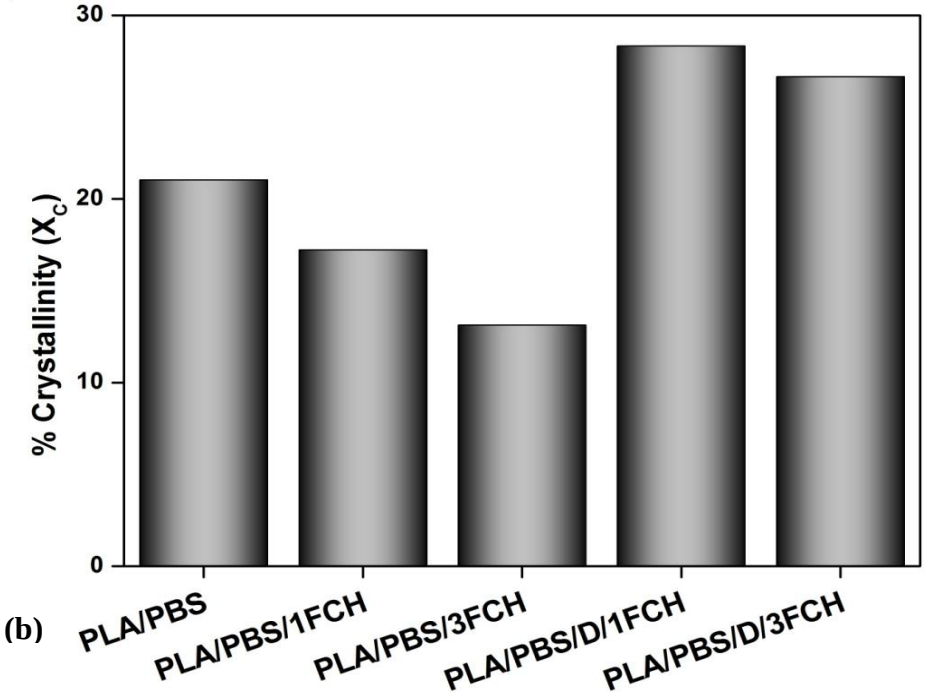

(b)

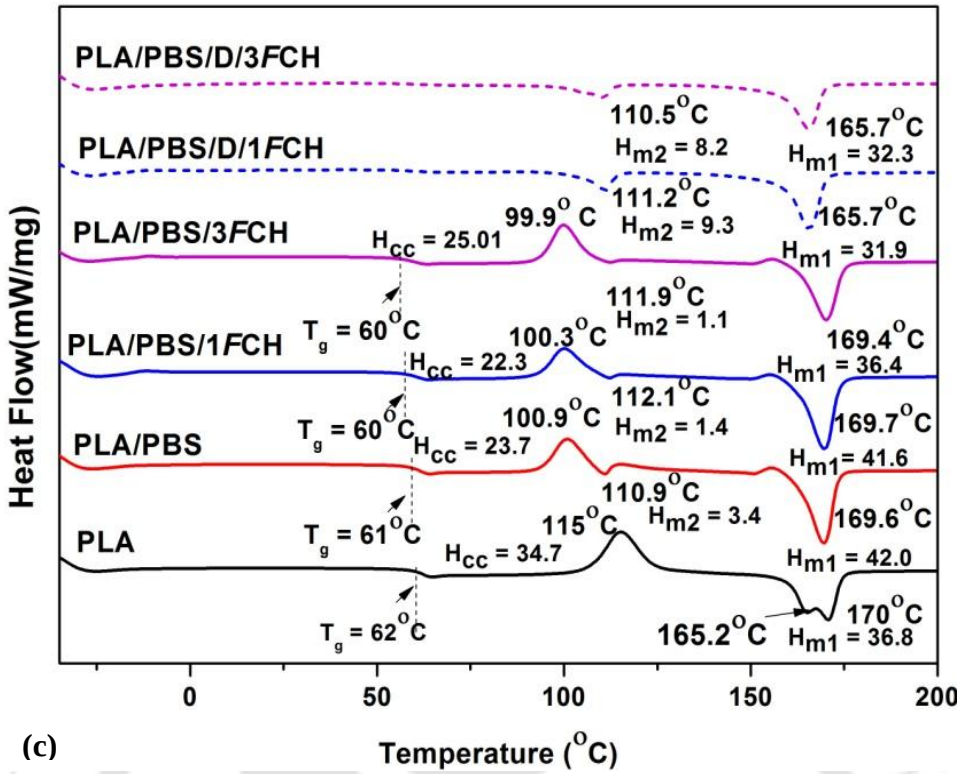

(c)

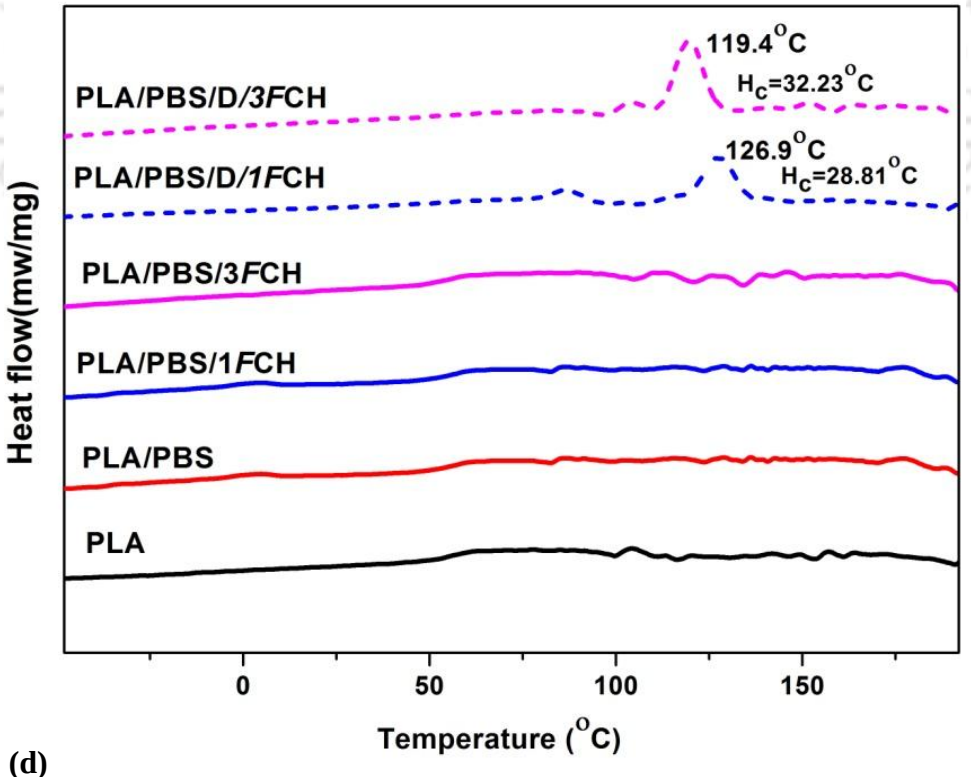

(d)

Figure 6.5: *Wide angle XRD analysis (a), Crystallinity (% X_c) fron XRD (b) DSC thermograms of PLA, PLA/PBS blend, PLA/PBS/FCH and their reactive bionanocomposite films (c) second heating cycles and (d) first cooling cycles.*

- ***Mechanical properties of reactively extruded PLA/PBS/FCH bionanocomposites films with and without addition of DCP***

Ultimate tensile strength (TS) of PLA is 48 MPa and elongation at break (% ε) is 8% due to its brittle nature. After addition of 20 wt% PBS, the elongation at break has been enhanced up to 14%, whereas tensile modulus (TM) and strength have been dropped. This finding confirms the improvement in ductility of PLA during tensile test. The mechanical analysis has been carried out to investigate the influence of *F*CH on PLA/PBS blend with and without DCP, including the elongation at break (%), tensile strength (MPa) and modulus (GPa). Mechanical properties of all the strips have been displayed in Figure 6.6 (a) and (b) respectively. As expected, the elongation at break has gradually increased from 13% to 24% (approximately 45% increment) for PLA/PBS/*F*CH bionanocomposite due to the presence of low molecular weight *F*CH which has the plasticizing effect. These results indicate that the ductility is improved which makes it more stretchable in comparison to neat PLA. Meanwhile, influence of *F*CH is detrimental to the young modulus and tensile strength. This could be ascribed that shorter *F*CH segments that has tendency to align faster than the long polymeric segments under the tensile run **(Pal et al., 2016)**. Therefore, presence of shorter polymer chains reduce the Young's modulus and strength, but the calculated tensile strength is lower in comparison to polyethylene (40 MPa) **(Nagarajan et al., 2016)**. However, further addition of 3 wt % *F*CH in PLA/PBS blend, the elongation at break is decreased probably due to agglomeration of *F*CH but the tensile strength and modulus almost remains constant. In fact, this is probably due to the insufficient transfer of stress across the interphase of either PLA or PBS phase to the *F*CH, due to their poor interphase adhesion.

When the *F*CH is 1 wt% and DCP content is 1 phr, PLA based ternary bionanocomposite exhibits balanced mechanical properties. For PLA/PBS/D/1*F*CH bionanocomposite, the tensile strength and modulus is improved and a reduction in elongation at break is noticed in

comparison to PLA/PBS/*F*CH bionanocomposite. Improvement in tensile strength and modulus can be assigned to the formation of some cross-linked/branched structure, which subsequently leads to the restricted mobility of the polymer chains to dissipate energy under tensile load. But the determined value of tensile strength is close to polyethylene (40 MPa), and elongation at break is still higher than that of PLA/PBS blend.

Hence, PLA/PBS/D/1*F*CH bionanocomposites may be considered as a very useful material for food packaging application. For PLA/PBS/D/3*F*CH bionanocomposite, the grafting efficiency is also reduced due to the agglomeration of *F*CH. It may lead to the reduction in elongation at break but tensile strength and modulus are almost constant.

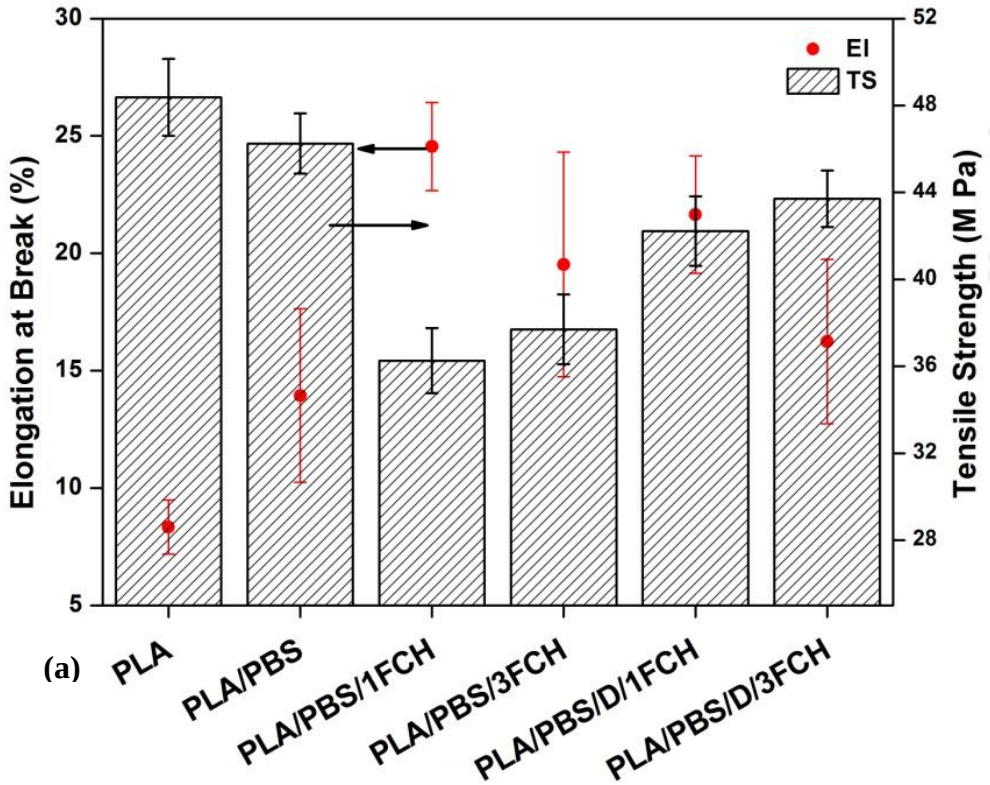

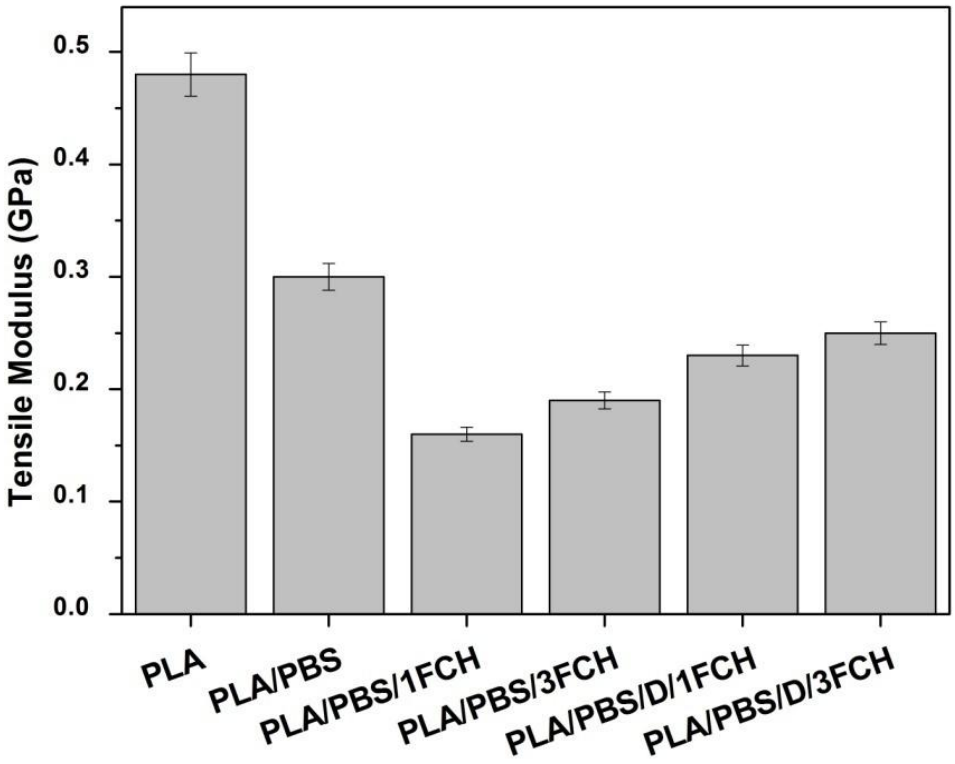

(b)

Figure 6.6: *Mechanical properties such as (a) Tensile modulus (b) Tensile strength and elongation at break (%) of the PLA, PLA/PBS blend, PLA/PBS/FCH and their reactive bionanocomposite films.*

- ***UV transmittance of the reactively extruded PLA/PBS/FCH film with or without addition of DCP***

The percentage transmission of PLA/PBS and PLA/PBS/*F*CH bionanocomposite with or without DCP is displayed in Figure 6.8 (a). PLA/PBS based film is the most transparent representing the maximum percentage of transmission in the visible region (400-800 nm). Further the incorporation of *F*CH into PLA/PBS blend provokes a remarkable reduction in the transparency of the biocomposite in the visible and UV (400-200 nm) region which is probably due to its brownish color **(Pal et al., 2018)**. Subsequently, at 275 nm (UV-C region), the transmittance of the PLA/PBS/*F*CH bionanocomposite films is decreased 10, 36, 49 and 62% with the incorporation of 1, 3 wt% *F*CH without or with DCP in comparison to PLA/PBS blend as seen in Figure 6.8 (b). Therefore, the result suggests that DCP treated

PLA/PBS/*F*CH enhanced UV barrier which is an interesting characteristic for the UV sensitive food packaging application.

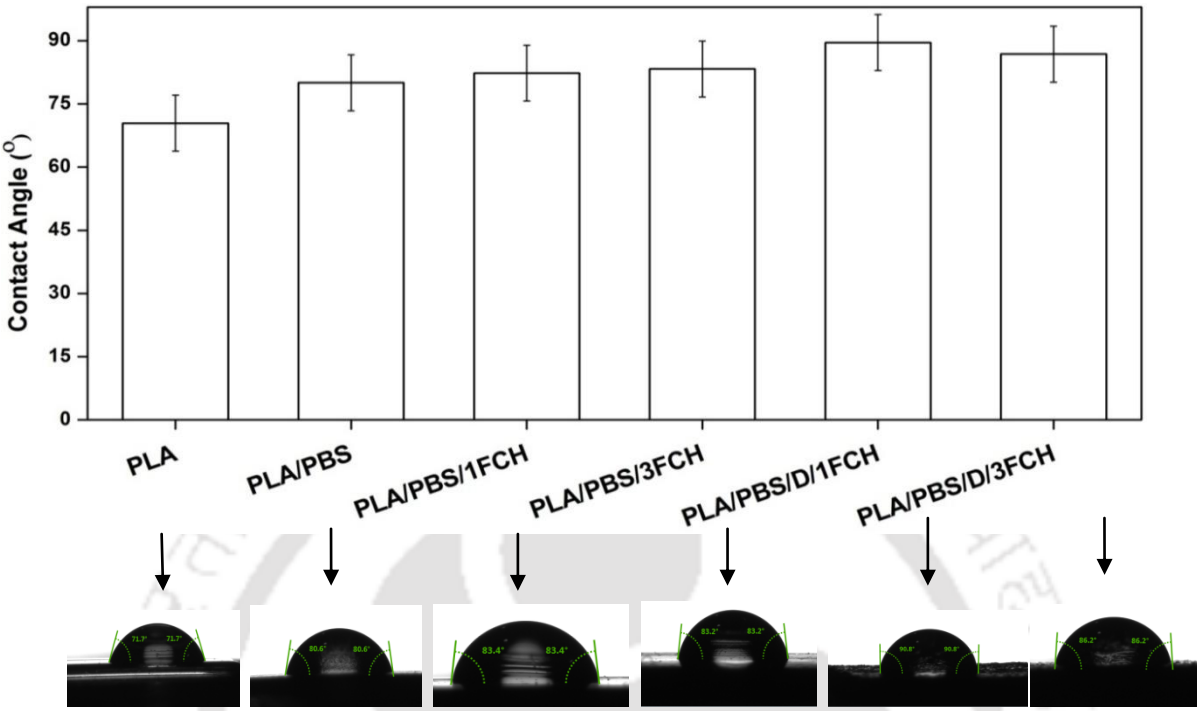

Figure 6.7: *Determination of static contact angle (at 25°C) to confirm wettability of PLA, PLA/PBS and PLA/PBS/FCH and their reactive bionanocomposite films.*

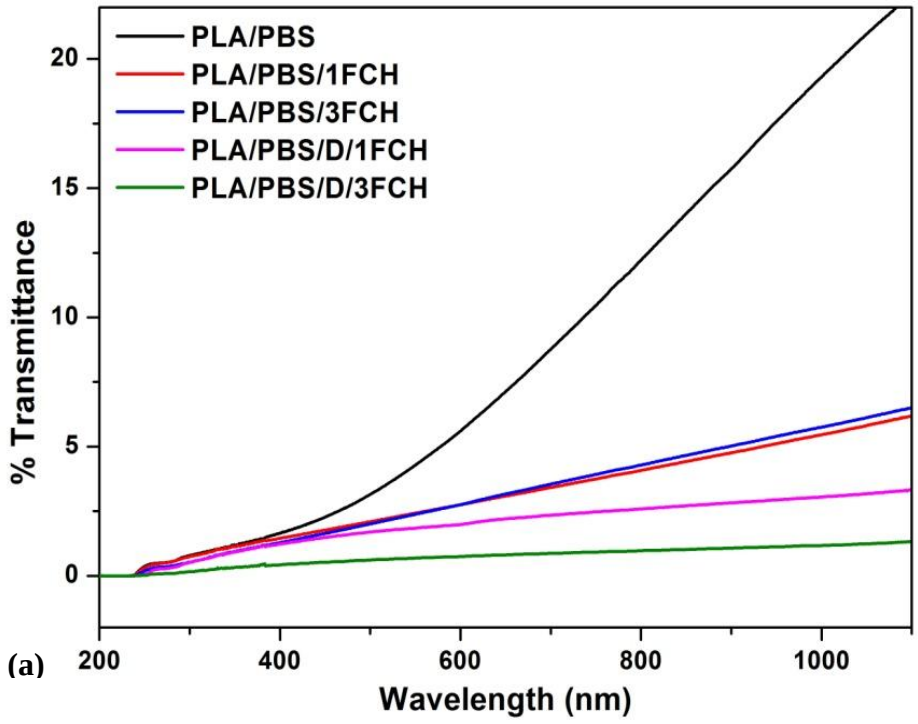

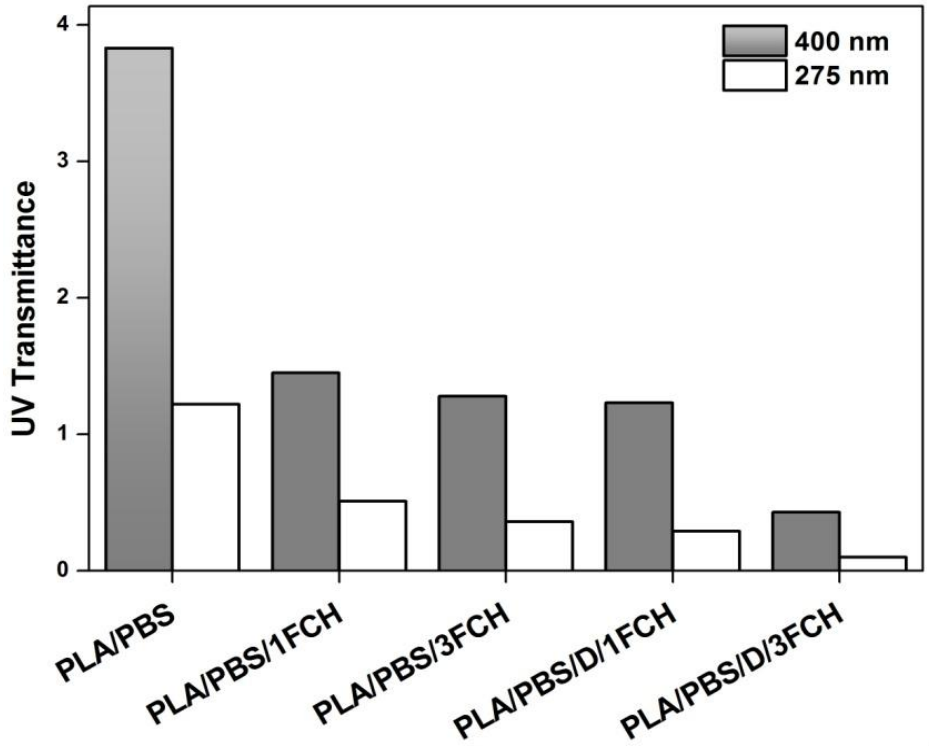

(b)

Figure 6.8: *(a) UV visible spectra (b) in full range (1100-200 nm), (c) Comparison of % transmittance at 700, 400 and 275 nm of PLA/PBS, PLA/PBS/FCH and their reactive bionanocomposite films.*

- ***Polarized optical microscopic analysis of the reactively extruded PLA/PBS/FCH film with and without addition of DCP***

POM investigation for the spherulites growth patterns developed in PLA/PBS, PLA/PBS/1*F*CH, PLA/PBS/3*F*CH, PLA/PBS/D/1*F*CH and PLA/PBS/D/3*F*CH during isothermal crystallization at 126°C and 140°C are depicted in Figure 6.9 (a) and (b) respectively. For all samples, Maltese cross patterns for only PLA spherulites have been observed and the nucleation density is enhanced gradually with time. The POM result confirms that the growth of PBS spherulites is not observed at a temperature above T_c (80 °C) of PBS in the PLA-rich blend. This is probably due to the fact that PLA macromolecule chains in the PLA/PBS (80/20) blend strongly inhibit the crystallization of PBS chains. In case of PLA/PBS blend, large and distinct spherulites are developed which show the weak

nucleation ability. Moreover, the incorporation of *F*CH into PLA/PBS blend could slightly improve the nucleation ability. PLA/PBS/D/1*F*CH displays the strongest nucleation ability and after 15 min, the spherulites of PLA cover the bulk region. The effect and differences among the PLA/PBS blend and their bionanocomposite in the presence and absence of DCP are clearly noticed after the isothermal crystallization at 140 °C. The growth of spherulites (slope determined from the spherulites radius (µm) against the crystallization time (min)) and nucleation density (total number of spherulites millimeters^{-2}) are displayed in Figure 12 c,d, for PLA/PBS, PLA/PBS/1*F*CH and PLA/PBS/D/1*F*CH respectively at 140 °C. At 140 °C, PLA/PBS/D/1*F*CH nanobiocomposite represents the strong nucleation ability, which is due to the crosslinking/branching sites which possibly function as nucleation sites **(Tesfaye et al., 2017; Nanthananon et al., 2015)**. Both DSC and POM analyses confirm that the crystallization of the PLA/PBS blend is accelerated by the presence of FCH with DCP. According to the **Kim et al., 2001** and **Ji et al., 2015**, the DSC result confirmed that the crosslinked/branched structures during reactive blending may act as nucleation sites.

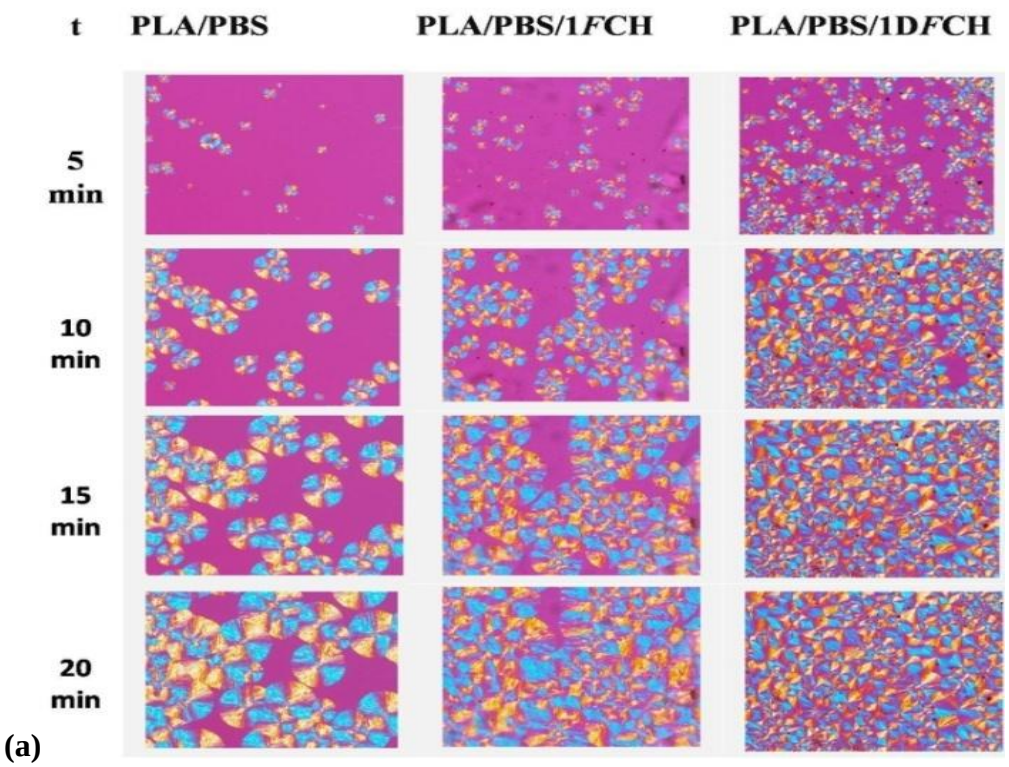

(a)

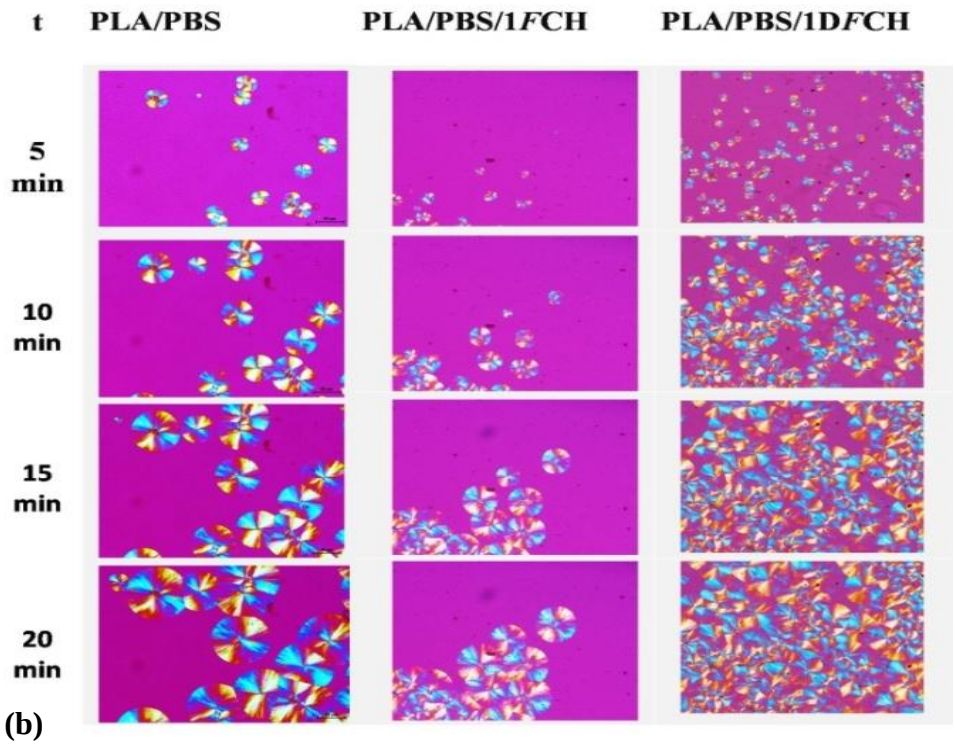

Figure 6.9: *Selected POM images of PLA/PBS blend and, PLA/PBS/FCH and their reactive bionanocomposite films crystallized isothermally at (a) 126 °C and (b) 140 °C (0 to 20 min).*

Dependency of number of nuclei on time, spherulites growth and nucleation density

Figure 6.10 (a) – (b) represent the dependency of number of spherulites on time at 126 and 140 °C respectively. From the findings, it is observed that the number and growth rate of spherulites are reduced as the nucleation become slightly difficult at elevated temperature. Figure 6.11 (a)-(b) displays the spherulites growth rate and nucleation density at 140 °C, respectively. At 126 °C, it is observed that after a primary delay time, number of spherulites increase gradually with time, as seen in Figure 6.10 (a). At 126 °C, linear region of each dependency has a straight-line are fit where nucleation delay (θ) time is estimated from the intercept of the line with the time. The estimated apparent nucleation delay time (θ_a) is 1.31, 1.05 and 0.96 minute for PLA/PBS, PLA/PBS/1*F*CH and PLA/PBS/D/1*F*CH respectively at 126 °C. The last regions of the dependencies are excluded due to the growth and overlapping

of the spherulites. The lowest value of θ also confirms the enhanced nucleation ability in case of PLA/PBS/D/1*F*CH. Moreover, the growth rate of spherulites of PLA/PBS/D/1*F*CH is inhibited (after 10 min) due to the entanglement of polymeric chains which has subsequently led to the overlapping of high density spherulites and finally deformation in their shapes. It is found that the lowest crystal size and the highest nuclear density **(maximum number of spherulites mm^{-2})** are noticed for PLA/PBS/D/1*F*CH.

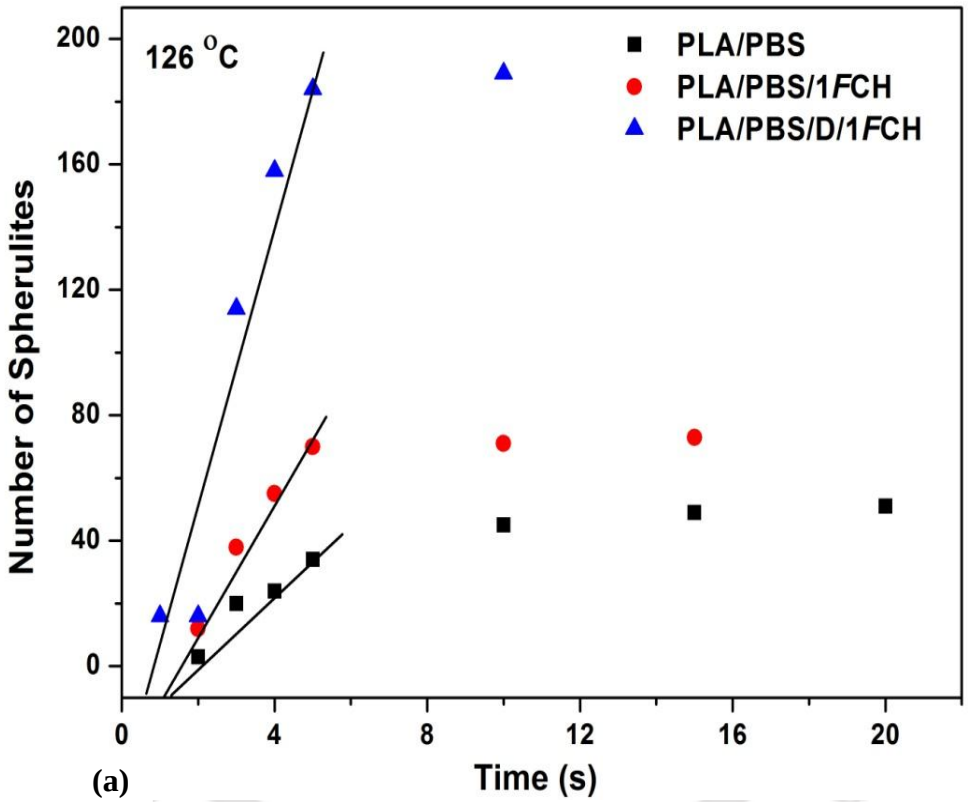

(a)

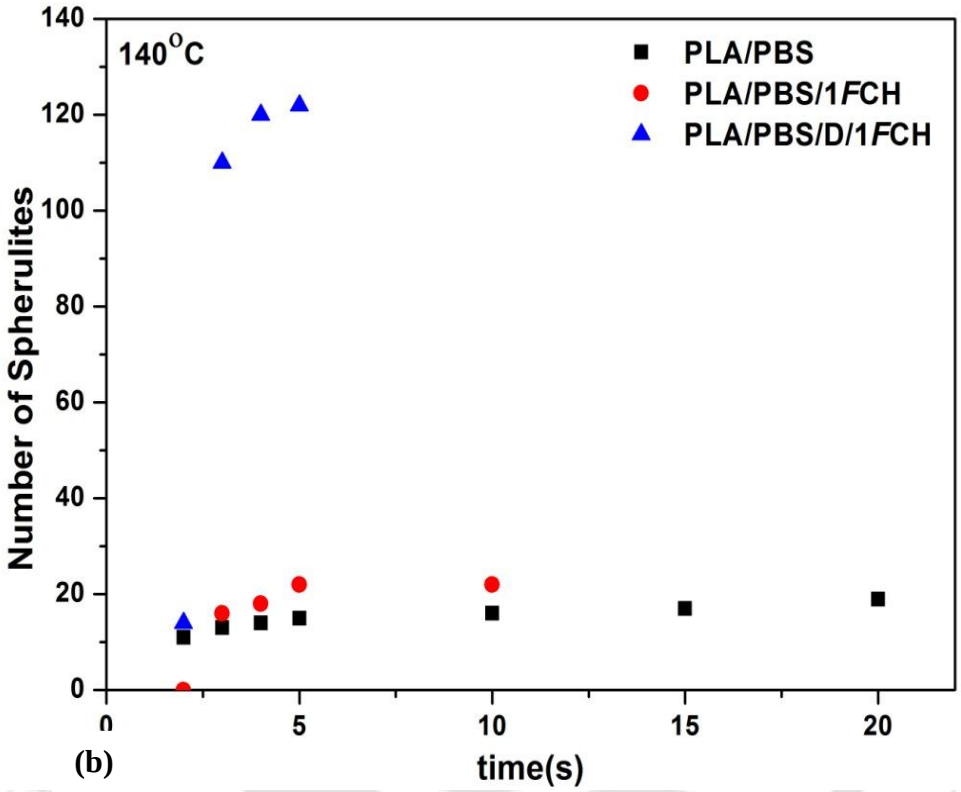

Figure 6.10: *Dependency of number of spherulites on time at (a) 126 and (b) 140 °C respectively for PLA/PBS blend, PLA/BS/1FCH and PLA/PBS/D/1FCH bionanocomposite films.*

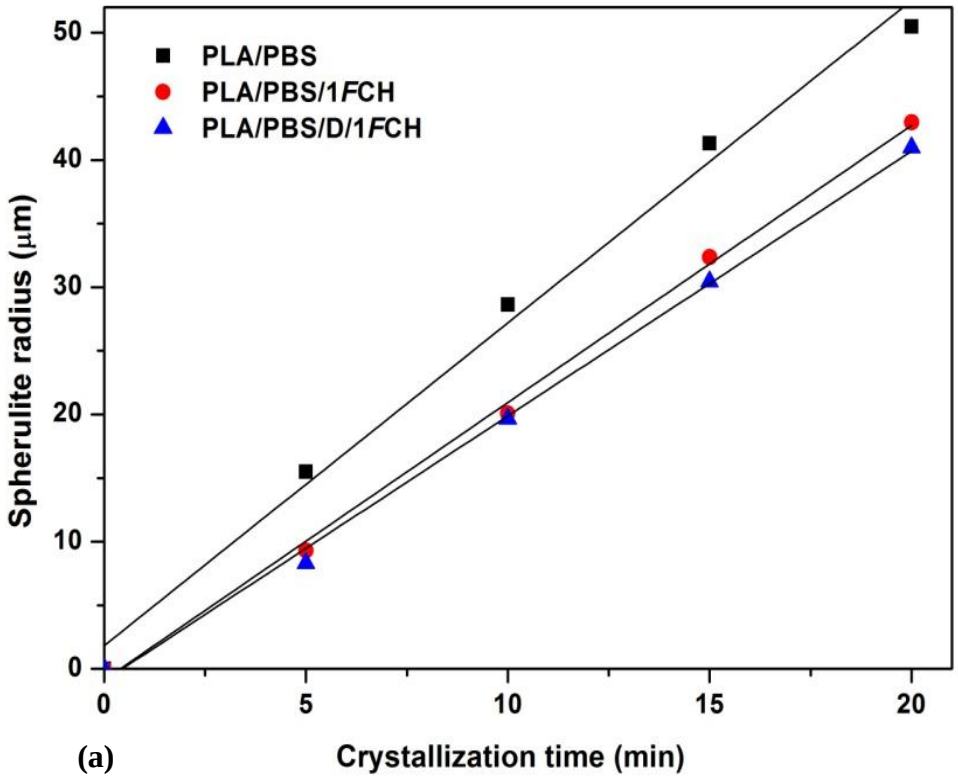

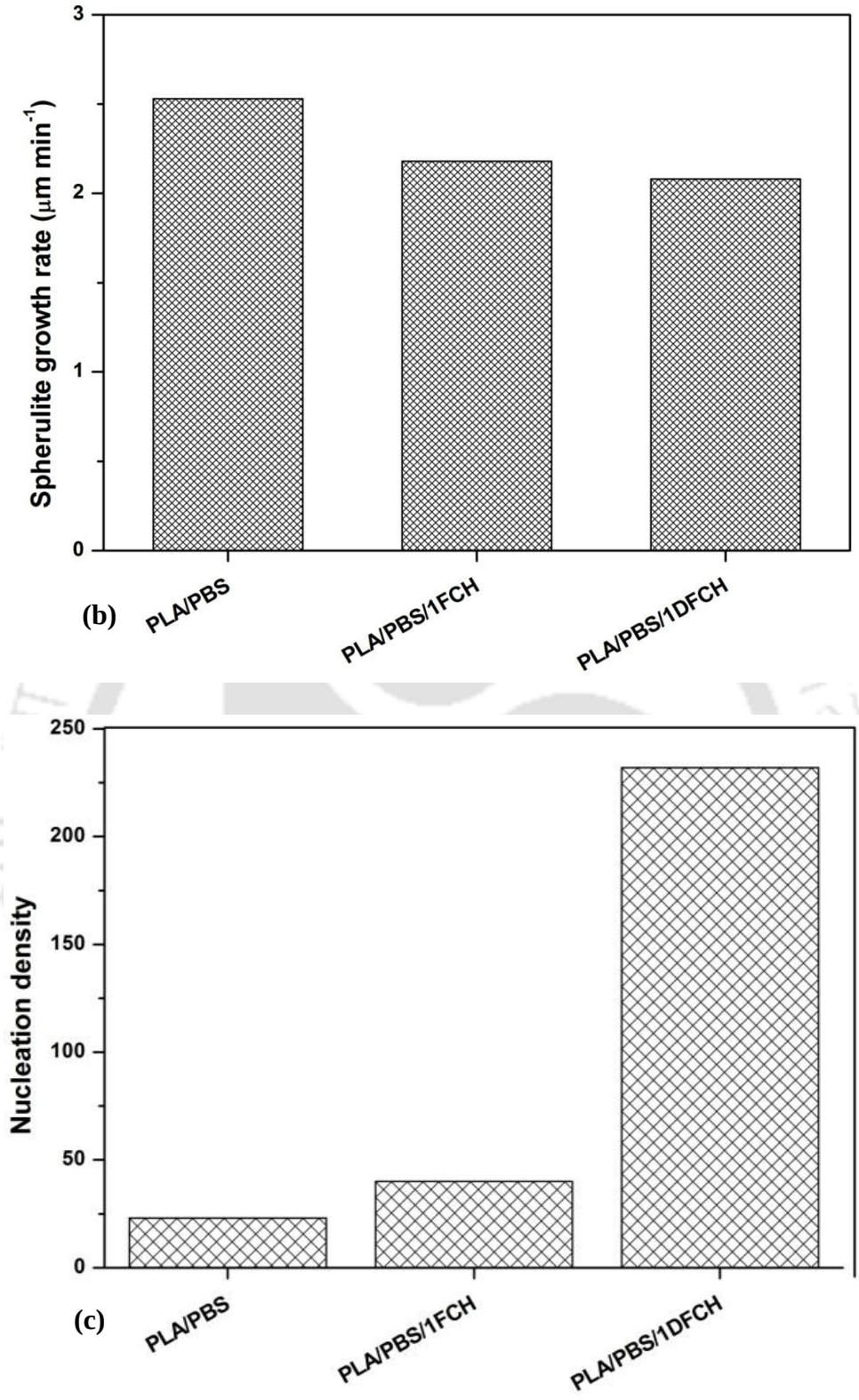

Figure 6.11: *Dependency of Spherulite radius on time (a), growth rate of spherulites and (b) and nucleation density (number of spherulites mm^{-2}) at 140°C (c) for PLA/PBS blend,PLA/PBS/FCH and their bionanocomposite films.*

6.3 CONCLUSIONS

The present investigation provides a simple industrially viable (melt extrusion) technique to fabricate PLA/PBS/*F*CH based ternary bionanocomposite with or without DCP, and structure modification confirmed by FTIR analysis. The surface morphology confirms that no PBS droplet is observed in PLA continuous phase after incorporating DCP or 1 wt% FCH. Further a well dispersion of *F*CH is observed for PLA/PBS/D/1*F*CH bionanocomposite in both polymer domains, which helps to obtain a balanced set of mechanical properties with improvised crystallization efficiency. Interestingly, X_c of PLA is enhanced to 33% and 27% as confirmed by wide angle XRD and DSC respectively for PLA/PBS/D/1*F*CH. Also, DSC investigation confirms that the crystallization rate of PLA is promoted after the incorporation of DCP in PLA/PBS/*F*CH bionanocomposite; mostly because the developed crosslinked structure acts as nucleating sites. Further, as evident by POM results, the spherulites formed in reactive bionanocomposite are larger in number and smaller in size than those formed in PLA/PBS blend and their bionanocomposite (0% DCP). In addition, nucleation density is also the highest which refers to the active participation of *F*CH in the presence of DCP. For PLA/PBS/D/1*F*CH, the static contact angle is significantly increased (~7º) as compared to PLA. The remarkable UV-C blocking effect of the reactive modified bionanocomposite may may be suitable for the packaging of UV sensitive materials.

Table 6.1: FTIR peak analysis for PLA/PBS blend, PLA/PBS/FCH with or without addition of DCP.

Assignments	PLA/PBS	PLA/PBS/1*F*CH	PLA/PBS/D/1*F*CH
asymmetric stretching C–H in CH_3	2996	2996	2992
symmetric stretching C–H in CH_3	2946	-	2945
CH_2 vibration	2964	2964	-
stretching C–H in PLA + stretching CH_2 in PBS	2880	2880	-
asymmetric stretching C–H in CH_3	-	-	2918
symmetric stretching C–H in CH_3	-	-	2851
stretching C(=O) in PLA	1748	1748	1746
stretching C(=O) in PBS	-	-	1713
doublet corresponding to CH_2 twisting appeared in PBS	-	-	1338-1312
C-OH bending of PBS	-	-	917
stretching C-COO & also attribute to amorphous phase of PLA	868	868	866
formation of new C-C linkage	-	-	805
CH_2 stretching	2964	2964	-

Table 6.2: Percentage crystallinity (% X_c) of PLA/PBS and reactive bionanocomposite films.

DSC parameters	PLA/ PBS	PLA/PBS/ 1*F*CH	PLA/PBS/ 3*F*CH	PLA/PBS/D/ 1*F*CH	PLA/PBS/D/ 3*F*CH
% $X_{c, PLA}$	24	27	14	49	43
% $X_{c, PBS}$	15	0.6	0.5	4	3

Chapter 7

Thermal Degradation Study on Poly (lactic acid)/ Poly (butylene succinate)/Functionalized Chitosan based Reactive Bionanocomposite Films

This chapter focuses on the nonisothermal degradation and melt rheological investigation of PLA/PBS/FCH based reactive bionanocomposite films. To address the poor rheological properties as well as the melt strength of PLA/PBS/FCH, reactive modification in the melt state has been performed to control the shear and thermal induced decomposition of fabricated films. The kinetic parameters and thermodynamic variables of the films are investigated using model free approach during the thermal decomposition process. The generalized master plots are selected to predict the decomposition mechanism.

The work in this chapter is under revision:

Monika & Katiyar, V. (2018) Generalized thermal degradation kinetic mechanism and melt rheology for PLA/PBS/functionalized chitosan (FCH) based reactive bionanocomposite, (Status: Under revision in International Journal of Biological Macromolecules).

ABSTRACT

A systematic kinetics of melt-blended poly (lactic acid) (PLA)/poly (butylene succinate) (PBS) and PLA/PBS/functionalized chitosan (*F*CH) bionanocomposite films with dicumyl peroxide (DCP) and chemical changes thereof at degradation temperatures have been evaluated using hyphenated thermogravimetry (TGA) and hyphenated TGA to Fourier transform infrared spectroscopy (TGA–FTIR). A comprehensive kinetic model is employed on the above blended samples, including (i) Flynn–Wall–Ozawa, Kissinger and modified Coat-Redfern methods to investigate the kinetic and thermodynamic variables, and (ii) generalized master plots to propose the thermal induced mechanism. The thermal stability of PLA/PBS is reduced with the increasing *F*CH loading up to 3wt%, which is improved for DCP treated PLA/PBS/1*F*CH at the maximum degradation temperature (T_{max}). The values of activation energy estimated from Flynn-Wall-Ozawa method are (129–139 $kJmol^{-1}$), (116–152 $kJmol^{-1}$), (109–146 $kJmol^{-1}$), (132–169 $kJmol^{-1}$) and (120–166 $kJmol^{-1}$) for PLA/PBS, PLA/PBS/1*F*CH, PLA/PBS/3*F*CH, PLA/PBS/D/1*F*CH and PLA/PBS/D/3*F*CH respectively. The generalized master plots depicts that the PLA/PBS blend exhibited L2–F1 mechanism whereas their bionanocomposite with or without DCP followed L2–D_n and A2–L2–D_n mechanism respectively. Hyphenated TGA–FTIR highlights the similar kinds of products such as lactide, acetaldehyde, esters, CO_2 and CO which are liberated during the thermal degradation of PLA/PBS blend and their bionanocomposite films. It is postulated from the rheological investigation that *F*CH is grafted onto PLA/PBS system to form crosslink/branched structure.

Graphical Abstract

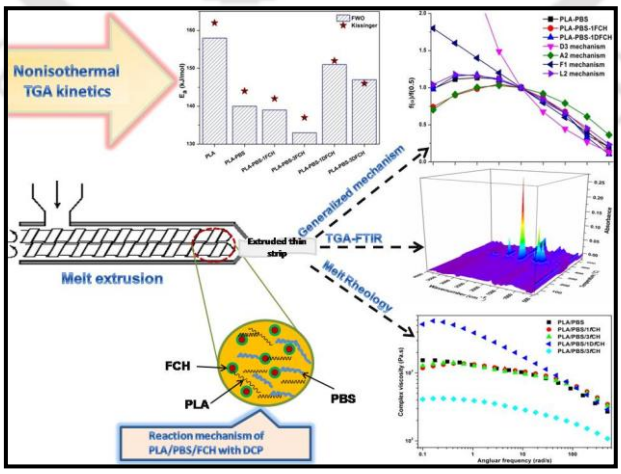

Scheme 7.1: *Schematic representation of thermal decomposition behavior of PLA/PBS/FCH bionanocomposite in the presence of DCP.*

7.1 INTRODUCTION

Due to the economic and environmental concerns, the quest for the development of renewable bio-based material as the potential replacement for synthetic polymer based packaging is an emerging area for the scientists as well as manufacturer **(Wu et al., 2005)**. In past, some bio-based and biodegradable polymers such as the poly lactic acid (PLA), poly (butylenes succinate) (PBS), poly (ε-caprolactone) (PCL), polybutylene adipate-co-terephthalate (PBAT) were introduce in the commercial market **(Nerantzaki et al., 2014)**. Of the entire biopolymer family, PLA has seen a notable surge of research due to its easy processability, biocompatibility and the properties that are comparable to many commodity plastic **(Kamal et al., 2015; Gu et al., 2008)**. In spite of various significant characteristics, it has some limitation such as brittle nature, low thermal stability, narrow processing window and poor melt strength **(Nerkar et al., 2015)**. However, these limitations are challenging for its industrial acceptance and inadequate for large scale applications **(Nerkar et al., 2015; Al-etry et al., 2012)**. Among the various approaches, blending with other biopolymers such as PBS may be a good choice to tailor the properties such as toughness **(Cherykhunthod et al., 2015)**. Despite this interest, PLA/PBS blend has limited application as the requirements of many products may not be satisfied due to its poor melt strength and barrier properties. Therefore, various strategies have been developed to overcome these limitations. One possible approach is the incorporation of inexpensive bio-filler in the polymer blend **(Muthuraj et al., 2017)**. Moreover, this perspective shows fabrication of bionanocomposite from biofiller with PLA/polyester blend for commercially viable applications.

Chitosan (CH) is a typical cationic polysaccharide, produced by deacetylation of chitin, which is utilized due to its antimicrobial nature, biodegradability, bio-compatibility, and non toxicity **(Balau et al., 2004; Ou et al., 2010; Muraleedharan et al., 2010)**. It has gained attention in various applications such as wastewater treatment, biomedicine and agricultural

sectors. Applications of chitosan are limited due to its solubility and hydrophilic nature in packaging sectors. To solve this issue, chitosan can be chemically modified by grafting some other hydrophobic oligomer or biopolymer to convert into hydrophobic material using one pot synthesis in the absence of solvent or catalyst. Hence, the dispersion of chitosan in hydrophobic PLA phase can also be enhanced by the functionalized chitosan (*F*CH) **(Pal et al., 2016)**. In this work, DCP plays a role of cross-linking agent **(Zheng et al., 2011)** to modify the properties of PLA/PBS/*F*CH based system in order to develop the bionanocomposites with balanced thermo–mechanical characteristics. Melt extrusion is one of the promising techniques for the development of polymeric bionanocomposites. In general, the polymeric materials such as PLA and PBS are susceptible to thermal decomposition at high temperature, which assists in the reduction of properties due to the severe mass loss. The probable reason for mass loss is the evolution of small volatile fragments after autocatalytic degradation **(Fitaroni et al., 2015)**.

TGA is the most accepted tool for calculating the thermal stability, degradation kinetic triplets such as activation energy (E_a), rate constant (k) and pre-exponential factor (A) **(Carrasco et al., 2010)**. For the systematic investigation, non-isothermal kinetic modeling helps for the better understanding of the decomposition behavior of all the systems and conducting quantitative results from the TGA data. Moreover, kinetic parameters are estimated using Kissinger, Flynn Wall Ozawa (FWO) and modified Coat-Redfern (C-R) methods. Hyphenated TGA–FTIR technique is further utilized to study the release of gas species during the decomposition process. Also, this study evaluated the influence of *F*CH with or without DCP on the thermal behavior of PLA/PBS based bionanocomposite, which is important to determine the processing of bionanocomposites without suffering serious thermal decomposition to make it feasible at an industrial level. Further, the rheological properties are beneficial in the detailed investigation of structure vs. property relationship of

polymer bionanocomposites which plays an essential role in effective processing during the molten state. Measurements of the rheological characteristics under shear are utilized to analyze the interaction between the polymer and filler during the molten state. For better understanding of structural-properties relationship, rheological response is investigated to observe the tailored flow characteristics of bionanocomposite films by modifying the molecular architecture through reactive extrusion with DCP, as well as altering the resultant properties of the system **(Al-Itry et al., 2012)**. The perspective of this research is to explore the rheological and thermal performance of DCP treated PLA/PBS/*F*CH bionanocomposite films with potential utilization in the packaging sector, by means of TGA kinetics, hyphenated TGA–FTIR and melt rheology.

7.2 RESULTS AND DISCUSSION

- ***FETEM of reactively extruded PLA/PBS/FCH based bionanocomposite films***

Figure 7.2 (a)-(b) displays FETEM micrographs of *F*CH, PLA/PBS/*F*CH based bionanocomposite with DCP at higher magnification. PBS is depicted as light spherical domains in Figure 7.2 (b), whereas the dark spherical spots confirm the presence of *F*CH nanoparticles in Figure 7.2 (b'). As observed, sizes of FCH nanoparticles are reduced after addition of DCP into PLA/PBS/*F*CH bionanocomposite.

- ***Thermal performance of reactively extruded PLA/PBS/FCH bionanocomposite films***

From the TGA analysis, the thermal stability in terms of temperature for 15% weight loss temperature (T_{15}), 50% weight loss temperature (T_{50}) and maximum degradation temperature (T_{max}) are mentioned in Table 7.1. TGA is performed to investigate the thermal decomposition behavior of PLA, PLA/PBS blend and their PLA/PBS/*F*CH bionanocomposites with or without DCP. Figure 7.2 (a) – (b) represents the TGA profiles of PLA/PBS, PLA/PBS/FCH and their reactive modified bionanocomposite films and their quantified parameters are displayed in Table 7.1. All of the samples showed two-stage

degradation process, which is revealed from the first derivative thermograms (DTG). Although the incorporation of 1wt% *F*CH into PLA/PBS blend shows no significant reduction in T_{15} and T_{max}, it has been varied insignificantly in comparison to PLA/PBS blend which may be due to the improved compatibility between the PLA and PBS phase in the presence of 1 wt % *F*CH. Further increasing the *F*CH loading with 3 wt %, bionanocomposite has shown reduction in the thermal parameters. The possible reason behind this is the increase in short OLLA chain attached with chitosan which cause the plasticization effect and supported the thermal decomposition of bionanocomposites at lower temperature **(Pal et al., 2016; Ambrosio-Martín et al., 2014)**. For DCP treated PLA/PBS/1*F*CH, the maximum degradation temperature (T_{max}) has been shifted to the higher temperature while no significant change in 15% wt. loss temperature (T_{15}) is observed in comparison to PLA/PBS/1*F*CH bionanocomposite. This result could ascribe that the thermal stability has been slightly improved due to the development of the branching/cross-linking sites at the interface of polymers which may be trying to control the decomposition process at higher temperature **(Luo et al., 2016; Dhar et al., 2016)**.

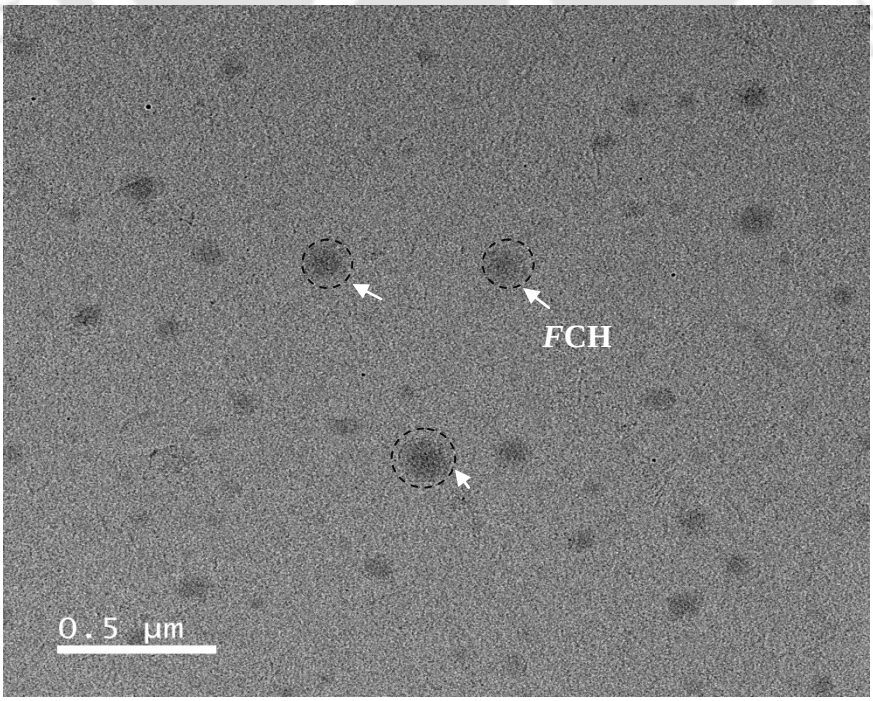

(a)

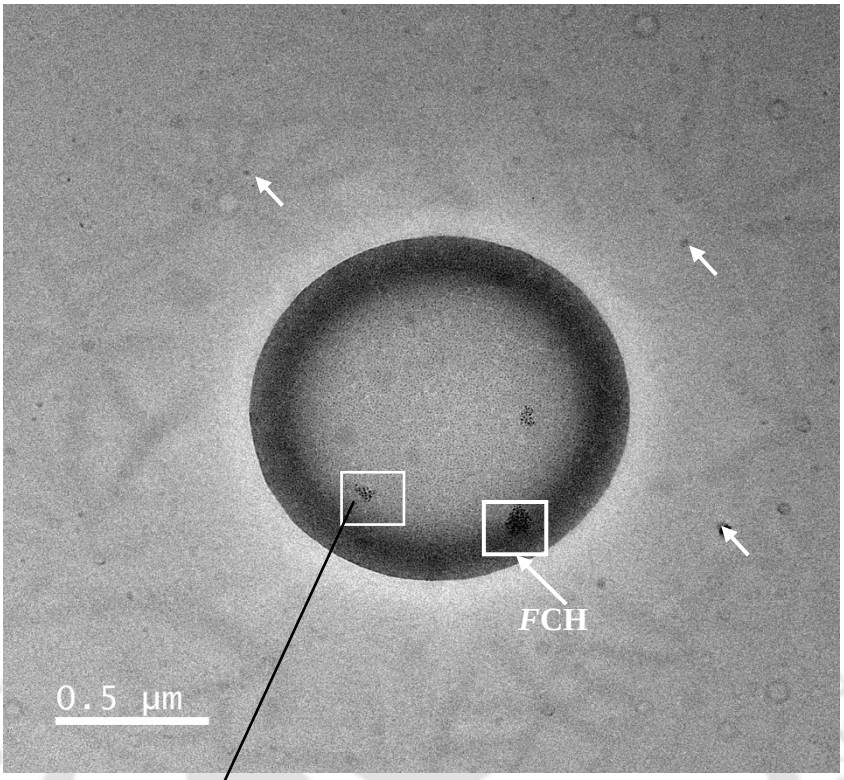

(b)

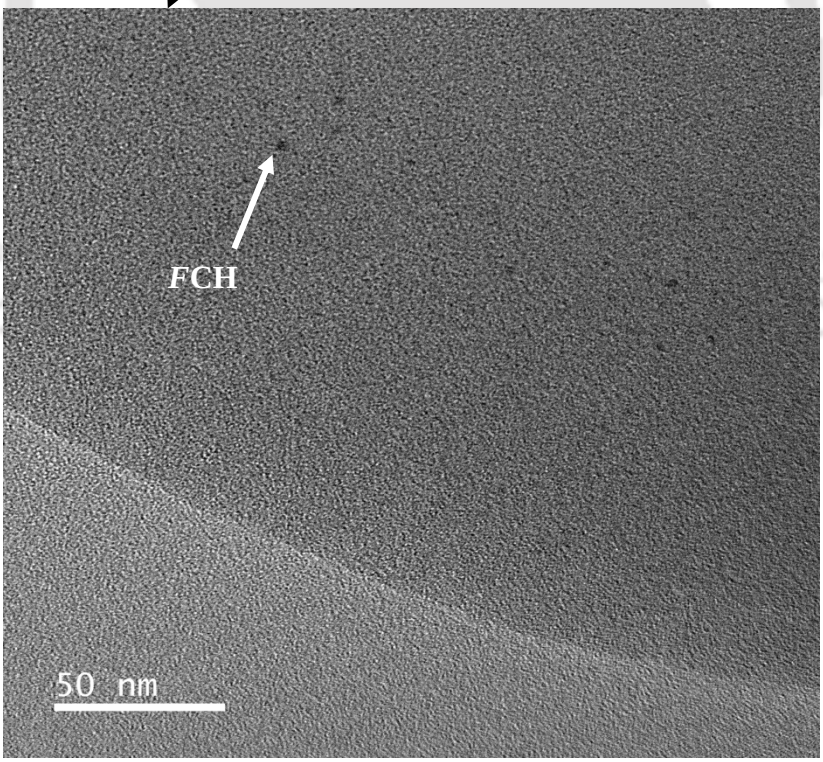

(b′)

Figure 7.1: *FETEM analysis of (a) FCH (b) PLA/PBS/D/1FCH and (b') enlarge image of PLA/PBS/D/1FCH bionanocomposite films.*

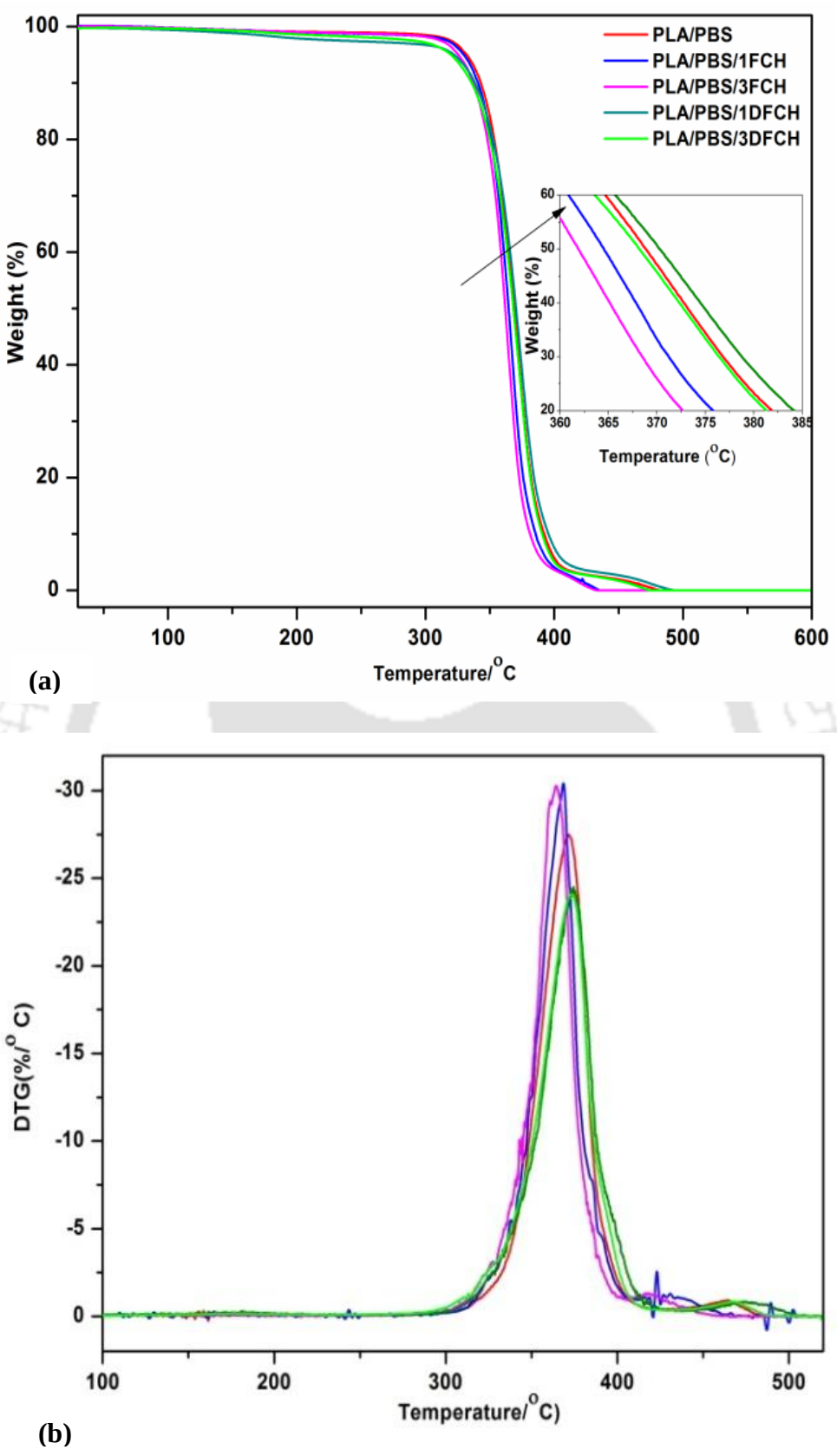

Figure 7.2: *(a) TGA and (b) DTG profiles of PLA/PBS blend, PLA/PBS/FCH and their reactive modified bionanocomposite films at 10 °C min^{-1}.*

Table 7.1: *Influence of the reactive modification on the thermal stability of PLA/PBS blend and their bionanocomposite films.*

Samples	T_{15} (°C)	T_{max} (°C)	T_{50} (°C)
PLA	353	376	371
PLA/PBS	349	371	368
PLA/PBS/1*F*CH	347	369	366
PLA/PBS/3*F*CH	343	365	361
PLA/PBS/D/1*F*CH	346	373	370
PLA/PBS/D/3*F*CH	345	371	369

- ***Nonisothermal degradation kinetics study of the reactively extruded PLA/PBS/FCH based bionanocomposite films***

The influence of different loadings of *F*CH (1 and 3 wt %) on the PLA/PBS in the presence or absence of DCP has systematically been investigated using non-isothermal TGA kinetics. TGA and DTG plots of PLA/PBS blend and their bionanocomposite films have been plotted at different heating rates (5, 10, 15 and 20 °C) as illustrated in Figure 7.3 (a) – (f). It is a well-known fact that the mass-loss plot shifts to the right due to less retention time at the higher heating rate and vice versa **(Yuzay et al., 2010)**. Moreover, the kinetic parameters are calculated by widely used model-free methods such as Kissinger, FWO and KAS method.

- ***Estimation of activation energy (kJ mol $^{-1}$) for reactively extruded PLA/PBS/FCH films***

Analytical methods have been utilized to determine E_a from TGA data, which are already described in theoretical approach. FWO (log β vs 1000/T) and modified CR (ln β/T^2 vs 1000/T) plots for PLA, PLA/PBS blend, PLA/PBS/*F*CH bionanocomposite films with and without DCP are displayed in Figure 7.4 (a) – (f) and Figure 7.5 (a) – (f) respectively; the slope of linear fit has been used to estimate the E_a. Notably, the linear fit corresponding to α range (0.1–0.9), indicates that both the isoconversional methods are appropriate choices to the analyzed system.

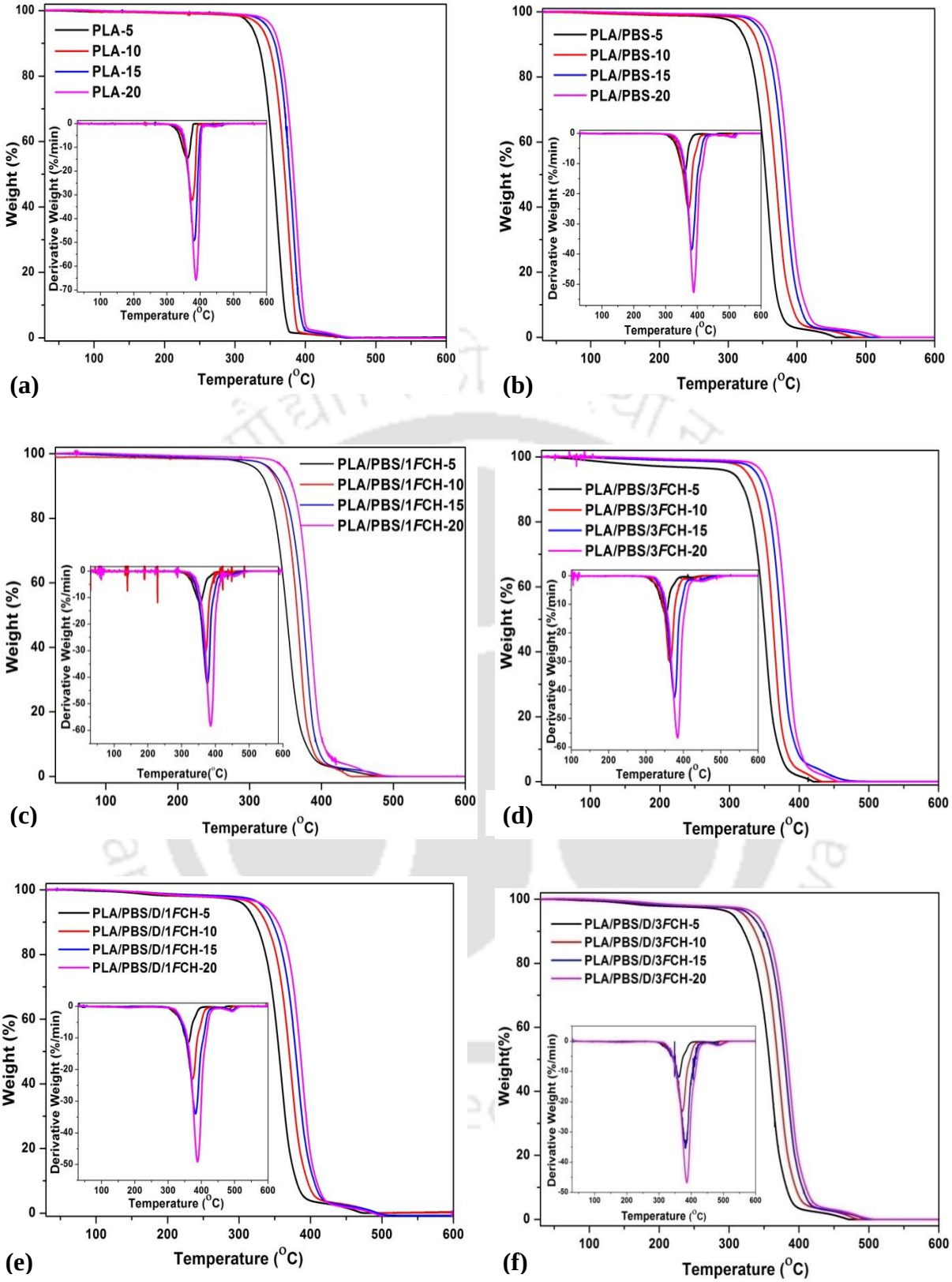

Figure 7.3: *TGA and DTG profiles of (a) PLA, (b) PLA/PBS, (c) PLA/PBS/1FCH, (d) PLA/PBS/3FCH, (e) PLA/PBS/D/1FCH, and (f) PLA/PBS/D/3FCH films at 5, 10, 15 and 20 °C min^{-1}.*

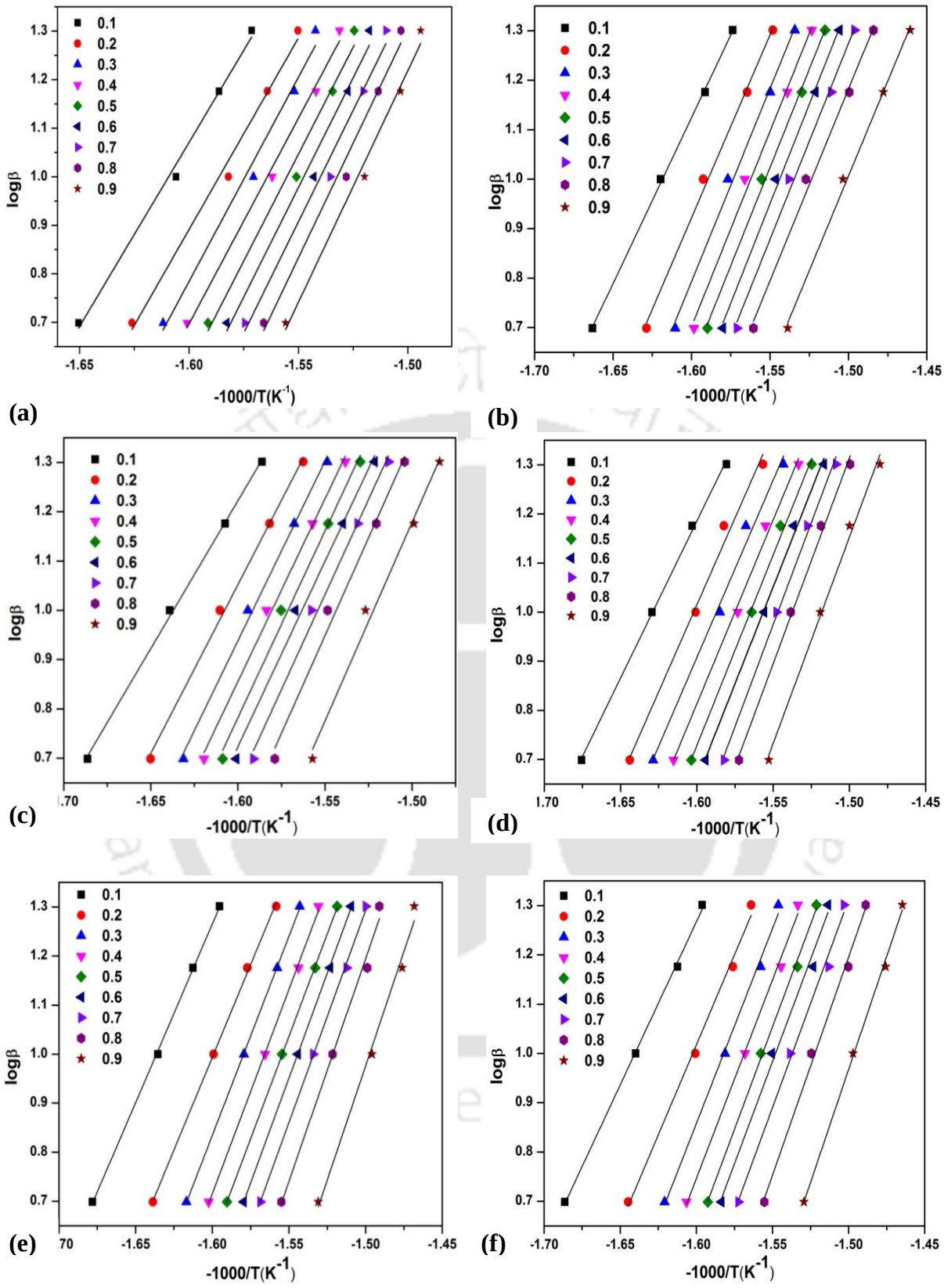

Figure 7.4: *FWO plots for (a) PLA, (b) PLA/PBS, (c) PLA/PBS/1FCH, (d) PLA/PBS/3FCH (e) PLA/PBS/D/1FCH and (f) PLA/PBS/D/3FCH bionanocomposite films.*

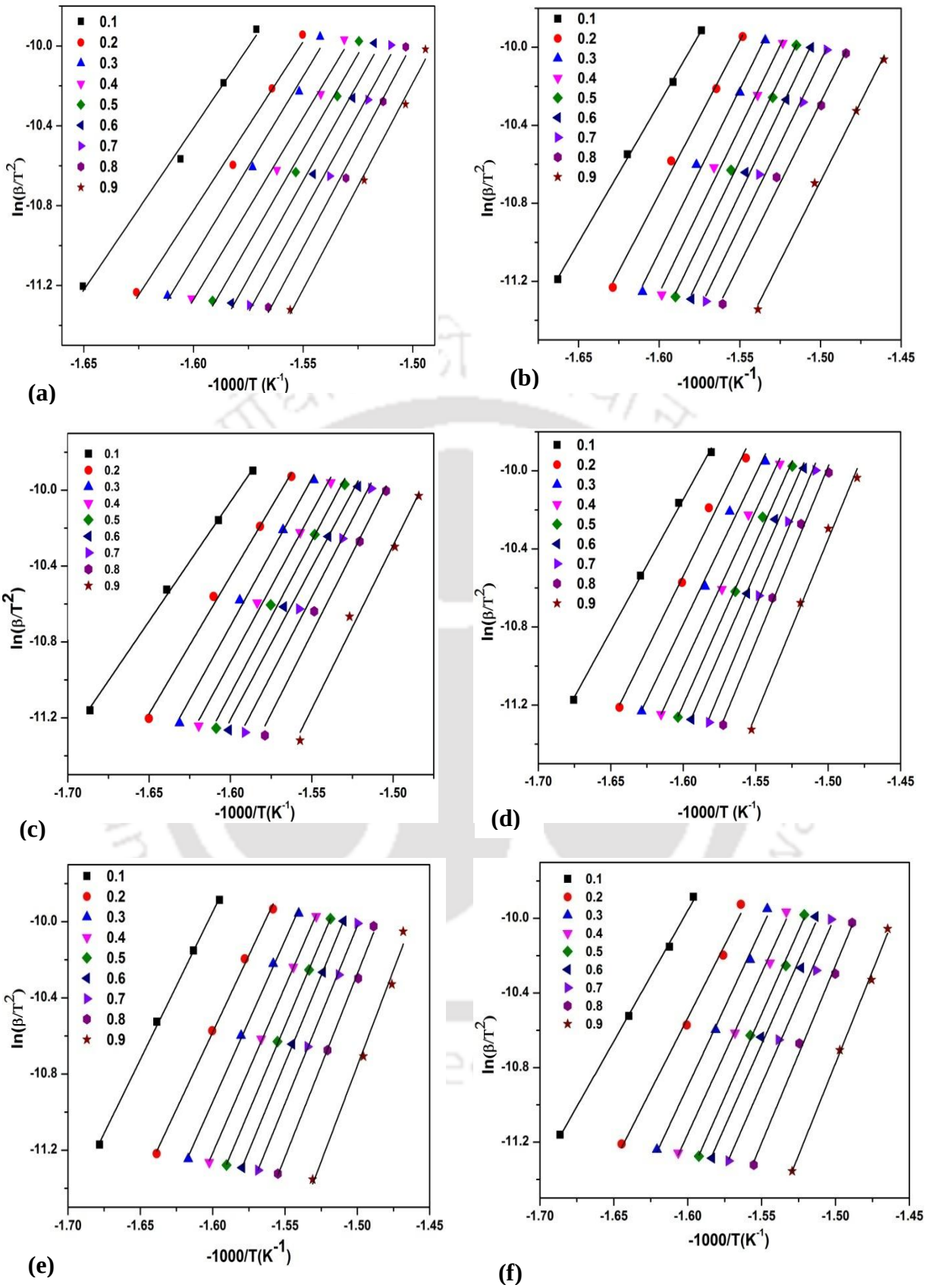

Figure 7.5: *Modified CR plots for (a) PLA, (b) PLA/PBS, (c) PLA/PBS/1FCH, (d) PLA/PBS/3FCH,(e)PLA/PBS/D/1FCH and (f)PLA/PBS/D/3FCH films.*

For all the samples, the distribution of E_a against α has been shown in Figure 7.6 (a) – (b) respectively; and summarized in Table 7.2. Moreover, the similar values of E_a are observed from methods within the experimental uncertainty using the isoconversional methods. When E_a remained unchanged for the various conversion degrees, the single step mechanism is involved. The variation of E_a with α is a sign of multiple reactions; since many reactions are further involved with increase in temperature. From Figure 7.6, it has been noticed that the value of E_a varies with α in case of PLA. Therefore, the decomposition behaviour of PLA is not processed by simple phenomena because of several reactions occurring concurrently. In general, PLA decomposition occurred by the cleavage of the ester group and chain scission of typical C–C and C–O bond on the backbone chain. It has been suggested that PLA chains undergo degradation by hydrolysis due to the presence of the trace of water, the presence of cyclic oligomer due to the intermolecular transesterification reaction, acrylic acid, acetaldehyde, and CO_2 produced due to cis-elimination and fragmentation respectively **(Kopinke et al. 1996; Tesfaye et al., 2016; Mofokeng et al., 2016)**.

For PLA/PBS blend, the determined value of E_a is ~129 kJ mol^{-1} at the initial level. It is suggested that less energy is needed to bond scission at a primary stage to commence the decomposition process, due to the existence of more active sites at the polymer chain ends. It is observed that the E_a remains unchanged at the conversion range (0.2–0.7) and slightly decrease after it which subsequently leads to the participation of two mechanisms in this case. The probable reason can be the blend morphology and the comparatively poor interaction between the PLA and PBS phase, which somehow varied the energy needed for the decomposition of each of the components. For PLA/PBS/1*F*CH bionanocomposite, the dependence on E_a can be separated into three distinct regions. It shows remarkable improvement in E_a up to ~153 kJ mol^{-1} in the first (I) region with increasing α~0.3, estimated value of E_a changes slowly in the second (II) region ($0.3 \leq \alpha \geq 0.6$). From the third (III)

region, a slight enhancement in value of E_a is noticed. This confirms that it promotes the decomposition process which involves at least three distinct types of mechanisms. It is supported by the fact that the calculated E_a of PLA/PBS/*F*CH based bionanocomposite is lower than PLA/PBS blend. A similar trend has also been noticed when 3 wt% *F*CH is added into PLA/PBS. This means that less energy is required due to the availability of more active terminal sites which subsequently leads to the enhancement in the auto-catalytic effect during the thermal decomposition of polymer bionanocomposite. It is probably due to the anhydrous chitosan produced by the dismissal of bound, unbound water during degradation; which produces more H^+ ions. The higher concentrations of H^+ ions also enhance the chain scission of ester groups in the random fashion for polymer bionanocomposite **(Pal et al. 2016; Valapa et al. 2014)**. There is a major possibility that the developed intermediates further face the random chain scission type decomposition which is probably due to the hydrolysis of ester group at the chain ends **(Pal et al., 2016; Li et al., 2009)**. Therefore, the thermal consistency is reduced to increase in the FCH loading in polymer bionanocomposite. For DCP treated PLA/PBS/1FCH bionanocomposite, it is observed that the E_a is gradually enhanced with α. Such variation in value of E_a is related to the multi-stage decomposition process **(Zou et al., 2009)**. This result shows that the delayed thermal decomposition of polymer bionanocomposite is due to inducing branching/crosslinking effect **(Luo et al., 2016; Wei et al., 2015)**. This can be further explained by the more energy input required to cleave the new C-C linkage. For DCP treated PLA/PBA/3*F*CH, a slight decrement in E_a is observed as compared to PLA/PBS/D/1*F*CH which is due to the possible reduction in the extent of branching/crosslinking linkage in the system.

From Figure 7.6, it is clear that more than two different types of mechanism are deployed to explain the decomposition behaviour for DCP treated PLA/PBS/1*F*CH and PLA/PBS/3*F*CH bionanocomposite films.

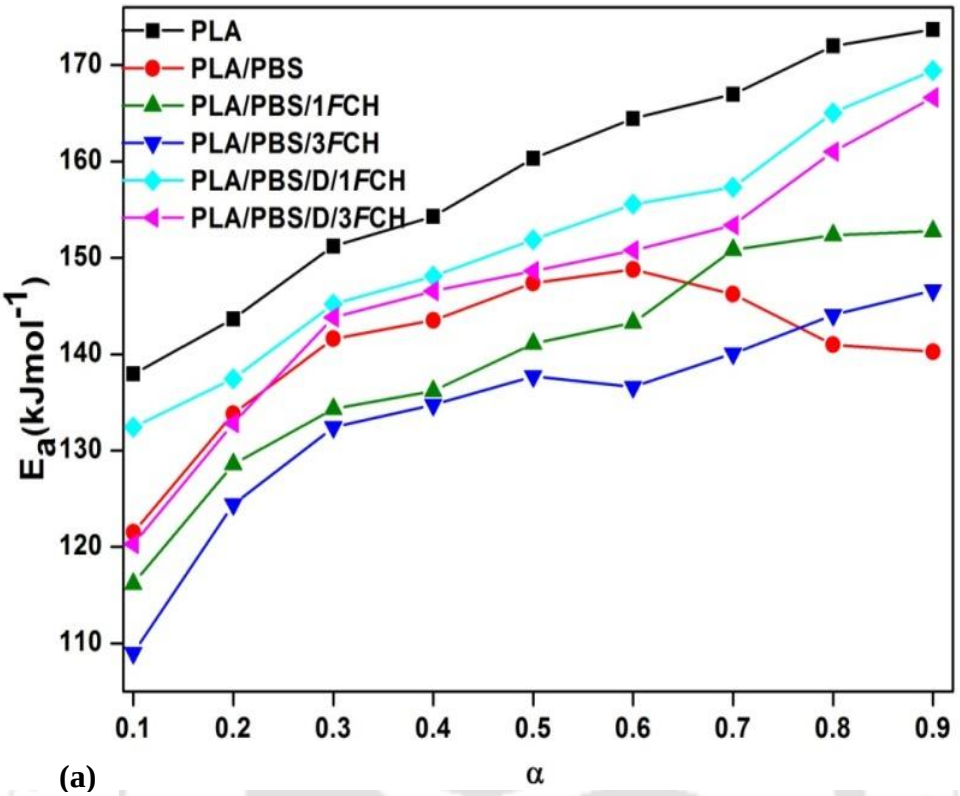

(a)

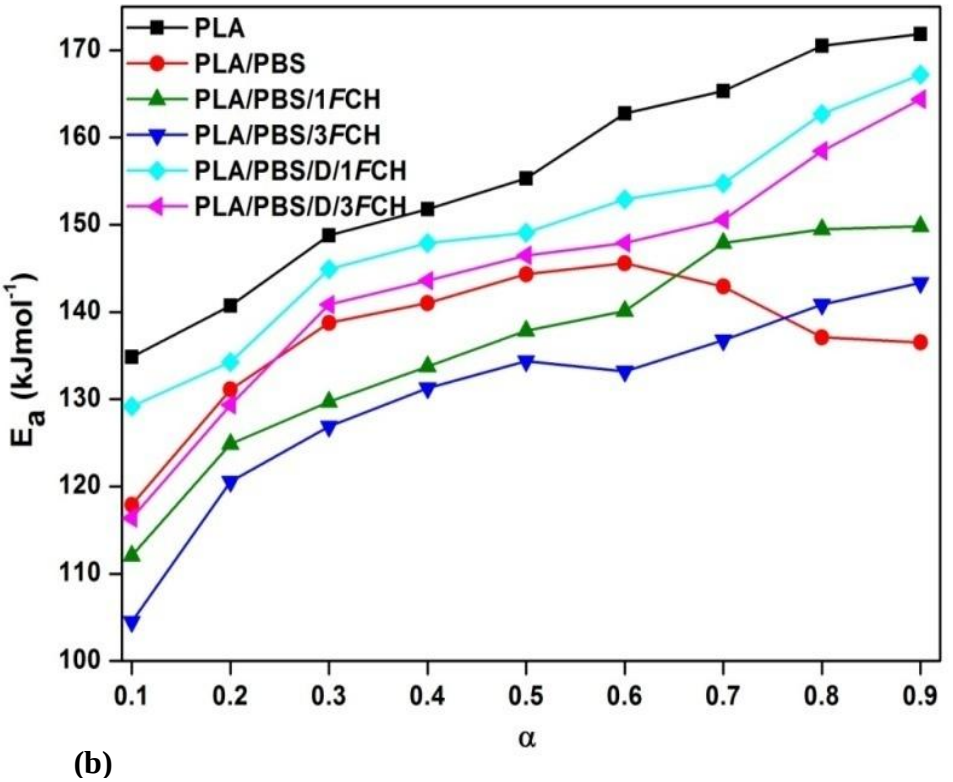

(b)

Figure 7.6: *Distribution of E_a with α profiles using (a) FWO (b) modified CR methods for PLA, PLA/PBS blend, PLA/PBS/FCH and their reactive bionanocomposite films.*

For the Kissinger method, the smooth relativity of the linear fits affirms the feasibility of this method **(Tiptipakoran et al., 2007)**, as clearly seen in Figure 7.7. The obtained E_a from the Kissinger method is higher than FWO and modified CR methods, which is due to different approximations utilized to solve the methods.

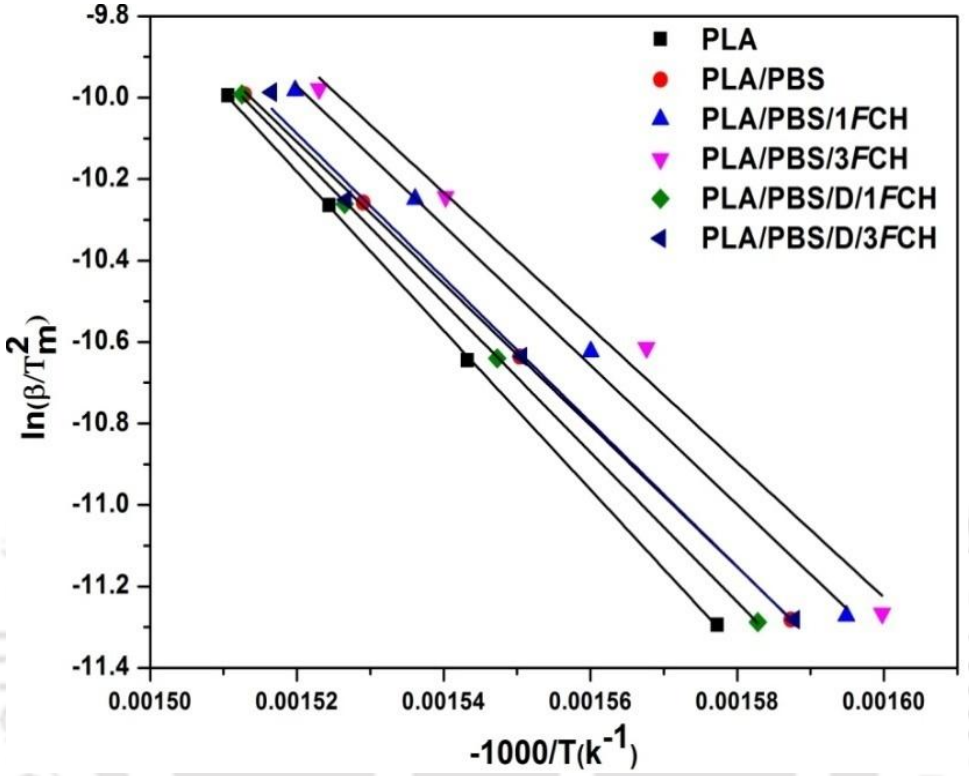

Figure 7.7: *Kissinger plots for PLA, PLA/PBS blend, PLA/PBS/FCH and their reactive bionanocomposite films.*

- ***Calculation of thermodynamic variables for reactively extruded PLA/PBS/FCH based bionanocomposite films***

Thermodynamic variables such as ΔG, ΔS and ΔH are obtained at T_{max} using the Kissinger method for all the samples, as mentioned in Table 7.3. The calculated value of ΔG, ΔH found positive while ΔS shows negative sign. The positive value of ΔH suggests that the possible decomposition processes are endothermic in nature and confirms that the bond dissociation increases with an increase in temperature. For all the samples, a positive sign of ΔG indicates that bond dissociation process is non-spontaneous at T_{max}. The negative sign of ΔS confirms

that the activated complex are produced at the higher temperature.

Table 7.2: *Estimated apparent E_a with regression coefficient (R^2) for PLA, PLA/PBS blend, and their bionanocomposite films with and without DCP obtained using FWO, modified CR and Kissinger methods.*

Samples	FWO method			modified C-R method			Kissinger method	
	E_a (0.1-0.9)	E_a	R^2	E_a (0.1-0.9)	E_a	R^2	E_a	R^2
PLA	137-173	158	0.994	134-171	156	0.996	162	0.994
PLA/PBS	129-139	140	0.995	117-136	136	0.996	144	0.999
PLA/PBS/1*F*CH	116-152	139	0.995	112-149	135	0.993	142	0.998
PLA/PBS/3*F*CH	109-146	133	0.994	104-143	130	0.993	137	0.994
PLA/PBS/D/1*F*CH	132-169	151	0.997	129-167	148	0.997	152	0.999
PLA/PBS/D/3*F*CH	120-166	147	0.996	116-164	144	0.995	146	0.995

Table 7.3: *Thermodynamic variables for PLA, PLA/PBS blend and their bionanocomposite films calculated using the Kissinger method.*

Samples	Thermodynamic variables			
	A (s^{-1})	ΔH (kJ mol^{-1} K^{-1})	ΔS (kJ mol^{-1})	ΔG (kJ mol^{-1})
PLA				
PLA/PBS	1.98E+11	144.79	-0.14055	235.3
PLA/PBS/1*F*CH	5.75E+13	167.59	-0.11062	238.6
PLA/PBS/3*F*CH	1.90E+13	161.20	-0.11727	236.1
PLA/PBS/D/1*F*CH	9.57E+13	170.95	-0.10707	240.1
PLA/PBS/D/3*F*CH	5.56E+13	168.80	-0.10931	239.3

- ***Prediction of degradation mechanism for the reactively extruded PLA/PBS/FCH based bionanocomposite films***

The generalized experimental curves are determined on the basis of Equation (9) and predict

the mechanism by comparing it with the master plots. The kinetic parameters obtained for Kissinger method are utilized in Equation (9) and Equation (11). Figure 7.8 (a)–(f) depicts master and experimental plots for PLA, PLA/PBS blend and their ternary bionanocomposite films with or without DCP.

It can be clearly seen in Figure 7.8 (a) that PLA follows the mechanism according to the A2 and shift the R3 to D2 **(Papageorgiou et al., 2010)**. In this type of solid-state mechanism, the degradation starts from the generation of nuclei sites that act as growth centre to initiate the thermal decomposition **(Kopinke et al., 1996)**. In general, the polymer crystals have imperfections due to the presence of impurities and some point defects. These imperfections are available sites for nuclei formation. In case of PLA/PBS blend, it follows via L2 (random scission mechanism) up to 0.7 conversions, shifts slowly towards the F1 (random nucleation mechanism) at higher conversion. PLA/PBS/*F*CH based bionanocomposite films (with 1 and 3 wt% *F*CH) exhibits degradation mechanism which is overlapped with A2 type mechanism at the conversion range (0.1–0.4). At $\alpha>0.5$ degradation mechanism change towards L2 ($\alpha\sim0.6$ to 0.7) to D2 ($\alpha\sim0.8$) and follow D3 ($\alpha\sim0.9$) type mechanism. For DCP treated PLA/PBS/*F*CH (with 1 wt% and 3 wt% *F*CH) bionanocomposite films, the thermal degradation proceeds via L2 (0.1-0.7) mechanism and system shifts towards D3 type mechanism at higher temperature. It may be said that L2 is the rate controlling step for DCP treated PLA/PBS/*F*CH bionanocomposite films.

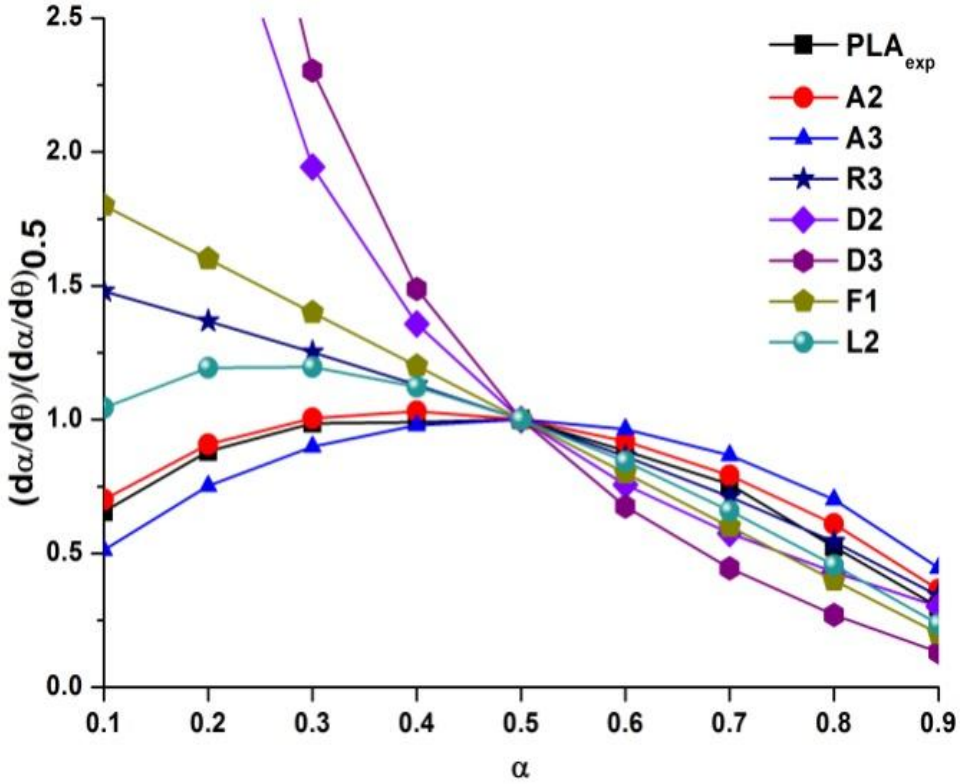

(a)

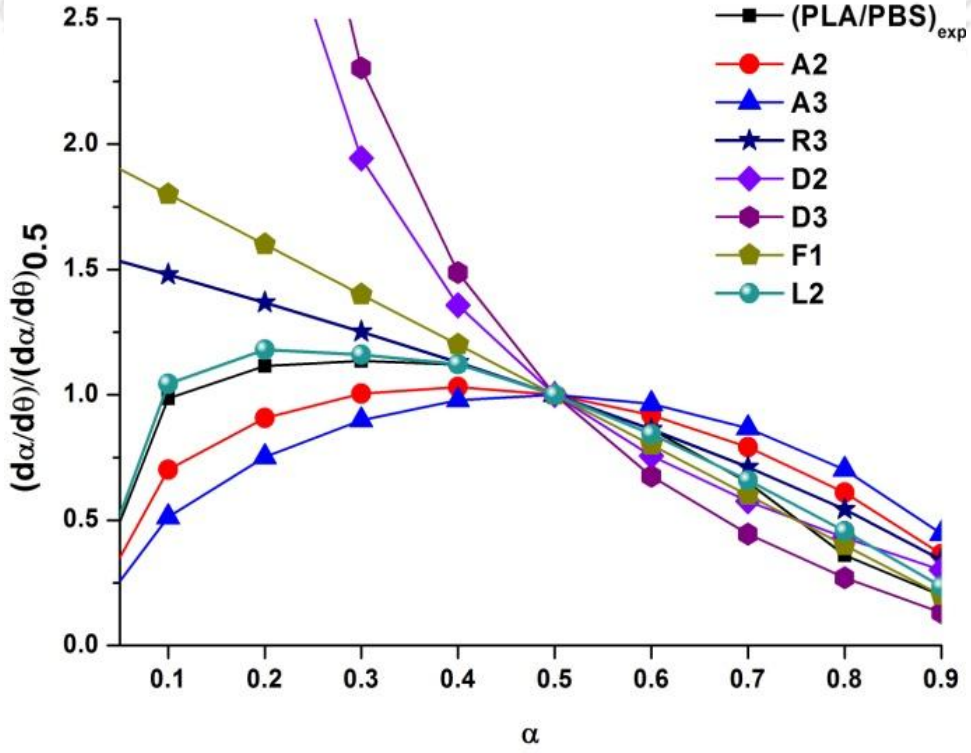

(b)

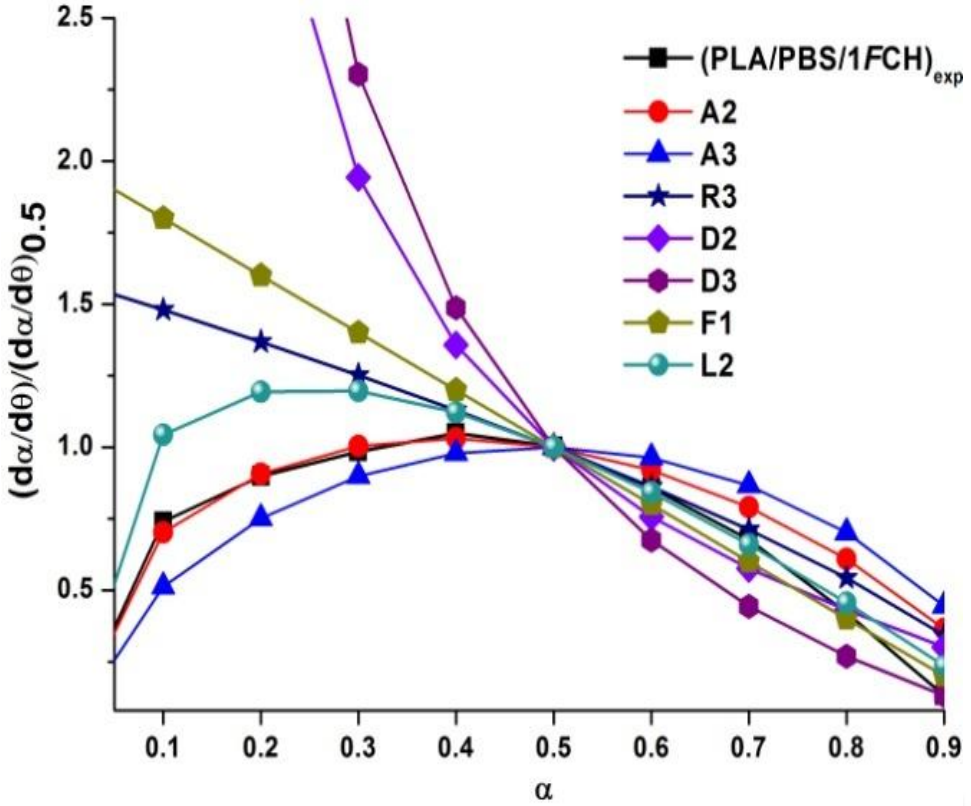

(c)

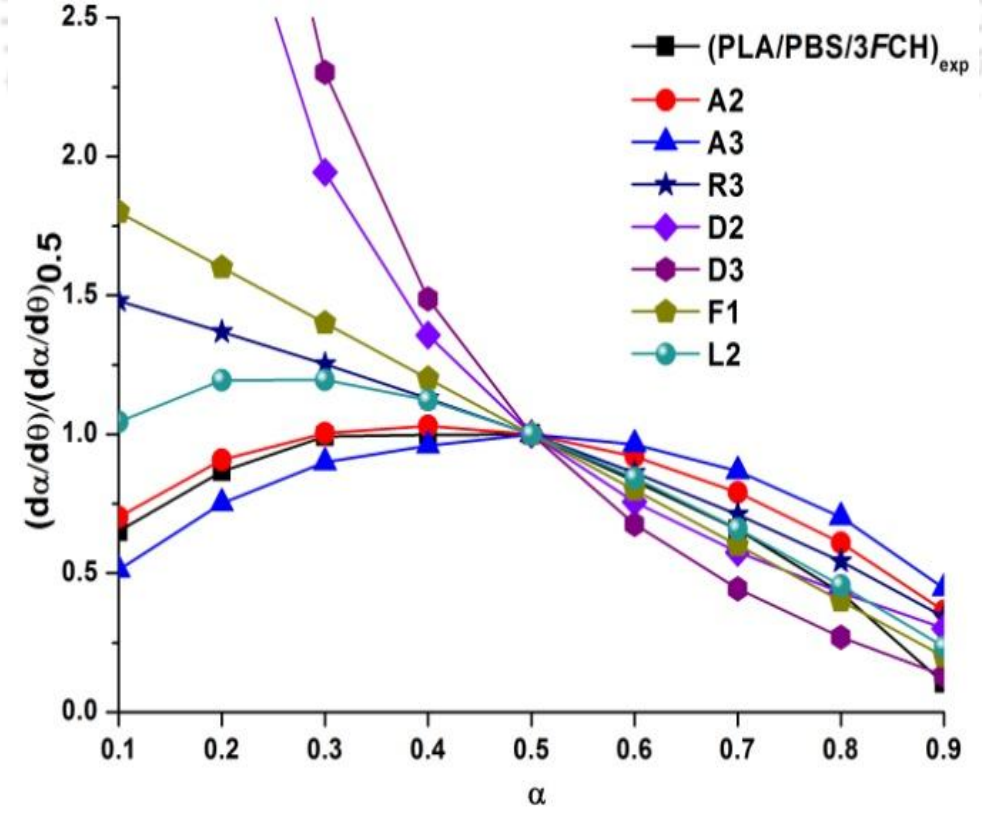

(d)

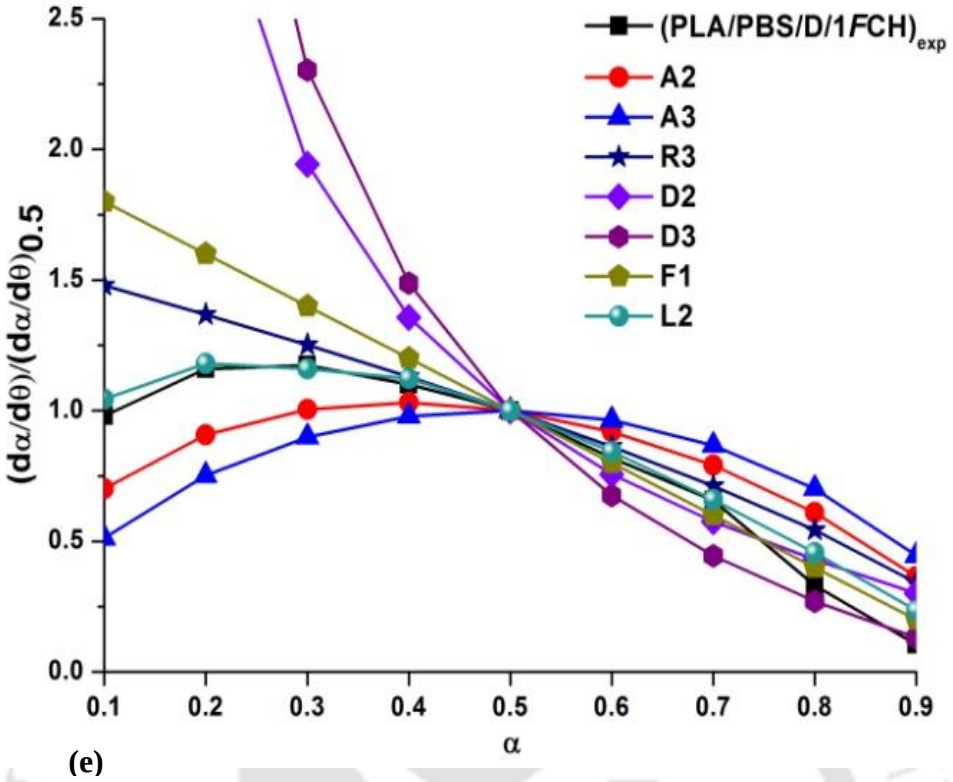

(e)

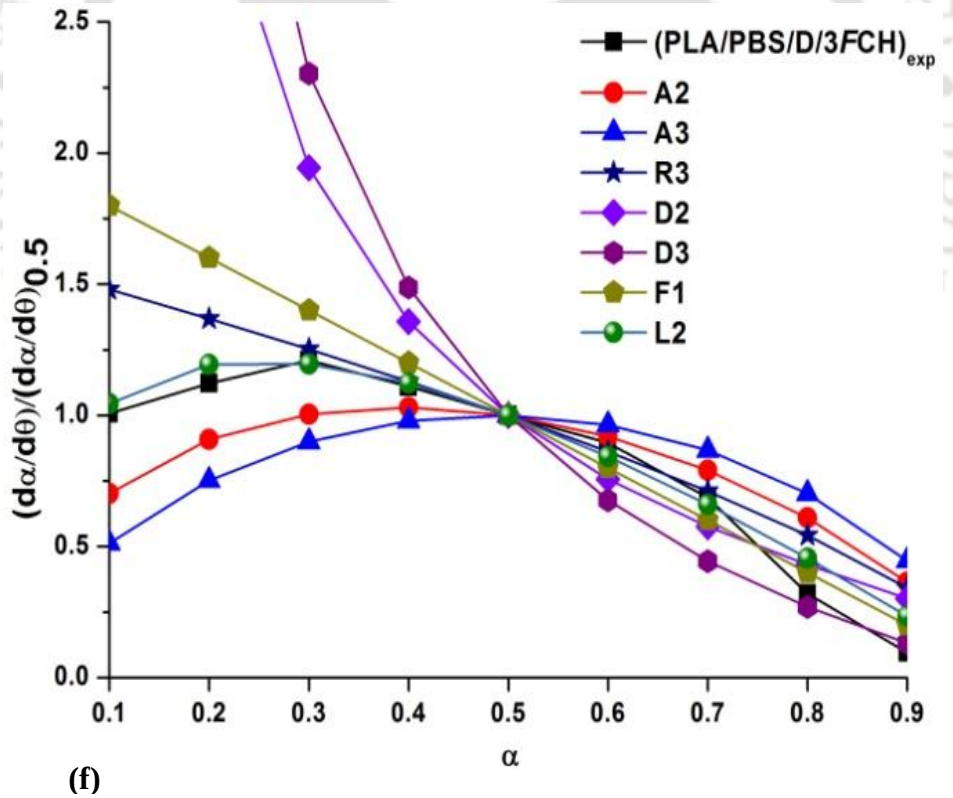

(f)

Figure 7.8: *Reaction mechanism obtained using the generalized mehtods for (a) PLA, (b) PLA/PBS, (c) PLA/PBS/1FCH, (d) PLA/PBS/3FCH, (e) PLA/PBS/D/1FCH and (f) PLA/PBS/D/3FCH bionanocomposite films.*

- ***Released of gaseous products analyzed by hyphenated TGA-FTIR technique***

Hyphenated TGA–FTIR technique is beneficial for understanding the thermal decomposition behaviour of PLA/PBS blend and its bionanocomposite films **(Wilkie et al., 1999)**. In hyphenated TGA-FTIR technique, the intensity of IR absorbance peak related to the concentration of the release volatile components. Figure 7.9 (a) – (a') and (b) – (b') shows the 3D and 2D IR spectrogram to detect the volatile species, related to the thermal decomposition of PLA/PBS blend and its bionanocomposite films. From the 3D plots, it could be inferred that there is no release of volatile component below 300°C. In fact, the intensity of absorption peaks is related to gaseous species emission attains its maximum at 365^{o}C and monotonically decreased after it. This result is found in agreement with the TGA data. From the 2D stack plot, it is clear that the major decomposition product **(Vogel et al., 2008; Tudorachi et al., 2012)** lactide shows the absorption bands due to stretching of C–H, asymmetric stretching of CH_3 and symmetric stretching of CH_3 at 3002, 2951 and 2893 cm^{-1} respectively. The band at 1792 cm^{-1} (stretching of C=O), 1377 cm^{-1} (bending of CH_3), subsequent two peaks at 1240 and 1106 cm^{-1} (stretching of C–O–C) and 930 cm^{-1} (ring skeleton) represent the major groups. Two noteworthy bands at 1765 cm^{-1} (stretching of C=O) and 2738 cm^{-1} (stretching of –CH=O), weak bands at 2963 cm^{-1} (stretching of CH_2) and 1371cm^{-1} (bending of CH_2), confirm that acetaldehyde is produced. Moreover, the bands appearing at 2358-2310 cm^{-1} (asymmetric stretching of O=C=O), 669 cm^{-1} (bending of O=C=O) is related to carbon dioxide (CO_2) and it is produced by decarboxylation of carboxyl group during the decomposition process. The IR peak related to carbon monoxide (CO) at 2176–2118 cm^{-1} (bending of C–O) is noticed. The shoulder peak at 1735 cm^{-1} also confirms the release of ester components. The FTIR spectrum of PLA/PBS/D/1*F*CH bionanocomposite films exhibited the similar kind of main gaseous product emission. When the temperature reaches around 450 ^{o}C, all the bands almost disappear except the band of CO_2 that exist till the end.

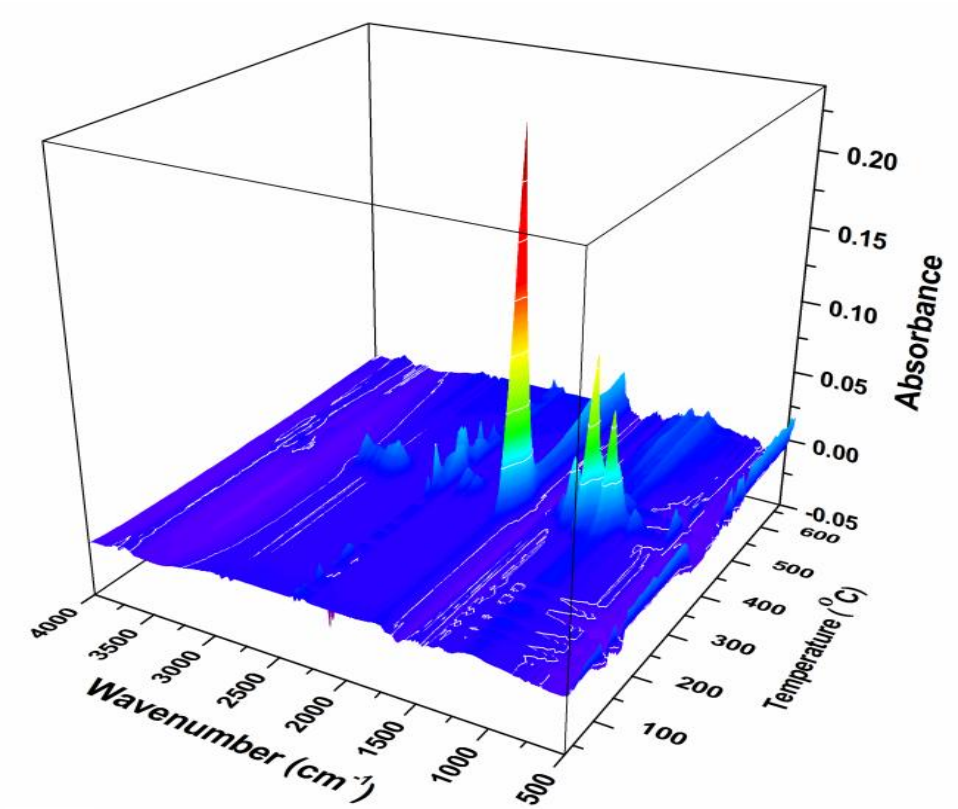

(a)

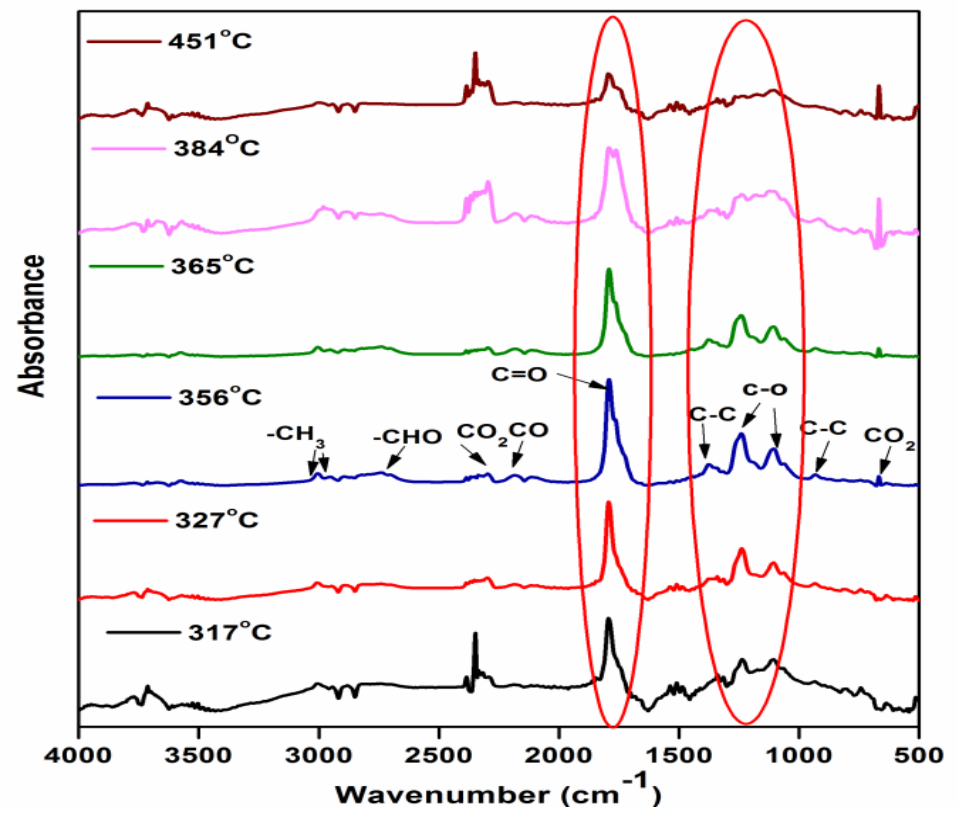

(b)

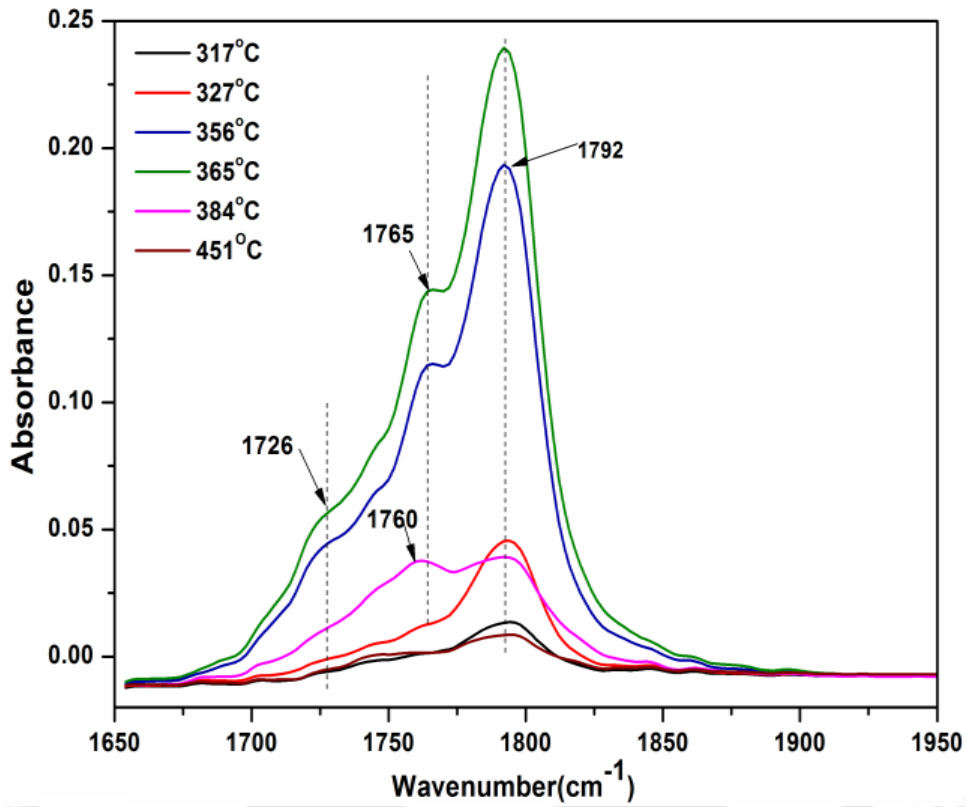

(c)

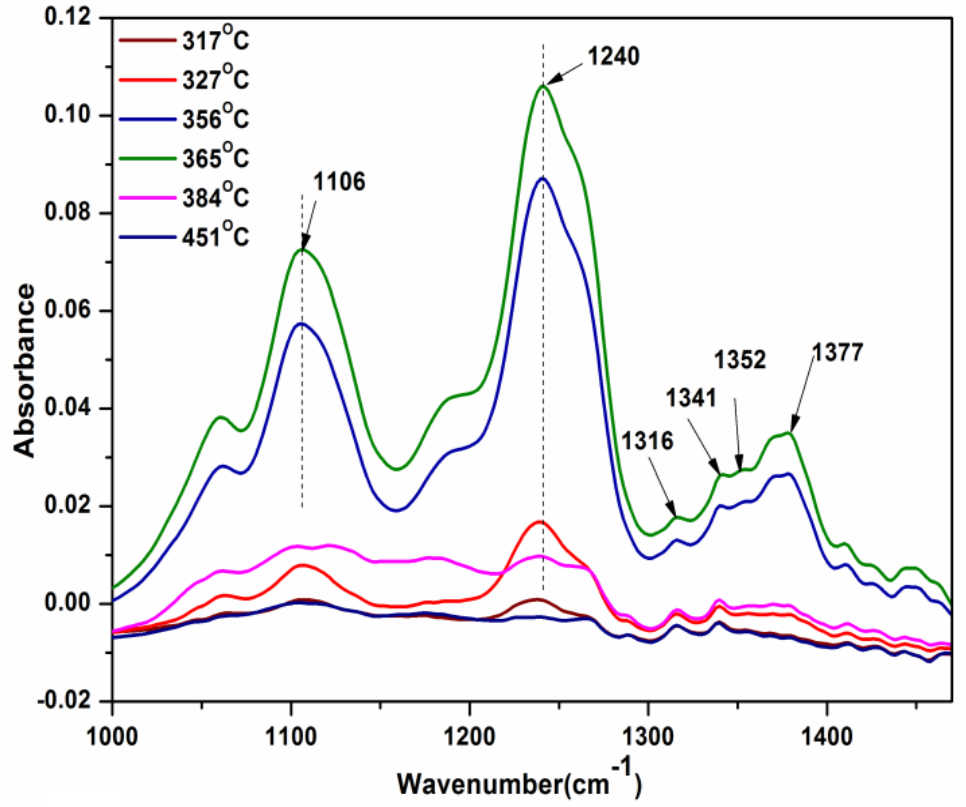

(d)

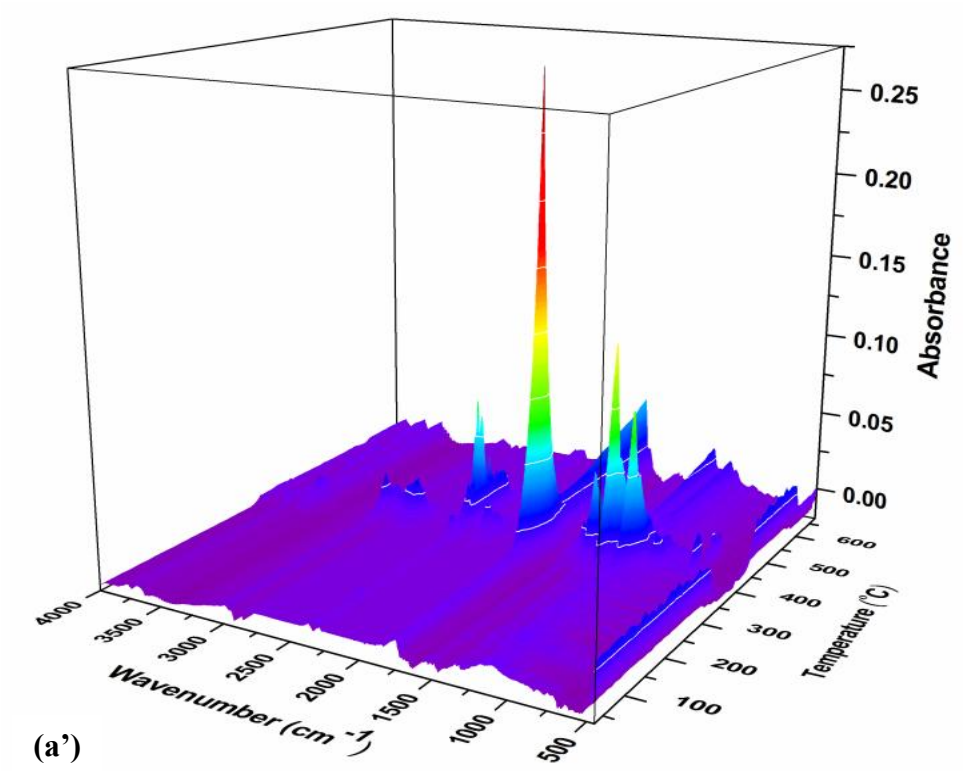

(a')

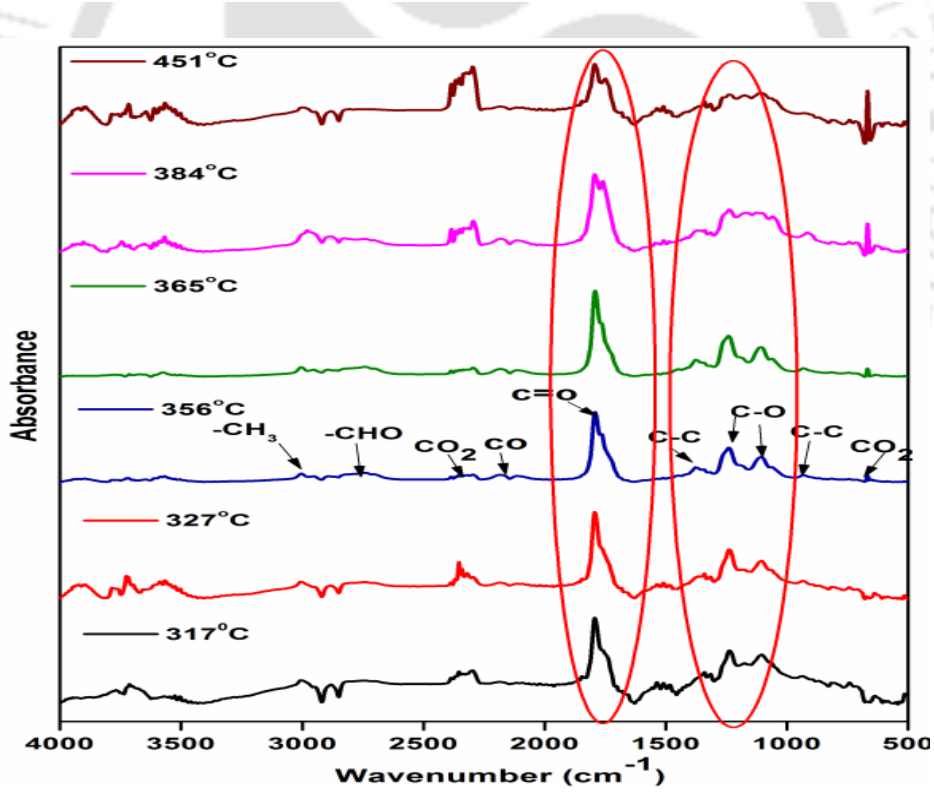

(b')

Figure 7.9: *3D-FTIR spectrogram (a), (a'), 2D stack plot (b), (b') with the enlarged image around (1650-1950 cm^{-1}) (c), (1500-1000 cm^{-1}) (d) for the characterstics spectra of the volatile species emitted from PLA/PBS blend and their reactive bionanocomposite film.*

- ***Rheological behaviour for reactively extruded PLA/PBS/FCH bionanocomposite films***

Rheological analysis can ascribe a detail structural characteristic relationship of polymer and their bionanocomposite films. Therefore, the influence of *F*CH along with and without DCP content on the complex viscosity (η*) of PLA/PBS system was studied. The η* of PLA/PBS blend, PLA/PBS/*F*CH bionanocomposite films with and without DCP at 190°C as a function of angular frequency (ω) are displayed in Figure 7.10 (a). It is noticed that PLA/PBS, PLA/PBS/1*F*CH, and PLA/PBS/3*F*CH shows the similar trend with the pseudo-Newtonian behaviour whereas the shear thinning started at higher ω region (≥10 rad/s). Such phenomenon is generally observed in polymer melts and the main reason is the reduction in entanglement density of the polymeric chains with the gradual increase in the value of ω. In addition, the average end to end gaps of polymeric chain segments extend at high ω region. Beyond 10 rad/s, a shear thinning behaviour of PLA/PBS blend leads to lower η* as compared to PLA/PBS/*F*CH based bionanocomposite films. After the addition of 3 wt % *F*CH into PLA/PBS blend, η* is slightly lower than that of PLA/PBS/1*F*CH which shows shear thinning effect due to the aggregation of *F*CH. With the addition of DCP into PLA/PBS/1*F*CH, a remarkable enhancement in η* and shear thinning behaviour is observed, especially in the low ω region due to the formation of the interconnected network of polymeric segments and nano fillers. For PLA/PBS/D/1*F*CH, η* is improved significantly, taking the ω at 0.1 rad s^{-1} as a reference point, when compared with the PLA/PBS blend. Hence it is noteworthy to mention when DCP is added in PLA/PBS/1*F*CH, there is possibility of PLA (presence of free radicals on tertiary C atoms) and PBS (easier abstraction of secondary hydrogen atom as compared to PLA) crosslinking, which subsequently leads to the long chain branching, apart from free radicals generated on OLLA chains attached to *F*CH that may also make significant interactions with PLA and PBS segments. This significant enhancement in η* can be related to develop long chain branching/ crosslinking

sites. It would produce more complex system in presence of DCP. Due to the appearance of long chain branching/crosslinking sites, polymeric segments become more connected which further restricts the mobility of individual macromolecular chains by forming more entangled structures under shear force and finally change in flow behaviour is found **(He et al. 2014; Huang et al. 2013)**.

Similar to the η*, loss (G″) and storage (G′) modulus of all samples is also displayed the same trend where G″ and G′ denotes the viscous region and elastic region of the melt respectively. Both G′ and G″ versus ω for PLA/PBS blend and their bionanocomposite films (without DCP) is increased gradually with increasing ω, introducing terminal behaviour, as presented in Figure 7.10 (b) – (c), respectively. Also for all samples, the dominance of G″ over G′ at lower ω, suggests that the polymeric composite are liquid like **(Tesfaye et al., 2017)**. Meanwhile, the rise in G′ is emphasized, mainly at the low ω region for PLA/PBS/D/1*F*CH which could be ascribed to the formation of some crosslinked/branched chains as well as the increased chain entanglement **(Tesfaye et al., 2017)**. Moreover η, G′ and G″ have been significantly dropped which suggest the chain dissociation by shear during the melt extrusion of PLA/PBS/D/3*F*CH. The possible reason is decrement in crosslinking efficiency which enhances the chain dissociation of the polymeric system due to presence of *F*CH (3 wt %) at higher content. This result is consistent with GPC and % gel yield data shown in the previous chapter 6.

A logarithmic plot of real viscosity (η′ = G″/ω) versus imaginary viscosity (η″= G′/ω) is usually known as Cole-Cole plot to investigate the viscoelastic characteristics of the PLA/PBS, PLA/PBS/*F*CH in presence or absence of DCP with relaxation time distribution. It noticed that the two-phase structures in case of PLA/PBS blend, are mentioned in Figure 7.11 (a). When the phase separation occurs in PLA/PBS, a second semicircle found in the right side of the arc which confirms that the second relaxation mechanism happened at the melt

stage **(Zhang et al., 2013)**. PLA/PBS blend and PLA/PBS/*F*CH bionanocomposite films without DCP follow the similar kind of relaxation mechanism. It is found that the arc of semicircle becomes broad with the incorporation of DCP in PLA/PBS/1*F*CH bionanocomposite film which confirms that the complex structures such as branching, crosslinking and copolymers are formed without phase separation **(Tesfaye et al., 2017)**. All of these observations further inform that the melt strength of the PLA/PBS/1*F*CH system is enhanced due to presence of DCP. It is noteworthy to mention that DCP modified PLA/PBS/1*F*CH plays a vital role to produce significant rheological characteristics. For all the samples, Han plots (log–log graph of G′ against G″) are displayed in Figure 7.11 (b). Further, the diagonal line (corresponding to G′ is equal to G″) divides the plot into two portions and presented the phase transition from the viscous (when G′ < G″) to elastic (G′ > G″) response. Comparing with PLA/PBS blend, the curve of PLA/PBS/1*F*CH positioned at lower from the diagonal line over the entire range which confirms that the elastic contribution becomes smaller and further shows the decrease in elasticity of polymeric composite in melt system. With the DCP modified PLA/PBS/1*F*CH, the curve has to reach the diagonal line progressively and informs the higher elasticity of melt. The curve is passed across the diagonal, presuming the crosslinked/branched structure rather than the chain extension and showed more solid-like response **(Cai et al., 2017; Zhang et al., 2016)**. As expected, the addition of DCP with *F*CH into PLA/PBS decreased the value of the slope, as mentioned in Table 7.4. This shows that the topological structure of the polymeric melt is strongly affected at the transition point; the possible reason behind which is the formation of branched and crosslinked structure **(Zhang et al., 2016)**.

To further study the topological structure of PLA/PBS blend and their composites, Van Gurp Palmen (phase angle as a function of log G*) plot has been depicted in Figure 7.11 (c) which shows that the phase angle decreases with the DCP modified PLA/PBS/1*F*CH in comparison

of PLA/PBS blend and their bionanocomposite films. It could be due to the development of nonlinear as well as long-chain branched/crosslinked structures that limit the mobility of macromolecule.

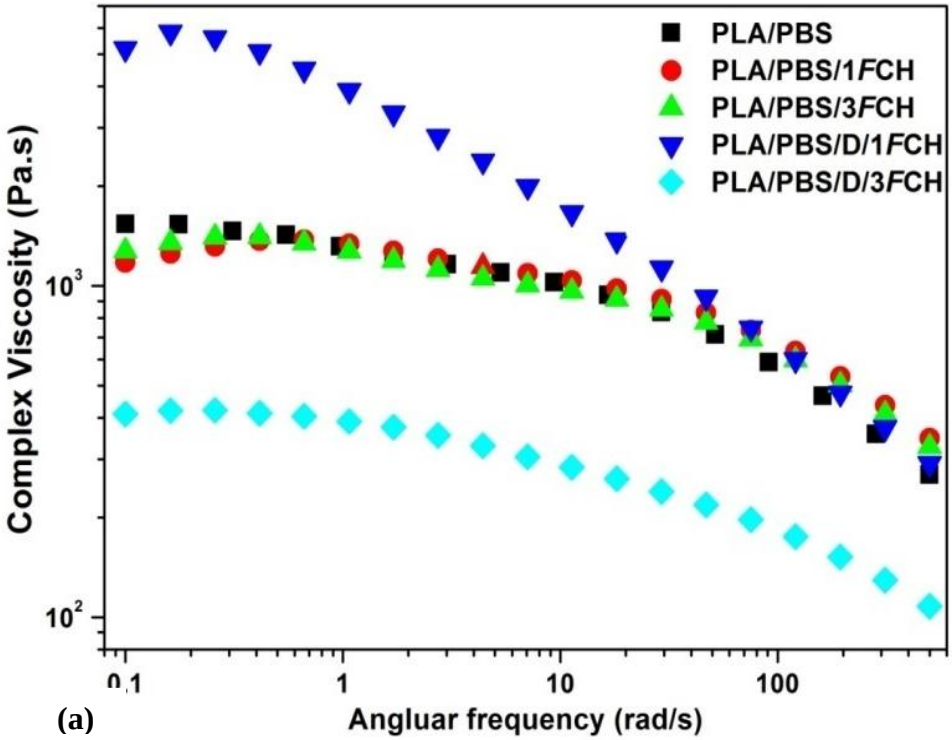

(a)

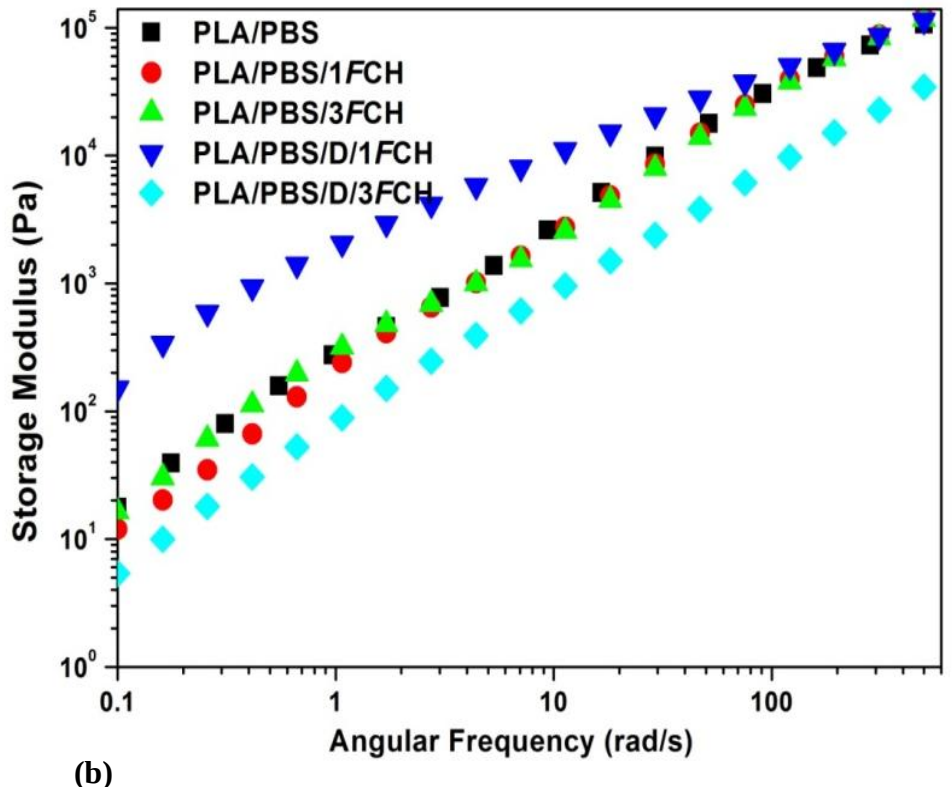

(b)

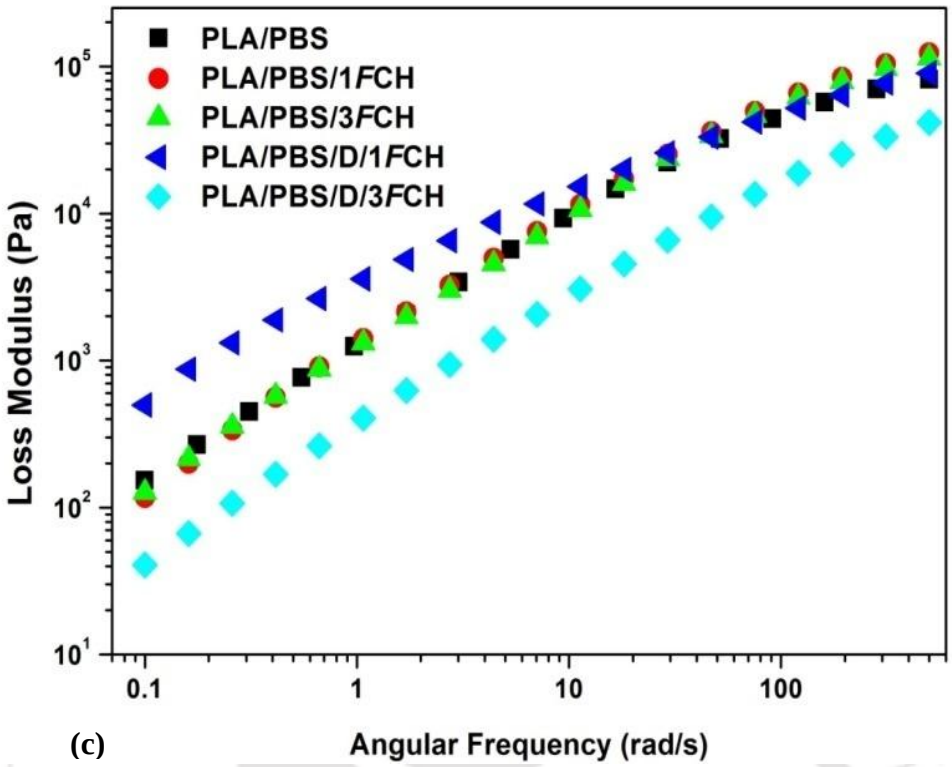

Figure 7.10: *Influence of modified macromolecular chains modifications on the complex viscosity (Pa.s) vs angular frequency (rad s^{-1}) (a), storage modulus (Pa) vs angular frequency (rad s^{-1}) (b), loss modulus (Pa) vs angular frequency (rad s^{-1}) (c) for PLA/PBS blend, PLA/PBS/FCH with and without DCP.*

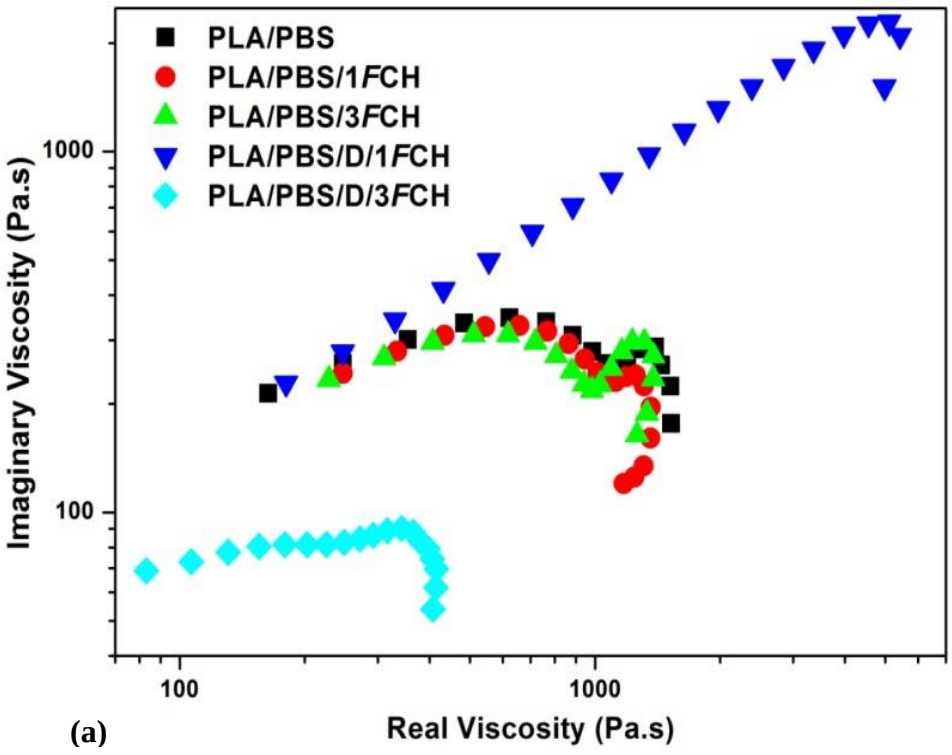

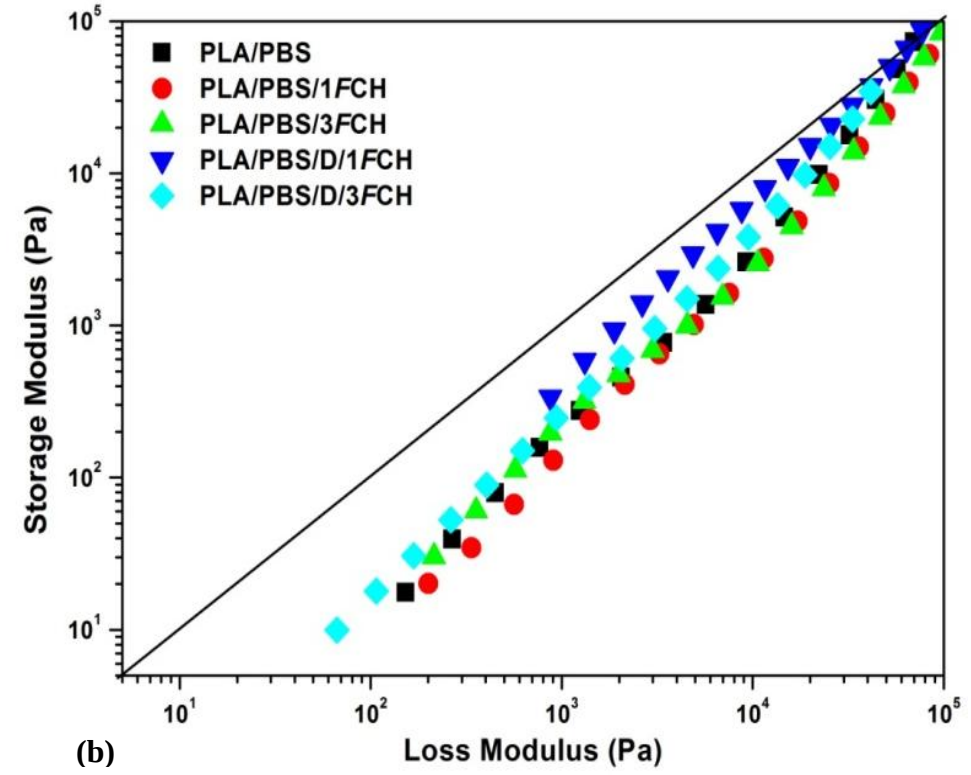

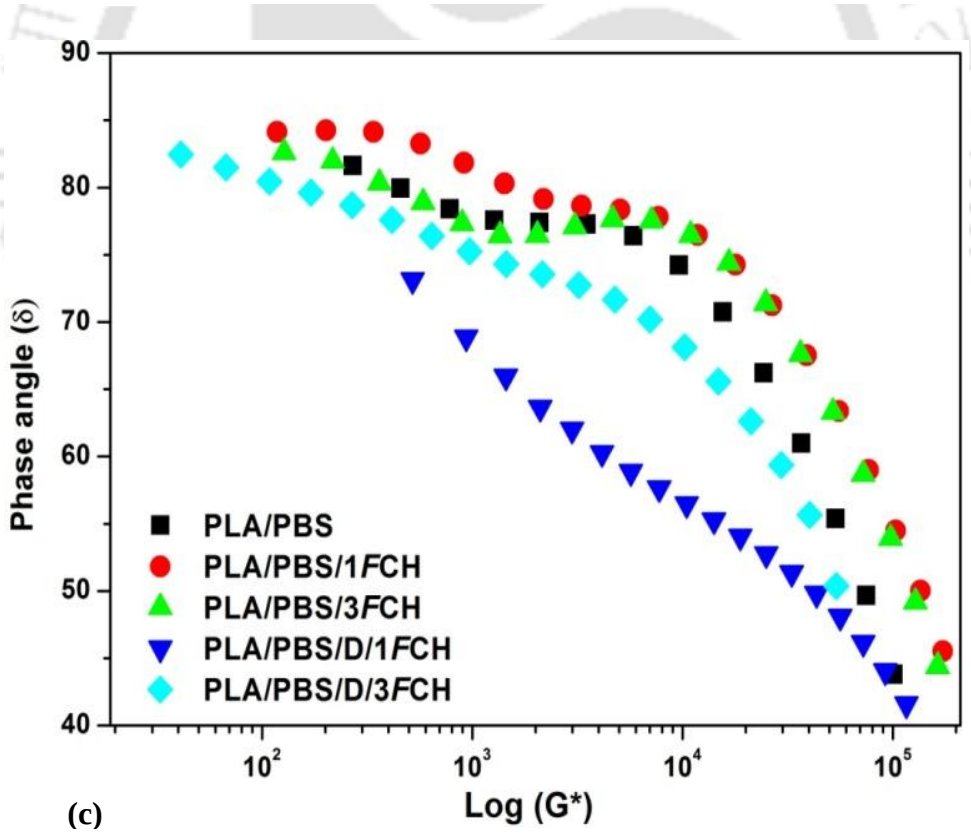

Figure 7.11: *Imaginary viscosity (Pa.s) vs real viscosity (Pa.s) as Cole –Cole Plot (a), storage modulus vs loss modulus as Han Plot (b), Phase angle vs complex modulus as Van-Grup plot(c) for PLA/PBS blend, PLA/PBS/FCH with and without DCP.*

- ***Shear behaviour for reactively extruded PLA/PBS/FCH based bionanocomposite films***

At a given shear rate ($5s^{-1}$), the shear viscosity (η_τ) can be obtained as a function of time (t) to understand how the η_τ of system changes with 't' due to the applied shear under the given processing conditions. Shear rheological behaviors of PLA/PBS blend, PLA/PBS/*F*CH bionanocomposite films with and without addition of DCP are displayed in Figure 7.12. It is found that η_τ decreases with 't' under the applied shear rate. At 5 s^{-1} shear rate, η_τ of PLA/PBS/*F*CH (1 and 3 wt%) are lower than those of PLA/PBS blend and decrease considerably with increasing *F*CH content due to the degrading character of the *F*CH. For DCP treated PLA/PBS/1*F*CH content, the value of η_τ is the highest in the entire range of t, as compared to PLA/PBS blend. This can be explained due to the presence of branched/crosslinked structure, where the polymeric system does not experience the degradation. Further, η_τ is reduced as function of t for PLA/PBS/D/3*F*CH due to the breakdown of polymeric system, as compared to PLA/PBS/D/1*F*CH bionanocomposite films.

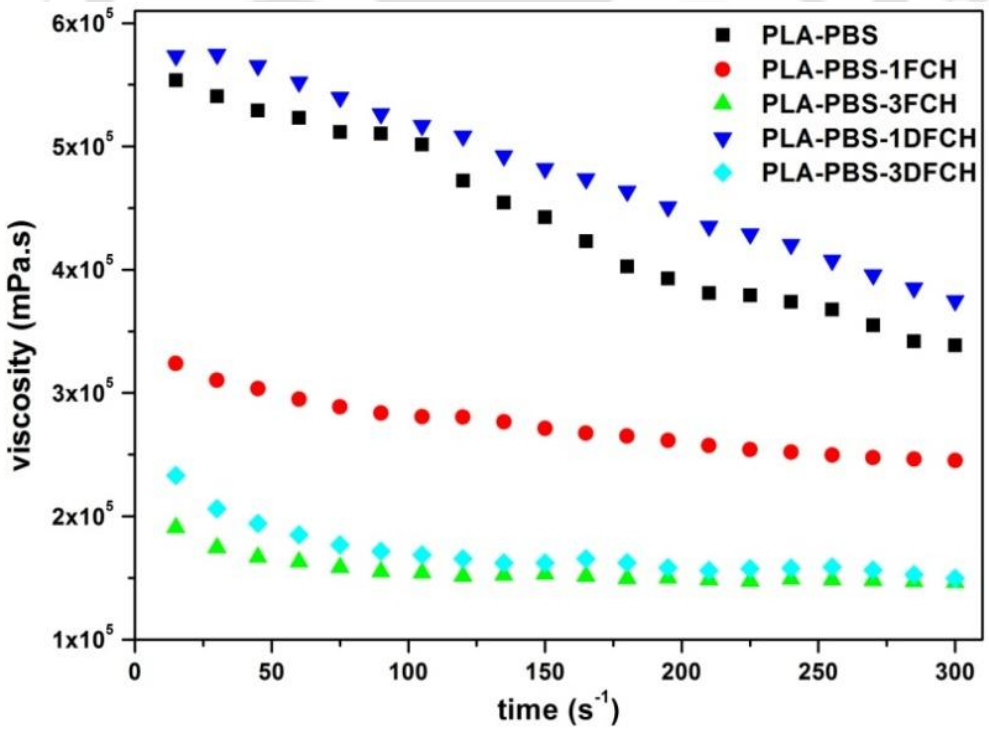

Figure 7.12: *Viscosity versus time graph for PLA/PBS blend, PLA/PBS/FCH and their reactive bionanocomposite films.*

7.3 CONCLUSIONS

This work reports the effect of *F*CH on PLA/PBS blends with or without DCP using TGA, TGA-FTIR and melt rheology analysis. TGA data shows that the thermal stability is slightly improved after the incorporation of 1 wt% *F*CH along with DCP in PLA/PBS blend at T_{max}. This is probably due to the development of crosslinking/branching sites in comparison to PLA/PBS/*F*CH bionanocomposite but merely affected as compared to PLA/PBS blend. Also, non-isothermal TGA kinetics results show that apparent E_a is highest in case of PLA/PBS/D/1*F*CH bionanocomposite. Based on the generalized mechanism plots, L2 D3 mechanism proposed for DCP treated PLA/PBS/*F*CH based nanocomposites. Thermal release investigations performed by hyphenated TGA–FTIR analysis indicates that the similar kinds of major volatile products are released such as lactide, acetaldehyde, cyclic oligomer, CO_2, CO for PLA/PBS blend and their bionanocomposite films. The rheological study indicates that the PLA/PBS/D/1*F*CH has shear thinning behavior which subsequently leads to the formation of interconnected networks of polymeric segments with *F*CH

Table 7.4: *Influence of FCH with and without DCP content on Han plot of PLA/PBS based bionanocomposite films.*

Samples	**PLA/ PBS**	**PLA/PBS/ 1*F*CH**	**PLA/PBS/ 3*F*CH**	**PLA/PBS/ D/1*F*CH**	**PLA/PBS/ D/3FCH**
Slope (R^2)	1.378 (0.987)	1.361 (0.993)	1.316 (0.995)	1.229 (0.999)	1.231 (0.998)

Chapter 8

Conclusions and Future Scope

This chapter summarizes the major key finding and conclusion drawn from the research work, and provides the future directive of the research on the thermally stably bionanocomposite film.

8.1 CONCLUSIONS

Melt processing of bio-based aliphatic polyesters with bio-fillers such as cellulose nano crystal, chitosan and gum arabic are a challenging task due to shear induced and thermal decomposition at elevated temperature, which limit the application of these bionanocomposite films for development of value added product at industrial scale. It is necessary to investigate how molten polymer is processed without serious thermal decomposition at specific temperature in presence of bio-filler. The knowledge of the thermal degradation kinetic of polymeric sample is required to obtain the relevant triplet kinetic parameters (E_a, A and n). This analysis is useful to understand the decomposition mechanism. Therefore, these parameters assist to estimate the service life of product at specific temperature as well as establishment of processing parameters. The detailed thermal degradation study may assist to choose the appropriate bionanocomposite for packaging applications. From the present research, it can be concluded that all the fillers used in the investigation are compatible with the PLA based system.

The key achievements reported in this regard are:

A remarkable improvement in the thermal stability as well as apparent value of activation energy in case of nitric acid hydrolysed CNC based PLA bionanocomposite (i), and reactive extrusion permits straightforward, feasible biocomposite and has great potential as a modification with DCP assists to overcome particular drawbacks of biofiller to modify structural and physiochemical properties belong to packaging application (ii). The conclusions drawn from the research work are summarized next:

- TGA study reveals that the HNO_3 derived CNC has strong interaction with the PLA matrix, which enhances it thermal stability. The E_a is the highest for PLA-HNO_3-CNC nanocomposite due to which more energy is required to break the stable C-N bond. This finding confirms that the PLA-HNO_3-CNC nanocomposite is the most suitable to be used as nano-filler since it controls the thermal decomposition of PLA matrix and the small release of volatile products such as CO_2, CO and aldehydes containing compound.
- DCP treated PLA/*F*G shows the improved interfacial interaction, elongation at break (~28%), UV–C blocking effect (~95%) and hydrophobicity (~14%). Thermal stability is also significantly improved for DCP treated PLA/1*F*G than that of PLA/*F*G. Therefore, this result confirms that the chemical modification using DCP, which leads to the tailored properties of the bionanocomposite films and enhance the utility of PLA/*F*G based bionanocomposite through an industrial viable twin screw extrusion technique.
- Melt blending of polymers is an economic and effective approach of achieving new materials with desired properties. However, the toughness improvement achieved in PLA/PBS blend is usually accompanied by the decrease in tensile modulus and tensile strength. This work successfully implements the peroxide initiating reaction in the melt along with FCH, to generate crosslinked/branched structure with PLA/PBS copolymer having a balanced set of mechanical properties, processibility, melt strength as well as

improvised crystallization efficiency. Also, the remarkable UV-C blocking effect of the reactive modified bionanocomposite may suggest possible application towards packaging of UV sensitive materials. In brief, DCP treated PLA/PBS/FCH bionanocomposite shows improvement in the processibility, melt strength and adequate physicochemical properties which confirm its applicability toward the packaging application without experiencing serious decomposition during extrusion.

8.2 FUTURE DIRECTIVE OF THE RESEARCH

Based on the findings of thesis work, it can be extended further. Some recommendations for future research have been summarized as follows:

- For food packaging application, oxygen permeability test should be examined for all film samples.
- Investigation in the direction of thermal recycling of the fabricated films.
- Thermo gravimetric analyzer coupled with Mass or Gas chromatography (GC-MS) spectroscopy to investigate the release of volatile components in presence of filler and finally establish the mechanism.
- Combined effect of dicumyl peroxide along with maleic anhydride may be effective approach to tailored properties of PLA nanobiocomposites.
- Influence of other free radical initiators such as benzyl peroxide (BPO) and chain extenders such as Joncryl chain extender on the thermal properties of PLA nanobiocomposite can be investigated.
- Extensional rheology work should be performed in future.

REFERENCES

Aboulkas et al. **2008**, Study of the kinetics and mechanism of thermal decomposition of Moroccan tarfaya oil shale and its kerogen, *Oil Shale*, 25, 426-443.

Adlim et al. **2015**, Chitosan based chemical sensors for determination of mercury in water: a review, AACL. *Bioflux*, 8, 665-666.

Aguirre et al. **2016**, Poly (lactic acid) - mass production, processing, industrial applications, and end of life, *Advanced Drug Delivery System*, 107, 333-366.

Al-Itry et al. **2012**, Improvement of thermal stability, rheological and mechanical properties of PLA, PBAT and their blends by reactive extrusion with functionalized epoxy, *Polymer Degradation and Stability*, 97, 1898-1914

Ali et al. **2010**, Gum arabic as a novel edible coating for enhancing shelf life and improving postharvest quality of tomato (Solanum lycopersicum L.) fruit, *Postharvest Biology and Technology*, 58, 42–47.

Ambrosio et al. **2014**, An effect of lactic acid oligomers on the barrier properties of polylactide, *Journal of Materials Science*, 49, 2975-2986.

Aoyagi et al. **2002**, Thermal degradation of poly [(R)-3-hydroxybutyrate], poly [ε-caprolactone], and poly [(S)-lactide], *Polymer Degradation and Stability*, 76, 53-59.

Ali et al. **2009**, Biological effects of gum Arabic: A review of some recent research, *Food and Chemical Toxicology*, 47, 1-8.

Arrieta et al. **2014**, Multifunctional PLA–PHB/cellulose nanocrystal films: Processing, structural and thermal properties. *Carbohydrate Polymer*, 107, 16-24.

Auras et al. **200**4, An overview of polylactide as packaging materials, *Macromolecular Bioscience*, 4, 835-864.

Auras et al. **2010**, Poly (lactic acid): synthesis, structure, properties, processing, and applications. John Wiley & Sons, Inc., New Jersy.

Badia et al. **2010**, Thermal analysis applied to the characterization of degradation in soil of polylactide: II. On the thermal stability and thermal decomposition kinetics, *Polymer Degradation and Stability*, 95, 2192-2199.

Bahari et al. **1998**, Radiation crosslinked poly(butylene succinate) foam and its biodegradation, *Polymer Degradation and Stability*, 62, 551-557.

Bai et al. **2014**, Studies on crystallization kinetics of bimodal long chain branched polylactides, *Cryst Eng Comm*, 16, 2452-2461.

Baloch et al. **2011**, Methods for the thermogravimetric analysis of polyethylene samples, *Journal of Applied Polymer Science*, 120, 3511-3518.

Balau et al. **2004**, Physico-chemical properties of chitosan films, *Central European Journal of Chemistry*, 2, 638-647.

Barun et al. **2012**, Supra-molecular ecobionanocomposites based on polylactide and cellulose nanwhiskers: synthesis and properties, *Biomacromolecules*, 13, 2013-2019.

Bhasney et al. **2017**, Plasticizing effect of coconut oil on morphological, mechanical, thermal, rheological, barrier, and optical properties of poly(lactic acid): A promising candidate for food packaging, *Journal of Applied Polymer Science*, 134, 1-12.

Bhatia et al. **2017**, Compatibility of biodegradable poly (lactic acid) (PLA) and poly

(butylene succinate) (PBS) blends for packaging application, *Korean-Australiz Rheology Journal*, 19, 125-131.

Bher et al. **2018**, Improving the toughening in poly (lactic acid)-thermoplastic cassava starch reactive blends, *Journal of Applied Polymer Science*, 46140, 1-15.

Bondeson et al. **2017**, Dispersion and characteristics of surfactant modified cellulose whisker nanocomposite, *Composite Interface*, 14, 617-630.

Bonilla et al. **2013**, Effects of chitosan on the physicochemical and antimicrobial properties of PLA films, *Journal of Food Engineering*, 119, 236-243.

Borkotoky et al. **2018**, Thermal degradation behaviour and crystallization kinetics of poly (lactic acid) and cellulose nanocrystals based microcellular composite foams, *International Journal of Biological Macromolecules*, 118, 1518-1531.

Bourmaud et al. **2016**, Recycling of L-poly-(lactide)-poly-(butylene-succinate)-flax biocomposite, *Polymer Degradation and Stability*, 128, 77-88.

Brigham et al. **2012**, Applications of poly (hydroxyalkanoates) in the medical industry, *International Journal of Biotechnology for Wellness Industries*, 1, 53-60.

Broido et al. **1969**, A simple, sensitive graphical method of treating thermogravimetric analysis data, *Journal of Polymer Science: Part A*, 7, 1761-1773.

Brydson et al. **1999**, The historical development of plastics materials, in plastic materials (seventh edition), Butterworth-Heinemann: Oxford, 1-18.

Budrugeac et al. **2000**, The evaluation of the non-isothermal kinetic parameters of the thermal and thermo-oxidative degradation of polymers and polymeric materials: its use and

abuse, *Polymer Degradation and Stability*, 71, 185-187.

Cai et al. **2017**, The flame retardancy and rheological properties of PA6/MCA modified by DOPO-based chain extender, *RSC Advance*, 7, 19593-19603.

Cao et al. **2017**, Effects of the chain extender content on the structure and performance of poly (lactic acid)/poly (butylene succinate)/-microcrystalline cellulose composite, *Journal of Applied Polymer Science*, 44895, 1-8.

Carrasco et al. **2010**, Processing of poly (lactic acid): characterization of chemical structure, thermal stability and mechanical properties, *Polymer Degradation and Stability*, 95, 116-125.

Carrasco et al. **2013**, Enhanced general analytical equation for the kinetics of the thermal degradation of Poly (lactic acid) driven by random scission, *Polymer Testing*, 32, 937-945.

Carrasco et al. **2014**, Enhanced general analytical equation for the kinetics of the thermal degradation of poly(lactic acid)/montmorillonite nanocomposite driven by random scission, *Polymer Degradation and Stability*, 10, 52-59.

Chaiwutthinan et al. **2015**, Biodegradable plastics prepared from poly(lactic acid), poly(butylene succinate) and microcrystalline cellulose extracted from waste-cotton fabric with a chain extender, *Journal of the Polymer and Environment*, 23, 114-125.

Chen et al. **2007**, Isothermal crystallization kinetics and thermal behaviour of poly (ε-caprolactone)/multi-walled carbon nanotube composite, *Polymer Degradation and Stabilty*, 92, 1009-1015.

Chen et al. **2012**, Thermal degradation characteristics of flame retardant polylactide using

TG-IR, *Polymer Degradation and Stability*, 97, 2143-2147.

Chen et al. **2014**, Bioplastics and their role in achieving global sustainability. *Journal of Chemical and Pharmaceutical Research*, 6, 226-231.

Cherykhunthod et al. **2015**, Effect of peroxide and chain extender on mechanical properties and morphology of poly (butylenes succinate)/poly (lactic acid) blends, *IOP: Conference Series*: *Material Science Engineering*, 87, No.012073.

Cheung et al. **2015**, Chitosan: An update on potential biomedical and pharmaceutical applications, *Marine Drugs*, 13, 5156-5186.

Chianga et al. **2011**, Effect of layered double hydroxides on the thermal degradation behaviour of biodegradable poly (L-lactide) nanocomposite, *Polymer Degradation and Stability*, 96, 60-66.

Chrissafis et al. **2011**, Detail kinetic analysis of the thermal decomposition of PLA with oxidized multi-walled carbon nanotubes, *Thermochimic Acta*, 511, 163-167.

Chrissafis et al. **2012**, Effect of different nanoparticles on thermal decomposition of poly (propylene sebacate) nanocomposites: Evaluation of mechanism using TGA and TG-FTIR-GC/MS, *Journal of Analytical and Applied Pyrolysis*, 96, 92-99.

Chuayjuljit et al. **2017**, Biodegradable poly (lactic acid)/poly (butylene succinate)/wood flour composites: physical and morphological properties, *Polymer Composite*, 38, 2841-2851.

Coats et al. **1964**, Kinetic parameters from Thermogravimetric data, *Nature*, 201, 68-69.

Coles et al. **2011**, Bioplastics, Food and Beverage Technology: Second edition Wiley.

Corre et al. **2011**, Melt strengthening of poly (lactic acid) through reactive extrusion with epoxy functionalized chain, *Rheological Acta*, 50, 613-629.

Criado et al. **1989**, Applicability of the master plots in kinetic analysis of non-isothermal data, *Thermochimica Acta*, 147,377–385.

Carrasco et al. **2017**, Thermal degradation of poly (lactic acid) and acrlonitrile-butadine-styrene bioblends: Elucidation of reaction mechanism, *Thermochimica Acta*, 654, 157-167.

Dai et al. **2013**, Study on thermal degradation kinetics of cellulose grafted poly (L-lactic acid) by thermogravimetric analysis, *Polymer Degradation and Stability*, 99, 233-239.

Das et al. **2017**, Thermal degradation kinetics of plastic and model selection, *Thermochimica Acta*, 654, 191-202

Dhar et al **2014,** Thermal degradation kinetics of poly (3-hydroxybutyrate)/cellulose nanocrystals based nanobiocomposite, *Journal Thermodynamic Catalyst*,5, 1-7.

Dhar et al. **2015**, Effect of cellulose nanocrystals polymorphs on mechanical, barrier and thermal properties of poly (lactic acid) based bionanocomposites, *RSC Advances*, 60426-60440.

Dhar et al. **2016**, Thermally recyclable poly (lactic acid)/ cellulose nanocrystals films through reactive extrusion, *Polymer*, 87, 268-282.

Dhar et al. **2016**, Acid functionalized cellulose nanocrystals and its effect on mechanical, thermal, crystallization and surface properties of poly (lactic acid) bionanocomposite films: a comprehensive study, *Polymer*, 101, 75-92.

Don et al. **2010**, Preparation and properties of blends from poly (3-hydroxybutyrate) with poly (vinyl acetate)-modified starch, *Polymer Engineer Science*, 50, 709-718.

Doyle et al. **1962**, Estimating isothermal life from thermogravimetric data, *Journal of Applied Polymer Science*, 6, 639-642.

Drumright et al. **2000**, Polylactic acid Technology, *Advanced Materials*, 12, 1841-1846.

Elsawy et al. **2017**, Hydrolytic degradation of polylactic acid and its composites, *Renewable and sustainable energy reviews*, 79, 1346-1352.

Elsabee et al. **2013**, Chitosan based edible films and coatings: A review, *Material science and engineering C*, 33, 1819-1841.

Emadian et al. **2017**, Biodegradation of bioplastics in natural environment, *Waste Management*, 59, 526-536.

Eng et al. **2013**, Enhancement of mechanical and thermal properties of Polylactic acid/polycaprolactone blends by hydrophilic nanoclay, *Indian Journal of Material Science*, 2013, 1-11.

Espinosa et al. **2013**, Isolation of thermally stable cellulose nanocrystals with phosphoric acid hydrolysis, *Biomacromolecules*, 14, 122-1230.

Espinosa bioplastics **2012**, Driving the evolution of bio-plastics, http://en.european-bioplastics.org/wp-content/uploads/2012/publications/image brouchers_Dec 2012.pdf.

Fan et al. **2004**, Thermal degradation behaviour of poly (lactic acid) stereocomplex, *Polymer Degradation and Stability*, 86, 197-208.

Fischer et al. **1987**, Obtaining the kinetic parameters from thermogravimetry using a modified

coat and redfern technique, 26, 1037-1040.

Filson et al. **2009**, Sono-chemical preparation of cellulose nanocrystals from lignocelluloses derived materials, *Bioresource Technology*, 100, 2259–2264.

Filson et al. **2009** Enzymatic-mediated production of cellulose nanocrystals from recycled pulp, *Green Chemistry*, 11, 1808–1814.

Fitaroni et al. **2015**, Thermal stability of propylene-montmorillonite clay nanocomposites: limitation of the thermogravimetric analysis, *Polymer Degradation and Stability*, 111,102-108.

Flynn et al. **1983**, The isoconversional method for determination of energy of activation at constant heating rates, *Journal of Thermal Analysis*, 27, 95-102.

Foutunati et al. **2013**, Combined effects of cellulose nanocrystals and silver nanoparticles on the barrier and migration properties of PLA nanobiocomposites, *Journal of Food Engineering*, 118, 117–124.

Friedman et al. **1964**, Kinetics of thermal degradation of char-forming plastics from thermogravimetry-Application to a phenolic plastic, *Journal of Polymer Science Part C: Polymer Symposia Banner*, 6, 183-195.

Freeman et al. **1958**, The application of thermo analytical techniques to reaction kinetics: the thermogravimetric evaluation of the kinetics of the decomposition of calcium oxalate monohydrate, *Journal of Physical Chemistry*, 62, 394-397.

George et al. **2015**, Cellulose nanocrystals: synthesis, functional properties, and applications, *Nanotechnology Science and Application*, 8, 45–54.

Girdthep et al. **2014**, Biodegradable nanocomposite blown films based on poly(lactic acid)

containing silver-loaded kaolinite: a route to controlling moisture barrier property and silver ion release with a prediction of extended shelf life of dried longan. *Polymer*, 55, 6776-6788.

Goffin et al. **2011**, From interfacial ring opening polymerization to melt processing of cellulose nanowhisker-filled polylactide based nanocomposites, *Biomacromolecules*, 12, 2456-2465.

Gonc et al. **2014**, Thermal behaviour of cashew gum by simultaneous TG/DTG/DSC–FTIR and EDXRF, *Journal of Thermal Analysis and Calorimetry*, 111, 1509-1514.

Gotor et al. **2000**, Kinetic analysis of solid-state reactions: The University of Master plots for analyzing isothermal and non-isothermal experiments, *Journal of Physical Chemistry A*, 104, 10777–10782.

Gurunathan et al. **2015**, A review of the recent developments in biocomposite based on natural fibres and their application perspectives. *Compost Part A: Applied Science and Manufacturing*, 77, 1-25.

Gu et al. **2008**, Melt rheology of polylactide/poly (butylene adipate-co-terephthalate) blends. *Carbohydrate Polymer*, 74, 79-85.

Gu et al. **2012**, The effect of PP and peroxide on the properties and morphology of HDPE and HDPE/PP blends, *Advances in Polymer Technology*, 21326, 1–9.

Habibi et al. **2018**, Bionanocomposites based on poly (ε-caprolactone)-grafted cellulose nanocrystals by ring-opening polymerization, *Journal of Material Chemistry*, 18, 5002-5010.

Habibi et al. **2010**, Cellulose nanocrystals: chemistry, self-assembly, and applications,

Chemical Reviews, 110, 3479-3500.

Hamad et al. **2015**, Properties and medical applications of poly (lactic acid): A review, *eExpress Polymer Letters*, 9, 435-455.

Harada et al. **2007**, Increased impact strength of biodegradable poly (lactic acid)/poly (butylene succinate) blend composites by using isocyanate as a reactive processing agent, *Journal of Applied Polymer Science*, 106, 1813-1820.

He et al. **2014**, Super-tough poly (L-lactide)/crosslinked polyurethane blends with tunable impact toughness, *RSC Advances*, 4, 12857-12866

Henrique et al. **2015**, Kinetic study of thermal decomposition of cellulose nanocrystals with different polymorphs, cellulose I and II, extracted from different sources and using different type of acids, *Industrial Crops and Products*, 76, 128-140.

Horowitz et al. **1963**, A new analysis of TGA traces, *Analytical Chemistry*, 35, 1464-1468.

Hsieh et al. **2013**, Lamellar assembly and orientation induced internal micro voids by cross sectional dissection of poly (ethylene oxide)/poly (L lactic acid) blend, *eXPRESS Polymer Letters*, 7, 396–405.

Huang et al. **2012**, Thermal properties and thermal degradation of cellulose tri-stearate (CTs), *Polymers*, 4, 1012-1024.

Huang et al. **2015**, Thermal degradation of poly (lactide-co-propylene carbonate) measured by TG/FTIR and py GC-MS, *Polymer Degradation and Stability*, 117, 16-21.

Huang et al. **2017**, Study on the effect of dicumyl peroxide on structure and properties of poly (lactic acid)/natural rubber blend, *Journal of Polymers and the Environment*, 21, 375–387.

Formela et al. **2018**, Reactive extrusion of bio-based polymer blends and composite-current trends and future devlopments, *Express Polymer Lett*er, 12, 24-57.

Frone et al. **2013**, Morphology and thermal properties of PLA-cellulose nanofibers composites, *Carbohydrate Polymer*, 91, 377-384.

Imre et. al. **2013**, Compatibilization in bio-based and biodegradable polymer blends, *European Polymer Journal*, 49, 1215-1233.

Ishak et al. **2013**, Reactive processing of maleic anhydride-grafted poly(butylene succinate) and the compatibilizing effect on poly(butylene succinate) nanocomposites, *Express Polymer Letter*,7, 340-354.

Jayakumar et al. **2010**, Biomedical applications of chitin and chitosan based nanomaterials-A short review, *Carbohydrate Polymers*, 82, 227-232.

Jambeck et al. **2015**, Plastic waste inputs from the land into the ocean, *Science*, 347, 768-771.

Jamshidian et al. **2010**, Poly-lactic acid: production, applications, nanocomposites and release studies, *Comprehensive Reviews in Food Science and Food safety*, 9, 552-571.

Jiang et al. **2006**, Study of biodegradable polylactide/poly (butylene adipate-co-terephthalate) blends, *Biomacromolecules*, 7, 199-207.

Jia et al. **2017**, Morphology, crystallization and thermal behaviors of PLA based composites: wonderful effects of hybrid GO/PEG via dynamic impregnating, *Polymers*, 9, 1-18.

Jaratrokamjorn et al. **2011**, Toughness enhancement of poly (lactic acid) by melt blending with natural rubber, *Journal of Applied Polymer Science*, 124, 5027-5036.

Jonoobi et al. **2012**, Comparison of modified and unmodified cellulose nanofiber reinforced

polylactic acid (PLA) prepared by twin screw extrusion, *Journal of Polymer and the Environment*, 20, 991-997.

Ji et al. **2012**, Study on the crystallization behaviour of PLA/PBS/DCP reactive blends, *Acta Polymerica Sinica*, 7, 694-697.

Ji et al. **2014**, Morphology, rheology, crystallization behaviour and mechanical properties of poly(lactic acid)/poly (butylenes succinate)/dicumyl peroxide reactive blends, *Journal of Applied Polymer Science*, 131, 1-8.

Jung et al. **2018**, Polymer identification of plastic debris ingested by pelagic-phase sea turtles in the central pacific, *Environmental Science and Technology*, 52, 11535-11544.

Juntuek et al. **2011**, Thermal, morphological and mechanical properties of biobased and biodegradable blends of poly(lactic acid) and chemically modified thermoplastic starch, *Polymer Engineering Science*, 51, 826-834.

Kamal et al. **2015**, Effect of cellulose nanocrystals (CNC) on rheological and mechanical properties and crystallization behaviour of PLA/CNC nanocomposite, *Carbohydrate Polymer*, 123, 105-114.

Kameno et al. **2016**, Thermal degradation of poly (lactic acid) oligomers reaction mechanism and multistep kinetic behaviour, *Polymer Degradation and Stability*, 134, 284-295.

Kangwanwatthanasiri et al. **2013**, Biocomposites from cassava pulp/poly (lactic acid)/poly (butyene succinate), *Advance Materials Research*, 747, 367-370.

Kan et al. **2016**, Effects of the heating rate on the thermochemical behaviour and bio fuel properties, *Energy Fuels*, 30, 1564−1570.

Kawai et al. **2007**, Crystallization and melting behaviour of poly (L-lactic acid), *Macro*

molecules, 40, 9463-9469.

Khawam et al. **2005**, Complementary use of model free and modelistic methods in the analysis of solid-state, *Kinetics Journal of Physical Chemistry*, 109, 10073-10080.

Khawam et al. **2006**, Solid-state kinetic models: basics and mathematical fundamentals, *Journal of Physical Chemistry B*, 110, 17315-17328.

Khoo et al. **2016**, Thermal and morphological properties of poly (lactic acid)/nanocellulose nanocomposite, *Procedia Chemistry*, 19, 788-794.

Kister et al. **1998**, Effects of morphology, conformation and configuration on the IR and Raman spectra of various poly(lactic acid), *Polymer*,39, 267-273.

Kiangkitiwan et al. **2013**, Poly (lactic acid) filled with cassava starch grafted soybean oil maleate, *The Scientific World Journal*, 2013, 860481-860487.

Kijchavengkul et al. **2008**, Compostability of polymers, *Polymer International*, 57, 793-804.

Kim et al. **2001**, Modification of poly (butylene succinate) with peroxide: Crosslinking, physical and thermal properties, and biodegradation, *Journal of Applied Polymer Science*, 81, 1115-1124.

Kissinger et al. **1957**, Reaction kinetics in differential thermal analysis, *Analysis Chemistry*, 29, 1702-1706.

Kopinke et al. **1996**, Thermal decomposition of biodegradable polyesters II: poly (lactic acid), *Polymer Degradation and Stability*, 53, 329-342.

Kumar et al. **2017**, Bioplastic classification, production and their potential food applications, Journal of hill agriculture, 8, 118-129.

Chilson et al. **2008**, The difference between ABS and PLA for 3D printing, http://www.protoparadigm.com/news-updates/the difference between ABS and PLA for 3D printing.

Leroy et al. **2010**, Kinetic study of forest fuels by TGA: Model-free kinetic approach for the prediction of phenomena, *Thermochimica Acta*, 497, 1-6.

Li et al. **2009**, Thermal degradation kinetic of gHA/PLA composite, *Thermochimica Acta*, 493, 90-95.

Li et al. **2004**, Preparation and degradation of PLA/chitosan composite materials, *Journal of Applied Polymer Science*, 91, 274-277.

Li et al. **2015**, Crystalline structures and crystallization behaviors of poly(l-lactide) in poly(l-lactide)/graphene nanosheet composites. *Polymer Chemistry*, 6, 3988-4002.

Lim et al. **2008**, Processing technology for poly (lactic acid), *Progress in Polymer Science*, 33, 820-852.

Lim et al. **2000**, processing of poly (lactide), in: Auras, R. (Eds.), Poly (lactic acid). Synthesis, structure, properties, processing and applications, John Wiley & Sons, Inc. New Jersey, 191-215.

Liu et al. **1999**, Critical consideration on the Freeman and Carroll method for evaluating global mass loss kinetics of polymer thermal degradation, *Thermochimica Acta*, 338, 85-94.

Liu et al. **2010**, Effects of hydrophilic fillers on the thermal degradation of poly (lactic acid), *Thermochimica Acta*, 509, 147-151.

Liu et al. **2014**, Thermal-oxidative degradation of high-amylose corn starch, *Journal of*

Thermal Analysis and Calorimetry, 115, 659-665.

Lopes et al. **2012**, Poly (lactic acid) production for tissue engineering applications, *Procedia Engineering*, 42, 1402-1413.

Luo et al. **2016**, Interfacial improvements in a green biopolymer alloy of poly(3-hydroxybutyrate-co-3-hydroxyvalerate) and lignin via in situ reactive extrusion. *ACS Sustainable Chemical Engineering*, 4, 3465-3476.

Lyu et al. **2007**, Kinetics and time temperature equivalence of polymer degradation, *Biomacromolecules*, 8, 2301-2310.

Martino et al. **2015**, Chitosan grafted low molecular weight polylactic acid for protein encapsulation and burst effect reduction. *International Journal of Pharmaceutics, 496*, 912-921.

Martin et al. **2001**, Poly (lactic acid): plasticization and properties of biodegradable multiphase system, *Polymer*, 42, 6209–6219.

Ma et al. **2012**, Toughening of PHBV/PBS and PHB/PBS Blends via in situ compatibilization using dicumyl peroxide as a free-radical grafting initiator. *Macromolecular Material and Engineering*, 297, 402-410.

Ma et al. **2014**, Lemstra In-situ compatibilization of poly (lactic acid) and poly (butylenes adipate-co-terephthalate) blends by using dicumyl peroxide as a free radical initiator, *Polymer Degradation and Stability*, 102, 145–151.

Maio et al. **2015**, Effect of polymer/organoclay composition on morphology and rheological properties of polylactide nanocomposites. *Polymer Composite, 36*, 1135-1144.

Mujica et al. **2016**, Poly (lactic acid) melt-spun fibres reinforced with functionalized cellulose nanocrystals, *RSC Advance*, 6, 9221-9231.

Mallakpour et al. **2009**, Kinetics of thermal degradation study of optically active and thermally stable aromatic polyamides with flame retardancy properties, *Polymer Journal*, 41, 308-318.

Manafi et al. **2015**, Thermal stability and thermal degradation kinetics (model-free kinetics)

of nanocomposites based on poly (lactic acid)/graphene: the influence of functionalization, *Polymer Bulletin*, 72, 1095–111.

Marechal et al. **1987**, IR spectra of carboxylic acids in the gas phase: A quantitative reinvestigation, *The Journal of Chemical Physics*, 87, 6344-6353.

Masutani et. al. **2014**, PLA synthesis, from the monomer to the polymer, in: Jimenez (Eds.), Poly (lactic acid) science and technology: processing, properties, additives and applications, *Royal Society of Chemistry*, 1-36.

Materazzi et al. **1997**, Thermogravimetry–infrared spectroscopy (TG–FTIR) coupled analysis, *Journal of Applied Spectroscopy Reviews*, 32, 385-404.

Mili et al. **2017**, Designing of poly (L-lactide)-nicotine conjugates: mechanistic and kinetic studies and thermal release behaviour of nicotine, *ACS Omega*, 2017, 6131-6142.

Mofokeng et al. **2015**, Dynamic mechanical properties of PLA/PHBV, PLA/PCL, PHBV/PCL blends and their nanocomposites with TiO_2 as nanofiller, *Thermochimica Acta*, 613, 41-53.

Monika et al. **2017,** Thermal degradation kinetics of poly (lactic acid)/acid fabricated

cellulose nanocrystals based bionanocomposites, *International Journal of Biological Macromolecules*, 104, 827-836.

Haque et al. **2017**, Effect of reactive functionalization on properties and degradability of poly (lactic acid)/poly(vinyl acetate) nanocomposites with cellulose nanocrystals, *Reactive and Functional Polymer*, 110, 1–9.

Montanari et al. **2008**, Top chemistry of carboxylated cellulose nanocrystals resulting from TEMPO-mediation oxidation, *Macromolecules*, 38, 1665-1671.

Muraleedharan et al. **2015**, Kinetic studies on the thermal dehydration and degradation of chitosan and citralidene chitosan, *Journal of Environmental Polymer Degradation, 23*, 1-10.

Muthuraj et al. **2017**, Biocomposite consisting of miscanthus fiber and biodegradable binary blend matrix: compatibilization and performance evaluation. *RSC Advances*, 7, 27538-27548.

Nair et al. **2007**, Thermogravimetric analysis of PVC/ELNR blends, *Polymer Degradation and Stability*, 92, 189-196.

Nagarajan et al. **2016**, Perspective on polylactic Acid (PLA) based sustainable materials for durable applications: focus on toughness and heat resistance, *ACS Sustainable Chemistry and Engineering*, 4, 2899-2916.

Najafi et al. **2013**, Crystallization behavior and morphology of polylactide and PLA/clay nanocomposites in the presence of chain extenders, *Polymer Engineering Science,* 53, 1053-1064.

Nanthananon et al. **2017**, Enhanced crystallization of poly(lactic acid) through reactive

aliphatic bisamide, *IOP conference Series: Material Science Engineering*, 87, 1-7.

Nasrin et al. **2017**, Preparation of chitin-PLA laminated composite for implantable products, bioactive materials, 2, 199-207.

Nayak et al. **2012**, Calcium alginate/gum arabic beads containing glibenclamide: development and in vitro characterization, *International Journal of Biological Macromolecules*, 51, 1070-1078.

Nie et. al. **2013**, A further amendment to the classical core structure of gum Arabic (acacia Senegal), *Food Hydrocolloids*, 31, 42-48.

Nerkar et al. **2015**, Improvement in the melt and solid state properties of poly (lactic acid), poly-3-hydroxyoctanoate and their blends through reactive modification, *Polymer*, 64, 51-61.

Nerantzaki et al. **2014**, Effect of nanofiller's type on the thermal properties and enzymatic degradation of poly (ε-caprolactone), *Polymer Degradation and Stability*, 108, 257-268.

Nishida et al. **2010**, Thermal degradation, in: Auras R (Eds.), Poly (Lactic acid). Synthesis, structure, properties, processing and applications, John Wiley & Sons, Inc. New Jersey, 401-412.

No et al. **2000**, Application of chitosan for treatment of wastewaters, in reviews of environmental contamination and toxicology: continuation of residue reviews. G. W. Ware, Editor. Springer New York: NY, 1-27.

Nofar et al. **2011**, Crystallization kinetics of linear and long chain branched polylactide, *Industrial Engineering Chemistry Research*, 50, 13789-13798.

Oliveira et al. **2016**, The role of shear and stabilizer on PLA degradation, *Polymer Testing*, 51, 109-116.

Onyari et al. **2008**, Biodegradability of poly (lactic acid), preparation and characterization of PLA/gum arabic blends, *Journal of Polymers and the Environment*, 16, 205-212.

Ounas et al. **2011**, Pyrolysis of olive residue and sugar cane bagasse: Non-isothermal thermogravimetric kinetic analysis, *Bioresource Technology*, 102, 11234-11238.

Ou et al. **2010**, Thermal degradation kinetics of chitosan-cobalt complex as studied by thermogravimetric analysis, *Carbohydrate Polymer*, 82, 1284-1289.

Oza et al. **2014**, Effect of surface treatment on thermal stability of the hemp-PLA composites: correlation of activation energy with thermal degradation, *Composites Part B: Engineering*, 67, 227-232.

Ozawa et al. **1965**, A new method of analyzing thermogravimetric data, *Bulletin of Chemical Society of Japan*, 38, 1881-1886.

Ozawa et al. **1986**, Non-isothermal kinetics and the generalized time, *Thermochimica Acta*, 100, 109-118.

Pal et al. **2016**, Nanoamphiphilic chitosan dispersed poly (lactic acid) bionanocomposite films with improved thermal, mechanical and gas barrier properties, *Biomacromolecules*, 17, 2603-2618.

Pal et al. **2017**, Thermal degradation behaviour of nanoamphiohilic chitosan dispersed poly (lactic acid) bionanocomposite films, *International Journal of Biological Macromolecules*, 95, 1267-1279.

Pal et al. **2018**, Chemomechanical, morphological and rheological studies of chitosan graft lactic acid oligomers reinforced poly (lactic acid) bionanocomposite films, Journal of Applied Polymer Science, 45546, 1-10.

Pallathadka et al. **2017**, Characteristics of biodegradable poly (butylene succinate) nanocomposites with thermally induced graphene nanosheets, *Polymer composites*, 38, 42-48.

Pandey et. al. **2005**, An overview on the degradation of polymer nanocomposite, *Polymer Degradation and Stability*, 88, 234-250.

Pan et al. **2016**, Validating carbonation parameters of alkaline solid waste via integrated thermal analyses: principle and applications, *Journal of Hazardous Material*, 307, 253-262.

Papageorgiou et al. **2010**, PLA nanocomposites: Effect of filler type on nonisothermal crystallization, *Thermochimica Acta*, 511, 129-139.

Papageorgiou et al. **2014**, Thermal degradation kinetics and decomposition mechanism of PBSu nanocomposites with silica-nanotubes and strontium hydroxyapatite nanorods. *Physical Chemistry Chemical Physics*, 16, 4830-4842.

Park et al. **2002**, Phase behaviour and morphology in blends of poly (L-lactic acid) and poly (butylene succinate), *Journal of Applied Polymer Science*, 86, 647-655.

Patel et al. **2015**, Applications of natural polymer gum Arabic: a review. *International Journal of Food Properties*, 18, 986-998.

Patwa et al. **2018**, Kinetic modelling of thermal degradation and nonisothermal crystallization of silk nano-disc reinforced poly (lactic acid) bionanocomposite, *Polymer Bulletin*, 1-

34, DOI: 10.1007/s00289-018-2434-7.

Paula et al. **2005**, Polylactide/montmorillonite nanocomposites: study of the hydrolytic degradation, *Polymer Degradation and Stability*, 87, 535-542.

Peng et al. **2011**, Chemistry and applications of nanocrystalline cellulose and its derivatives: a nanotechnology perspective, *The Canadian Journal of Chemical Engineering*, 9999, 1-16.

Perinovic et al. **2010**, Thermal properties of poly (l-lactide)/olive stone flour composites, *Thermochimica Acta*, 510, 97-102.

Petersson et al. **2007**, Structure and thermal properties of poly (lactic acid)/ cellulose whiskers nanocomposite materials, *Composites Science and Technology*, 67, 2535-2544.

Pilla et al. **2011**, Engineering applications of bioplastic and biocomposites-An overview, in Handbook of Bioplastic and Biocomposites Engineering Applications, John Wiley & Sons, Inc. 1-15.

Pilawka et al. **2014**, Thermal degradation kinetics of PET/SWCNTs nanocomposite prepared by the in situ polymerization, *Journal of Thermal Analysis and Calorimetry*, 115, 451-460.

Quero et al. **2012**, Isothermal cold-crystallization of PLA/PBAT blends with and without the addition of acetyl tributyl citrate, *Macromolecular Chemistry and Physics*, 213, 36-48.

Ramajo-Escalera et al. **2006**, Model-free kinetics applied to sugarcane bagasse combustion, *Thermochimica Acta*, 448, 111–116.

Ramukutty et al. **2014**, Reaction rate models for the thermal decomposition of ibuprofen crystals, *Journal of Crystallization Process and Technology*, 4, 71-78.

Rinaudo et al. **2006**, Chitin and chitosan: properties and applications, *Progress in polymer science*, 31, 603-632.

Rudnik et al. **2010,** Compostable polymer materials, Elsevier publishing, 1-224.

Ruseckaite et al. **2003**, Thermal degradation of mixture of polycaprolactone with cellulose derivates, *Polymer Degradation and Stability*, 81, 353-358.

Sa'nchez-Jime'nez et al. **2010**, Generalized Kinetics master plots for the thermal degradation of polymers following a random scission mechanism, *Journal of Physical Chemistry A*, 2010; 114:7868.

Song et al. **2012**, Flame retardance and thermal degradation behaviour of phosphate in combination with POSS in polylactide composite, *Thermochimica Acta*, 527, 1-7.

Sajna et al. **2015**, Effect of poly (lactic acid)-grafted-glycidyl methacrylate as a compatibilizer on properties of poly (lactic acid)/banana fiber biocomposites, *Polymers Advanced Technologies*, 27, 515-524.

Sanchez-Jimenez et al. **2010**, Generalized kinetic master plots for the thermal degradation of polymers following a random chain scission, *The Journal of Physical Chemistry A*, 114, 7868-7876.

Sbirrazzuoli et al. **2009**, Integral, Differential and advanced isoconversional methods, *Chemometrics and Intelligent Laboratory System*, 96, 219–226.

Shayan et al. **2015**, Effect of modified starch and nanoclay particles on biodegradability and

mechanical properties of crosslinked poly (lactic acid), *Carbohydrate Polymer*, 124, 237-244.

Shen et al. **2009**, The mechanism for thermal decomposition of cellulose and its main products, *Bioresource Technology*, 100, 6496-6504.

Shibata et al. **2006**, Mechanical properties, morphology and crystallization behaviour of blends of poly (L-lactide) with poly (butylenes succinate-co-L-lactate) and poly (butylenes succinate), *Polymer*, 47, 3557-3564.

Signori et al. **2009**, Thermal degradation of poly (lactic acid) and poly (butylenes adiapate-co-terephthalate) and their blends upon melt processing, *Polymer Degradation and Stability*, 94, 74-82.

Singh et al. **2008**, Mechanistic implications of plastic degradation, *Polymer Degradation and Stability*, 93, 561-584.

Sinha et al. **2013**, Influence of organomodified Ni-Al layered double hydroxide (LDH) content on the thermal properties and degradation kinetics of polystyrene (PS)/Ni-Al LDH nanocomposite prepared via solvent blending method, *Advanced Material Research*, 747, 23-26.

Silva et al. **2015**, Immobilization of trypsin onto poly(ethylene terephthalate)/poly(lactic acid) nonwoven nanofiber mats, *Biochemical Engineering Journal*,104, 48-56.

Sodergard et al. **1994**, Stabilization of poly (L-lactide) in the melt, *Polymer Degradation and Stability*, 46, 25-30.

Kangwanwatthanasiri et al. **2013**, Biocomposites from cassava pulp/Polylactic acid/Poly (butylene succinate), *Advanced Materials Research*, 747 (2013) 367-370.

Song et al. **2009**, Biodegradation and compostable alternatives to conventional plastics, *Philosophical Transactions of the Royal Society B: Biological Sciences, 364,* 2127-2139.

Shen et al. **2009**, Product overview and market projection of emerging biobased plastics, Final report of Utrecht University to European Bioplastics; 2009.

Spinella et al. **2016**, Green and efficient synthesis of dispersible cellulose nanocrystals in biobased polyesters for engineering applications, *ACS Sustainable Chemistry and Engineering*, 4, 2517–2527.

Sullivan et al. **2015**, Processing and characterization of cellulose nanocrystals/polylactic acid nanocomposite films, *Materials*, 8, 8106–8116.

Su et al. **2008**, Thermal stabilities and the thermal degradation kinetics of Poly (ε-caprolactone), *Polymer Plastic Technology and Engineering*, 47, 398-403.

Takamura et al. **2008**, Effect of type of peroxide on cross-linking of poly(l-lactide), *Polymer Degradaion and Stability*, 93, 1909-191.

Tachibana et al. **2009**, Utilization of a biodegradable mulch sheet produced from Poly (lactic acid)/ecoflex/modified starch in mandarin orange groves, *International Journal of molecular science*, 10, 3599-3615.

Teamsinsungvon et al. **2013**, Preparation and characterization of poly(lactic acid)/poly(butylene adipate-co-terepthalate) blends and their composite. *Polymer-Plastic Technology and Engineering*, 52, 1362-1367.

Tesfaye et al. **2017**, Nanosilk grafted poly (lactic acid) films: Influence of crosslinking on rheology and thermal stability, *ACS Omega*, 2, 7071-7984.

Tesfaye et al. **2016**, Silk nanocrystals stabilized melt extruded poly (lactic acid) nanocomposite films: Effect of recycling on thermal degradation kinetics and optimization studies, *Thermochimica Acta*, 643, 41-52.

Tesfaye et al. **2017**, Recycling of poly (lactic acid)/silk based bionanocomposites films and its influence on thermal stability, crystallization kinetics, solution and melt rheology. *International Journal of Biological Macromolecules*, 101, 580-594.

Teixeira et al. **2010**, Nanofibras de algodão obtidas sob diferentes condic ões de hidrólise ácida, *Polímeros*, 20, 264-268.

Thompson et al. **2009**, Plastics, the environment and human health: current consensus and future trends. *Philosophical Transactions of the Royal Society B: Biological Sciences*, 364, 2153-2166.

Tiptipakorn et al. **2007**, Thermal degradation behaviours of polybenzoxazine and silicon containing polyimide blends, *Polymer Degradation and Stability*, 92, 1265-1278.

Triphati et al. **2016**, PLA/functionalized-gum Arabic based bionanocomposite films for high gas barrier applications, *Journal of Applied Polymer Science*, 43458, 1-8.

Tripathi et al. **2017**, Poly (lactic acid)/modified gum arabic based biocomposite film: Thermal degradation kinetics, *Polymer Engineering Science*, 57, 1193.

Tripathi et al. **2018**, Lactic acid oligomer (OLLA) grafted gum arabic based green adhesive for structural application, *International Journal of Biological Macromolecules*, 120:711.

Tudorachi et al. **2012**, Thermal degradation of carboxymethyl starch-g-poly (lactic acid) copolymer by TG-FTIR-MS analysis, *Industrial Engineering Chemistry Research*, 51,

15537-15545.

Turmanova et al. **2011**, Kinetics of nonisothermal degradation of some polymer composite: change of entrophy at the formation of the activated complex from the reagents, *Journal of Thermodyanamic*, 1-10.

Ummartyotin et al. **2015**, A critical review on cellulose: from fundamental to an approach on sensor technology, *Renewable and Sustainable Energy Reviews*, 41, 402-412.

Vink et al. **2015**, Life cycle inventory and impact assessment data for 2014, Ingeo polylactide production, *Industrial Biotechnology*, 11, 167-180.

Valapa et al. **2014**, Thermal degradation kinetics of sucrose palmitate reinforced poly (lactic acid) biocomposite, *International Journal of Biological Macromolecules*, 2014, 65, 275.

Valapa et al. **2015**, Effect of graphene content on the properties of poly (lactic acid) nanocomposites, *RSC Advance*, 5, 28410-28423.

Vasanthakumari et al. **1983**, Crystallization kinetics of poly (L-lactic acid), *Polymer*, 24, 175–178.

Vogel et al. **2008**, Thermal Degradation of Poly (ε-caprolactone), Poly (L-lactic acid) and their Blends with Poly (3-hydroxy-butyrate) studied by TGA/FT-IR Spectroscopy. *Polymer Science & Technology General, Macromolecular Symposia*, 265, 183–194.

Volli et al. **2014**, Physico-chemical properties and thermal degradation studies of commercial oils in nitrogen atmosphere, *Fuel*, 117, 1010-1019.

Vyazovkin et al. **2001**, Modification of the integral isoconversional methods to account for

variation in the activation energy, *Journal of Computational Chemistry*, 22, 178-183.

Wachsen et al. **1997**, Thermal degradation of poly-L-lactide-studies on kinetics, modelling and melt stabilization, *Polymer Degradation and Stability*, 57, 87-94.

Wang et al. **2011**, Flame retardancy and thermal degradation of intumescent flame retardant poly (lactic acid)/starch biocomposite, 50, 713-720.

Wang et al. **2013**, Fabrication and characterization of heparin-grafted poly-L-lactic acid-chitosan core-shell nanofibers scaffold for vascular gasket, *ACS applied material interfaces*, 5, 3757-3763.

Wang et al. **2014**, Synthesis, characterization and emulsification properties of dodecenyl succinic anhydride derivatives of gum arabic, *Food Hydrocolloids*, 37, 143-148.

Wang et al. **2015**, Supertoughened biobased poly (lactic acid)-epoxidized natural rubber thermoplastic vulcanizates: Fabrication, co-continuous phase structure, interfacial in situ compatibilization and toughening mechanism, *Journal of Physical Chemistry B*, 119, 12138-12146.

Wei et al. **2015**, Interfacial improvement in biocomposites based on poly (3-hydroxybutyrate) and poly (3-hydroxybutyrate-co-3-hydroxyvalerate) bioplastics reinforced and grafted with α-cellulose fibers, *Green Chemistry*, 17, 4800-4814.

Wilkie et al. **1999**, TGA/FTIR: an extremely useful technique for studying polymer degradation, *Polymer Degradation and Stability*, 66, 301-306.

Wu et al. **2005**, Improving poly lactide/starch biocomposite by grafting poly lactide with acrylic acid-characterization and biodegradability assessment, *Macromolecular Bioscience*, 5, 352-361.

Wu et al. **2012**, Interfacial properties, visco-elasticity and thermal behaviour of poly (butylenes succinate)/poly lactide blend, *Industrial and Engineering Chemistry Research*, 51, 2290-2298.

Xilei et al. **2012**, Thermal degradation characteristics of flame retardant polylactide using TG-IR, *Polymer Degradation and Stability*, 2143-2147.

Xu et al. **2005**, Observation of banded spherulites in pure poly (l-lactide) and its miscible blend with amorphous polymer, *Polymer*, 46, 9176–9185.

Xu et al. **2010**, Poly (butylenes succinate) and its copolymers: Research, development and industrialization, *Biotechnology Journal*, 5, 1149-1163.

Xu et al. **2017**, Interfacial modification on polyhydroxyalkanoates/starch blend by grafting in situ, *Carbohydrate Polymer*, 174, 716–722.

Xiong et al. **2013**, Preparation and characterization of poly(lactic acid)/starch composites toughened with epoxidized soybean oil. *Carbohydrate Polymer, 92*, 810-816.

Yang et al. **2007**, Characteristics of hemicelluloses, cellulose and lignin pyrolysis, *Fuel*, 86 1781–1788.

Yang et al. **2017**, A study on the mechanical properties, thermal properties and crystallization behaviour of poly (lactic acid)/thermoplastic poly (propylene carbonate) polyurethane blends, *RSC Advance*, 7, 46183–46194.

Yang et al. **2009**, Measurement and simulation of thermal stability of poly (lactic acid) by thermogravimetric analysis, *Journal of Testing Evaluation*, 37, 364-370.

Yang et al. **2015**, Stereoselective polymerization of rac-lactide catalyzed by zinc complexes

with tetradenated aminephenolate ligands in different coordinateion patterns: kinetic and mechanism, *Inorganic chemistry*, 54, 5834-5854.

Yang et al. **2008**, Thermal and mechanical properties of chemical crosslinked polylactide (PLA), *Polymer Testing*, 27, 957-963.

Yang et al. **2016**, Poly(lactide)-g-poly(butylene succinate-co-adipate) with high crystallization capacity and migration resistance, *Materials*, *9*, 313.

Yao et al. **2017**, Investigation of Structure and Crystallization Behavior of Poly(butylene succinate) by Fourier Transform Infrared Spectroscopy, *Journal Physical Chemistry B*, *121*, 9476-9485.

Yarsley et. al. **1945**, Plastics Middlesex: Penguin Books Limited.

Yasuniwa et al. **2008**, Behavior of poly(L-lactic acid): X-ray and DSC analyses of the melting process, *Polymer*, 49, 1943–1951.

Yildirim et al. **2012**, Synthesis, characterization, and thermal degradation kinetic of Polystyrene-g-Polycaprolactone, *Journal of Applied Polymer Science*, 126, 1236-1246.

Yokohara et al. **2008**, Structure and properties for biomass-based polyester blends for PLA and PBS, *European Polymer Journal*, *44*, 677-685.

Yutaka et al. **2009**, Biodegradability of plastics, *International Journal of Molecular Science*, 10, 3722-3742.

Yuzay et al. **2010**, Effects of synthetic and natural zeolites on morphology and thermal degradation of poly (lactic acid) composites, *Polymer Degradation and Stability*, 95, 1769-1777.

Yoshikawa et al. **2014**, Multistep kinetic behaviour in the thermal degradation of poly (L-lactic acid): A physico-geometrical kinetic, *Journal of Physical Chemistry B*, 38, 11397-11405.

Zargar et al. **2015**, A review on chitin and chitosan polymers: structure, chemistry, solubility, derivatives and applications, *Chem Bio Eng Reviews*, 2, 204-226.

Zeng et al. **2012**, Chitin whisker: an overview, *Biomacromolecules*, 13, 1-11.

Zhang et al. **2012**, Fully Biodegradable and Biorenewable Ternary Blends from Polylactide, Poly(3-hydroxybutyrate-co-hydroxyvalerate) and Poly(butylene succinate) with Balanced Properties, *ACS Applied Material Interfaces*, 4, 3091-3101.

Zhang et al. **2013**, Enhance ductility of polylactide materials: Reactive blending with pre-hot sheared natural rubber, *Journal of Polymer Research*, 20, 1-9.

Zhang et al. **2014**, Toughened sustainable green composites from poly (3-hydroxybutyrate-co-3-hydroxyvalerate) based ternary blends and miscanthus biofiber, *ACS Sustainable Chemistry and Engineering*, 2, 2345-2354.

Zhang et al. **2015**, Compatibilization strategies in poly (lactic acid)-based blends, *RSC Advance*, 5, 32546–32565.

Zhang et al. **2016**, Reinforcement effect of poly (butylene succinate) (PBS)-grafted cellulose nanocrystals on the toughened PBS/Polylactic acid blends, *Carbohydrate Polymer*, 140, 374-382.

Zhang et al. **2016**, Toughening advance of PLLA by combination of copolymerization and in situ reactive blending, *RSC Advance*, 6, 113366-113376.

Zhao et al. **2014**, A new super-efficiently flame retardant bioplastic poly (lactic acid): flammability, thermal decomposition behaviour and tensile properties, *ACS Sustainable Chemical Engineering*, 2014, 4:1.

Zheng et al. **2011**, Synthesis, characterization and properties of novel biodegradable multi block copolymers compromising poly (butylene succinate) and poly (1, 2-propylene terephthalate) with hexamethylene diisocynate as a chain extender, *Polymer International*, 60, 666-675.

Zho et al. **2016**, Effect of N, N'-diallyl –phenylphosphoricdiamide on ease of ignition, thermal decomposition behaviour and mechanical properties of poly(lactic acid), *Polymer Degradation and stability*, 127, 2-10.

Zhou et al. **2018**, Enhancing mechanical properties of poly (lactic acid) through its in-situ crosslinking with maleic anhydride-modified cellulose nanocrystals from cottonseed hulls, *Industrial Crops and Products*, 112, 449–459.

Zhu et al. **2001**, Fire properties of polystyrene-clay nanocomposites, *Chemistry of Material*, 13, 3774-3780.

Zong et al. **2005**, Thermal degradation kinetics of polyethylene and silane crosslinked polyethylene, *Journal of Applied Polymer Science*, 98, 1172-1179.

Zou et al. **2009**, Thermal degradation of poly (lactic acid) measured by thermogravimetry coupled to fourier transform infrared spectroscopy, *Journal of Thermal Analysis Calorimetry*, 97, 929-935.

Zou et al. **2011**, Thermal stability and thermal degradation kinetics of poly (trimethylene-co-butylene terepthalate) copolymers, *Journal of Macromolecular Science, Part B*: *Physics*, 50, 1559-1570.

Supplementary file

FTIR

Functionalized chitosan

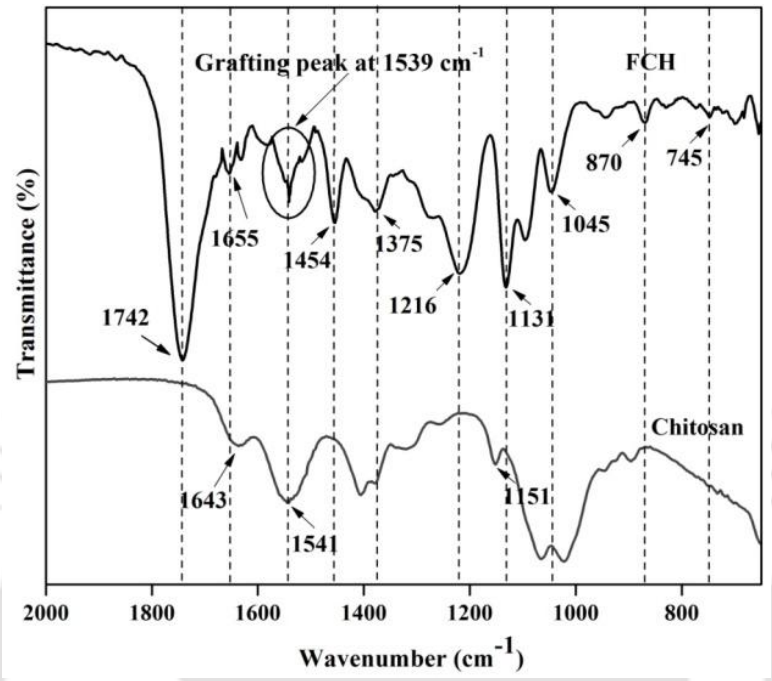

Fig. 2.1S FTIR profiles of Chitosan and FCH.

Functionalized gum arabic

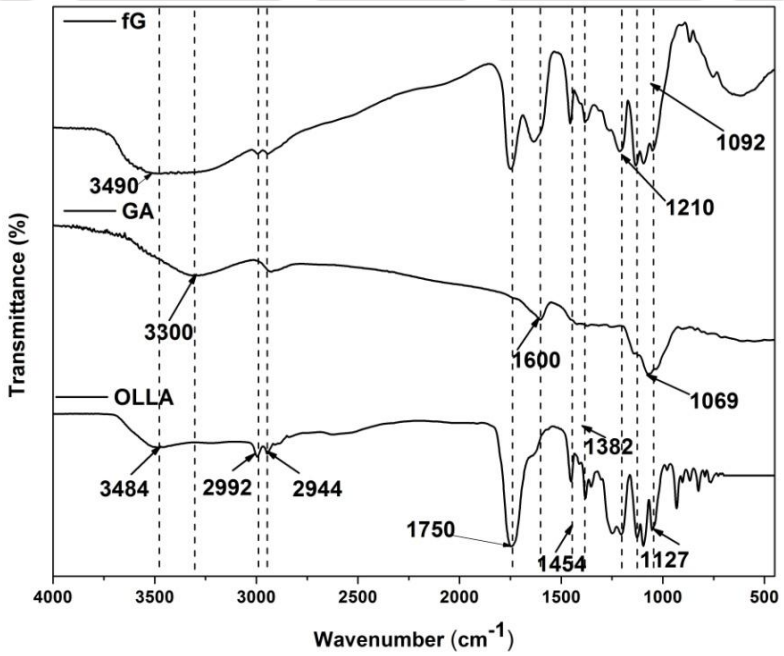

Fig. 2.2S FTIR profiles of OLLA, GA and fG.

3D plot of TGA-FTIR

Gum Arabic

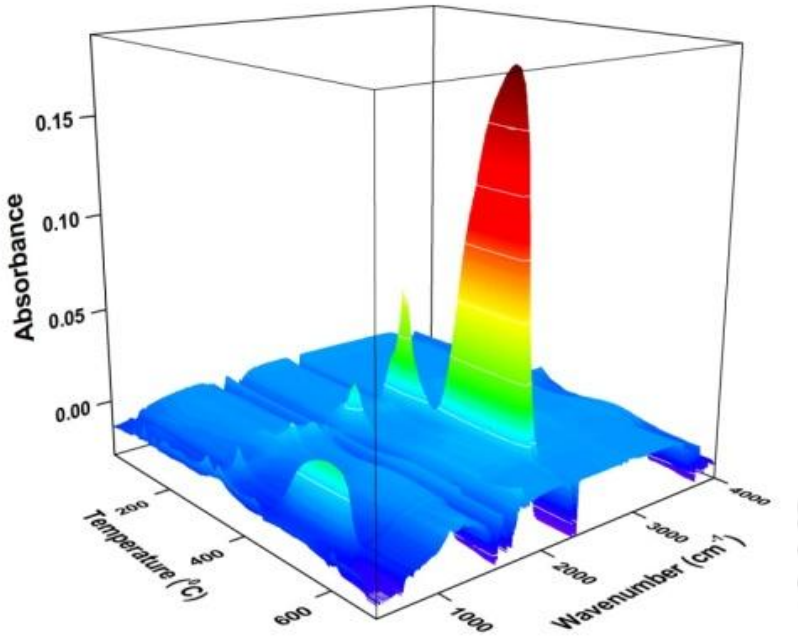

(a)

Functionalized Gum

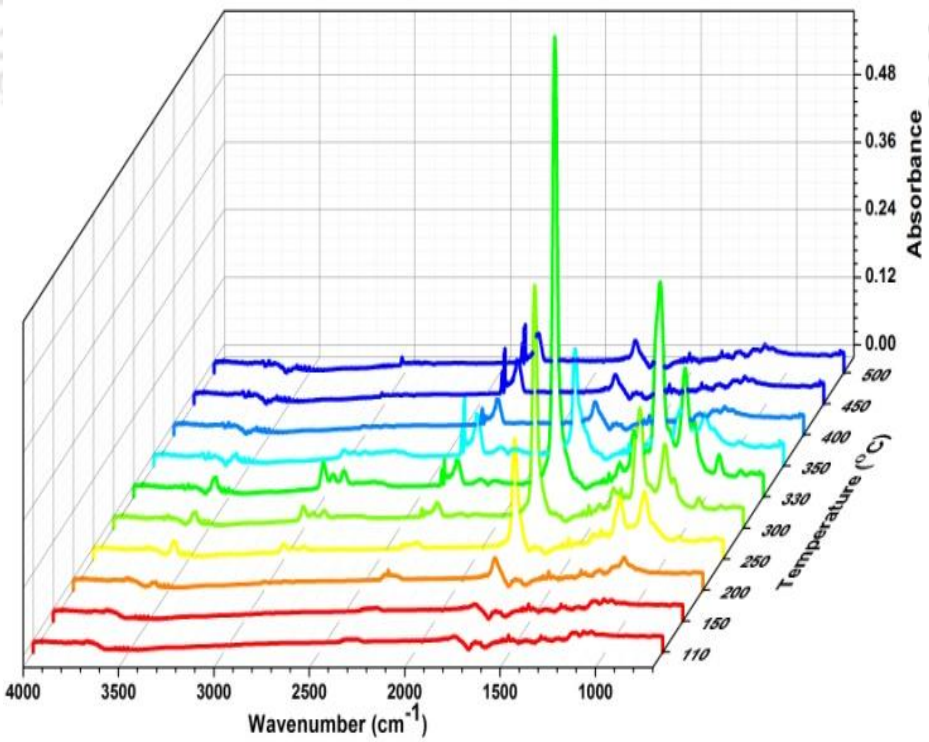

(b)

PLA-1FG bionanocomposite

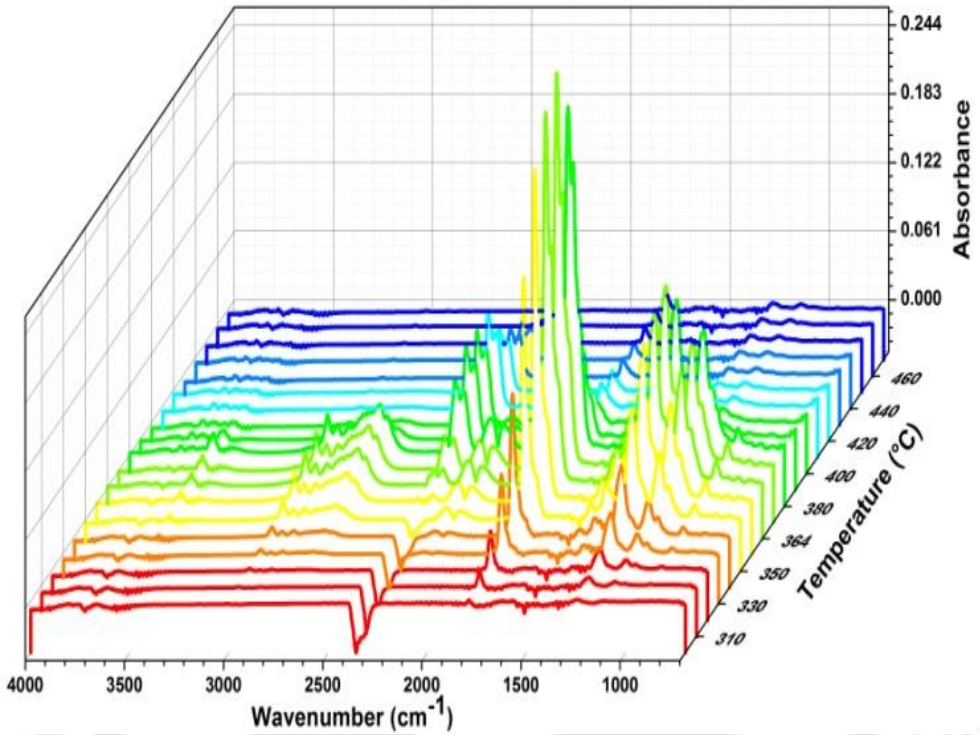

(c)

DCP treated PLA-1FG bionanocomposite

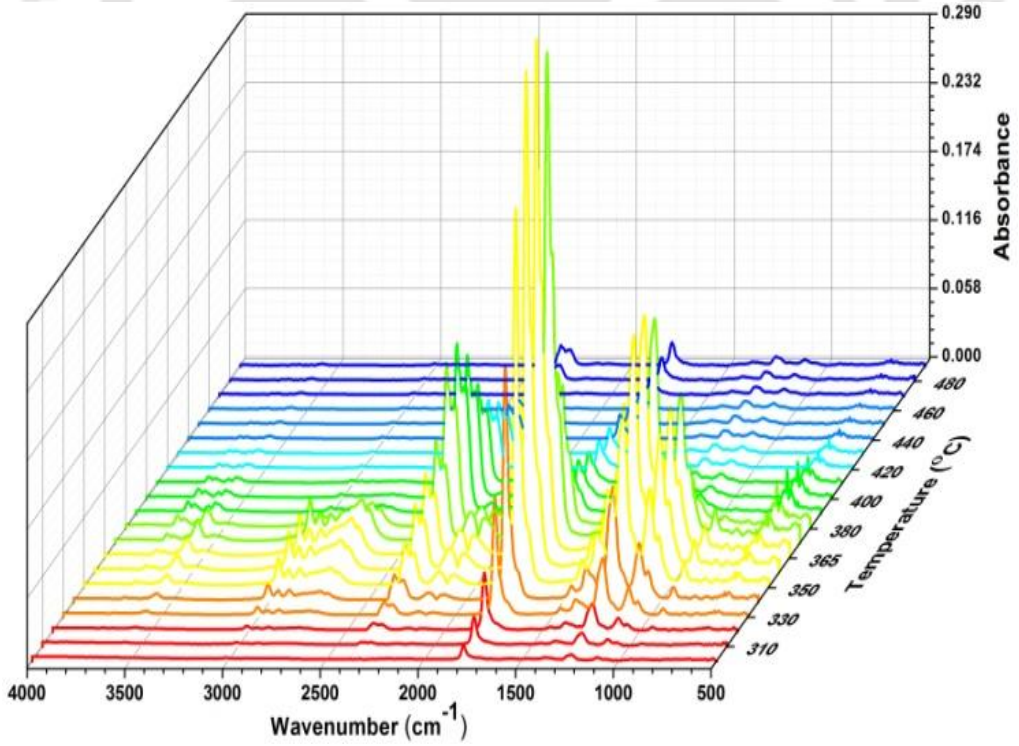

(d)

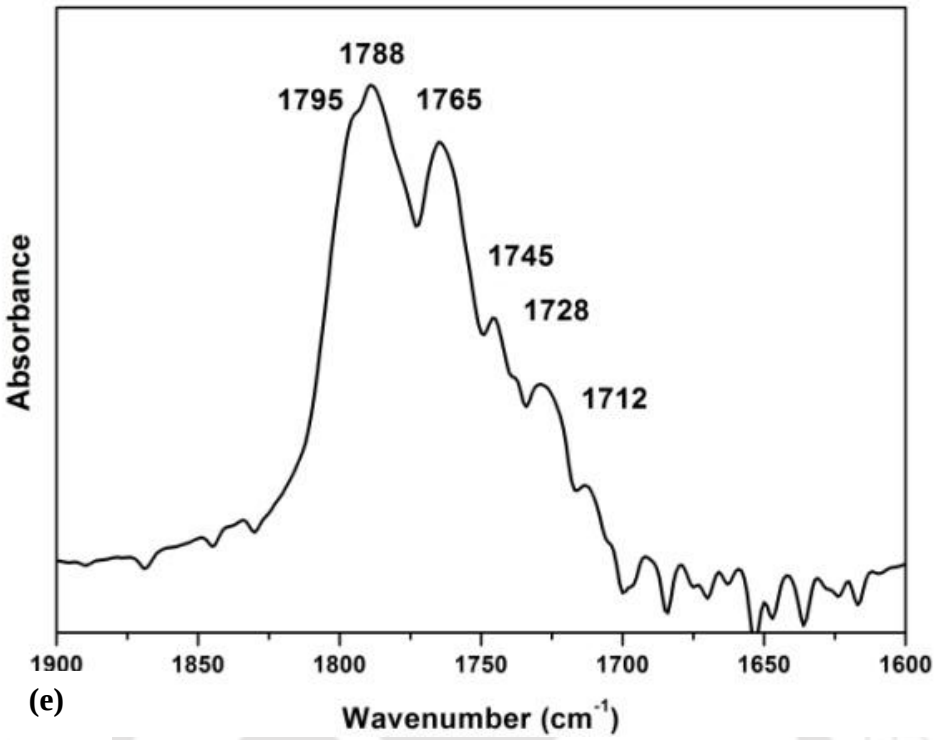

Figure 4.1 S: *Evolution of volatile products as a function of temperature from (a) GA, (b) FG (c) PLA-1FG (d) PLA-D-1FG (e) enlarge image of PLA-D-1FG in the range of 1900-1600 cm^{-1} bionanocomposite films.*

Research Outcomes

In Manuscript

Monika, Prodyut Dhar and Vimal Katiyar (2017), Thermal Degradation Kinetics of Poly (lactic acid)/Different Acid Fabricated Cellulose Nanocrystals based Bionanocomposite, "***International Journal of Biological Macromolecules"***, 104, 827-836.

Monika, Akhilesh Kumar Pal, Siddhartha Mohan Bhasney, Purabi Bhagabati and Vimal Katiyar (2018), Effect of Dicumyl Peroxide on a Poly (lactic acid)/Poly (butylene succinate)/Functionalized Chitosan based Nanobiocomposite for Packaging: A Reactive Extrusion Study, ***ACS Omega***, 3, 13298-13312.

Monika and Vimal Katiyar (2019), Non-Isothermal Degradation Kinetics of PLA/Functionalized Gum (fG) Biocompsite with Dicumyl Peroxide (DCP), "***Journal of Thermal Analysis and Calorimetry***" 1-16.

Monika, Neha Mulchandani and Vimal Katiyar, Generalized Kinetic for Thermal Degradation and Melt Rheology for Poly (lactic acid) PLA/Poly (butylene succinate) PBS/Functionalized chitosan (*F*CH) based Reactive Nanobiocomposite (**Status**: Under Revision International Journal of Biological Macromolecules).

Monika, Khalid Mehmood and Vimal Katiyar, Compatibilized PLA/Functionalized Gum Arabic based Bionanocomposite Films with Dicumyl Peroxide (DCP): A Reactive Extrusion Approach (**Status**: Submitted to Polymer Bulletin)

Other contributions

Neelima Triphati, **Monika** and Vimal Katiyar (2007), Poly (lactic acid)/Modified Gum Arabic based Bionanocomposite Films: Thermal Degradation Kinetics, ***Polymer Engineering and Science***, 1-14.

Rahul Patwa, **Monika** and Vimal Katiyar (2018), Kinetic modelling of thermal degradation and non-isothermal crystallization of silk nano-disc reinforced poly (lactic acid) bionanocom

posite, ***Polymer Bulletin***, 1-34.

Medha Mili, Arvind Gupta, **Monika** and Vimal Katiyar (2017), Designing of Poly (lactide)-nicotine conjugates: mechanistic, kinetic studies and thermal release behaviour of nicotine, ***ACS Omega***, 2, 6131-6142.

Prodyut Dhar, **Monika** and Vimal Katiyar, Reactive Extrusion of Poly (lactic acid)/Cellulose nanocrystals film for packaging: Influence of fillers on biodegradation and thermal behaviour (Under Writing).

Conference Proceedings

Monika, Khalid Mehmood and Vimal Katiyar, Poly (lactic acid)/functionalized gum arabic based reactive modified biocomposite: Mechanism, mechanical and UV properties, *International Symposium on Sustainable Polymers & Launch SPSI-North East Chapter*, August 23-25, 2019, Guwahati, India.

Monika and Vimal Katiyar, Influence of functionalized chitosan on poly (lactic acid)/poly (butylene succinate) based reactive nanobiocomposite: to investigate morphology and melt rheology, ***Sixth International Symposium Frontiers in Polymer Science***, May 5-8, 2019, Budapest, Hungary.

Monika and Vimal Katiyar, poly (lactic acid)/poly (butylene succinate)/functionalized chitosan based reactive nanobiocomposite for packaging application, ***Poly Char 19***, May 19-23, 2019, Kathmandu, Nepal.

Monika and Vimal Katiyar, Functionalized Gum grafted PLA film: Elucidation of Degradation Kinetic Parameters and Mechanism, "***SPSI MACRO 18"***, IISER Pune, 19-22 December 2018.

Monika and Vimal Katiyar, Non-Isothermal Degradation Kinetic Study of PLA/PBS based Ternary Bionaocomposites, "***Indo Japan Bilateral Symposium on future perspective of Bio resource Utilization 17 (IJBS 17)****"*, February 1-4, 2018, Guwahati, India.

Monika and Vimal Katiyar, Effect of functionalized chitosan on PLA/PBS based biocomposite for morphological, thermal and mechanical properties analysis, "***Forth international symposium on Advance in Sustainable Polymer 17 (ASP 17)****"*, January 8-11, 2018, Guwahati, India.

Monika, Prodyut Dhar and Vimal Katiyar, Thermal Degradation Kinetics of PLA/CNC based Bionanocomposites, "***Indo Japan Bilateral Symposium on future perspective of Bioresource Utilization 17 (IJBS 17)****"*, February 1-4, 2018, Guwahati, India.

Monika and Vimal Katiyar, Thermal Degradation Study of Xanthan Gum, Guar Gum and Gum Arabic using Hyphenated TGA-FTIR Analysis: A Comparative Study, "***International Conference on Polymer Science and Technology* (*MACRO 2017*)**", January 8-11, 2017, Thiruvananthapuram, Kerala, India.

Rahul Patwa, **Monika**, Amit Kumar and Vimal Katiyar, Influence of Silk Nanocrystals on Thermal Degradation Behaviour of PLA based Bionanocomposite Film: Assessment of Mechanism using TGA and TG-IR Studies, "***International Conference on Advanced Materials for Energy and Health* (*ICAM 2016*)**", March 4-7, 2016, IIT Roorkee, India.

Medha Mili, Arvind Gupta, **Monika**, Prakash Kotecha and Vimal Katiyar, Synthesis Characterization and Thermal Release Behavior of Poly (L-lactic Acid) Conjugates, "***Advance in Sustainable Polymer 16 (ASP 16)",*** Kyoto Institute of Technology, Kyoto, Japan.

Awards

Springer Award for poster presentation in the ***Indo Japan Bilateral Symposium on Future Perspective of Bioresource Utilization 17*** *(IJBS 17),* February 1-4, 2018.